

DISSERTATION

NOVEL *IN VITRO* APPROACHES TO DELINEATE
PRION STRAIN CONFORMATIONAL VARIATION

Submitted by

Vanessa Villegas Selwyn

Graduate Degree Program in Cellular and Molecular Biology

In partial fulfillment of the requirements

For the Degree of Doctor of Philosophy

Colorado State University

Fort Collins, Colorado

Fall 2019

Doctoral Committee:

Advisor: Glenn Telling

Mark Zabel

Eric Ross

Karen Dobos

Copyright by Vanessa Villegas Selwyn 2019

All Rights Reserved

ABSTRACT

NOVEL *IN VITRO* APPROACHES TO DELINEATE PRION STRAIN CONFORMATIONAL VARIATION

Prions cause in invariably lethal, transmissible neurodegenerative diseases. There are no effective treatments or cures for prion diseases. Unlike other known pathogens, prions replicate in the absence of nucleic acids. Prion diseases stem from the conformational corruption of the cellular prion protein (PrP^C) by the pathogenic form (PrP^{Sc}) (Prusiner, 1982). The prion phenomenon, protein-templated misfolding, is no longer limited to the prion protein (PrP). Other neurodegenerative disorders, including but not limited to Alzheimer's, Parkinson's, Huntington's are now being recognized as prion-like disorders (Soto, 2012). By exploring the intricacies of prion protein-misfolding, therapeutic approaches might emerge that will be useful in treating other neurodegenerative protein-misfolding disorders.

Although the structure of PrP^C has been solved (Riek et al 1997, Zahn et al 2000, Garcia et al 2000, Donne et al 2007, Antonyuk et al 2009), the three-dimensional structure of PrP^{Sc} has yet to be resolved. A confounding issue to identifying PrP^{Sc} structure is the existence of prion strains (Bett et al 2012). In the absence of nucleic acids, prion strain properties are propagated through variations in the conformational structure of PrP^{Sc} (Telling et al 1996). As such, prion strains can be defined as an infectious prion protein particle with a specific tertiary conformation that produces a

specific neurodegenerative phenotype (Colby et al., 2009). Specifically, a prion strain can be considered to have a strain-specific (Peretz et al 2001) disease phenotype (Collinge et al 1996) based on the prion's ability to be stably propagated, fidelity to neuropathology, disease length, glycosylation profile, molecular weight of PK-resistant PrP^{Sc}, resistance to denaturation, amyloid seeding potential and other molecular characteristics. Ultimately, revealing PrP^{Sc} structure will provide better understanding of the basis of strains, species adaption and ultimately the species barrier.

The traditional methodologies to examine prion strains are costly, time consuming, and do not provide adequate resolution of the PrP^{Sc} structure. The overarching aim of my research is to better understand how prions encrypt strain information. In Chapter 1, I outline essential background regarding prions and prion strains. In Chapter 2 and 3, I address the creation of the expanded Cell-Based Conformational Stability Assay, Epitope Stability Assay, and use of a new 7-5 ELISA Conformational Stability Assay. These represent novel tools that use chaotropic agents to probe epitope-mapped regions to identify subtle differences in prion strain structure. The prion strains evaluated were cervid (deer and elk) chronic wasting disease, murine-adapted scrapie (RML, 22L, 139A), murine-adapted chronic wasting disease (mD10) and cervid-adapted (deer and elk) RML. These techniques revealed subtle but significant prion strain structural variations within and between these strains. In Chapter 4, the techniques were used to better understand drug-induced prion evolution and strain evolution in cell culture. Drug-induced prion evolution of PrP^{Sc} structure was subtle but detectable within 24 hours of treatment. Additionally, the structural

changes were not stable, but in flux. Prion strains evolve in cell culture through serial passaging, they do not recapitulate molecular characteristics of a biological prion infection. Moreover, the prion structure is not stably passaged into naïve cells, or transgenic mice. This makes reliance on chronically infected cells as a basis for anti-prion therapeutic testing inadvisable. In conclusion, the subtle variations encoded in prion strain structure can be detected with the three new techniques in this dissertation: C-CSA, ESA, and 7-5 ELISA-CSA.

ACKNOWLEDGEMENTS

Although this document is the ultimate culmination of my work, research and effort, I would never have achieved this pinnacle of knowledge without the graciousness and support of those around me. First and foremost, I want to acknowledge my family. I love and thank you all, especially: my mother, MariaElena Selwyn, my sibling, S. Cesaria Selwyn, father, David Selwyn, grandpa, J.Ventura Garcia, grandma, MariaInez Garcia, and partner, Bashar Matrix. Throughout my four degrees my family rallied around me with their love, strength, funds, unconditional support, and true belief that I could succeed. They have championed me, consoled me, and reminded me that failure is part of success.

To my New Mexico State University mentors and friends, I sincerely offer my gratitude. I was fortunate to have wise and gracious scientists to start my path into research: Dr. Daniel Howard, Dr. Elba Serrano, Dr. James Kroger, and Dr. Antonio Lara. They taught me, guided me, and pushed me to grow as an individual and as a scientist. Each of you had an influence on me, and I'm grateful.

To those at Colorado State University who offered me mentorship and advice, I genuinely offer my appreciation. Without you to help me, I would have been lost in the multiple occasions that the valleys of my journey became nearly insurmountable peaks. I want to especially thank Dr. Jodie Hanzlik, Dr. Lupe Salazar, Dr. Carol Wilusz, Dr. Paul Laybourn, Dr. Greg Florant, Dr. Mary Ontiveros, Dr. Deryl Keney, Dr. Roxann Karkhoff-Schwiezer, Dr. Mark Brown, Dr. Mark Zabel, Dr. Howard Liber, Nancy

Graham, Lori Williams, Heidi Runge, and Charlene Spencer. Additionally, I need to thank my peers who offered moral support and reminded me that I'm never truly alone in this degree, especially: Dr. Phillida Charley, Dr. SarahJo Kane, Dr. Melissa Edwards, Dr. Stephanie Morphet, Zin Telling, and Kelly Hassell.

I want to express gratitude to my laboratory collaborators and mentors, Dr. Glenn Telling, Dr. Julie Moreno, Dr. Jifang Bian, Dr. Hae-Eun Kang, Carla Calvi, Dr. SarahJo Kane, SeHun Kim, Dr. Vadim Khaychuk, and Jenna Crowell for helping make the Telling lab my scientific home-base at CSU. Each member of my lab pushed me, and encouraged me to the best of their ability. The long discussions where we bounced ideas off of each other, the camaraderie, the long hours in lab; they helped make me better scientists.

To all the individuals who have served on my PhD committee, thank you for offering guidance through the process and helping me develop as a scientist. I wish to acknowledge Dr. Glenn Telling, Dr. Mark Zabel, Dr. Eric Ross, Dr. Kathy Partin, Dr. Karen Dobos, and Dr. Carol Wilusz. Your willingness to thrust me ever onward has propelled me to finish.

Last, but not least, to my PhD advisor Dr. Glenn Telling. Thank you for finding patience when I tried you, for being willing to bear with me though all these years. You have challenged me the way no other advisor ever has.

DEDICATION

*To those who loved me enough to endure the
rollercoaster ride that accompanied this journey.*

¡Gracias por todo!

TABLE OF CONTENTS

ABSTRACT	ii
ACKNOWLEDGEMENTS.....	v
DEDICATION	vii
LIST OF TABLES.....	x
LIST OF FIGURES.....	xi
CHAPTER 1 - BACKGROUND	1
A. BRIEF HISTORICAL OVERVIEW.....	1
B. PRION DISEASES AND STRAINS.....	2
C. PRION PROTEIN STRUCTURE AND REPLICATION	19
D. APPROACHES FOR STUDYING PRIONS.....	28
E. INVESTIGATIONAL AIMS.....	34
i. AIM 1: Expand the prion Cell-Based Conformational Stability Assay to better understand prion strain structural characteristics	
ii. AIM 2: Create a new prion Epitope Stability Assay (ESA) to more directly examine epitope accessibility differences in prion strain structural characteristics and provide previously inaccessible structural information about the prion protein	
iii. AIM 3: Compare emerging and evolving strains to better understand the basis of strain/species adaption and ultimately the species barrier	
BIBLIOGRAPHY	41
CHAPTER 2 - PRION STRAIN DIFFERENCES ARE DETECTABLE WITH AN EXPANDED CELL-BASED CONFORMATIONAL ASSAY IN FRESHLY INFECTED RK-PrP CELLS	66
A. INTRODUCTION	66
B. MATERIALS AND METHODOLOGY	73
C. RESULTS	85
D. DISCUSSION.....	109
BIBLIOGRAPHY	114
CHAPTER 3 - A NOVEL EPITOPE ACCESSIBILITY ASSAY REVEALS STRAIN DIFFERENCES AND NATIVE PrP ^{Sc} STRUCTURAL INFORMATION	125
A. INTRODUCTION	125
B. MATERIALS AND METHODOLOGY	129
C. RESULTS	141
D. DISCUSSION.....	190
BIBLIOGRAPHY	192
CHAPTER 4 - MONITORING PRION STRAIN EVOLUTION	200
A. INTRODUCTION	200
B. MATERIALS AND METHODOLOGY	207

C. RESULTS	211
D. DISCUSSION	248
BIBLIOGRAPHY	254
CHAPTER 5 - DISCUSSION	260
A. OVERALL SUMMARY	260
B. HYPOTHESES WITH CONJOINING CONCLUSIONS.....	265
C. FUTURE DIRECTIONS.....	273
BIBLIOGRAPHY	277
LIST OF ABBREVIATIONS.....	278
CURRICULUM VITAE	280

LIST OF TABLES

TABLE 1.1 – Prion Diseases	16
TABLE 1.2 – Iatrogenic Human Prion Disease Causes.....	18
TABLE 2.1 - Murine-adapted prion strains properties.	99
TABLE 3.1 - Prion strain properties and infection paradigm.	140

LIST OF FIGURES

FIGURE 1.1 - Schematic representation of the human prion cellular protein (PrP ^C), polymorphisms	17
FIGURE 1.2 - Schematic representation of prion cellular protein (PrP ^C),.....	25
FIGURE 1.3 - Traditional techniques utilize proteinase K (PK) treatment to differentiate between PrP ^C and PrP ^{Sc}	26
FIGURE 1.4 - Schematic representation of prion replication (Conversion PrP ^C → PrP ^{Sc}) Models	27
FIGURE 2.1 - Schematic representation of the mouse cellular prion protein (PrP ^C) and Epitopes of Anti-Prion Antibodies	82
FIGURE 2.2 - Schematic representation of the Cell-Based Conformational Stability Assay with representative example of data garnered.	83
FIGURE 2.3 - C-CSA method can differentiate CWD strains in both chronically infected and freshly infected cell lines.	98
FIGURE 2.4 - C-CSA method can detect murine-adapted prion strains, RML and 22L	100
FIGURE 2.5 - Overall reaction to denaturation, protease resistance, and amyloid deposition is more heterogeneous in Deer passaged CWD compared to Elk passaged CWD	101
FIGURE 2.6 - C-CSA method can differentiate CWD strains at multiple epitopes	103
FIGURE 2.7 - Subtle structural micro-regions responses to denaturation and protease cleavage define murine-adapted prion strains	105
FIGURE 2.8 - C-CSA method can differentiate between subtle differences in murine-adapted prion strains	107
FIGURE 3.1 - Schematic representation of the mouse cellular prion protein (PrP ^C) and Epitopes of Anti-Prion Antibodies	137
FIGURE 3.2 - Schematic representation of the Epitope Stability Assay with representative example of data garnered	138
FIGURE 3.3 - Infection specific, 7-5 ELISA-CSA, is able to differentiate between prion strains via differences in epitope binding without requiring PK ablation of PrP ^C	169
FIGURE 3.4 - Ablating PrP ^C signal with Proteinase K and denaturation with a chaotropic agent alters epitope accessibility of PrP ^{Sc} but not PrP ^C at most epitopes.....	171
FIGURE 3.5 - PrP ^{Sc} epitope accessibility can be used to differentiate between Elk-CWD and Deer-CWD	173
FIGURE 3.6 - PrP ^{Sc} epitope accessibility can be used to differentiate between classically defined murine-adapted scrapie strains (RML and 22L)	175
FIGURE 3.7 - PK-treated, non-denatured PrP ^{Sc} epitopes are accessible and create strain and host-PrP ^C specific patterns	177
FIGURE 3.8 - A single amino acid difference in the inoculum and/or the substrate make drastic differences on the tertiary shape of PrP ^{Sc}	179
FIGURE 3.9 - A single amino acid difference in the inoculum and/or the substrate can cause differences in the tertiary shape of PrP ^{Sc} in newly adapted strains	181

FIGURE 3.10 - Species-adapted strains have different tertiary structures than those passed within their native host PrP ^C	183
FIGURE 3.11 - The tertiary structure of PrP ^{Sc} is different at multiple epitopes along the molecule even in prion strains sharing the same PrP ^C substrate	185
FIGURE 3.12 - Prion resistance to protease degradation after partial denaturation (C-CSA) is <u>not</u> equivalent to epitope accessibility (ESA)	187
FIGURE 3.13 - PrP ^{Sc} epitope folded (non-denatured) and GdnHCl _{1/2} values create an individual fingerprint for each strain.	189
FIGURE 4.1 - Pilot study, ESA can be used to examine changes due to quinacrine but published methodology is insufficient to gauge daily changes	234
FIGURE 4.2 - ESA can uncover subtle conformational changes to PrP ^{Sc} over the first 5 days that the prion is exposed to quinacrine at the 6H4 epitope	236
FIGURE 4.3 - ESA can uncover subtle conformational changes to PrP ^{Sc} over the first 5 days that the prion is exposed to quinacrine at multiple epitopes	238
FIGURE 4.4 - Traditional techniques do not adequately distinguish fresh and chronically infected cells	239
FIGURE 4.5 - Chronic prion infection alters PK-treated, non-denatured PrP ^{Sc} epitopes accessibility	240
FIGURE 4.6 - Chronically infected cell lines do not have the same PrP ^{Sc} structure as Freshly infected cells	242
FIGURE 4.7 - PrP ^{Sc} structure from chronically infected cell lysate does not recapitulate the brain source material <u>or</u> the cells they were derived from in chronically infected; the PrP ^{Sc} structure in chronically infected cells is not stable, and undergoes changes when it is passaged	244
FIGURE 4.8 - Passaging chronically infected cell material through Tg(Deer) mice alters PK-treated, non-denatured PrP ^{Sc} epitopes accessibility. Additionally, PrP ^{Sc} structure from chronically infected cell material passaged through Tg(Deer) mice does not recapitulate the brain source material <u>or</u> the chronically infected cells they were derived from; the PrP ^{Sc} structure in chronically infected cells is not stable, and undergoes changes when it is passaged	246

CHAPTER 1 - BACKGROUND

A. BRIEF HISTORICAL OVERVIEW

Since the dawn of humankind, humans have been inspired to battle diseases by searching for cures and preventative treatments^{1, 2, 3}. It was no surprise that a lethal neurological disease affecting domesticated livestock would garner human attention. The first recognized prion disease was in sheep in the mid 1700s^{4, 5, 6} when animals exhibited pruritus, defined as an itchiness that led them to scrape off their wool, tremors and recumbency that progressed to death. Over the next 250 years, other similar diseases were recognized in a range of animals and humans (Table 1.1). Due to a lack of molecular understanding, these diseases were not originally considered to have the same etiology. As scientific understanding and molecular techniques advanced, transmissible spongiform encephalopathies (TSE's), also called prion diseases, were linked together⁷ due to a shared disease phenotype and shared molecular characteristics⁸. TSE's are invariably lethal, neurodegenerative diseases that disrupt and destroy nervous tissue⁹. There are no current effective treatments or cures for prion disease³.

A slow virus etiology for these transmissible encephalopathies was erroneously proposed in the 1950s¹⁰. Groundbreaking research published in the 1960s done by Alper^{11, 12} and Pattison^{13, 14} provided evidence that prion diseases could not stem from nucleic acid-based infections. Specifically, unlike known infectious agents, such as bacteria, fungi, and viruses, the infectious prion particle was UV resistant¹², radiation

resistant⁸, formalin resistant¹³, and it did not conform to the expected viral size¹¹. With evidence piling up, a novel idea emerged: an infectious source that was not based on nucleic acids. Griffith¹⁵ proposed the most logical alternative: an infectious proteinaceous particle.

The two proposed etiologies, the slow virus hypothesis and the protein-based hypothesis, were scrutinized from the 1960s – 1980s^{16, 7, 17}. As evidence supported the protein hypothesis mounted, the prion hypothesis emerged: conformational corruption of cellular prion protein (PrP^C) by the pathogenic form (PrP^{Sc})^{18, 19, 20}. Prions replicate in the absence of nucleic acids; they undergo pathological endogenous protein misfolding. The prion hypothesis preceded the discovery of the prion gene (*PRNP*) by 3 years²¹. The inability to transmit prions into mice lacking the prion protein^{22, 23, 24} and the creation of *de novo* prions from misfolded cellular prion protein²⁵ have been further evidence to validate the prion hypothesis.

B. PRION DISEASES AND STRAINS

Prion Diseases Overview

Prototypical transmissible spongiform encephalopathies (TSE's) present with neuropathological features, specifically: spongiform degeneration, which is defined as neuronal vacuolation and loss, reactive astrocyte gliosis, and amyloid deposition. Additionally, there is a prolonged disease incubation periods and a rapidly progressive clinical phase. There is a hallmark absence of immune response to infection. Often there are similar presentations of clinical signs in mice models, such as: truncal ataxia, loss of

weight, plastic tail, and head bobbing. The route of infection has bearing on how this neurotropic disease reaches the brain²⁶.

The infectious source (PrP^{Sc}) may be introduced naturally via consumption or animal-animal contact. PrP^{Sc} can also be introduced artificially via medical procedures²⁷, and research methodology²⁸. Consumption of contaminated dirt²⁹, plants³⁰, or infected tissues^{31, 32} can result prion infection. Human risk due to exposure to animal prion diseased tissues is a prevailing concern. A variant of a human prion Creutzfeldt-Jakob disease appeared after exposure to prion infected cows, specifically bovine spongiform encephalopathy, (BSE) infected tissues³¹. This implies that there is a potential for humans to be susceptible to other animal prion diseases, like chronic wasting disease (CWD)^{33, 34}, via consumption of prion-infected materials.

As correctly hypothesized in 1913⁵, prion diseases originate from genetic predisposition or infection. Genetic variations, such as mutations and polymorphisms, in the prion protein gene can alter the amino acid composition of the mature protein. Although prion diseases stem from protein-templated misfolding, single amino acid changes to the prion protein can have intense impact on transmission and susceptibility³⁵. Genetic mutations can predispose the prion protein to misfold and spontaneously cause disease. Genetic polymorphism can affect susceptibility to infection. For example, a single human PrP^C polymorphism (M/V 129)³⁶ has been shown to confer susceptibility or resistance for BSE prions containing bovine PrP^C to convert human PrP^C into PrP^{Sc}.

As scientific understanding of the prion hypothesis grows the prion realm expands. Yeast was found to have prions that convey epigenetic information³⁷. As the 21st century dawned, other protein misfolding neurodegenerative diseases and amyloidoses were examined for prion-like properties³⁸. It was found that prion pathogenesis no longer limited to prototypical transmissible spongiform encephalopathies. Other neurodegenerative disorders, like Alzheimer's, Parkinson's, and Huntington's are now beginning to be recognized as prion diseases³⁸. This makes understanding prion biology even more essential to human health and fits our driving human need to heal illness^{1, 2, 3}.

Prion Species Barrier

The species barrier describes the ease or difficulty with which a disease from one species can cause disease in a different species. In the case of prions, the species barrier relates to the ability for PrP^{Sc} containing the amino acid sequence of one species to convert the PrP^C of a different species into the misfolded conformer³⁹. Zoonotic events occur when an animal disease can jump the species barrier and infect humans. This barrier has served, thus far, as an obstacle to zoonotic events with most known animal prions⁴⁰. The only verified example of humans contracting an animal prion disease is after exposure to bovine spongiform encephalopathy (BSE) prion infected cattle, a new form of variant Creutzfeldt-Jakob (vCJD) disease appeared³¹. Since the titre required for a zoonotic event to occur is not clear⁴¹, consumption of prion-infected tissues should be prevented for human health and safety.

The species barrier can often be overcome through the use of bioassay, the experimental serial passaging of infected materials in a living model. For example, transmitting chronic wasting disease infected deer brain tissue into an inbred mouse, then taking the brain from the first passage mouse, and re-transmitting it into the same inbred mouse strain to abrogate the species barrier⁴². Upon serial passage, many species barriers can be removed. Additionally, *in vitro* techniques can be used to overcome the species barrier⁴³. Prions that have crossed a species barrier and now preferentially infect the new host are considered adapted⁴⁴, e.g. mouse-adapted scrapie (RML)²⁸. Adaption is often accompanied by a shortening of the first passage incubation time, changes in the biochemical properties of PrP^{Sc}, and changes in the neuropathology.

Prion research has resoundingly shown that the primary structure of the prion protein has direct consequences on transmission⁴⁵, especially across the species barrier^{46, 47}. The beta 2 - alpha 2 loop region is one site that has been implicated as an important zoonotic barrier both *in vivo*⁴⁸ and *in vitro*⁴⁹. The reliance on the primary structure to dictate seeding potential is shared with other amyloidogenic proteins⁵⁰, for example Hyp-FN protein⁵¹, α -synuclein⁵², and β -Amyloid⁵³.

A new dimension to the species barrier was just uncovered: non-adaptive prion amplification⁵⁴. Within this new paradigm, prions may cross the species barrier, but then fail to adapt upon second and third passages while remaining infectious to their original host species. This might lessen the fear of a zoonotic epidemic because if a prion can weakly cross the species barrier but not adapt, then risk of infection due to exposure to contaminated medical supplies/materials is low.

Prion Strains Overview

A further confounding issue to understanding the species barrier, and prions in general is the existence of prion strains⁵⁵. Transmission of hamster-adapted transmissible mink encephalopathy (TME) was invaluable for the discovery⁵⁶ and characterization⁵⁷ of the first identified prion strains. In the early 1990s, the studies to differentiate between these first prion strains, Hyper (Hy) and Drowsy (Dy), helped set the molecular standard for what prion strains were, how to elucidate them, and reinforced that strains existed. Moreover, Hy and Dy strains contained the same amino acid sequence and yet produce distinctly different diseases.

As such, prion strains defy the conventional genetic-based definition that is applied to strains of viruses, bacteria, and fungi. Instead, prion strains properties rely on specific prion protein tertiary conformations⁵⁸. A prion strain is an infectious prion protein particle with a specific tertiary conformation⁵⁹ that produces a specific neurodegenerative phenotype⁶⁰. Specifically, a prion strain can be considered to have a strain-specific⁶¹ disease phenotype⁶² based on the prion's ability to be stably propagated, fidelity to neuropathology, disease length, glycosylation profile, molecular weight of PK-resistant PrP^{Sc}, resistance to denaturation, amyloid seeding potential and other molecular characteristics.

The conformational selection model⁶³ tries to reconcile why copious possible prion protein conformational structures exists and a specific strain can be both faithfully propagated via bioassay within the same species or produce a completely different adaptive disease in a new species. The selection model proposes that there are quasi-

species of prions; essentially, that means there are different tertiary conformers of the same primary amino acid sequence, and the interaction between PrP^{Sc} and PrP^C structures selects a specific PrP^{Sc} conformation to be propagated. Strain diversity undergoes strain-dependent or species-dependent selection that resolves a preferred PrP^{Sc} conformation²³³.

The need to sort through the chaos to find meaningful structural data that is useful is crucial. By exploring the intricacies of prion protein-misfolding, prion strains can be better understood and therapeutic approaches might emerge that will be useful in treating both prion diseases and other neurodegenerative protein-misfolding disorders.

Human Prion Diseases & Strains

There is currently no known treatment or cure to any human prion diseases³. Three main pathways currently exist for the etiology of human prion diseases: hereditary, sporadic and acquired. Each pathway contains a divergent source of the disease, but ultimately they all involve the misfolded self-propagating prion protein that leads to neurodegeneration and death. Distinct human prion strains are naturally created primarily due protein structural differences dictated by *PRPN* polymorphisms⁶⁴ (Figure 1.1). The strains present with different symptoms, molecular characteristic, and ultimately are different diseases that are caused by the same gene^{65, 66}.

Dr. Jakob^{67, 68} and Dr. Creutzfeld⁶⁹ first described Creutzfeldt-Jakob Disease (CJD), a human prion disease, in the early 1920s. In the 1960s, CJD was first transmitted into chimpanzees⁷⁰. At this point, historically, CJD was erroneously thought to be

caused by a slow virus. In the 1980s, the prion diseases were unified under the prion hypothesis¹⁸: protein-misfolding self-replication. There are four known version of CJD: sporadic (sCJD), familial (fCJD), iatrogenic (iCJD), and variant (vCJD).

Sporadic CJD presents in older individuals aged 50-75 years old⁷¹ and makes up roughly 85% of CJD⁷². sCJD presents with rapid clinical signs: cerebellar ataxia⁷³, rapidly progressing dementia⁷⁴, myoclonus⁷⁵, akinetic mutism⁷⁵, and death occurs within ~2 years of diagnosis⁷¹. Strains of sCJD differentiate on symptoms and molecular properties based on the M/V129 polymorphism present in the human *PRNP* gene⁷⁶. Familial CJD is due to mutations in the *PRNP* gene⁷⁷, the most common mutation being D178N and E200K (Figure 1.1). Iatrogenic CJD is due to contaminated medical supplies (Table 1.2). The risks associated with medical procedures have created a necessity to find better methodology to decontaminate surgical equipment⁷⁸. Variant CJD appeared following the bovine spongiform encephalopathy ('mad cow') epidemic^{79, 80} in the UK. Those affected by vCJD were significantly younger individuals than those presenting with classical CJD^{81, 82}. vCJD is the result of zoonotic jump of BSE prions from cattle into humans^{31, 83}. The zoonotic ability of BSE created a concern that other animal prion diseases, like scrapie⁸⁴ and chronic wasting disease^{33, 34} might also bridge the zoonotic gap.

Fatal familial insomnia (FFI) was first described in the 1980s⁸⁵. FFI is due to mutations in the *PRNP* gene⁷⁷, the most common mutation being D178N⁸⁶ (Figure 1.1). As the name 'fatal familial insomnia' implies, this disease presents with insomnia and ends in death; other symptoms include: dysautonomia, hyperthermia, hypertension,

tachycardia, hallucinations, stupor, and coma⁸⁶. There is a sporadic version of FFI: fatal sporadic insomnia (FSI). FSI was described about 20 years⁸⁷ after FFI, with a relatively similar phenotype. However, FSI is not attributed to a hereditary genetic mutation, but rather a somatic mutation⁸⁷. Dr.'s Gerstmann, Straussler, and Scheinker⁸⁸ first described Gerstmann-Straussler-Scheinker syndrome (GSS) in the 1930s. GSS presents at around 45 years of age with ataxia, dementia, myoclonus and ends in death⁸⁹. GSS is due to mutations in the *PRNP* gene, the most common mutation being P102L^{90, 91}(Figure 1.1). The disease phenotype can be recapitulated in mice transgenic for the prion protein but missing the GPI-anchor⁹².

Kuru appeared in the Fore tribes of Papua New Guinea as a direct result of ritualistic funeral cannibalism⁹³. Gajdusek first described Kuru in the 1950s³² as a brutal human epidemic. The disease progressed extremely rapidly, with women and children presenting more prevalently due to their high consumption of infected brain and visceral tissues. Kuru in the Fore language means 'to shake or tremble'⁹⁴. The most prominent symptom of Kuru is tremors, unlike the dementia and cognitive decline that accompanies other human prion disease. Hadlow correctly proposed in 1959, that an animal prion disease (scrapie) and human prion disease (Kuru) stem from the same source⁹⁵. The connection between human and animal prion diseases helped to expedite scientific understanding of prion diseases.

Animal Prion Diseases & Strains: Scrapie

The first recognized prion disease was in sheep in the mid 1700s⁴. These animals exhibited pruritus, tremors and recumbency that progressed to death^{4, 5, 6}. The pruritus,

itchiness, directly lead to the permanent name “scrapie” for the disease, as the sheep would scrape off their wool. It would take over 200 years before the protein hypothesis¹⁸ would expose the novel protein misfolding process that is prion infection.

Fear of economic reprisals made farmers conceal sick animals and the actual prevalence of the disease was difficult to ascertain⁵. They correctly feared the impact that herds would have to be culled, and farms with diseased animals would have a harder time selling their livestock. Although the idea that the infectious agent was a misfolded protein was unimaginable at the time, in 1913⁵ it was hypothesized that scrapie originates from genetic predisposition and from infection.

Scientists attempted infecting live sheep to maintain the disease for study, believing they were searching for a bacterial or virus etiology. However, they had difficulties intentionally infecting sheep. Scrapie was accidentally passaged as part of the louping-ill vaccine that was administered by the Animal Disease Research Association in the early 1930s⁹⁶. The first successful experimental scrapie infection in sheep occurred in 1936⁹⁷. Once scrapie could be successfully passaged, the etiological search intensified. Infectious tissue homogenates were purified, and showed no bacterial growth even though they infected sheep⁹⁸. Erroneously, a slow virus etiology was proposed¹⁰. Scrapie was successfully passaged into goats in 1959⁹⁹. It is now considered a disease of ovids, a taxonomical group including sheep and goats.

As Hadlow correctly proposed in 1959, scrapie and Kuru stem from the same disease factor⁹⁵. Groundbreaking research published in the 1960s done on scrapie and Kuru by Alper^{11, 12} and Pattison^{13, 14} provided evidence that prion diseases could not

stem from nucleic acid-based infections. Specifically, unlike known infectious agents (bacteria, fungi, viruses, etc.) the infectious particle (scrapie/Kuru) was UV resistant¹², radiation resistant⁸, formalin resistant¹³, and it did not conform to the expected viral size¹¹. From this data, the prion hypothesis¹⁸ was born: the infectious particle was a misfolded self-templating protein. This led to the search for the gene responsible for the infectious protein; reverse engineering the prion protein to get cDNA and compare infected to uninfected gene products confirmed the scrapie infectious particle to be the same protein²⁰.

Although scrapie transmission studies continued from the late 1800s-1960s in sheep¹⁰⁰ and goats¹⁰¹, incubation times were lengthy making these experiments costly to perform. In the 1960s, more research amenable models were explored with mice²⁸, rats¹⁰² and hamsters¹⁰². Due to molecular techniques, mice became the most convenient model system^{103, 104}. With the genetic tools available for mice, the genetic susceptibility for scrapie was ascertained^{105, 106, 35, 107}. This genetic knowledge^{108, 109}, led to selective breeding to eliminate susceptible sheep¹¹⁰.

Multiple strains of scrapie were murine-adapted: RML²⁸, 22L¹¹¹, 139A¹¹², etc. In fact, scrapie strains were identified in mice before the protein hypothesis or the gene was identified¹¹³. To expand the understanding of prion strains, scrapie has also been transmitted into cervids, like white tail deer¹¹⁴ and elk¹¹⁵, and into mice transgenic for cervid prion protein Tg(Elk)¹¹⁶. This was done in part with the hope of discovering if scrapie was the origin of chronic wasting disease, and to better understand strains and the species barrier.

Recently, a new strain of scrapie (atypical / Nor98) was identified¹¹⁷. Atypical scrapie presents with an absence of pruritus, lacking the very feature that named scrapie, with the predominant trait being ataxia. Molecularly, the neuropathology and migration pattern of PK-resistant PrP^{Sc} is different for atypical scrapie vs. classical scrapie. The molecular data further supported the physiological data indicating that atypical scrapie was indeed a new strain of scrapie.

Animal Prion Diseases & Strains: Transmissible Mink Encephalopathy (TME)

Transmissible mink encephalopathy is a prion disease of farmed mink. It has occurred as discrete epidemics¹¹⁸ on mink fur farms. TME was scientifically described in the 1960s¹¹⁹, although it was first observed on a farm in the 1940s¹²⁰. Mink infected with TME present with a loss of cleanliness, difficulty eating/swallowing, excitability, ataxia, seizures, self-mutilation and death¹¹⁹.

The origin of TME has been associated with mink consuming bovine spongiform encephalopathy (BSE) contaminated feed¹²¹. TME was passaged into non-mink organisms to examine its host range: mice^{122, 123}, Squirrel Monkeys¹²⁴, hamsters¹²³, cat¹²³, ferret¹²³, goat¹²³, cattle¹²³, chicken¹²³, rhesus monkey¹²³, and others. TME gave most species a cryptic/lymphatic infection, and only the ferrets and goat presented clinical signs.

Serial transmission of TME into hamsters to create a hamster-adapted TME¹²⁵ was invaluable for the discovery⁵⁶ and characterization⁵⁷ of two prion strains: Hyper (Hy) and Drowsy (Dy). In the early 1990s, these strains helped set the molecular standard for what prion strains were, how to elucidate them, and reinforced that strains

existed.

Animal Prion Diseases & Strains: Bovine Spongiform Encephalopathy (BSE)

Bovine spongiform encephalopathy is a fatal neurological prion disease affecting cattle and exotic ungulates, e.g. antelope, bison, and zoo-housed ungulates. The disease was first described in 1986 in Great Britain¹²⁶. The cattle presented with inconsistency in posture and movement, altered mental status, weight loss, and reduced milk yield¹²⁷. Most BSE cases occurred in dairy cows between 3-6 years of age and had an incubation time of 2-8 years¹²⁸. BSE originated from the process of meat and bone meal, which is an agricultural practice of reusing dead animals in feed¹²⁷. The disease decimated the cattle industry because impacted herds were culled¹²⁹ to prevent the spread of the disease.

Variant CJD (vCJD) appeared in humans following the BSE ('mad cow') epidemic^{79, 90} in the UK. Those affected by vCJD were significantly younger individuals presenting classical CJD. vCJD is the result of zoonotic jump of prions from cattle (BSE) into humans^{31, 83}. Due to vCJD, there was a dramatic increase in the surveillance of cattle^{130, 131}. Increased surveillance¹³² led to the discovery of novel atypical BSE strains^{133, 134, 135, 136}. There are three known types of BSE: classical BSE, atypical H-type BSE, and atypical L-type BSE. The atypical forms are named for their appearance on a western immunoblot. Specifically, the atypical BSE banding pattern is either Higher or Lower than classical BSE banding patterns. Atypical BSE type is identified by molecular characteristics¹³⁷, as both atypical forms present similarly to classical BSE with subtle differences with locomotor changes and increased anxiety/dullness¹³⁸. BSE

has been murine-adapted^{139, 140}, and passaged through other species, e.g. transgenic cervid-PrP^C mice¹⁴¹.

Animal Prion Diseases & Strains: Chronic Wasting Disease (CWD)

Chronic wasting disease is a prion disease endemic to cervids. Cervids are a taxonomic family of ruminant mammals composed of deer, elk, moose, reindeer, caribou, and other similar animals. CWD was first described in the 1980s when mule deer presented with behavior alterations, weight loss, ataxia, patchy coats, and lowered head¹⁴². Unlike other prion diseases, CWD is the only known prion disease affecting wild herds of animals. Unfortunately, it has shown unparalleled transmission efficiency in the wild¹⁴³. Moreover although prion animal diseases, scrapie¹⁴⁴ and BSE¹⁴⁵, tend to occur as discrete outbreaks, CWD shows a persistent burgeoning outbreak¹⁴⁶. CWD has been detected across over half the states in the United States¹⁴⁷, two Canadian Provinces¹⁴³, South Korea¹⁴⁸, Norway¹⁴⁹, Finland¹⁵⁰ and Sweden¹⁵¹.

PrP^{Sc} is detectable in muscle³³ and antler velvet³⁴ which means that CWD infectious material has been seen in tissues humans consume. This emphasizes the zoonotic potential of CWD. Additionally, it was recently uncovered that PrP^{Sc} can be bound to soil¹⁵², contaminate local water sources¹⁵³, and even absorbed by plants³⁰; implying not even vegetarians are truly “safe” from potential exposure. It is crucial for the overall survival of cervids and protection of humans that we understand CWD and the structure of the cervid prion protein better. Human risk, due to exposure to animal CWD-diseased tissue, is a prevailing concern¹⁴⁶ since a variant of a human prion disease appeared after human exposure to prion infected bovine tissues¹⁵⁴. This exposure risk

creates an overall potential for humans to be susceptible to other animal prion diseases. It is crucial for the overall survival of cervids and protection of humans that we understand CWD and the structure of the cervid prion protein better. A species barrier exists in cervids due to differences in the amino acid sequence, specifically, at residue 226 in deer (Q) and elk (E) primary structures^{155, 156}. This single difference has been the source of a clear but weak species barrier¹⁵⁷. Two specific CWD types¹⁵⁶ have been identified. The same CWD isolate has been shown to present differently dependent on the host PrP^C (deer or elk

Unlike the early murine adaption of scrapie²⁸, CWD has only recently been adapted into inbred mice; unfortunately the strain term for mouse-adapted chronic wasting disease “mCWD” encompasses 4 very distinct murine adaption events: deer CWD (isolate D10) into FVB inbred mice into C57BL/6 inbred mice¹⁵⁸, mule deer CWD isolate into Tg20¹⁵⁹, Elk CWD (brain pool E190Y+2229Y) into VM/Dk inbred mice¹⁶⁰, and white-tail deer CWD (Wisconsin isolate) into wild mice¹⁶¹. Due to this further complication along with such a recent adaption, mCWD is not well characterized. This dissertation further characterizes the mD10 adaption¹⁵⁸ of CWD.

Table 1.1: Prion Diseases A list of prion diseases, primary affected species, year discovered, and the known source of the disease.

Disease	Natural Host	Year first described	Ultimate pathogenic source
Familial Creutzfeldt - Jakob disease	Human	1924	Genetic Mutation in <i>PRNP</i> gene
Iatrogenic Creutzfeldt - Jakob disease	Human	1974	Infection with contaminated medical supplies/equipment
Sporadic Creutzfeldt - Jakob disease	Human	1920	Spontaneous Conversion of PrP ^C to PrP ^{Sc}
Kuru	Human	1957	Infection through Ritualistic Cannibalism
Fatal Familial Insomnia	Human	1986	Genetic Mutation in <i>PRNP</i> gene
Fatal Sporadic Insomnia	Human	1999	Spontaneous Conversion of PrP ^C to PrP ^{Sc}
Gerstmann-Straussler-Scheinker syndrome	Human	1936	Genetic Mutation in <i>PRNP</i> gene
(Classic) Scrapie	Ovid (Sheep & Goats)	1700's	Infection or Sporadic
Atypical Scrapie	Ovid (Sheep & Goats)	2003	Infection or Sporadic
(Classic) Bovine Spongiform Encephalopathy	Cattle, Exotic Ungulates	1986	Infection or Sporadic
Atypical H-Type Bovine Spongiform Encephalopathy	Cattle	2004	Infection or Sporadic
Atypical L-Type Bovine Spongiform Encephalopathy	Cattle	2004	Infection or Sporadic
Feline Spongiform Encephalopathy	Cats (Domestic & Zoo)	1990	Infection or Sporadic
Transmissible Mink Encephalopathy	Farmed Mink	1965	Infection
Chronic Wasting Disease	Cervid (deer, elk, moose, reindeer, etc.)	1967	Infection or Sporadic
Chronic Wasting Disease Type-1	Cervid (deer, elk, moose, reindeer, etc.)	2010	Infection or Sporadic
Chronic Wasting Disease Type-2	Cervid (deer, elk, moose, reindeer, etc.)	2010	Infection or Sporadic

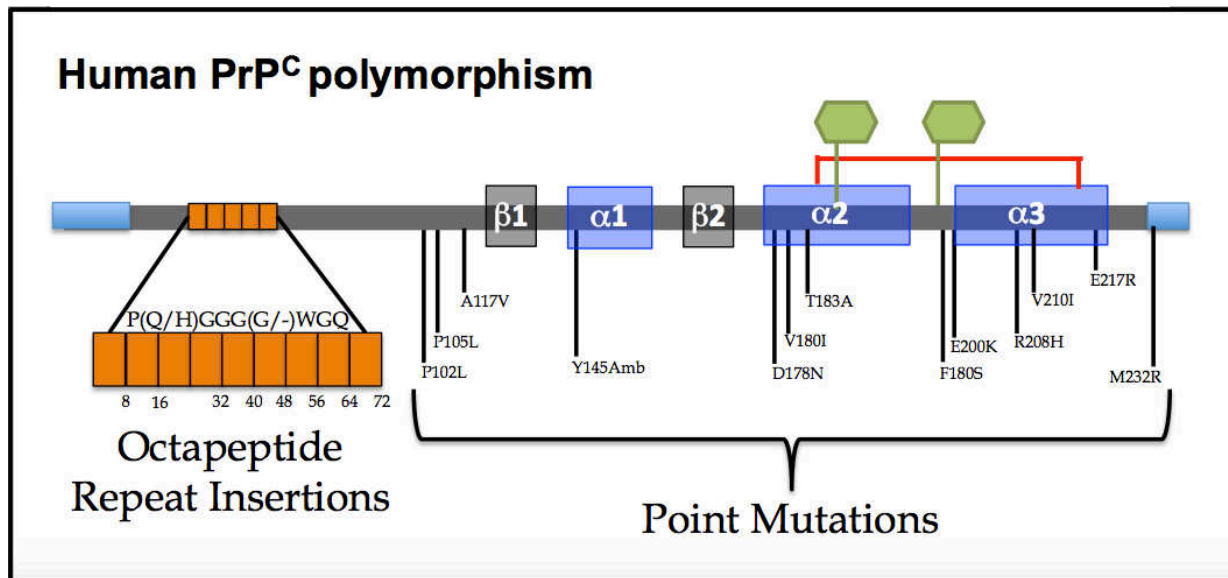


Figure 1.1: Schematic representation of the human prion cellular protein (PrP^C) polymorphism. The human prion protein (PrP^C) is shown as a grey line with distinct areas indicated. An N-terminal target sequence (left solid blue box) is cleaved during protein processing prior to insertion into the plasma membrane. The remaining N-terminus is charged, primarily unstructured, and contains the copper octapeptide repeat binding motif (orange boxes), which can contain multiple repeats. Point mutations range from before the first beta sheet motifs (grey boxes), through the alpha helices (blue boxes), and into the Glycosylphosphatidylinositol (GPI) anchor attached at the C-terminus (right solid blue box). Post-translational glycosylation at asparagine residues (green hexagons) and stabilizing disulfide bridge (red line) are indicated.

Table 1.2: Iatrogenic Human Prion Disease Causes Expanded Bonda *Neurosurgical Focus* (2016) with more recent data

Causes	# Cases
Dura mater graft	238
Surgical Instruments	4
Corneal Transplant	2
EEG depth electrode	2
Human pituitary (growth hormone)	238
Human pituitary (Gonadotropin)	4
Blood Transfusion	3
Total	491

C. PRION PROTEIN STRUCTURE AND REPLICATION

Prion Protein: Cellular Form (PrP^C)

The prion hypothesis¹⁸ prompted a search for the gene of the protein responsible for prion diseases¹⁶². The prion protein gene (*PRNP*) was named for the disease it created²¹ and it is part of a family of genes. There are three proteins encoded in the prion genetic family (*PRN*): Prion protein (*PRNP*), Doppel protein (*PRND*), and Shadoo protein (*SPRN*). The three genes share structural similarities and endoproteolytic processing¹⁶³.

The function of PrP^C is the source of endless debates in the field. The *PRNP* gene is conserved across mammals^{164, 165}. However, knocking out the prion gene (PrP-KO) in mice does not result in an embryonic lethal phenotype^{22, 23}. The PrP-KO mice do exhibit some phenotypic differences: altered stress response¹⁶⁶, abnormal circadian rhythm¹⁶⁷, increased locomotor activity¹⁶⁸, increased brain damage by alcohol¹⁶⁹ and traumatic brain injury¹⁷⁰, and abnormal teeth¹⁷¹. Each phenotype suggests a purpose for PrP^C: embryonic development¹⁷² and cell differentiation^{173, 174}, as a modulator of metabotropic glutamate receptors^{175, 176, 177}, a co-receptor for β -Amyloid receptor¹⁷⁸ or facilitator of disease in Alzheimer's¹⁷⁹, immune regulation¹⁸⁰ and there are more functions are being found each year. There are recent studies that associate PrP^C and cancer¹⁸¹, higher PrP^C expression is associated with poor prognosis in breast cancer¹⁸². Additionally, anti-prion antibodies reduce colon cancer in a mouse model¹⁸³. Surprisingly, the unstructured region of PrP^C has anti-viral (HIV-1) properties¹⁸⁴.

Once the *PRNP* gene was uncovered, the structure of both the cellular prion protein and pathogenic prion protein were necessary to fully understand prion replication and disease. The prion cellular protein (Figure 1.2) is a GPI-anchored protein¹⁸⁵ composed of an unstructured N-terminus region, copper binding octapeptide repeat¹⁸⁶, hydrophobic region¹⁸⁷ and a globular region that contains three alpha helices, two short beta sheets, a single disulfide bond, and two N-linked glycosylation sites^{188, 189, 190, 191, 192}. The region between beta sheet 2 and alpha helix 2 is well defined in some species, e.g. cervids¹⁹³. This beta sheet 2 and alpha helix 2 region has been implicated in prion stability and transmission across the species barrier¹⁹⁴.

Glycosylation of the prion protein is necessary for trafficking to the cellular membrane¹⁹⁵ where PrP^C localizes to lipid rafts^{196, 197}. The mature PrP^C contains two N-linked glycosylation sites^{198, 199} can present in four glycosylation states: aglycosylated, mono-1 glycosylation, mono-2 glycosylation, and diglycosylated²⁰⁰. PrP^C is primarily found in the nervous system²⁰¹ and lymphoreticular system²⁰². The localization of the prion protein can change over the organism's development, using alternative tissue-specific polyadenylation²⁰³.

The prion cellular protein (unlike the prion infectious form) is proteinase K (PK) sensitive²⁰⁴. This sensitivity serves as a basis for traditional molecular techniques (Figure 1.3) to separate PrP^C and PrP^{Sc} signals¹⁶².

Prion Protein: Infectious Form (PrP^{Sc})

The infectious form of the prion protein (PrP^{Sc}, prion) consists of misfolded cellular prion protein (PrP^C). Although yeast were found to have prions that convey

epigenetic information³⁷, the only verified function of PrP^{Sc} in mammals is to cause transmissible spongiform encephalopathies.

The general tertiary structural difference between PrP^C and PrP^{Sc} has been known for over 20 years²⁰⁵. Specifically, PrP^{Sc} is more β -sheet rich than the α -helix dominated PrP^C. Under the umbrella term (PrP^{Sc}) there are various forms: single misfolded PrP^{Sc} monomers, small soluble PrP^{Sc} oligomers, and insoluble PrP^{Sc} amyloid fibrils²⁰⁶. There is some debate in the field on whether the soluble oligomers or amyloid fibrils are the infectious fraction or toxic species of prion protein²⁰⁷.

Unlike PrP^C, PrP^{Sc} is a hardy, persistent molecule that is resistant to proteinase digestion^{204, 208}, UV radiation¹², gamma radiation⁸, formalin¹³, and linger in soil for years²⁹ evading environmental degradation. Unlike most proteins, PrP^{Sc} resists proteinase K (PK) degradation. Several stable cleavage products are made²⁰⁹, but relative resistance to PK degradation depends on salt concentrations²¹⁰ and can be tissue-dependent²¹¹ or strain-specific²¹². Additionally, other proteinases^{208, 213} can be used to examine the PK-sensitive, and possibly toxic, species of PrP^{Sc}.

A further confounding issue to understanding PrP^{Sc} is the existence of prion strains⁵⁵. As described earlier (Chapter 1B), prion strain properties rely on specific tertiary conformations⁵⁸ of PrP^{Sc}. A prion strain is an infectious prion protein particle with a specific tertiary conformation⁵⁹ that produces a specific neurodegenerative phenotype⁶⁰. Since the three-dimensional structure of PrP^{Sc} has yet to be identified, there is a barrier in our understanding of prion strains and the species barrier. The species barrier depends on the structure of both PrP^C and PrP^{Sc} and prion strains can

present a variety of tertiary PrP^{Sc} structures. Strain properties have direct importance in possible zoonotic events because the more versions of PrP^{Sc} that exist, the higher the mathematical possibility that a strain will be compatible to corrupt human PrP^C.

Prion Replication, Conversion PrP^C → PrP^{Sc}

A unique pathway is involved in prion diseases: conformational corruption of cellular prion protein (**PrP^C**) by the pathogenic form (**PrP^{Sc}**)¹⁸. Fundamentally, the cellular prion protein must denature enough to be perturbed and refold into the infectious prion proteins misfolded tertiary conformation. Models to describe this novel process were abound²¹⁴.

Currently, two conceptually different models are regarded as plausible (Figure 1.4): (1) template-assisted model and (2) nucleation/ polymerization model. The template-assisted model depends on PrP^{Sc} monomers being more stable than PrP^C ²¹⁵. There has been conjecture that a 'protein X' could facilitate misfolding²¹⁶. The nucleation/ polymerization model depends on PrP^C monomers being incorporated into growing PrP^{Sc} amyloid fibrils²¹⁷. This leads to a slow initial nucleation phase, which then grows exponentially (elongation), until it reaches a plateau phase^{218, 219}. Two *in vitro* prion replication assays (PMCA²²⁰ and RT-QuIC²²¹) support the nucleation/ polymerization model.

The interaction between the PrP^C substrate and infectious PrP^{Sc} seed is at the crux of prion replication. This interaction can be impacted by genetic variations²²², glycosylation²²³, route of infection^{224, 225}, immune involvement²²⁶, gene dosage²²⁷,

infectious titre²²⁴, a species barrier²²⁸ and other yet undiscovered properties. Ultimately, the exact process of conversion from PrP^C to PrP^{Sc} is still a resounding mystery.

This protein-misfolding pathway is shared with other amyloidogenic proteins²²⁹. Due to this shared pattern, neurodegenerative protein misfolding disorders, like Alzheimer's, Huntington's, and Parkinson's, are now considered members of the prion field. This allows the prion protein to serve as a model for these human diseases and increases the need for stringent well-designed prion protein experiments.

Prion Protein Structural Models

Like the artistic complexity that can turn a piece of paper into an origami masterpiece, the primary structure of the prion cellular protein can bend and fold into multiple forms. The folding differences of these forms of the prion protein are fundamental to the ability to cause and propagate disease. The secondary structure of PrP^C was determined to be alpha-helical rich²⁰⁵. The tertiary structure of PrP^C was ascertained via NMR^{188, 189, 190} and crystallization^{192, 230} in the early 2000s.

The structure of PrP^{Sc} is still unresolved²³¹. The difficulty uncovering the structure stems from several obstacles. First, as mentioned above, PrP^{Sc} is an umbrella term that includes monomers, soluble oligomers, amyloid fibrils, and aggregates can range in size^{232, 233}. This complicates determining a single unified structure for PrP^{Sc}, especially since the insoluble nature of fibrils/aggregates defies crystallization and solution-based NMR. There are further perplexities involving prion strains. Without a genetic basis, strains depend on structural differences in the misfolded conformations of PrP^{Sc}. As such, the number of possible PrP^{Sc} structures grows with each new strain

discovered. Although the tertiary structure of PrP^{Sc} has yet to be identified, there are several models based on of PrP^{Sc} and prion amyloid fibrils. Structural information has been garnered from mutational analysis within the prion protein. However, short segments of PrP^{Sc} have been examined with crystallography.

Mutational analysis involves examining natural polymorphisms⁴⁵, changing a single amino acid²³⁴ or several^{235, 236}, or even deleting sections of the protein²³⁷ and using the changes to determine changes in prion folding, infectious nature, or conformational stability²³⁸. The glycosylation state has also been used to differentiate and form ideas about PrP^{Sc} structure^{239, 240}. Even the interactions between the extra-cellular matrix have informed indirectly on PrP^{Sc} structure²⁴¹. Using shortened version of the prion protein with more traditional structural delineating techniques has also been done, along with other techniques. One of the newest techniques being put forth is using quantum dots²⁴² to track subtle changes in real time.

With all this complexity, there are several models^{243, 244, 245, 246} being championed in the prion field: steric zippering, beta sheet model, beta helix model, and beta spiral model. Each is an attempt to better understand how PrP^{Sc} exists in multiple forms. Detailed information about the infectious form of the prion protein has been insufficient to serve as a template for treatment options. Ultimately, understanding the tertiary structure of PrP^{Sc} and structural differences encoding strains is important²⁴⁷. The research contained in this dissertation aims to further our knowledge of the structure of PrP^{Sc}.

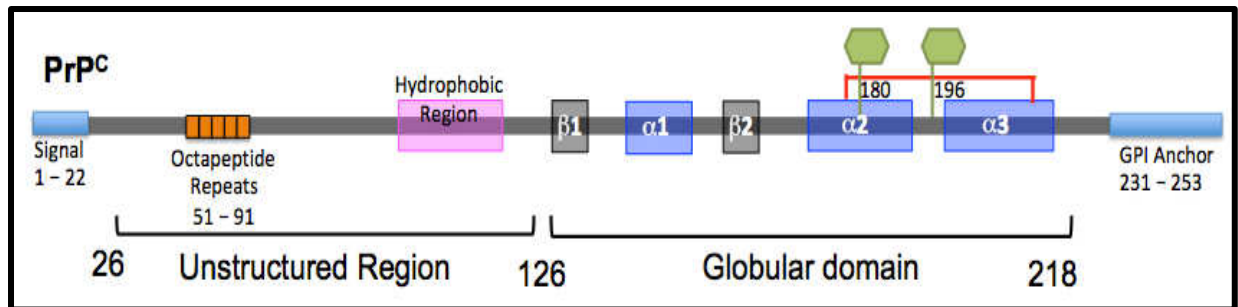


Figure 1.2: Schematic representation of the cellular prion protein (PrP^C). The mouse prion protein (PrP^C) is shown as a grey line with distinct areas indicated; the numbers shown represent amino acid locations along the molecule. An N-terminal target sequence (solid blue box) is cleaved during protein processing prior to insertion into the plasma membrane. The remaining N-terminus is charged, primarily unstructured, and contains the copper octapeptide repeat binding motif (orange boxes), and a hydrophobic region (pink box). The C-terminal domain is structured with three alpha helices (blue boxes), two beta sheet motifs (grey boxes) and post-translational glycosylation at asparagine residues (green hexagons). A stabilizing disulfide bridge forms between alpha helix 2 and alpha helix 3 (red line). Finally, there is a Glycosylphosphatidylinositol (GPI) anchor attached at the C-terminus (solid blue box) which anchors the protein to the cellular plasma membrane.

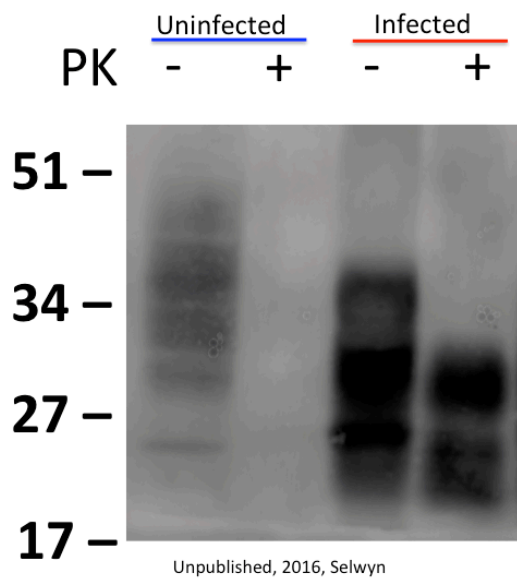


Figure 1.3: Traditional techniques utilize proteinase K (PK) treatment to differentiate between PrP^C and PrP^{Sc}. Brain homogenate from terminally ill C57BL/6 inbred mice infected with RML (infected) and age-matched uninfected C57BL/6 inbred mice were interrogated with anti-prion antibody PRC5 via western blot. PK indicates usage (+) of proteinase K to ablate PrP^C signal and allow detection of PrP^{Sc}, lack of PK (-) indicates total PrP^C and PrP^{Sc} fraction

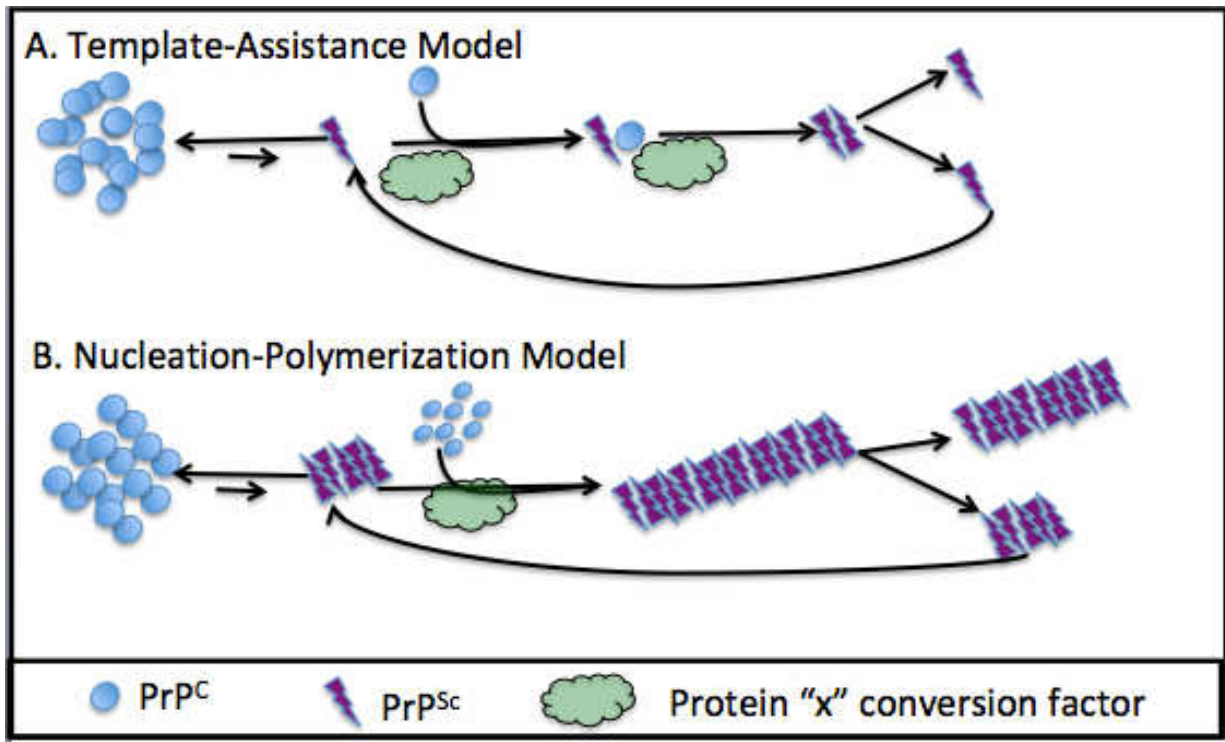


Figure 1.4: Schematic representation of prion replication (Conversion PrP^C → PrP^{Sc}) models Conformational corruption of cellular prion protein (PrP^C) by the pathogenic form (PrP^{Sc}) is proposed to occur in four forms based on two models (with or without the possibility of a protein "x" conversion factor).

(A) Template Assistance Model

(B) Nucleation-Polymerization Model

D. APPROACHES FOR STUDYING PRIONS

As mentioned throughout this chapter, prions have been studied in animal models, immunoblot (western) assays, ELISA, neuropathological evidence, newer *in vitro* analyses (PMCA, RT-QuIC), and more²⁴⁸. Prion research has delved into every facet of the prion gene^{164, 165}, folding of mRNA²⁴⁹, protein^{243, 244}, and diseases³. Bioassay was the one of the first ways scientists examined prion diseases via scrapie transmission studies in the early 1900's^{5, 6}. Bioassay is a technique where an infectious agent is passaged/transmitted into a living host. Specifically, infectious prion materials, such as brain, lymph, or muscle, are given via intracerebral inoculation, interparietal inoculation, or orally/nasally, to animals. Transmitting prions within animals preceded understanding the etiology of prion diseases. Transmission studies implied a novel concept: unlike known diseases, scrapie had a hereditary component and infectious properties⁵. Although scrapie transmission studies continued from the late 1800s-1960s in sheep and goats, incubation times were lengthy¹⁰¹ making experiments costly to perform. In the 1960s, more research amenable models were explored with mice²⁸, rats¹⁰² and hamsters¹⁰². Few rat transmission studies^{250, 251} have occurred due to the genetic molecular tools available making mice a more tractable model. Recently, non-mammalian animal models have been explored: zebrafish^{252, 253}, *drosophila*^{254, 255}, and *c. elegans*²⁵⁶. All the evidence so far indicates that understanding strains and the species barrier is momentarily important. The lack of a detailed infectious prion structure creates a barrier in our understanding of prion strains and further prevents the development of effective treatments.

In Vivo Model: Hamsters

Hamster transmission studies of scrapie²⁵⁷ led to transmission of other prion diseases, like transmissible mink encephalopathy (TME). Transmission of hamster-adapted TME was invaluable for the discovery⁵⁶ and characterization⁵⁷ of two prion strains: Hyper (Hy) and Drowsy (Dy). The 139A mouse-adapted scrapie strain discussed later in this dissertation originated from hamsters^{258, 112}. Strain differences were seen with hamster prions, when sucrose gradients were applied²⁵⁹.

In Vivo Model: Mice

For research purposes and ease of study, prions have been adapted to infect mice in a more time efficient laboratory setting, such as scrapie²⁸, TME¹²³, BSE¹³⁹, and CWD⁴². Traditionally, mice that are inbred (WT), PrP^C over expressing mice, or mice that are transgenic (Tg)/Gene-targeted (Gt) for a heterologous PrP on a mouse-PrP null background are used. Until recently bioassay, the passaging of an infectious agent in a living host, had been the sole means of assessing prion infectivity and the standard for strain characterization. However, bioassay is costly for both time and financial resources.

Although murine-adapted Rocky Mountain Laboratory (RML)²⁸ and 22L¹¹¹ scrapie strains have been around for over 50 years, the specific conformational differences between strains have not been clarified. Although conformational stability has been established by western blots for these strains, many studies have focused on a single antibody/epitope^{260, 61} or a single strain²⁶¹. The most detailed examination murine-adapted RML strain via conformational stability evaluated eight antibody

epitopes via western blotting²⁶².

As mentioned, unlike the early murine adaption of scrapie, chronic wasting disease (cervid prion disease) has only recently been adapted into mice; unfortunately the strain term “mCWD” encompasses 4 very distinct murine adaption events: deer CWD (isolate D10) into FVB inbred mice into C57BL/6 inbred mice²⁶³, mule deer CWD isolate into Tg20²⁶⁴, Elk CWD (brain pool E190Y+2229Y) into VM/Dk inbred mice²⁶⁵, and white-tail deer CWD (Wisconsin isolate) into wild mice²⁶⁶. Due to this further complication along with such a recent adaptations, mCWD is not well characterized.

Prion Cell Culture Models

The N2a²⁶⁷, PK1²⁶⁸, RK-PrP²⁶⁹, NpL2²⁷⁰, and HEK293²⁷⁰ prion cell culture models, have been advantageous to examine a range of prion questions ranging from: prion adaption²⁷¹, spontaneous prion generation^{272, 273}, genetic variables that increase susceptibility^{274, 275}, the role of PrP^C in cellular function²⁷⁰, modulators of infectivity (e.g. estrogen²⁷⁶, siRNA²⁷⁷, glycosides²⁷⁸), to test anti-prion compounds^{279, 280, 281, 282, 283, 284, 285}, examine drug-induced prion evolution²⁸⁶, and more. Prion cell-based models provide advantages over cell-free systems (Protein Misfolding Cyclic Amplification^{287, 288} and Real Time-Quaking Induced Conversion²⁸⁹) that have been recently developed because cell-free systems focus primarily on amyloidogenesis, whereas cell-based models can examine prion infection in living cells. Furthermore, new techniques, like the scrapie cell assay (SCA)²⁹⁰, were generated specifically for use in prion cell culture models. The SCA was the first highly sensitive, reliable method to examine prion titre in cell culture; however, it had limited applications²⁹¹ due to a small subset of cell types²⁹² and

laboratory-generated strains²⁹³.

Unlike the cell lines used in the SCA, the rabbit kidney epithelial²⁹⁴ (RK13) cell culture model has vastly expanded the species and prion strains that could be examined. Specifically, RK13 cells transfected^{295, 296} to stably to express a pIRESpuro3 vector containing the PrP^C gene of choice²⁹⁷ and pcDNA3-gag expressing HIV-1 GAG precursor protein to enhance the release of PrP^C ²⁹⁸. This transfection paradigm works because RK13 cells do not endogenously express PrP^C ²⁹⁹ and rabbits are relatively immune to prion disorders^{300, 301, 302, 303}. RK-PrP cell lines have been useful to examine prion titre²⁹⁵, anti-prion drug screening^{304, 305}, and strain differentiation³⁰⁶. A significant advancement in the prion field^{307, 308} was the ability to infect naïve cell culture models and perpetually propagate prion infection, also called “chronically infected” cell lines. These chronically infected lines effectively expanded the ability to address questions about prion structure and further characterize strains³⁰⁹. The chosen prion cell culture model for this dissertation was RK-PrP in both naïve and chronically infected forms.

Chaotropic Agents

Chaotropic agents disturb the hydrogen bonding of water³¹⁰ around a protein, destabilizing the three-dimensional structure of a protein. This destabilization causes proteins to undergo a denaturation-renaturation event, where they unfold and re-fold. This denaturation and renaturation can be seen in a variety of proteins, for example Lysozyme^{311, 312}. Bacteriorhodopsin³¹³, and more importantly, in bacterial grown PrP³¹⁴, yeast prions³¹⁵, mammalian prions⁶¹, and PrP^{Sc} ³¹⁶. This is because the hydrogen bonding of water is important to prion protein structural stability³¹⁷.

The chaotropic agent predominantly used in this dissertation is guanidine hydrochloride (GdnHCl). The structure of guanidine is known^{318, 319} and as a chaotropic agent, GdnHCl, is a highly effective tool to denature proteins³²⁰ via its interactions with water^{321, 322, 323}. Interestingly, GdnHCl stabilizes proteins during the transition period between the original form and renatured form³²⁴ of the protein by pairing with positively charged Arginine side chains³²⁵.

Although the use of chaotropic agents to indirectly study protein structure is not unique to the prion field^{326, 327, 328}, the prion field utilizes chaotropic agents via denaturation curves as a means to interrogate PrP^{Sc} structure and distinguish between different prion strains. Prion conformational stability assays (CSA) use chaotropic agents to assess relative resistance of prions to protease degradation after partial denaturation to examine PrP^{Sc}. Traditionally, CSA's depends on western blot²⁷¹, dot blot or enzyme linked immunosorbent assays (ELISA)³²⁹ to visualize prion response to protease degradation after partial denaturation. The cell-based conformational stability assay²⁹⁵ (C-CSA) utilizes GdnHCl in the RK-PrP cell system to examine differences between prion strains.

Epitope-Mapped Anti-Prion Protein Antibodies

Often when scientists grasp for new knowledge, the tools available limit them. Epitope-mapping an antibody is a process to identify the amino acids that the antibody Fab region binds^{330 331}. The use of denaturation, epitope-mapped antibodies, and conformational specific antibodies to probe protein structure is not unique to the prion protein, e.g. vitronectin³³², lysozyme³³³, and neurofilament³³⁴. To expand understanding

of the prion protein, a plethora of anti-prion antibodies^{335, 336, 337, 338}, glycosylation specific antibodies²⁴⁰, and anti-amyloid antibodies³³⁹ have been generated. Epitope mapping has been done with several anti-prion antibodies^{340, 341, 342, 343, 344}. Mapped antibodies have been explored for anti-prion qualities^{345, 346, 347}. In hopes of understanding more about the structure of both PrP^C and PrP^{Sc}, conformationally dependent antibodies³⁴⁸ have been used to examine prion structure. Conformationally dependent antibodies require the protein to be in a specific conformation, as the epitope regions are discontinuous.

Combining methodology using chaotropic agents with epitope-mapped antibodies has produced the prion conformational stability assays (CSA). The CSA uses chaotropic agents to assess relative resistance of prions to protease degradation after partial denaturation as a means to interrogate PrP^{Sc} structure and distinguish between different prion strains. Traditionally, CSA's depends on western blot²⁷¹, dot blot or enzyme linked immunosorbent assays (ELISA)³²⁹ to visualize prion response to protease degradation after partial denaturation. Conformational stability of mouse-adapted scrapie strains RML and 22L have been established by western blots previously; however, many of these have focused on a single antibody (epitope)^{260, 61} or a single strain²⁶¹. The knowledge garnered from interrogating a single antibody epitope is limited. Using a wide array of antibodies with varied epitopes clarifies subtle structural variation present between strains. The most detailed examination of RML via conformational stability evaluated eight antibody epitopes via western blotting²⁶². The most comprehensive use of epitope-mapped antibodies examined three murine-

adapted scrapie strains, Chandler (RML), 22L, and Me7 with twelve epitope-mapped antibodies via an ELISA system³²⁹.

E. INVESTIGATIONAL AIMS

The overarching goal is to understand structural differences within and between strains of prions (infectious proteinaceous agents) by examining prion structure after exposure to denaturing chaotropic agents. Understanding prion disease transmission, the species barrier, and finding treatment options depends on resolving the structure of PrP^{Sc}; yet, this very basic need is still unfulfilled²⁴⁷. It remains a driving question that the research presented in this dissertation aims to shed light on. **My overall hypothesis** is that detailed structural information about the prion protein can be garnered through new and innovative techniques we developed. Specifically, chaotropic agents used to probe epitope-mapped regions of the prion protein will allow us to create a map of specific regional differences between strains. The aims of this dissertation focus on two questions:

QUESTION 1: What are the subtle structural ways that infectious proteins encrypt strain information?

Hypothesis: Structural characteristics of the prion protein can be elucidated through new assays via examination of stability and epitope availability within the infectious prion protein.

Aim 1: Expand the prion Cell-Based Conformational Stability Assay to better understand prion strain structural characteristics. Rationale: Bioassay had been the sole means of assessing prion infectivity and the standard for strain characterization until

the advent of the scrapie cell assay (Klohn et al 2003). Cell culture models are significant for addressing questions about prion structure and characterizing strains (van Der Merwe et al. 2015). Recent technical advancements use cell-based approaches: the cervid prion cell assay assesses prion infectivity (Bian et al 2010); whereas, the Cell-Based Conformational Stability Assay (**C-CSA**) can be used to distinguish differences between prion strains (Bian et al 2014). The C-CSA uses chaotropic agents and epitope-mapped antibodies to examine prion stability, essentially, generating a map of the tertiary structure of PrP^{Sc}. These new techniques will be novel approaches to save time and the funding required when performing similar bioassay examinations, while examining the prion structure in a new light.

Aim 2: Create a new prion Epitope Stability Assay (ESA) to more directly examine epitope accessibility differences in prion strain structural characteristics and provide previously inaccessible structural information about the prion protein.

Rationale: The C-CSA can be used to distinguish differences between prion strains (Bian et al 2014); however, the resultant data is constrained due to the methodology. The C-CSA methodology (Aim 1) establishes the Proteinase K (**PK**) sensitivity of PrP^C and PrP^{Sc} that has been exposed to denaturing conditions at different epitopes. The C-CSA relies on methodology traditionally referred to in the prion field as a “conformational stability assay” (Safar et al 1998, Novitskaya et al 2006, Shindoh et al 2009, Bian et al 2014). A shift in methodology originates from the advantage of the 7-5 ELISA to distinguish PrP^C and PrP^{Sc} without the necessary PK step via the glycosylation state of the prion protein A modification that alters the C-CSA methodology to recapitulate

current 7-5 ELISA methodology will provide information about the epitope accessibility of PrP^{Sc} under different denaturing (GdnHCl) conditions at different epitopes.

We address the molecular basis for prion strains seen in murine-adapted prions. The basis for murine prion strains can be uncovered with detailed structural characteristics via examination of prion stability. Mouse prion variants (RML, 22L, 139A, and mD10) all share the same amino acid sequence; yet, each ultimately produce different diseases. Tertiary structural differences between each infectious particle must be the culprit since they share the same amino acid sequence. Using the experimental methodology we developed, 7-5 ELISA, C-CSA (Aim 1), and ESA (Aim 2) a new map of specific regional differences between strains between murine prion strains were uncovered; specifically,. Classically defined murine-adapted scrapie strains (RML and 22L) respond to degradation by proteinase K after denaturation with a chaotropic agent along the prion protein differently even though they contain the same amino acid sequence; specifically, this feature occurred at 4 of 5 epitope-mapped regions (unstructured and globular regions) examined. These two strains differ drastically in their transition point; this recapitulates previous lab data showing that RML contains at least 2 quasi-species, whereas 22L has been serially cloned into a single conformer. Classically defined murine-adapted scrapie strains (RML, 22L, and 139A) and newly murine-adapted CWD have different epitope accessibility along the prion protein even though they contain the same amino acid sequence. These strains differ drastically in their transition point, resistance to denaturation, and “native” PrP^{Sc} epitope accessibility.

We address the molecular basis for prion strains, prion strain adaptation and species barriers seen in cervids. Single amino acid changes to the prion protein can have intense impact on transmission and susceptibility (Belt et al 1995); e.g. the difference amino acid at position 226 [deer (Q), elk (E)] has profound effects on the presentation of chronic wasting disease (Angers et al 2010). The C-CSA, ESA and 7-5 ELISA are able to uncover detailed molecular differences by using chaotropic agents to probe epitope-mapped regions of the prion protein to uncover specific regional differences between strains. Chronic wasting disease (CWD) infected deer are more resistant than CWD infected elk to degradation by proteinase K after denaturation with a chaotropic agent along the prion protein; specifically, this feature occurred at 6 of 6 epitope-mapped regions (unstructured and globular regions) examined. There is a higher heterogeneity in the conformations and transition point in CWD infected deer as opposed to CWD infected elk. This is in concert with previous lab data (IHC and SDD-AGE). The Q/E 226 difference between the deer and elk prion protein sequence is recapitulated and can be seen with multiple inoculums (i.e. more than one version of CWD). This made these new methodologies ideal tools to examine the differences between CWD in deer and elk and newly cervid-adapted prion strains. Chronic wasting disease (CWD) infected deer have different epitope accessibility than CWD infected elk along the prion protein at epitope-mapped regions (unstructured and globular regions). The Q/E 226 difference between the deer and elk prion protein sequence is recapitulated when examining cervid-adapted RML.

QUESTION 2: What are the subtle structural ways that prion structure evolves?

Hypothesis: Subtle tertiary structural changes occurring as prions emerge/evolve can be tracked via chaotropic agents and epitope-mapped antibodies.

Aim 3: Compare emerging and evolving strains to better understand the basis of strain/species adaptation and ultimately the species barrier. Rationale: Prion strain characteristics and the species barrier are dependent on the conformational structure of the misfolded prion protein (PrP^{Sc}). Understanding what prion structural changes occur during evolution and emergence will provide vital information for future emergent strains; for example, newly emergent chronic wasting disease in Europe and drug-induced evolution.

Rationale: Drug-Induced Prion Evolution: Drug-induced evolution can alter the characteristics of the prion protein and is considered to create new strains of infectious prions, e.g. Swansonine (Li et al 2010), IND24/IND81 (Berry et al 2013), and Quinacrine (Doh-Ura et al 2000). Quinacrine was touted as an anti-prion potential therapy due to effectiveness in murine cell culture systems (Doh-Ura et al 2000; Korth et al 2001); however, it failed in human trials (Benito-León et al 2004; Nakijima et al 2004; Collinge et al 2009; Mead et al 2011; Geschwind et al 2013) and was shown to increase prion load in a cervid-PrP transgenic cell culture system (Bian et al 2014). Quinacrine perturbation of the prion protein was detectable in the cell culture system by day 6. We used chaotropic agents and epitope-mapped antibodies (Aim 2) to track daily drug-induced effects change in epitope-localized prion structure. Quinacrine-induced evolution of chronic wasting disease causes rapid emergence of conformational perturbation of the

prion protein, measurable at some epitopes within 24 hours of drug application. The evolution yields a more epitope-inaccessible protein.

Rationale: Evolution in cell culture: Potential prion diseases therapeutic testing relies on the assumption that cell culture systems recapitulate natural prion diseases in higher order animals (human, deer, elk, sheep, etc.). This assumption has not been reliable, e.g., quinacrine was promising in cell culture systems (Doh-Ura et al 2000; Korth et al 2001) but failed in human trials (Benito-León et al 2004; Nakijima et al 2004; Collinge et al 2009; Mead et al 2011; Geschwind et al 2013). To ensure scientific facts are accurate and for science to move forward, we must continually challenge our assumptions. A fundamental prion biology assumption that is challenged: chronically prion infected cell models will recapitulate molecular characteristics of a biological prion infection. To test the validity that prion strains are truly stable within cell culture, chaotropic agents and epitope-mapped antibodies (Aim1, Aim 2) were used to compare fresh prion infection to chronic (long-term) prion infection in cell culture. Repeated passaging of a prion strain in cell culture selects for the most stable quasi-species, leading to a PrP^{Sc} native conformation that is inaccessible at some epitopes (without denaturation) unlike primarily infected cell material. Cell-induced selection of prion quasi-species potentially confounds current drug screening methodologies. Using chronically infected (repeatedly passaged) cell material as an infectious source yields different epitope accessibilities than either primarily infected or chronically infected materials. Generalizability in science is the basis of using models (animal, cell, etc.); however, like psychology having a wealth of data about college undergraduates, the

concept of using chronically infected cells may be more specific than previously thought.

In summary, the proposed research will expand our understanding of the structure of infectious prions, prion strains, adaption, and prion cell culture models. The ultimate benefit of the proposed research will be from the structural knowledge gained; this knowledge, in turn, could serve as a basis for new therapeutics.

BIBLIOGRAPHY

- ¹ Aboelsoud, N. H. (2010). Herbal medicine in ancient Egypt. *Journal of Medicinal Plants Research*, 4(2), 082-086.
- ² Gossell-Williams, M., Simon, O. R., & West, M. E. (2006). The past and present use of plants for medicines. *West Indian Medical Journal*, 55(4), 217-218.
- ³ Aguzzi, A., & O'Connor, T. (2010). Protein aggregation diseases: Pathogenicity and therapeutic perspectives. *Nature Reviews Drug Discovery*, 9(3), 237-248.
- ⁴ Comber, T. (1772). Real improvements in agriculture:(on the principles of A. Young, Esq.;) recommended to accompany improvements of rents; in a letter to Reade Peacock, esq; alderman of Huntingdon. To which is added, a letter to Dr. Hunter, physician in York. Concerning the rickets in sheep. Printed for W. Nicoll.
- ⁵ Stockman, S (1913, November 8) "Scrapie." *The Scottish Farmer*, vol. xxi., No. 1088, p. 1059: Glasgow
- ⁶ M'GOWAN, J. P. (1914). Investigation into the Disease of Sheep called "Scrapie"(Traberkrankheit; La Tremblante) with Especial Reference to its Association with Sarcosporidiosis. With an Appendix on a Case of Johne's Disease in the Sheep.
- ⁷ Gajdusek, D. C. (1972). Spongiform virus encephalopathies. *Journal of Clinical Pathology. Supplement (Royal College of Pathologists).*, 6, 78.
- ⁸ Gibbs, C. J., Gajdusek, D. C., & Latarjet, R. (1978). Unusual resistance to ionizing radiation of the viruses of kuru, Creutzfeldt-Jakob disease, and scrapie. *Proceedings of the National Academy of Sciences*, 75(12), 6268-6270.
- ⁹ Cui, H. L., Guo, B., Scicluna, B., Coleman, B. M., Lawson, V. A., Ellett, L., & Hill, A. F. (2014). Prion infection impairs cholesterol metabolism in neuronal cells. *Journal of Biological Chemistry*, 289(2), 789-802.
- ¹⁰ Sigurðsson, B. (1954). *Rida, a chronic encephalitis of sheep: with general remarks on infections which develop slowly and some of their special characteristics.*
- ¹¹ Alper T, Haig DA, Clarke MC. The exceptionally small size of the scrapie agent. *Biochem Bioph Res Co* 1966;**22**:278-84.
- ¹² Alper T, Cramp WA, Haig DA, et al. Does the agent of scrapie replicate without nucleic acid? *Nature* 1967;**214**:764-6.
- ¹³ Pattison IH. Resistance of the scrapie agent to formalin. *J Comp Pathol* 1965;**75**:159-64.
- ¹⁴ Pattison IH, Jones KM. The possible nature of the transmissible agent of scrapie. *Vet Rec* 1967;**80**:2-9.
- ¹⁵ Griffith JS. Self-replication and scrapie. *Nature* 1967;**215**:1043-4.
- ¹⁶ Eklund CM, Kennedy RC, Hadlow WJ. Pathogenesis of scrapie virus infection in the mouse. *J Infect Dis* 1967;**117**:15-22.
- ¹⁷ Diener, T. O., McKinley, M. P., & Prusiner, S. B. (1982). Viroids and prions. *Proceedings of the National Academy of Sciences*, 79(17), 5220-5224.
- ¹⁸ Prusiner SB (1982) Novel proteinaceous infectious particles cause scrapie. *Science* 216: 136-144

-
- ¹⁹ Oesch, B., Teplow, D. B., Stahl, N., Serban, D., Hood, L. E., & Prusiner, S. B. (1990). Identification of cellular proteins binding to the scrapie prion protein. *Biochemistry*, 29(24), 5848-5855.
- ²⁰ Basler, K., Oesch, B., Scott, M., Westaway, D., Wälchli, M., Groth, D. F., & Weissmann, C. (1986). Scrapie and cellular PrP isoforms are encoded by the same chromosomal gene. *Cell*, 46(3), 417-428.
- ²¹ Oesch, B., Westaway, D., Wälchli, M., McKinley, M. P., Kent, S. B., Aebersold, R., & Prusiner, S. B. (1985). A cellular gene encodes scrapie PrP 27-30 protein. *Cell*, 40(4), 735-746.
- ²² Autenried, P., Ague&, M., Weissmann, C., Zentraliabor, S., & Zurich, U. (2004). Mice Devoid of PrP Are Resistant to Scrapie. *Cell*, 116(116), 1339-1347.
- ²³ Sailer, A., Büeler, H., Fischer, M., Aguzzi, A., & Weissmann, C. (1994). No propagation of prions in mice devoid of PrP. *Cell*, 77(7), 967-968.
- ²⁴ Büeler, H., Aguzzi, A., Sailer, A., Greiner, R. A., Autenried, P., Aguet, M., & Weissmann, C. (1993). Mice devoid of PrP are resistant to scrapie. *Cell*, 73(7), 1339-1347.
- ²⁵ Legname, G., Baskakov, I. V., Nguyen, H. O. B., Riesner, D., Cohen, F. E., DeArmond, S. J., & Prusiner, S. B. (2004). Synthetic mammalian prions. *Science*, 305(5684), 673-676.
- ²⁶ Sisó, S., González, L., & Jeffrey, M. (2010). Neuroinvasion in prion diseases: the roles of ascending neural infection and blood dissemination. *Interdisciplinary perspectives on infectious diseases*, 2010.
- ²⁷ Bonda, D. J., Manjila, S., Mehndiratta, P., Khan, F., Miller, B. R., Onwuzulike, K., & Cali, I. (2016). Human prion diseases: surgical lessons learned from iatrogenic prion transmission. *Neurosurgical Focus*, 41(1), E10.
- ²⁸ Chandler, R. (1961). Encephalopathy in mice produced by inoculation with scrapie brain material. *The Lancet*, 1(7191), 1378-1379.
- ²⁹ Seidel, B., Thomzig, A., Buschmann, A., Groschup, M. H., Peters, R., Beekes, M., & Terytze, K. (2007). Scrapie agent (strain 263K) can transmit disease via the oral route after persistence in soil over years. *PLoS One*, 2(5), e435.
- ³⁰ Pritzkow, S., Morales, R., Moda, F., Khan, U., Telling, G. C., Hoover, E., & Soto, C. (2015). Grass Plants Bind, Retain, Uptake, and Transport Infectious Prions. *Cell reports*, 11(8), 1168-1175.
- ³¹ Bruce, M. E., Will, R. G., Ironside, J. W., McConnell, I., Drummond, D., Suttie, A., & Cousens, S. (1997). Transmissions to mice indicate that 'new variant' CJD is caused by the BSE agent. *Nature*, 389(6650), 498-501.
- ³² Zigas, V., & Gajdusek, D. C. (1957). Kuru: clinical study of a new syndrome resembling paralysis agitans in natives of the Eastern Highlands of Australian New Guinea. *Medical Journal of Australia*, 2(21), 745-54.
- ³³ Angers, R. C., S. R. Browning, T. S. Seward, C. J. Sigurdson, M. W. Miller, E. A. Hoover, and G. C. Telling. 2006. Prions in skeletal muscles of deer with chronic wasting disease. *Science* 311:1117.

-
- ³⁴ Angers, R. C., T. S. Seward, D. Napier, M. Green, E. A. Hoover, T. Spraker, K. O'Rourke, A. Balachandran, and G. C. Telling. 2009. Prions in Antler Velvet of CWD-Infected Elk. *Emerging Infectious Diseases* 15:696-703
- ³⁵ Belt, P. B., Muileman, I. H., Schreuder, B. E., Bos-de Ruijter, J., Gielkens, A. L., & Smits, M. A. (1995). Identification of five allelic variants of the sheep PrP gene and their association with natural scrapie. *Journal of General Virology*, 76(3), 509-517.
- ³⁶ Wadsworth, J. D., Asante, E. A., Desbruslais, M., Linehan, J. M., Joiner, S., Gowland, I., & Brandner, S. (2004). Human prion protein with valine 129 prevents expression of variant CJD phenotype. *Science*, 306(5702), 1793-1796.
- ³⁷ Ross, E. D., Minton, A., & Wickner, R. B. (2005). Prion domains: Sequences, structures and interactions. *Nature Cell Biology*, 7(11), 1039-1044.
- ³⁸ Soto, C., Estrada, L., & Castilla, J. (2006). Amyloids, prions and the inherent infectious nature of misfolded protein aggregates. *Trends in Biochemical Sciences*, 31(3), 150-155.
- ³⁹ Torres, J. M., Espinosa, J. C., Aguilar-Calvo, P., Herva, M. E., Relaño-Ginés, A., Villa-Díaz, A., & Castilla, J. (2014). Elements modulating the prion species barrier and its passage consequences. *PloS one*, 9(3), e89722.
- ⁴⁰ Collinge, J. (2012). The risk of prion zoonoses. *Science*, 335(6067), 411-413.
- ⁴¹ Fryer HR, McLean AR (2011) There Is No Safe Dose of Prions. *PLoS ONE* 6(8): e23664.
- ⁴² Sigurdson, C. J., Manco, G., Schwarz, P., Liberski, P., Hoover, E. A., Hornemann, S., & Aguzzi, A. (2006). Strain fidelity of chronic wasting disease upon murine adaptation. *Journal of virology*, 80(24), 12303-12311.
- ⁴³ Castilla, J., Gonzalez-Romero, D., Saá, P., Morales, R., De Castro, J., & Soto, C. (2008). Crossing the species barrier by PrP Sc replication in vitro generates unique infectious prions. *Cell*, 134(5), 757-768.
- ⁴⁴ Baskakov, I. V. (2014). The many shades of prion strain adaptation. *Prion*, 8(2), 169-172.
- ⁴⁵ Cobb, N. J., Apostol, M. I., Chen, S., Smirnovas, V., & Surewicz, W. K. (2014). Conformational stability of mammalian prion protein amyloid fibrils is dictated by a packing polymorphism within the core region. *Journal of Biological Chemistry*, 289(5), 2643-2650.
- ⁴⁶ Telling, G. C., Scott, M., Hsiao, K. K., Foster, D., Yang, S. L., Torchia, M., & Prusiner, S. B. (1994). Transmission of creutzfeldt-jakob disease from humans to transgenic mice expressing chimeric human- mouse prion protein. *Proceedings of the National Academy of Sciences*, 91(21), 9936-9940.
- ⁴⁷ Telling, G. C., M. Scott, J. Mastrianni, R. Gabizon, M. Torchia, F. E. Cohen, S. J. DeArmond, and S. B. Prusiner. 1995. Prion propagation in mice expressing human and chimeric PrP transgenes implicates the interaction of cellular PrP with another protein. *Cell* 83:79-90.
- ⁴⁸ Sigurdson, C. J., Joshi-Barr, S., Bett, C., Winson, O., Manco, G., Schwarz, P., & Peretz, D. (2011). Spongiform encephalopathy in transgenic mice expressing a point mutation in the $\alpha 2$ loop of the prion protein. *Journal of Neuroscience*, 31(39), 13840-13847.

-
- ⁴⁹ Kyle, L. M., John, T. R., Schätzl, H. M., & Lewis, R. V. (2013). Introducing a rigid loop structure from deer into mouse prion protein increases its propensity for misfolding in vitro. *PLoS one*, 8(6), e66715.
- ⁵⁰ Krebs, M. R., Morozova-Roche, L. A., Daniel, K., Robinson, C. V., & Dobson, C. M. (2004). Observation of sequence specificity in the seeding of protein amyloid fibrils. *Protein Science*, 13(7), 1933-1938.
- ⁵¹ Campioni, S., Mannini, B., Zampagni, M., Pensalfini, A., Parrini, C., Evangelisti, E., & Chiti, F. (2010). A causative link between the structure of aberrant protein oligomers and their toxicity. *Nature chemical biology*, 6(2), 140.
- ⁵² Cremades, N., Cohen, S. I., Deas, E., Abramov, A. Y., Chen, A. Y., Orte, A., & Bertoncini, C. W. (2012). Direct observation of the interconversion of normal and toxic forms of α -synuclein. *Cell*, 149(5), 1048-1059.
- ⁵³ Bernstein, S. L., Dupuis, N. F., Lazo, N. D., Wyttenbach, T., Condron, M. M., Bitan, G., & Bowers, M. T. (2009). Amyloid- β protein oligomerization and the importance of tetramers and dodecamers in the aetiology of Alzheimer's disease. *Nature chemistry*, 1(4), 326-331.
- ⁵⁴ Bian, J., Khaychuk, V., Angers, R. C., Fernández-Borges, N., Vidal, E., Meyerett-Reid, C., & Agrimi, U. (2017). Prion replication without host adaptation during interspecies transmissions. *Proceedings of the National Academy of Sciences*, 114(5), 1141-1146.
- ⁵⁵ Bett C, Joshi-Barr S, Lucero M, Trejo M, Liberski P, et al. (2012) Biochemical Properties of Highly Neuroinvasive Prion Strains. *PLoS Pathog* 8(2)
- ⁵⁶ Bessen, R. A., & Marsh, R. F. (1992). Identification of two biologically distinct strains of transmissible mink encephalopathy in hamsters. *Journal of General Virology*, 73(2), 329-334.
- ⁵⁷ Bessen, R. A., & Marsh, R. F. (1992). Biochemical and physical properties of the prion protein from two strains of the transmissible mink encephalopathy agent. *Journal of virology*, 66(4), 2096-2101.
- ⁵⁸ Tanaka, M., Collins, S. R., Toyama, B. H., & Weissman, J. S. (2006). The physical basis of how prion conformations determine strain phenotypes. *Nature*, 442(7102), 585-589.
- ⁵⁹ Telling, G. C., Parchi, P., DeArmond, S. J., Cortelli, P., Montagna, P., Gabizon, R., & Prusiner, S. B. (1996). Evidence for the conformation of the pathologic isoform of the prion protein enciphering and propagating prion diversity. *Science*, 274(5295), 2079-2082.
- ⁶⁰ Colby, D. W., Giles, K., Legname, G., Wille, H., Baskakov, I. V., DeArmond, S. J., & Prusiner, S. B. (2009). Design and construction of diverse mammalian prion strains. *Proceedings of the National Academy of Sciences*, 106(48), 20417-20422.
- ⁶¹ Peretz, D., Scott, M. R., Groth, D., Williamson, R. A., Burton, D. R., Cohen, F. E., & Prusiner, S. B. (2001). Strain-specified relative conformational stability of the scrapie prion protein. *Protein Science*, 10(4), 854-863.

-
- ⁶² Collinge, J., Sidle, K. C., Meads, J., Ironside, J., & Hill, A. F. (1996). Molecular analysis of prion strain variation and the aetiology of 'new variant' CJD. *Nature*, 383(6602), 685.
- ⁶³ Collinge, J., & Clarke, A. R. (2007). A general model of prion strains and their pathogenicity. *Science*, 318(5852), 930-936.
- ⁶⁴ Nyström, S., & Hammarström, P. (2014). Is the prevalent human prion protein 129M/V mutation a living fossil from a Paleolithic panzootic superprion pandemic?. *Prion*, 8(1), 2-10.
- ⁶⁵ Schoch G, Seeger H, Bogousslavsky J, Tolnay M, Janzer RC, et al. (2006) Analysis of prion strains by PrP^{Sc} profiling in sporadic Creutzfeldt-Jakob disease. *PLoS Med* 3(2): e14
- ⁶⁶ Cracco, L., Notari, S., Cali, I., Sy, M. S., Chen, S. G., Cohen, M. L., & Safar, J. G. (2017). Novel strain properties distinguishing sporadic prion diseases sharing prion protein genotype and prion type. *Scientific Reports*, 7.
- ⁶⁷ Jakob, A. (1921). Über eigenartige Erkrankungen des Zentralnervensystems mit bemerkenswertem anatomischen Befunde. *Zeitschrift für die gesamte Neurologie und Psychiatrie*, 64(1), 147-228.
- ⁶⁸ Jakob, A. (1921). Über eine der multiplen Sklerose nahestehende Erkrankung des Zentralnervensystems (spastische Pseudosklerose) mit bemerkenswertem anatomischen Befunde. *Med. Klin*, 1, 372-376.
- ⁶⁹ Creutzfeldt, H. G. (1920). Über eine eigenartige herdförmige Erkrankung des Zentralnervensystems (vorläufige Mitteilung). *Zeitschrift für die gesamte Neurologie und Psychiatrie*, 57(1), 1-18.
- ⁷⁰ Gibbs, C. J., Gajdusek, D. C., Asher, D. M., Alpers, M. P., Beck, E., Daniel, P. M., & Matthews, W. B. (1968). Creutzfeldt-Jakob disease (spongiform encephalopathy): transmission to the chimpanzee. *Science*, 161(3839), 388-389.
- ⁷¹ Parchi, P., Giese, A., Capellari, S., Brown, P., Schulz-Schaeffer, W., Windl, O., & Poser, S. (1999). Classification of sporadic Creutzfeldt-Jakob disease based on molecular and phenotypic analysis of 300 subjects. *Annals of neurology*, 46(2), 224-233.
- ⁷² CDC online: <https://www.cdc.gov/prions/cjd/occurrence-transmission.html>
- ⁷³ Cooper, S. A., Murray, K. L., Heath, C. A., Will, R. G., & Knight, R. S. (2006). Sporadic Creutzfeldt-Jakob disease with cerebellar ataxia at onset in the United Kingdom. *Journal of Neurology, Neurosurgery & Psychiatry*.
- ⁷⁴ Van Everbroeck, B., Pals, P., Dzedzic, T., Dom, R., Godfraind, C., Sciot, R., & Cras, P. (2000). Retrospective study of Creutzfeldt-Jakob disease in Belgium: neuropathological findings. *Acta neuropathologica*, 99(4), 358-364.
- ⁷⁵ Will, R. G., & Matthews, W. B. (1984). A retrospective study of Creutzfeldt-Jakob disease in England and Wales 1970-79. I: Clinical features. *Journal of Neurology, Neurosurgery & Psychiatry*, 47(2), 134-140.
- ⁷⁶ Sikorska, B., Knight, R., Ironside, J. W., & Liberski, P. P. (2012). Creutzfeldt-jakob disease. *Neurodegenerative Diseases*, 76-90.
- ⁷⁷ Goldfarb, L. G., Petersen, R. B., Tabaton, M., Brown, P., LeBlanc, A. C., Montagna, P., & Haltia, M. (1992). Fatal familial insomnia and familial Creutzfeldt-Jakob

-
- disease: disease phenotype determined by a DNA polymorphism. *SCIENCE-NEW YORK THEN WASHINGTON-*, 806-806.
- ⁷⁸ Lipscomb, I. P., Pinchin, H., Collin, R., & Keevil, C. W. (2007). Effect of drying time, ambient temperature and pre-soaks on prion-infected tissue contamination levels on surgical stainless steel: concerns over prolonged transportation of instruments from theatre to central sterile service departments. *Journal of Hospital Infection*, 65(1), 72-77.
- ⁷⁹ Will, R. G., Ironside, J. W., Zeidler, M., Estibeiro, K., Cousens, S. N., Smith, P. G., & Hofman, A. (1996). A new variant of Creutzfeldt-Jakob disease in the UK. *The Lancet*, 347(9006), 921-925.
- ⁸⁰ Zeidler, M., Stewart, G. E., Barraclough, C. R., Bateman, D. E., Bates, D., Burn, D. J., & Mackenzie, J. M. (1997). New variant Creutzfeldt-Jakob disease: neurological features and diagnostic tests. *The Lancet*, 350(9082), 903-907.
- ⁸¹ Bateman, D., Hilton, D., Love, S., Zeidler, M., Beck, J., & Collinge, J. (1995). Sporadic Creutzfeldt-Jakob disease in a 18-year-old in the UK. *The Lancet*, 346(8983), 1155-1156.
- ⁸² Britton, T. C., Al-Sarraj, S., Shaw, C., Campbell, T., & Collinge, J. (1995). Sporadic Creutzfeldt-Jakob disease in a 16-year-old in the UK. *The Lancet*, 346(8983), 1155.
- ⁸³ Scott, M. R., Will, R., Ironside, J., Nguyen, H. O. B., Tremblay, P., DeArmond, S. J., & Prusiner, S. B. (1999). Compelling transgenic evidence for transmission of bovine spongiform encephalopathy prions to humans. *Proceedings of the National Academy of Sciences*, 96(26), 15137-15142.
- ⁸⁴ Raymond, G. J., Hope, J., Kocisko, D. A., Priola, S. A., Raymond, L. D., Bossers, A., & Gambetti, P. (1997). Molecular assessment of the potential transmissibilities of BSE and scrapie to humans. *Nature*, 388(6639), 285-288.
- ⁸⁵ Lugaresi, E., Medori, R., Montagna, P., Baruzzi, A., Cortelli, P., Lugaresi, A., & Gambetti, P. (1986). Fatal familial insomnia and dysautonomia with selective degeneration of thalamic nuclei. *New England Journal of Medicine*, 315(16), 997-1003.
- ⁸⁶ Medori, R., Tritschler, H. J., LeBlanc, A., Villare, F., Manetto, V., Chen, H. Y., & Tinuper, P. (1992). Fatal familial insomnia, a prion disease with a mutation at codon 178 of the prion protein gene. *New England Journal of Medicine*, 326(7), 444-449.
- ⁸⁷ Parchi, P., Capellari, S., Chin, S., Schwarz, H. B., Schechter, N. P., Butts, J. D., & Gambetti, P. (1999). A subtype of sporadic prion disease mimicking fatal familial insomnia. *Neurology*, 52(9), 1757-1757.
- ⁸⁸ Gerstmann, J., Sträussler, E., & Scheinker, I. (1935). Über eine eigenartige hereditär-familiäre Erkrankung des Zentralnervensystems. *Zeitschrift für die gesamte Neurologie und Psychiatrie*, 154(1), 736-762.
- ⁸⁹ Budka, H., & Kovacs, G. G. (2013). Gerstmann-Sträussler-Scheinker Disease.
- ⁹⁰ Parchi, P., Chen, S. G., Brown, P., Zou, W., Capellari, S., Budka, H., & Gajdusek, D. C. (1998). Different patterns of truncated prion protein fragments correlate with

-
- distinct phenotypes in P102L Gerstmann-Sträussler-Scheinker disease. *Proceedings of the National Academy of Sciences*, 95(14), 8322-8327.
- ⁹¹ Wadsworth, J. D., Joiner, S., Linehan, J. M., Cooper, S., Powell, C., Mallinson, G., & Brandner, S. (2006). Phenotypic heterogeneity in inherited prion disease (P102L) is associated with differential propagation of protease-resistant wild-type and mutant prion protein. *Brain*, 129(6), 1557-1569.
- ⁹² Zanusso, G., Fiorini, M., Ferrari, S., Meade-White, K., Barbieri, I., Brocchi, E., & Monaco, S. (2014). Gerstmann-Sträussler-Scheinker disease and “anchorless Prion Protein” mice share prion conformational properties diverging from sporadic Creutzfeldt-Jakob disease. *Journal of Biological Chemistry*, 289(8), 4870-4881.
- ⁹³ Hotchin, J. (1966). Kuru as a persisting tolerated infection. *The Lancet*, 288(7453), 28-31.
- ⁹⁴ Hoskin, J. O., Kiloh, L. G., & Cawte, J. E. (1969). Epilepsy and guria: the shaking syndromes of New Guinea. *Social Science & Medicine* (1967), 3(1), 39-48.
- ⁹⁵ Hadlow, W. J. (1959). Scrapie and Kuru. *The Lancet*, 274(7097), 289-290.
- ⁹⁶ Greig, J. R. (1950). Scrapie in sheep. *Journal of Comparative Pathology and Therapeutics*, 60, 263-266.
- ⁹⁷ Cuillé, J. & Chelle, P. L. (1936). La maladie dite tremblante du mouton est-elle inoculable. *CR Acad Sci* 203, 1552-1554
- ⁹⁸ Wilson, D. R., Anderson, R. D., & Smith, W. (1950). Studies in scrapie. *Journal of Comparative Pathology and Therapeutics*, 60, 267-282.
- ⁹⁹ Pattison, I. H., Gordon, W. S., & Millson, G. C. (1959). Experimental production of scrapie in goats. *Journal of Comparative Pathology and Therapeutics*, 69, 300-312.
- ¹⁰⁰ Parry, H. B. (1962). Scrapie: a transmissible and hereditary disease of sheep. *Heredity*, 17(Pt. 1), 75-105.
- ¹⁰¹ Pattison, I. H., & Millson, G. C. (1962). Distribution of the scrapie agent in the tissues of experimentally inoculated goats. *Journal of Comparative Pathology and Therapeutics*, 72, 233-244.
- ¹⁰² Zlotnik, I., & Rennie, J. C. (1965). Experimental transmission of mouse passaged scrapie to goats, sheep, rats and hamsters. *Journal of comparative pathology*, 75(2), 147IN3157-156IN6.
- ¹⁰³ Eklund, C. M., Hadlow, W. J., & Kennedy, R. C. (1963). Some properties of the scrapie agent and its behavior in mice. *Experimental Biology and Medicine*, 112(4), 974-979.
- ¹⁰⁴ Mould, D. L., Dawson, A. M., Slater, J. S., & Zlotnik, I. (1967). Relationships between chemical changes and histological damage in the brains of scrapie affected mice. *Journal of comparative pathology*, 77(4), 393IN5403-402IN6.
- ¹⁰⁵ Westaway, D., Zuliani, V., Cooper, C. M., Da Costa, M., Neuman, S., Jenny, A. L., & Prusiner, S. B. (1994). Homozygosity for prion protein alleles encoding glutamine-171 renders sheep susceptible to natural scrapie. *Genes & development*, 8(8), 959-969.
- ¹⁰⁶ Elsen, J. M., Amigues, Y., Schelcher, F., Ducrocq, V., Androletti, O., Eychenne, F., & Laplanche, J. L. (1999). Genetic susceptibility and transmission factors in scrapie:

-
- detailed analysis of an epidemic in a closed flock of Romanov. *Archives of virology*, 144(3), 431-445.
- ¹⁰⁷ Clouscard, C., Beaudry, P., Elsen, J. M., Milan, D., Dussaucy, M., Bounneau, C., ... & Laplanche, J. L. (1995). Different allelic effects of the codons 136 and 171 of the prion protein gene in sheep with natural scrapie. *Journal of General Virology*, 76(8), 2097-2101.
- ¹⁰⁸ Bruce, M. E. (1993). Scrapie strain variation and mutation. *British Medical Bulletin*, 49(4), 822-838.
- ¹⁰⁹ Baylis, M., & Goldmann, W. (2004). The genetics of scrapie in sheep and goats. *Current molecular medicine*, 4(4), 385-396.
- ¹¹⁰ Melchior, M. B., Windig, J. J., Hagenaaars, T. J., Bossers, A., Davidse, A., & van Zijderveld, F. G. (2010). Eradication of scrapie with selective breeding: are we nearly there?. *BMC veterinary research*, 6(1), 24.
- ¹¹¹ Kim, Y. S., Carp, R. I., Callahan, S. M., Natelli, M., & Wisniewski, H. M. (1990). Vacuolization, incubation period and survival time analyses in three mouse genotypes injected stereotactically in three brain regions with the 22L scrapie strain. *Journal of Neuropathology & Experimental Neurology*, 49(2), 106-113.
- ¹¹² Kimberlin, R. H., Cole, S., & Walker, C. A. (1987). Temporary and permanent modifications to a single strain of mouse scrapie on transmission to rats and hamsters. *Journal of General Virology*, 68(7), 1875-1881.
- ¹¹³ Fraser, H., & Dickinson, A. G. (1973). Scrapie in mice: agent-strain differences in the distribution and intensity of grey matter vacuolation. *Journal of comparative pathology*, 83(1), 29-40.
- ¹¹⁴ Greenlee, J. J., Smith, J. D., & Kunkle, R. A. (2011). White-tailed deer are susceptible to the agent of sheep scrapie by intracerebral inoculation. *Veterinary research*, 42(1), 107.
- ¹¹⁵ Hamir, A. N., Miller, J. M., Cutlip, R. C., Kunkle, R. A., Jenny, A. L., Stack, M. J., & Richt, J. A. (2004). Transmission of sheep scrapie to elk (*Cervus elaphus nelsoni*) by intracerebral inoculation: final outcome of the experiment. *Journal of Veterinary Diagnostic Investigation*, 16(4), 316-321.
- ¹¹⁶ Tamgüney, G., Miller, M. W., Giles, K., Lemus, A., Glidden, D. V., DeArmond, S. J., & Prusiner, S. B. (2009). Transmission of scrapie and sheep-passaged bovine spongiform encephalopathy prions to transgenic mice expressing elk prion protein. *Journal of general virology*, 90(4), 1035-1047.
- ¹¹⁷ Benestad, S. L., Sarradin, P., Thu, B., Schönheit, J., Tranulis, M. A., & Bratberg, B. (2003). Cases of scrapie with unusual features in Norway and designation of a new type, Nor98. *The Veterinary Record*, 153(7), 202-208.
- ¹¹⁸ Marsh, R. F., & Hadlow, W. J. (1992). Transmissible mink encephalopathy. *Revue scientifique et technique (International Office of Epizootics)*, 11(2), 539-550.
- ¹¹⁹ Hartsough, G. R., & Burger, D. (1965). Encephalopathy of mink: I. Epizootiologic and clinical observations. *Journal of Infectious Diseases*, 115(4), 387-392.

-
- ¹²⁰ Liberski, P. P., Sikorska, B., Guiroy, D., & Bessen, R. A. (2009). Transmissible mink encephalopathy-review of the etiology of a rare prion disease. *Folia Neuropathol*, 47(2), 195-204.
- ¹²¹ Robinson, M. M., Hadlow, W. J., Huff, T. P., Wells, G. A., Dawson, M., Marsh, R. F., & Gorham, J. R. (1994). Experimental infection of mink with bovine spongiform encephalopathy. *Journal of General Virology*, 75(9), 2151-2155.
- ¹²² Barlow, R. M., & Rennie, J. C. (1970). Transmission experiments with a scrapie-like encephalopathy of mink. *Journal of comparative pathology*, 80(1), 75-79.
- ¹²³ Marsh, R. F., Burger, D., Eckroade, R., Rhein, G. Z., & Hanson, R. P. (1969). A preliminary report on the experimental host range of the transmissible mink encephalopathy agent. *The Journal of infectious diseases*, 713-719.
- ¹²⁴ Eckroade, R. J., Zu Rhein, G. M., Marsh, R. F., & Hanson, R. P. (1970). Transmissible mink encephalopathy: experimental transmission to the squirrel monkey. *Science*, 169(3950), 1088-1090.
- ¹²⁵ Marsh, R. F., & Bessen, R. A. (1994). Physicochemical and biological characterizations of distinct strains of the transmissible mink encephalopathy agent. *Philosophical Transactions of the Royal Society of London B: Biological Sciences*, 343(1306), 413-414.
- ¹²⁶ Wells, G. A., Scott, A. C., Johnson, C. T., Gunning, R. F., Hancock, R. D., Jeffrey, M., ... & Bradley, R. (1987). A novel progressive spongiform encephalopathy in cattle. *Veterinary Record*, 121(18), 419-420.
- ¹²⁷ Wilesmith, J. W., Wells, G. A., Cranwell, M. P., & Ryan, J. B. (1988). Bovine spongiform encephalopathy: epidemiological studies. *The Veterinary Record*, 123(25), 638-644.
- ¹²⁸ West Greenlee MH, Smith JD, Platt EM, Juarez JR, Timms LL, Greenlee JJ (2015) Changes in Retinal Function and Morphology Are Early Clinical Signs of Disease in Cattle with Bovine Spongiform Encephalopathy. *PLoS ONE* 10(3)
- ¹²⁹ Aguzzi, A., & Calella, A. M. (2009). Prions: protein aggregation and infectious diseases. *Physiological reviews*, 89(4), 1105-1152.
- ¹³⁰ Doherr, M. G., Oesch, B., Moser, M., Vandeveld, M., & Heim, D. (1999). Targeted surveillance for bovine spongiform encephalopathy. *Investigative Ophthalmology and Visual Science*, 32, 1492-1498.
- ¹³¹ Doherr, M. G., Heim, D., Fatzer, R., Cohen, C. H., Vandeveld, M., & Zurbriggen, A. (2001). Targeted screening of high-risk cattle populations for BSE to augment mandatory reporting of clinical suspects. *Preventive Veterinary Medicine*, 51(1-2), 3-16.
- ¹³² Buschmann, A., Biacabe, A. G., Ziegler, U., Bencsik, A., Madec, J. Y., Erhardt, G., & Groschup, M. H. (2004). Atypical scrapie cases in Germany and France are identified by discrepant reaction patterns in BSE rapid tests. *Journal of virological methods*, 117(1), 27-36.
- ¹³³ Biacabe, A. G., Morignat, E., Vulin, J., Calavas, D., & Baron, T. G. (2008). Atypical bovine spongiform encephalopathies, France, 2001-2007. *Emerging infectious diseases*, 14(2), 298.

-
- ¹³⁴ Ducrot, C., Arnold, M., De Koeijer, A., Heim, D., & Calavas, D. (2008). Review on the epidemiology and dynamics of BSE epidemics. *Veterinary research*, 39(4), 1-18.
- ¹³⁵ Casalone, C., Zanusso, G., Acutis, P., Ferrari, S., Capucci, L., Tagliavini, F., & Caramelli, M. (2004). Identification of a second bovine amyloidotic spongiform encephalopathy: molecular similarities with sporadic Creutzfeldt-Jakob disease. *Proceedings of the National Academy of Sciences*, 101(9), 3065-3070.
- ¹³⁶ Masujin, K., Okada, H., Miyazawa, K., Matsuura, Y., Imamura, M., Iwamaru, Y., & Yokoyama, T. (2016). Emergence of a novel bovine spongiform encephalopathy (BSE) prion from an atypical H-type BSE. *Scientific reports*, 6.
- ¹³⁷ Sala, C., Morignat, E., Oussaïd, N., Gay, E., Abrial, D., Ducrot, C., & Calavas, D. (2012). Individual factors associated with L- and H-type Bovine Spongiform Encephalopathy in France. *BMC veterinary research*, 8(1), 74.
- ¹³⁸ Konold, T., Bone, G. E., Clifford, D., Chaplin, M. J., Cawthraw, S., Stack, M. J., & Simmons, M. M. (2012). Experimental H-type and L-type bovine spongiform encephalopathy in cattle: observation of two clinical syndromes and diagnostic challenges. *BMC veterinary research*, 8(1), 22.
- ¹³⁹ Lloyd, S. E., Linehan, J. M., Desbruslais, M., Joiner, S., Buckell, J., Brandner, S., & Collinge, J. (2004). Characterization of two distinct prion strains derived from bovine spongiform encephalopathy transmissions to inbred mice. *Journal of General Virology*, 85(8), 2471-2478.
- ¹⁴⁰ Bruce, M., Chree, A., McConnell, I., Foster, J. P., Pearson, G., & Fraser, H. (1994). Transmission of bovine spongiform encephalopathy and scrapie to mice: strain variation and the species barrier. *Philosophical Transactions of the Royal Society of London B: Biological Sciences*, 343(1306), 405-411.
- ¹⁴¹ Vickery, C. M., Lockey, R., Holder, T. M., Thorne, L., Beck, K. E., Wilson, C., & Dexter, I. (2014). Assessing the susceptibility of transgenic mice overexpressing deer prion protein to bovine spongiform encephalopathy. *Journal of virology*, 88(3), 1830-1833.
- ¹⁴² Williams, E. S., & Young, S. (1980). Chronic Wasting Disease of Captive Mule Deer: a Spongiform Encephalopathy 1. *Journal of wildlife diseases*, 16(1), 89-98.
- ¹⁴³ Nobert, B. R., Merrill, E. H., Pybus, M. J., Bollinger, T. K., & Hwang, Y. T. (2016). Landscape connectivity predicts chronic wasting disease risk in Canada. *Journal of applied ecology*, 53(5), 1450-1459.
- ¹⁴⁴ Caramelli, M., Ru, G., Casalone, C., Bozzetta, E., Acutis, P. L., Calella, A., & Forloni, G. (2001). Evidence for the transmission of scrapie to sheep and goats from a vaccine against *Mycoplasma agalactiae*. *Veterinary Record*, 148(17), 531-536.
- ¹⁴⁵ Collee, J. G., & Bradley, R. (1997). BSE: a decade on – Part I. *The Lancet*, 349(9052), 636-641.
- ¹⁴⁶ Ricci, A., Allende, A., Bolton, D., Chemaly, M., Davies, R., Fernandez Escamez, P. S., ... & Nørrung, B. (2017). Chronic wasting disease (CWD) in cervids. *EFSA Journal*, 15(1).
- ¹⁴⁷ http://www.nwhc.usgs.gov/disease_information/chronic_wasting_disease/

-
- 148 Lee, Y. H., Sohn, H. J., Kim, M. J., Kim, H. J., Lee, W. Y., Yun, E. I., & Balachandran, A. (2012). Strain characterization of the Korean CWD cases in 2001 and 2004. *Journal of Veterinary Medical Science*, 12-0077.
- 149 Benestad, S. L., Mitchell, G., Simmons, M., Ytrehus, B., & Vikøren, T. (2016). First case of chronic wasting disease in Europe in a Norwegian free-ranging reindeer. *Veterinary research*, 47(1), 88.
- 150 <https://www.ruokavirasto.fi/en/farmers/animal-husbandry/animal-health-and-diseases/animal-diseases/luonnonvaraiset-elaimet/chronic-wasting-disease-cwd-in-cervids/>
- 151 <https://www.sva.se/om-sva/pressrum/nyheter-fran-sva/avmagringssjuka-cwd-upptackt-pa-alg-i-norrbottens-lan>
- 152 Yuan Q, Eckland T, Telling G, Bartz J, Bartelt-Hunt S (2015) Mitigation of Prion Infectivity and Conversion Capacity by a Simulated Natural Process – Repeated Cycles of Drying and Wetting. *PLoS Pathog* 11(2)
- 153 Nichols, T. A., Pulford, B., Wyckoff, A. C., Meyerett, C., Michel, B., Gertig, K., & Zabel, M. D. (2009). Detection of protease-resistant cervid prion protein in water from a CWD-endemic area. *Prion*, 3(3), 171-183.
- 154 Hill, A. F., Desbruslais, M., Joiner, S., Sidle, K. C., Gowland, I., Collinge, J., & Lantos, P. (1997). The same prion strain causes vCJD and BSE. *Nature*, 389(6650), 448-450.
- 155 Moore, R. A., Vorberg, I., & Priola, S. A. (2005). Species barriers in prion diseases – brief review. In *Infectious Diseases from Nature: Mechanisms of Viral Emergence and Persistence* (pp. 187-202). Springer Vienna.
- 156 Angers, R. C., H. E. Kang, D. Napier, S. Browning, T. Seward, C. Mathiason, A. Balachandran, D. McKenzie, J. Castilla, C. Soto, J. Jewell, C. Graham, E. A. Hoover, and G. C. Telling. 2010. Prion strain mutation determined by prion protein conformational compatibility and primary structure. *Science* 328:1154–1158.
- 157 Johnson, C., Johnson, J., Vanderloo, J. P., Keane, D., Aiken, J. M., & McKenzie, D. (2006). Prion protein polymorphisms in white-tailed deer influence susceptibility to chronic wasting disease. *Journal of General Virology*, 87(7), 2109-2114.
- 158 Reid, C. M. (2014). *Prion strain adaptation: breaking and building species barriers* (Doctoral dissertation, Colorado State University. Libraries).
- 159 Sigurdson, C. J., Manco, G., Schwarz, P., Liberski, P., Hoover, E. A., Hornemann, S., & Aguzzi, A. (2006). Strain fidelity of chronic wasting disease upon murine adaptation. *Journal of virology*, 80(24), 12303-12311.
- 160 Lee, Y. H., Sohn, H. J., Kim, M. J., Kim, H. J., Park, K. J., Lee, W. Y., & Balachandran, A. (2013). Experimental chronic wasting disease in wild type VM mice. *Journal of Veterinary Medical Science*, 75(8), 1107-1110.
- 161 Heisey, D. M., Mickelsen, N. A., Schneider, J. R., Johnson, C. J., Johnson, C. J., Langenberg, J. A., & Barr, D. J. (2010). Chronic wasting disease (CWD) susceptibility of several North American rodents that are sympatric with cervid CWD epidemics. *Journal of virology*, 84(1), 210-215.

-
- ¹⁶² Prusiner, S. B., Groth, D. F., Bolton, D. C., Kent, S. B., & Hood, L. E. (1984). Purification and structural studies of a major scrapie prion protein. *Cell*, 38(1), 127-134.
- ¹⁶³ Mays, C. E., Coomaraswamy, J., Watts, J. C., Yang, J., Ko, K. W., Strome, B., & Westaway, D. (2014). Endoproteolytic processing of the mammalian prion glycoprotein family. *The FEBS journal*, 281(3), 862-876.
- ¹⁶⁴ Damberger, F. F., Christen, B., Pérez, D. R., Hornemann, S., & Wüthrich, K. (2011). Cellular prion protein conformation and function. *Proceedings of the National Academy of Sciences*, 108(42), 17308-17313.
- ¹⁶⁵ Martin, R., Gallet, P. F., Rocha, D., & Petit, D. (2009). Polymorphism of the prion protein in mammals: a phylogenetic approach. *Recent patents on DNA & gene sequences*, 3(1), 63-71.
- ¹⁶⁶ Nico, P. B. C., de-Paris, F., Vinadé, E. R., Amaral, O. B., Rockenbach, I., Soares, B. L., & Izquierdo, I. (2005). Altered behavioural response to acute stress in mice lacking cellular prion protein. *Behavioural brain research*, 162(2), 173-181.
- ¹⁶⁷ Tobler, I., Gaus, S. E., Deboer, T., & Achermann, P. (1996). Altered circadian activity rhythms and sleep in mice devoid of prion protein. *Nature*, 380(6575), 639.
- ¹⁶⁸ Roesler, R., Walz, R., Quevedo, J., de-Paris, F., Zanata, S. M., Graner, E., ... & Brentani, R. R. (1999). Normal inhibitory avoidance learning and anxiety, but increased locomotor activity in mice devoid of PrP C. *Molecular brain research*, 71(2), 349-353.
- ¹⁶⁹ Gains, M. J., Roth, K. A., & LeBlanc, A. C. (2006). Prion protein protects against ethanol-induced Bax-mediated cell death in vivo. *Neuroreport*, 17(9), 903-906.
- ¹⁷⁰ Hoshino, S., Inoue, K., Yokoyama, T., Kobayashi, S., Asakura, T., Teramoto, A., & Itohara, S. (2003). Prions prevent brain damage after experimental brain injury: a preliminary report. In *Brain Edema XII* (pp. 297-299). Springer Vienna.
- ¹⁷¹ Schneider, K., Korkmaz, Y., Addicks, K., Lang, H., & Raab, W. H. M. (2007). Prion protein (PrP) in human teeth: an unprecedented pointer to PrP's function. *Journal of endodontics*, 33(2), 110-113.
- ¹⁷² Málaga-Trillo, E., Solis, G. P., Schrock, Y., Geiss, C., Luncz, L., Thomanetz, V., & Stuermer, C. A. (2009). Regulation of embryonic cell adhesion by the prion protein. *PLoS Biol*, 7(3), e1000055.
- ¹⁷³ Lee, Y. J., & Baskakov, I. V. (2010). Treatment with normal prion protein delays differentiation and helps to maintain high proliferation activity in human embryonic stem cells. *Journal of neurochemistry*, 114(2), 362-373.
- ¹⁷⁴ Lee, Y. J., & Baskakov, I. V. (2013). The cellular form of the prion protein is involved in controlling cell cycle dynamics, self-renewal, and the fate of human embryonic stem cell differentiation. *Journal of neurochemistry*, 124(3), 310-322.
- ¹⁷⁵ Biasini, E., Unterberger, U., Solomon, I. H., Massignan, T., Senatore, A., Bian, H., & Luebke, J. (2013). A mutant prion protein sensitizes neurons to glutamate-induced excitotoxicity. *Journal of Neuroscience*, 33(6), 2408-2418.
- ¹⁷⁶ Haas, L. T., Kostylev, M. A., & Strittmatter, S. M. (2014). Therapeutic molecules and endogenous ligands regulate the interaction between brain cellular prion protein

-
- (PrPC) and metabotropic glutamate receptor 5 (mGluR5). *Journal of Biological Chemistry*, 289(41), 28460-28477.
- ¹⁷⁷ Beraldo, F. H., Arantes, C. P., Santos, T. G., Machado, C. F., Roffe, M., Hajj, G. N., & Lopes, M. H. (2011). Metabotropic glutamate receptors transduce signals for neurite outgrowth after binding of the prion protein to laminin α 1 chain. *The FASEB Journal*, 25(1), 265-279.
- ¹⁷⁸ Um, J. W., Kaufman, A. C., Kostylev, M., Heiss, J. K., Stagi, M., Takahashi, H., & Gunther, E. C. (2013). Metabotropic glutamate receptor 5 is a coreceptor for Alzheimer α oligomer bound to cellular prion protein. *Neuron*, 79(5), 887-902.
- ¹⁷⁹ Ostapchenko, V. G., Beraldo, F. H., Guimarães, A. L., Mishra, S., Guzman, M., Fan, J., & Prado, M. A. (2013). Increased prion protein processing and expression of metabotropic glutamate receptor 1 in a mouse model of Alzheimer's disease. *Journal of neurochemistry*, 127(3), 415-425.
- ¹⁸⁰ Liu, J., Zhao, D., Liu, C., Ding, T., Yang, L., Yin, X., & Zhou, X. (2015). Prion protein participates in the protection of mice from lipopolysaccharide infection by regulating the inflammatory process. *Journal of Molecular Neuroscience*, 55(1), 279-287.
- ¹⁸¹ Yang, X., Zhang, Y., Zhang, L., He, T., Zhang, J., & Li, C. (2014). Prion protein and cancers. *Acta Biochim Biophys Sin*, 1-10
- ¹⁸² Déry, M. A., Jodoin, J., Ursini-Siegel, J., Aleynikova, O., Ferrario, C., Hassan, S., & LeBlanc, A. C. (2013). Endoplasmic reticulum stress induces PRNP prion protein gene expression in breast cancer. *Breast cancer research*, 15(2), R22.
- ¹⁸³ McEwan, J. F., Windsor, M. L., & Cullis-Hill, S. D. (2009). Antibodies to prion protein inhibit human colon cancer cell growth. *Tumor Biology*, 30(3), 141-147.
- ¹⁸⁴ Alais, S., Soto-Rifo, R., Balter, V., Gruffat, H., Manet, E., Schaeffer, L., & Leblanc, P. (2012). Functional mechanisms of the cellular prion protein (PrPC) associated anti-HIV-1 properties. *Cellular and Molecular Life Sciences*, 69(8), 1331-1352.
- ¹⁸⁵ Stahl, N., Borchelt, D. R., Hsiao, K., & Prusiner, S. B. (1987). Scrapie prion protein contains a phosphatidylinositol glycolipid. *Cell*, 51(2), 229-240.
- ¹⁸⁶ Hornshaw, M. P., McDermott, J. R., & Candy, J. M. (1995). Copper binding to the N-terminal tandem repeat regions of mammalian and avian prion protein. *Biochemical and biophysical research communications*, 207(2), 621-629.
- ¹⁸⁷ Lopez, C. D., Yost, C. S., Prusiner, S. B., Myers, R. M., & Lingappa, V. R. (1990). Unusual topogenic sequence directs prion protein biogenesis. *Science*, 248(4952), 226.
- ¹⁸⁸ Zahn, R., Liu, A., Lührs, T., Riek, R., von Schroetter, C., García, F. L., & Wüthrich, K. (2000). NMR solution structure of the human prion protein. *Proceedings of the National Academy of Sciences*, 97(1), 145-150.
- ¹⁸⁹ García, F. L., Zahn, R., Riek, R., & Wüthrich, K. (2000). NMR structure of the bovine prion protein. *Proceedings of the National Academy of Sciences*, 97(15), 8334-8339.
- ¹⁹⁰ Riek, R., Hornemann, S., Wider, G., Glockshuber, R., & Wüthrich, K. (1997). NMR characterization of the full-length recombinant murine prion protein, mPrP (23-231). *FEBS letters*, 413(2), 282-288.

-
- ¹⁹¹ Donne, D. G., Viles, J. H., Groth, D., Mehlhorn, I., James, T. L., Cohen, F. E., ... & Dyson, H. J. (1997). Structure of the recombinant full-length hamster prion protein PrP (29–231): the N terminus is highly flexible. *Proceedings of the National Academy of Sciences*, 94(25), 13452-13457.
- ¹⁹² Antonyuk, S. V., Trevitt, C. R., Strange, R. W., Jackson, G. S., Sangar, D., Batchelor, M., & Khalili-Shirazi, A. (2009). Crystal structure of human prion protein bound to a therapeutic antibody. *Proceedings of the National Academy of Sciences*, 106(8), 2554-2558.
- ¹⁹³ Gossert, A. D., Bonjour, S., Lysek, D. A., Fiorito, F., & Wüthrich, K. (2005). Prion protein NMR structures of elk and of mouse/elk hybrids. *Proceedings of the National Academy of Sciences of the United States of America*, 102(3), 646-650.
- ¹⁹⁴ Kurt, T. D., Bett, C., Fernández-Borges, N., Joshi-Barr, S., Hornemann, S., Rüllicke, T., & Sigurdson, C. J. (2014). Prion transmission prevented by modifying the β 2- β 2 loop structure of host PrPC. *Journal of Neuroscience*, 34(3), 1022-1027.
- ¹⁹⁵ Salamat, M. K., Dron, M., Chapuis, J., Langevin, C., & Laude, H. (2011). Prion propagation in cells expressing PrP glycosylation mutants. *Journal of virology*, 85(7), 3077-3085.
- ¹⁹⁶ Naslavsky, N., Stein, R., Yanai, A., Friedlander, G., & Taraboulos, A. (1997). Characterization of detergent-insoluble complexes containing the cellular prion protein and its scrapie isoform. *Journal of Biological Chemistry*, 272(10), 6324-6331.
- ¹⁹⁷ Caputo, A., Sarnataro, D., Campana, V., Costanzo, M., Negro, A., Sorgato, M. C., & Zurzolo, C. (2010). Doppel and PrPC co-immunoprecipitate in detergent-resistant membrane domains of epithelial FRT cells. *Biochemical Journal*, 425(2), 341-351.
- ¹⁹⁸ Endo, T., Groth, D., Prusiner, S. B., & Kobata, A. (1989). Diversity of oligosaccharide structures linked to asparagines of the scrapie prion protein. *Biochemistry*, 28(21), 8380-8388.
- ¹⁹⁹ Haraguchi, T., Fisher, S., Olofsson, S., Endo, T., Groth, D., Tarentino, A., ... & Lycke, E. (1989). Asparagine-linked glycosylation of the scrapie and cellular prion proteins. *Archives of biochemistry and biophysics*, 274(1), 1-13.
- ²⁰⁰ Rogers, M., Taraboulos, A., Scott, M., Groth, D., & Prusiner, S. B. (1990). Intracellular accumulation of the cellular prion protein after mutagenesis of its Asn-linked glycosylation sites. *Glycobiology*, 1(1), 101-109.
- ²⁰¹ Salès, N., Rodolfo, K., Hässig, R., Faucheux, B., Di Gamberardino, L., & Moya, K. L. (1998). Cellular prion protein localization in rodent and primate brain. *European Journal of Neuroscience*, 10(7), 2464-2471.
- ²⁰² Weissmann, C., Raeber, A. J., Montrasio, F., Hegyi, I., Frigg, R., Klein, M. A., & Aguzzi, A. (2001). Prions and the lymphoreticular system. *Philosophical Transactions of the Royal Society of London. Series B*, 356(1406), 177-184.
- ²⁰³ Goldmann, W., O'Neill, G., Cheung, F., Charleson, F., Ford, P., & Hunter, N. (1999). PrP (prion) gene expression in sheep may be modulated by alternative polyadenylation of its messenger RNA. *Journal of general virology*, 80(8), 2275-2283.

-
- ²⁰⁴ Prusiner, S. B., Groth, D. F., Bildstein, C., Masiarz, F. R., McKinley, M. P., & Cochran, S. P. (1980). Electrophoretic properties of the scrapie agent in agarose gels. *Proceedings of the National Academy of Sciences*, 77(5), 2984-2988.
- ²⁰⁵ Pan, K. M., Baldwin, M., Nguyen, J., Gasset, M., Serban, A. N. A., Groth, D., & Cohen, F. E. (1993). Conversion of alpha-helices into beta-sheets features in the formation of the scrapie prion proteins. *Proceedings of the National Academy of Sciences*, 90(23), 10962-10966.
- ²⁰⁶ Come, J. H., Fraser, P. E., & Lansbury, P. T. (1993). A kinetic model for amyloid formation in the prion diseases: importance of seeding. *Proceedings of the National Academy of Sciences*, 90(13), 5959-5963.
- ²⁰⁷ Sandberg, M. K., Al-Doujaily, H., Sharps, B., Clarke, A. R., & Collinge, J. (2011). Prion propagation and toxicity in vivo occur in two distinct mechanistic phases. *Nature*, 470(7335), 540-542.
- ²⁰⁸ Cronier, S., Gros, N., Tattum, M. H., Jackson, G. S., Clarke, A. R., Collinge, J., & Wadsworth, J. D. (2008). Detection and characterization of proteinase K-sensitive disease-related prion protein with thermolysin. *Biochemical Journal*, 416(2), 297-305.
- ²⁰⁹ Vázquez-Fernández, E., Alonso, J., Pastrana, M. A., Ramos, A., Stitz, L., Vidal, E., & Requena, J. R. (2012). Structural organization of mammalian prions as probed by limited proteolysis. *PLoS One*, 7(11), e50111.
- ²¹⁰ Concha-Marambio, L., Diaz-Espinoza, R., & Soto, C. (2014). The extent of protease resistance of misfolded prion protein is highly dependent on the salt concentration. *Journal of Biological Chemistry*, 289(5), 3073-3079.
- ²¹¹ Dron, M., Moudjou, M., Chapuis, J., Salamat, M. K. F., Bernard, J., Cronier, S., & Laude, H. (2010). Endogenous proteolytic cleavage of disease-associated prion protein to produce C2 fragments is strongly cell-and tissue-dependent. *Journal of Biological Chemistry*, 285(14), 10252-10264.
- ²¹² Nicot, S., & Baron, T. G. (2010). Strain-specific proteolytic processing of the prion protein in prion diseases of ruminants transmitted in ovine transgenic mice. *Journal of general virology*, 91(2), 570-574.
- ²¹³ D'Castro, L., Wenborn, A., Gros, N., Joiner, S., Cronier, S., Collinge, J., & Wadsworth, J. D. (2010). Isolation of proteinase K-sensitive prions using pronase E and phosphotungstic acid. *PLoS One*, 5(12), e15679.
- ²¹⁴ Eigen, M. (1996). Prionics or the kinetic basis of prion diseases. *Biophysical chemistry*, 63(1), A1-A18.
- ²¹⁵ Prusiner, S. B. (1991). Molecular biology of prion diseases. *Science*, 252(5012), 1515-1523.
- ²¹⁶ Kaneko, K., Zulianello, L., Scott, M., Cooper, C. M., Wallace, A. C., James, T. L., & Prusiner, S. B. (1997). Evidence for protein X binding to a discontinuous epitope on the cellular prion protein during scrapie prion propagation. *Proceedings of the National Academy of Sciences*, 94(19), 10069-10074.

-
- ²¹⁷ Rubenstein, R., Gray, P. C., Cleland, T. J., Piltch, M. S., Hlavacek, W. S., Roberts, R. M., & Kim, J. I. (2007). Dynamics of the nucleated polymerization model of prion replication. *Biophysical chemistry*, 125(2), 360-367.
- ²¹⁸ Morris, A. M., Watzky, M. A., Agar, J. N., & Finke, R. G. (2008). Fitting Neurological Protein Aggregation Kinetic Data via a 2-Step, Minimal/"Ockham's Razor" Model: The Finke-Watzky Mechanism of Nucleation Followed by Autocatalytic Surface Growth. *Biochemistry*, 47(8), 2413-2427.
- ²¹⁹ Knowles, T. P., Waudby, C. A., Devlin, G. L., Cohen, S. I., Aguzzi, A., Vendruscolo, M., & Dobson, C. M. (2009). An analytical solution to the kinetics of breakable filament assembly. *Science*, 326(5959), 1533-1537.
- ²²⁰ Soto, C., Saborio, G. P., & Anderes, L. (2002). Cyclic amplification of protein misfolding: application to prion-related disorders and beyond. *Trends in neurosciences*, 25(8), 390-394.
- ²²¹ Atarashi, R., Wilham, J. M., Christensen, L., Hughson, A. G., Moore, R. A., Johnson, L. M., & Caughey, B. (2008). Simplified ultrasensitive prion detection by recombinant PrP conversion with shaking. *Nature Methods*, 5(3), 211-212.
- ²²² Robinson, S. J., Samuel, M. D., O'rourke, K. I., & Johnson, C. J. (2012). The role of genetics in chronic wasting disease of North American cervids. *Prion*, 6(2), 153-162.
- ²²³ Lehmann, S., & Harris, D. A. (1997). Blockade of glycosylation promotes acquisition of scrapie-like properties by the prion protein in cultured cells. *Journal of Biological Chemistry*, 272(34), 21479-21487.
- ²²⁴ Kimberlin, R. H., & Walker, C. A. (1978). Pathogenesis of mouse scrapie: effect of route of inoculation on infectivity titres and dose-response curves. *Journal of comparative pathology*, 88(1), 39-47.
- ²²⁵ Stumpf, M. P., & Krakauer, D. C. (2000). Mapping the parameters of prion-induced neuropathology. *Proceedings of the National Academy of Sciences*, 97(19), 10573-10577.
- ²²⁶ Mohan, J., Bruce, M. E., & Mabbott, N. A. (2005). Follicular dendritic cell dedifferentiation reduces scrapie susceptibility following inoculation via the skin. *Immunology*, 114(2), 225-234.
- ²²⁷ Manson, J. C., Clarke, A. R., McBride, P. A., McConnell, I., & Hope, J. (1994). PrP gene dosage determines the timing but not the final intensity or distribution of lesions in scrapie pathology. *Neurodegeneration: a journal for neurodegenerative disorders, neuroprotection, and neuroregeneration*, 3(4), 331-340.
- ²²⁸ Bett, C., Fernández-Borges, N., Kurt, T. D., Lucero, M., Nilsson, K. P. R., Castilla, J., & Sigurdson, C. J. (2012). Structure of the β 2- β 2 loop and interspecies prion transmission. *The FASEB Journal*, 26(7), 2868-2876.
- ²²⁹ Dovidchenko, N. V., Leonova, E. I., & Galzitskaya, O. V. (2014). Mechanisms of amyloid fibril formation. *Biochemistry (Moscow)*, 79(13), 1515-1527.
- ²³⁰ Haire, L. F., Whyte, S. M., Vasisht, N., Gill, A. C., Verma, C., Dodson, E. J., & Bayley, P. M. (2004). The crystal structure of the globular domain of sheep prion protein. *Journal of molecular biology*, 336(5), 1175-1183.

-
- ²³¹ Requena, J. R., & Wille, H. (2014). The structure of the infectious prion protein: experimental data and molecular models. *Prion*, 8(1), 60-66.
- ²³² Silveira, J. R., Raymond, G. J., Hughson, A. G., Race, R. E., Sim, V. L., Hayes, S. F., & Caughey, B. (2005). The most infectious prion protein particles. *Nature*, 437(7056), 257-261.
- ²³³ Tixador, P., Herzog, L., Reine, F., Jaumain, E., Chapuis, J., Le Dur, A., & Beringue, V. (2010). The physical relationship between infectivity and prion protein aggregates is strain-dependent. *PLoS Pathog*, 6(4), e1000859.
- ²³⁴ Groveman, B. R., Kraus, A., Raymond, L. D., Dolan, M. A., Anson, K. J., Dorward, D. W., & Caughey, B. (2015). Charge neutralization of the central lysine cluster in prion protein (PrP) promotes PrP^{Sc}-like folding of recombinant PrP amyloids. *Journal of Biological Chemistry*, 290(2), 1119-1128.
- ²³⁵ Hafner-Bratkovič, I., Bester, R., Pristovšek, P., Gaedtke, L., Verani, P., Gašperšič, J., & Aguzzi, A. (2011). Globular domain of the prion protein needs to be unlocked by domain swapping to support prion protein conversion. *Journal of Biological Chemistry*, 286(14), 12149-12156.
- ²³⁶ Welker, E., Wedemeyer, W. J., & Scheraga, H. A. (2001). A role for intermolecular disulfide bonds in prion diseases?. *Proceedings of the National Academy of Sciences*, 98(8), 4334-4336.
- ²³⁷ Biasini, E., Tapella, L., Restelli, E., Pozzoli, M., Massignan, T., & Chiesa, R. (2010). The hydrophobic core region governs mutant prion protein aggregation and intracellular retention. *Biochemical Journal*, 430(3), 477-486.
- ²³⁸ Lee, S., Antony, L., Hartmann, R., Knaus, K. J., Surewicz, K., Surewicz, W. K., & Yee, V. C. (2010). Conformational diversity in prion protein variants influences intermolecular β -sheet formation. *The EMBO journal*, 29(1), 251-262.
- ²³⁹ Rudd, P. M., Endo, T., Colominas, C., Groth, D., Wheeler, S. F., Harvey, D. J., & Dwek, R. A. (1999). Glycosylation differences between the normal and pathogenic prion protein isoforms. *Proceedings of the National Academy of Sciences*, 96(23), 13044-13049.
- ²⁴⁰ Moudjou, M., Treguer, E., Rezaei, H., Sabuncu, E., Neuendorf, E., Groschup, M. H., & Laude, H. (2004). Glycan-controlled epitopes of prion protein include a major determinant of susceptibility to sheep scrapie. *Journal of virology*, 78(17), 9270-9276.
- ²⁴¹ Quittot, N., Sebastiao, M., & Bourgault, S. (2017). Modulation of amyloid assembly by glycosaminoglycans: from mechanism to biological significance. *Biochemistry and Cell Biology*.
- ²⁴² Sobrova, P., Blazkova, I., Chomoucka, J., Drbohlavova, J., Vaculovicova, M., Kopel, P., & Adam, V. (2013). Quantum dots and prion proteins: is this a new challenge for neurodegenerative diseases imaging?. *Prion*, 7(5), 349-358.
- ²⁴³ Diaz-Espinoza, R., & Soto, C. (2012). High-resolution structure of infectious prion protein: the final frontier. *Nature structural & molecular biology*, 19(4), 370.
- ²⁴⁴ Rodriguez, J. A., Jiang, L., & Eisenberg, D. S. (2017). Toward the atomic structure of PrP^{Sc}. *Cold Spring Harbor perspectives in biology*, 9(9), a031336.

-
- ²⁴⁵ Sawaya, M. R., Sambashivan, S., Nelson, R., Ivanova, M. I., Sievers, S. A., Apostol, M. I., & Madsen, A. Ø. (2007). Atomic structures of amyloid cross- β spines reveal varied steric zippers. *Nature*, *447*(7143), 453-457.
- ²⁴⁶ Fitzpatrick, A. W., Debelouchina, G. T., Bayro, M. J., Clare, D. K., Caporini, M. A., Bajaj, V. S., & MacPhee, C. E. (2013). Atomic structure and hierarchical assembly of a cross- β amyloid fibril. *Proceedings of the National Academy of Sciences*, *110*(14), 5468-5473.
- ²⁴⁷ Falsig, J., Nilsson, K. P. R., Knowles, T. P., & Aguzzi, A. (2008). Chemical and biophysical insights into the propagation of prion strains. *HFSP journal*, *2*(6), 332-341.
- ²⁴⁸ Watts JC, Balachandran A, Westaway D (2006) The expanding universe of prion diseases. *PLoS Pathog* *2*(3): e26.
- ²⁴⁹ Barrette, I., Poisson, G., Gendron, P., & Major, F. (2001). Pseudoknots in prion protein mRNAs confirmed by comparative sequence analysis and pattern searching. *Nucleic Acids Research*, *29*(3), 753-758.
- ²⁵⁰ Bassant, M. H., Cathala, F., Court, L., Gourmelon, P., & Hauw, J. J. (1984). Experimental scrapie in rats: first electrophysiological observations. *Electroencephalography and clinical neurophysiology*, *57*(6), 541-547.
- ²⁵¹ Gomi, H., Ikeda, T., Kunieda, T., Itohara, S., Prusiner, S. B., & Yamanouchi, K. (1994). Prion protein (Prp) is not involved in the pathogenesis of spongiform encephalopathy in zitter rats. *Neuroscience letters*, *166*(2), 171-174.
- ²⁵² Málaga-Trillo, E., & Sempou, E. (2009). PrPs: Proteins with a purpose-Lessons from the zebrafish. *Prion*, *3*(3), 129-133.
- ²⁵³ Málaga-Trillo, E., Salta, E., Figueras, A., Panagiotidis, C., & Sklaviadis, T. (2011). Fish models in prion biology: underwater issues. *Biochimica et Biophysica Acta (BBA)-Molecular Basis of Disease*, *1812*(3), 402-414.
- ²⁵⁴ Choi, J. K., Jeon, Y. C., Lee, D. W., Oh, J. M., Lee, H. P., Jeong, B. H., ... & Kim, Y. S. (2010). A Drosophila model of GSS syndrome suggests defects in active zones are responsible for pathogenesis of GSS syndrome. *Human molecular genetics*, *19*(22), 4474-4489.
- ²⁵⁵ Fernandez-Funez, P., Casas-Tinto, S., Zhang, Y., Gómez-Velazquez, M., Morales-Garza, M. A., Cepeda-Nieto, A. C., ... & Rincon-Limas, D. E. (2009). In vivo generation of neurotoxic prion protein: role for hsp70 in accumulation of misfolded isoforms. *PLoS Genet*, *5*(6), e1000507.
- ²⁵⁶ Park, K. W., & Li, L. (2008). Cytoplasmic expression of mouse prion protein causes severe toxicity in *Caenorhabditis elegans*. *Biochemical and biophysical research communications*, *372*(4), 697-702.
- ²⁵⁷ Kimberlin, R. H., & Walker, C. A. (1977). Characteristics of a short incubation model of scrapie in the golden hamster. *Journal of General Virology*, *34*(2), 295-304.
- ²⁵⁸ Shi, Q., Zhang, B. Y., Gao, C., Zhang, J., Jiang, H. Y., Chen, C., & Dong, X. P. (2012). Mouse-adapted scrapie strains 139A and ME7 overcome species barrier to induce experimental scrapie in hamsters and changed their pathogenic features. *Virology journal*, *9*(1), 63.

-
- ²⁵⁹ Morales, R., Hu, P. P., Duran-Aniotz, C., Moda, F., Diaz-Espinoza, R., Chen, B., & Soto, C. (2016). Strain-dependent profile of misfolded prion protein aggregates. *Scientific reports*, 6, 20526.
- ²⁶⁰ Safar, J., Wille, H., Itri, V., Groth, D., Serban, H., Torchia, M., & Prusiner, S. B. (1998). Eight prion strains have PrP Sc molecules with different conformations. *Nature medicine*, 4(10), 1157.
- ²⁶¹ Novitskaya, V., Makarava, N., Bellon, A., Bocharova, O. V., Bronstein, I. B., Williamson, R. A., & Baskakov, I. V. (2006). Probing the conformation of the prion protein within a single amyloid fibril using a novel immunoconformational assay. *Journal of Biological Chemistry*, 281(22), 15536-15545.
- ²⁶² Shindoh, R., Kim, C. L., Song, C. H., Hasebe, R., & Horiuchi, M. (2009). The region approximately between amino acids 81 and 137 of proteinase K-resistant PrPSc is critical for the infectivity of the Chandler prion strain. *Journal of virology*, 83(8), 3852-3860.
- ²⁶³ Reid, C. M. (2014). *Prion strain adaptation: breaking and building species barriers* (Doctoral dissertation, Colorado State University Libraries).
- ²⁶⁴ Sigurdson, C. J., Manco, G., Schwarz, P., Liberski, P., Hoover, E. A., Hornemann, S., & Aguzzi, A. (2006). Strain fidelity of chronic wasting disease upon murine adaptation. *Journal of virology*, 80(24), 12303-12311.
- ²⁶⁵ Lee, Y. H., Sohn, H. J., Kim, M. J., Kim, H. J., Park, K. J., Lee, W. Y., & Balachandran, A. (2013). Experimental chronic wasting disease in wild type VM mice. *Journal of Veterinary Medical Science*, 75(8), 1107-1110.
- ²⁶⁶ Heisey, D. M., Mickelsen, N. A., Schneider, J. R., Johnson, C. J., Johnson, C. J., Langenberg, J. A., & Barr, D. J. (2010). Chronic wasting disease (CWD) susceptibility of several North American rodents that are sympatric with cervid CWD epidemics. *Journal of virology*, 84(1), 210-215.
- ²⁶⁷ Bosque, P. J., & Prusiner, S. B. (2000). Cultured cell sublines highly susceptible to prion infection. *Journal of virology*, 74(9), 4377-4386.
- ²⁶⁸ Marbiah, M. M., Harvey, A., West, B. T., Louzolo, A., Banerjee, P., Alden, J., & Bloom, G. S. (2014). Identification of a gene regulatory network associated with prion replication. *The EMBO journal*, e201387150.
- ²⁶⁹ Bian, J., Kang, H. E., & Telling, G. C. (2014). Quinacrine promotes replication and conformational mutation of chronic wasting disease prions. *Proceedings of the National Academy of Sciences*, 111(16), 6028-6033.
- ²⁷⁰ Ramljak, S., Asif, A. R., Armstrong, V. W., Wrede, A., Groschup, M. H., Buschmann, A., & Zerr, I. (2008). Physiological role of the cellular prion protein (PrPc): protein profiling study in two cell culture systems. *Journal of proteome research*, 7(7), 2681-2695.
- ²⁷¹ Oelschlegel, A. M., Fallahi, M., Ortiz-Umpierre, S., & Weissmann, C. (2012). The Extended Cell Panel Assay (ECPA) characterizes the relationship of RML, 79A and 139A prion strains and reveals conversion of 139A to 79A-like prions in cell culture. *Journal of virology*, JVI-00181.

-
- ²⁷² Zou, R. S., Fujioka, H., Guo, J. P., Xiao, X., Shimoji, M., Kong, C., & Moudjou, M. (2011). Characterization of spontaneously generated prion-like conformers in cultured cells. *Aging (Albany NY)*, 3(10), 968-984.
- ²⁷³ Edgeworth, J. A., Gros, N., Alden, J., Joiner, S., Wadsworth, J. D., Linehan, J., & Collinge, J. (2010). Spontaneous generation of mammalian prions. *Proceedings of the National Academy of Sciences*, 107(32), 14402-14406.
- ²⁷⁴ Brown, C. A., Schmidt, C., Poulter, M., Hummerich, H., Klöhn, P. C., Jat, P., & Lloyd, S. E. (2014). In vitro screen of prion disease susceptibility genes using the scrapie cell assay. *Human molecular genetics*, 23(19), 5102-5108.
- ²⁷⁵ Marbiah, M. M., Harvey, A., West, B. T., Louzolo, A., Banerjee, P., Alden, J., & Bloom, G. S. (2014). Identification of a gene regulatory network associated with prion replication. *The EMBO journal*, e201387150.
- ²⁷⁶ Molloy, B., & McMahon, H. E. (2014). A cell-biased effect of estrogen in prion infection. *Journal of virology*, 88(2), 1342-1353.
- ²⁷⁷ Pulford, B., Reim, N., Bell, A., Veatch, J., Forster, G., Bender, H., & Wyckoff, A. C. (2010). Liposome-siRNA-peptide complexes cross the blood-brain barrier and significantly decrease PrP C on neuronal cells and PrP RES in infected cell cultures. *PloS one*, 5(6), e11085.
- ²⁷⁸ Nishizawa, K., Oguma, A., Kawata, M., Sakasegawa, Y., Teruya, K., & Doh-ura, K. (2014). Efficacy and mechanism of a glycoside compound inhibiting abnormal prion protein formation in prion-infected cells: implications of interferon and phosphodiesterase 4D-interacting protein. *Journal of virology*, 88(8), 4083-4099.
- ²⁷⁹ Lu D, et al. (2013) Biaryl amides and hydrazones as therapeutics for prion disease in transgenic mice. *J Pharmacol Exp Ther* 347(2):325–338.
- ²⁸⁰ Li Z, et al. (2013) Discovery and preliminary SAR of arylpiperazines as novel, brain-penetrant antiprion compounds. *ACS Med Chem Letters* 4(4):397–401.
- ²⁸¹ Kimata A, et al. (2007) New series of antiprion compounds: Pyrazolone derivatives have the potent activity of inhibiting protease-resistant prion protein accumulation. *J Med Chem* 50(21):5053–5056.
- ²⁸² Geissen M, et al. (2011) From high-throughput cell culture screening to mouse model: Identification of new inhibitor classes against prion disease. *ChemMedChem* 6(10): 1928–1937.
- ²⁸³ Ghaemmaghami S, May BC, Renslo AR, Prusiner SB (2010) Discovery of 2-aminothiazoles as potent antiprion compounds. *J Virol* 84(7):3408–3412.
- ²⁸⁴ Bate, C., Salmons, M., Diomedes, L., & Williams, A. (2004). Squalenolol cures prion-infected neurons and protects against prion neurotoxicity. *Journal of Biological Chemistry*, 279(15), 14983-14990.
- ²⁸⁵ Kocisko, D. A., & Caughey, B. (2006). Searching for Anti-Prion Compounds: Cell-Based High-Throughput In Vitro Assays and Animal Testing Strategies. *Methods in enzymology*, 412, 223-234.
- ²⁸⁶ Li, J., Browning, S., Mahal, S. P., Oelschlegel, A. M., & Weissmann, C. (2010). Darwinian evolution of prions in cell culture. *Science*, 327(5967), 869-872.

-
- ²⁸⁷ Saborio, G. P., Permanne, B., & Soto, C. (2001). Sensitive detection of pathological prion protein by cyclic amplification of protein misfolding. *Nature*, *411*(6839), 810-813.
- ²⁸⁸ Soto, C., Saborio, G. P., & Anderes, L. (2002). Cyclic amplification of protein misfolding: application to prion-related disorders and beyond. *Trends in neurosciences*, *25*(8), 390-394
- ²⁸⁹ Atarashi, R., Wilham, J. M., Christensen, L., Hughson, A. G., Moore, R. A., Johnson, L. M., & Caughey, B. (2008). Simplified ultrasensitive prion detection by recombinant PrP conversion with shaking. *Nature Methods*, *5*(3), 211-212.
- ²⁹⁰ Klohn, P. C., L. Stoltze, E. Flechsig, M. Enari, and C. Weissmann. 2003. A quantitative, highly sensitive cell-based infectivity assay for mouse scrapie prions. *Proc Natl Acad Sci U S A* *100*:11666-71.
- ²⁹¹ van Der Merwe, J., Aiken, J., Westaway, D., & McKenzie, D. (2015). The standard scrapie cell assay: development, utility and prospects. *Viruses*, *7*(1), 180-198.
- ²⁹² Bosque, P. J., and S. B. Prusiner. 2000. Cultured cell sublines highly susceptible to prion infection. *J. Virol.* *74*:4377-4386.
- ²⁹³ Mahal, S. P., C. A. Demczyk, E. W. Smith, Jr., P. C. Klohn, and C. Weissmann. 2008. Assaying prions in cell culture: the standard scrapie cell assay (SSCA) and the scrapie cell assay in end point format (SCEPA). *Methods Mol. Biol.* *459*:49-68.
- ²⁹⁴ Christofinis, G. J., & Beale, A. J. (1968). Some biological characters of cell lines derived from normal rabbit kidney. *The Journal of Pathology*, *95*(2), 377-381.
- ²⁹⁵ Bian, J., Napier, D., Khaychuck, V., Angers, R., Graham, C., & Telling, G. (2010). Cell-based quantification of chronic wasting disease prions. *Journal of virology*, *84*(16), 8322-8326.
- ²⁹⁶ Khaychuk, V. (2012). Prion Characterization Using Cell Based Approaches. Doctoral Dissertation, University of Kentucky
- ²⁹⁷ Arellano-Anaya, Z. E., Savistchenko, J., Mathey, J., Huor, A., Lacroux, C., Andréoletti, O., & Vilette, D. (2011). A simple, versatile and sensitive cell-based assay for prions from various species. *PLoS One*, *6*(5), e20563.
- ²⁹⁸ Leblanc, P., S. Alais, I. Porto-Carreiro, S. Lehmann, J. Grassi, G. Raposo, and J. L. Darlix. 2006. Retrovirus infection strongly enhances scrapie infectivity release in cell culture. *EMBO J.* *25*:2674-2685.
- ²⁹⁹ Vilette, D., O. Andreoletti, F. Archer, M. F. Madelaine, J. L. Vilotte, S. Lehmann, and H. Laude. 2001. Ex vivo propagation of infectious sheep scrapie agent in heterologous epithelial cells expressing ovine prion protein. *Proc. Natl. Acad. Sci. U. S. A.* *98*:4055-4059
- ³⁰⁰ Sweeting B., Brown, E., Chakrabartty, A., & Pai, E. F. (2009). The structure of rabbit PrPC: clues into species barrier and prion disease susceptibility. *Canadian Light Source*, *28*.
- ³⁰¹ Sweeting, B, Brown E, Khan MQ, Chakrabartty A, Pai EF (2013) N-Terminal Helix-Cap in a-Helix 2 Modulates b-State Misfolding in Rabbit and Hamster Prion Proteins. *PLoS ONE* *8*(5)

-
- ³⁰² Chianini, F., Fernández-Borges, N., Vidal, E., Gibbard, L., Pintado, B., de Castro, J., & Pang, Y. (2012). Rabbits are not resistant to prion infection. *Proceedings of the National Academy of Sciences*, 109(13), 5080-5085.
- ³⁰³ Moore, R. A., Vorberg, I., & Priola, S. A. (2005). Species barriers in prion diseases – brief review. In *Infectious Diseases from Nature: Mechanisms of Viral Emergence and Persistence* (pp. 187-202). Springer Vienna.
- ³⁰⁴ Kocisko, D. A., & Caughey, B. (2006). Searching for Anti-Prion Compounds: Cell-Based High-Throughput In Vitro Assays and Animal Testing Strategies. *Methods in enzymology*, 412, 223-234.
- ³⁰⁵ Korth, C., May, B. C., Cohen, F. E., & Prusiner, S. B. (2001). Acridine and phenothiazine derivatives as pharmacotherapeutics for prion disease. *Proceedings of the National Academy of Sciences*, 98(17), 9836-9841.
- ³⁰⁶ Oelschlegel, A. M., Fallahi, M., Ortiz-Umpierre, S., & Weissmann, C. (2012). The Extended Cell Panel Assay (ECPA) characterizes the relationship of RML, 79A and 139A prion strains and reveals conversion of 139A to 79A-like prions in cell culture. *Journal of virology*, JVI-00181.
- ³⁰⁷ Lawson, V. A., L. J. Vella, J. D. Stewart, R. A. Sharples, H. Klemm, D. M. Machalek, C. L. Masters, R. Cappai, S. J. Collins, and A. F. Hill. 2008. Mouse-adapted sporadic human Creutzfeldt-Jakob disease prions propagate in cell culture. *Int. J. Biochem. Cell Biol.* 40:2793–2801.
- ³⁰⁸ Courageot, M. P., N. Daude, R. Nonno, S. Paquet, M. A. Di Bari, A. Le Dur, J. Chapuis, A. F. Hill, U. Agrimi, H. Laude, and D. Vilette. 2008. A cell line infectible by prion strains from different species. *J. Gen. Virol.* 89:341–347.
- ³⁰⁹ Oelschlegel, A. M., Fallahi, M., Ortiz-Umpierre, S., & Weissmann, C. (2012). The Extended Cell Panel Assay (ECPA) characterizes the relationship of RML, 79A and 139A prion strains and reveals conversion of 139A to 79A-like prions in cell culture. *Journal of virology*, JVI-00181.
- ³¹⁰ Pace, C. N., Fu, H., Fryar, K., Landua, J., Trevino, S. R., Schell, D., & Sevcik, J. (2014). Contribution of hydrogen bonds to protein stability. *Protein Science*, 23(5), 652-661.
- ³¹¹ Goldberg, M. E., Rudolph, R., & Jaenicke, R. (1991). A kinetic study of the competition between renaturation and aggregation during the refolding of denatured-reduced egg white lysozyme. *Biochemistry*, 30(11), 2790-2797.
- ³¹² Ohkuri, T., Nagatomo, S., Oda, K., So, T., Imoto, T., & Ueda, T. (2010). A protein's conformational stability is an immunologically dominant factor: evidence that free-energy barriers for protein unfolding limit the immunogenicity of foreign proteins. *The Journal of Immunology*, 185(7), 4199-4205.
- ³¹³ Huang, K. S., Bayley, H., Liao, M. J., London, E., & Khorana, H. G. (1981). Refolding of an integral membrane protein. Denaturation, renaturation, and reconstitution of intact bacteriorhodopsin and two proteolytic fragments. *Journal of Biological Chemistry*, 256(8), 3802-3809.

-
- ³¹⁴ Swietnicki, W., Petersen, R. B., Gambetti, P., & Surewicz, W. K. (1998). Familial mutations and the thermodynamic stability of the recombinant human prion protein. *Journal of Biological Chemistry*, 273(47), 31048-31052.
- ³¹⁵ Yeh, V., Broering, J. M., Romanyuk, A., Chen, B., Chernoff, Y. O., & Bommarium, A. S. (2010). The Hofmeister effect on amyloid formation using yeast prion protein. *Protein Science*, 19(1), 47-56.
- ³¹⁶ O'Brien, E. P., Dima, R. I., Brooks, B., & Thirumalai, D. (2007). Interactions between hydrophobic and ionic solutes in aqueous guanidinium chloride and urea solutions: lessons for protein denaturation mechanism. *Journal of the American Chemical Society*, 129(23), 7346-7353.
- ³¹⁷ De Simone, A., Dodson, G. G., Verma, C. S., Zagari, A., & Fraternali, F. (2005). Prion and water: tight and dynamical hydration sites have a key role in structural stability. *Proceedings of the National Academy of Sciences of the United States of America*, 102(21), 7535-7540.
- ³¹⁸ Yamada, T., Liu, X., Englert, U., Yamane, H., & Dronskowski, R. (2009). Solid-State Structure of Free Base Guanidine Achieved at Last. *Chemistry—A European Journal*, 15(23), 5651-5655.
- ³¹⁹ Mason, P. E., Neilson, G. W., Enderby, J. E., Saboungi, M. L., Dempsey, C. E., MacKerell, A. D., & Brady, J. W. (2004). The structure of aqueous guanidinium chloride solutions. *Journal of the American Chemical Society*, 126(37), 11462-11470.
- ³²⁰ Makhatadze, G. I., & Privalov, P. L. (1992). Protein interactions with urea and guanidinium chloride: a calorimetric study. *Journal of molecular biology*, 226(2), 491-505.
- ³²¹ Shih, O., England, A. H., Dallinger, G. C., Smith, J. W., Duffey, K. C., Cohen, R. C., & Saykally, R. J. (2013). Cation-cation contact pairing in water: Guanidinium. *The Journal of chemical physics*, 139(3), 07B616_1.
- ³²² Cooper, R. J., Heiles, S., DiTucci, M. J., & Williams, E. R. (2014). Hydration of guanidinium: second shell formation at small cluster size. *The Journal of Physical Chemistry A*, 118(30), 5657-5666.
- ³²³ Ball, P., & Hallsworth, J. E. (2015). Water structure and chaotropicity: their uses, abuses and biological implications. *Physical Chemistry Chemical Physics*, 17(13), 8297-8305.
- ³²⁴ Graziano, G. (2011). Contrasting the denaturing effect of guanidinium chloride with the stabilizing effect of guanidinium sulfate. *Physical Chemistry Chemical Physics*, 13(25), 12008-12014.
- ³²⁵ Kubíčková, A., Krátek, T., Coufal, P., Wernersson, E., Heyda, J., & Jungwirth, P. (2011). Guanidinium cations pair with positively charged arginine side chains in water. *The Journal of Physical Chemistry Letters*, 2(12), 1387-1389.
- ³²⁶ Hatefi, Y., & Hanstein, W. G. (1969). Solubilization of particulate proteins and nonelectrolytes by chaotropic agents. *Proceedings of the National Academy of Sciences*, 62(4), 1129-1136.

-
- ³²⁷ Salvi, G., De Los Rios, P., & Vendruscolo, M. (2005). Effective interactions between chaotropic agents and proteins. *Proteins: Structure, Function, and Bioinformatics*, 61(3), 492-499.
- ³²⁸ Sawyer, W. H., & Puckridge, J. (1973). The dissociation of proteins by chaotropic salts. *Journal of Biological Chemistry*, 248(24), 8429-8433.
- ³²⁹ Saijo E, Hughson AG, Raymond GJ, Suzuki A, Horiuchi M, Caughey B. 2016. PrPSc-specific antibody reveals C-terminal conformational differences between prion strains. *J Virol* 90:4905-4913.
- ³³⁰ Kunik, V., Peters, B., & Ofran, Y. (2012). Structural consensus among antibodies defines the antigen binding site. *PLoS Comput Biol*, 8(2), e1002388.
- ³³¹ Scarabelli, G., Morra, G., & Colombo, G. (2010). Predicting interaction sites from the energetics of isolated proteins: a new approach to epitope mapping. *Biophysical journal*, 98(9), 1966-1975.
- ³³² Stockmann, A., Hess, S., Declerck, P., Timpl, R., & Preissner, K. T. (1993). Multimeric vitronectin. Identification and characterization of conformation-dependent self-association of the adhesive protein. *Journal of Biological Chemistry*, 268(30), 22874-22882.
- ³³³ Amit, A. G., Mariuzza, R. A., Phillips, S. E. V., & Poljak, R. J. (1986). Three-dimensional structure of an antigen-antibody complex at 2.8 Å resolution. *Science*, 233, 747-754.
- ³³⁴ Schmidt, M. L., Murray, J., Lee, V. M., Hill, W. D., Wertkin, A., & Trojanowski, J. Q. (1991). Epitope map of neurofilament protein domains in cortical and peripheral nervous system Lewy bodies. *The American journal of pathology*, 139(1), 53.
- ³³⁵ McCutcheon S, Langeveld JPM, Tan BC, Gill AC, de Wolf C, et al. (2014) Prion Protein-Specific Antibodies That Detect Multiple TSE Agents with High Sensitivity. *PLoS ONE* 9(3)
- ³³⁶ Williamson, R. A., Peretz, D., Smorodinsky, N., Bastidas, R., Serban, H., Mehlhorn, I., & Burton, D. R. (1996). Circumventing tolerance to generate autologous monoclonal antibodies to the prion protein. *Proceedings of the national Academy of Sciences*, 93(14), 7279-7282.
- ³³⁷ Cordes, H., Bergström, A. L., Ohm, J., Laursen, H., & Heegaard, P. M. (2008). Characterisation of new monoclonal antibodies reacting with prions from both human and animal brain tissues. *Journal of immunological methods*, 337(2), 106-120.
- ³³⁸ Yuan, F. F., Biffin, S., Brazier, M. W., Suarez, M., Cappai, R., Hill, A. F., & Geczy, A. F. (2005). Detection of prion epitopes on PrP^C and PrP^{Sc} of transmissible spongiform encephalopathies using specific monoclonal antibodies to PrP. *Immunology and cell biology*, 83(6), 632-637.
- ³³⁹ Brannstrom K, Lindhagen-Persson M, Gharibyan AL, Iakovleva I, Vestling M, et al. (2014) A Generic Method for Design of Oligomer-Specific Antibodies. *PLoS ONE* 9(3)
- ³⁴⁰ Polymenidou, M., Moos, R., Scott, M., Sigurdson, C., Shi, Y. Z., Yajima, B., & Bellon, A. (2008). The POM monoclonals: a comprehensive set of antibodies to non-overlapping prion protein epitopes. *PLoS One*, 3(12), e3872.

-
- ³⁴¹ Doolan, K. M., & Colby, D. W. (2015). Conformation-dependent epitopes recognized by prion protein antibodies probed using mutational scanning and deep sequencing. *Journal of molecular biology*, 427(2), 328-340.
- ³⁴² Williamson, R. A., Peretz, D., Pinilla, C., Ball, H., Bastidas, R. B., Rozenshteyn, R., & Burton, D. R. (1998). Mapping the prion protein using recombinant antibodies. *Journal of Virology*, 72(11), 9413-9418.
- ³⁴³ Pan, T., Li, R., Kang, S. C., Wong, B. S., Wisniewski, T., & Sy, M. S. (2004). Epitope scanning reveals gain and loss of strain specific antibody binding epitopes associated with the conversion of normal cellular prion to scrapie prion. *Journal of neurochemistry*, 90(5), 1205-1217.
- ³⁴⁴ Kang, H. E., Weng, C. C., Saijo, E., Saylor, V., Bian, J., Kim, S., & Telling, G. C. (2012). Characterization of conformation-dependent prion protein epitopes. *Journal of Biological Chemistry*, 287(44), 37219-37232.
- ³⁴⁵ Sonati, T., Reimann, R. R., Falsig, J., Baral, P. K., O'Connor, T., Hornemann, S., & Swayampakula, M. (2013). The toxicity of anti-prion antibodies is mediated by the flexible tail of the prion protein. *Nature*, 501(7465), 102-106.
- ³⁴⁶ Klöhn, P. C., Farmer, M., Linehan, J. M., O'malley, C., de Marco, M. F., Taylor, W., & Collinge, J. (2012). PrP antibodies do not trigger mouse hippocampal neuron apoptosis. *Science*, 335(6064), 52-52.
- ³⁴⁷ Reimann, R. R., Sonati, T., Hornemann, S., Herrmann, U. S., Arand, M., Hawke, S., & Aguzzi, A. (2016). Differential toxicity of antibodies to the prion protein. *PLoS Pathog*, 12(1), e1005401.
- ³⁴⁸ Stanker, L. H., Serban, A. V., Cleveland, E., Hnasko, R., Lemus, A., Safar, J., & Prusiner, S. B. (2010). Conformation-dependent high-affinity monoclonal antibodies to prion proteins. *The Journal of Immunology*, 185(1), 729-737.

CHAPTER 2 - PRION STRAIN DIFFERENCES ARE DETECTABLE WITH AN EXPANDED CELL-BASED CONFORMATIONAL ASSAY IN FRESHLY INFECTED RK-PrP CELLS

A. INTRODUCTION

Prions cause invariably lethal, transmissible neurodegenerative diseases. There are no current effective treatments or cures for prion disease. Prion diseases affect a variety of mammals, including humans. Prion diseases do not stem from viruses, as originally proposed¹, instead these disease originate from genetic predisposition or infection². Prions replicate in the absence of nucleic acids, they instead undergo pathological endogenous protein misfolding via conformational corruption of cellular prion protein (PrP^C) by the pathogenic form (PrP^{Sc})^{3, 4, 5}. Single amino acid changes to the prion protein can have intense impact on transmission and susceptibility⁶. For example, a difference in amino acid at position 226 [deer (Q), elk (E)] has profound effects on the presentation of chronic wasting disease⁷.

The difference between the general tertiary structure between PrP^C and PrP^{Sc} was established over 20 years⁸ ago. Specifically, PrP^{Sc} is more β -sheet rich than the α -helix dominated PrP^C. Unlike PrP^C (Figure 1.2, 2.1A), PrP^{Sc} is a hardy, persistent molecule that resists proteinase digestion^{9, 10}, UV radiation¹¹, gamma radiation¹², formalin¹³, and environmental degradation¹⁴ because it can linger in soil for years¹⁵, contaminate local water sources¹⁶, and even absorbed by plants¹⁷. The stable cleavage products¹⁸ resulting from Proteinase K (PK) degradation^{9, 10} of PrP^{Sc} can be tissue dependent¹⁹ or strain specific²⁰. As such, PK resistance is a gold standard technique to

differentiate between PrP^C and PrP^{Sc}, and to differentiate between prion strains (Figure 1.3). Although PrP^C structure was resolved in the 1990s, the structure of PrP^{Sc} remains unresolved²¹. The existence of prion strains²² is a further complication in understanding prion structure.

Prion strains defy the conventional genetic-based definition that is applied to strains of viruses, bacteria, and fungi. Instead, prion strains properties rely on specific prion protein tertiary conformations²³ and as such a prion strain is defined as an infectious prion protein particle with a specific tertiary conformation²⁴ that produces a specific neurodegenerative phenotype²⁵. Specifically, a prion strain can be considered to have a strain-specific²⁶ disease phenotype²⁷ based on the prion's ability to be stably propagated, fidelity to neuropathology, disease length, glycosylation profile, molecular weight of PK-resistant PrP^{Sc}, resistance to denaturation, amyloid seeding potential and other molecular characteristics.

The scientific tools available to examine prions have evolved since scrapie was first described in 1772²⁸. The earliest prion research focused on bioassay, the passaging of infectious material in living animals^{29, 30}. The disease course and tissues collected from bioassay allowed researchers to develop tools to identify prions with neuropathology, disease length, and glycosylation profile, molecular weight of PK-resistant PrP^{Sc}, resistance to denaturation, and other molecular characteristics. Bioassay confirmed that the prion cellular protein is required for prion disease, i.e. PrP^C null (PrP-KO) mice do not get prion disease^{31, 32, 33}. However, studying prions in their host organism is inherently difficult due to the long incubation time, and ethical barriers to

empirical experimentation in humans. More amenable research models were explored by adapting prions into mice^{34, 35, 36, 37}, rats^{38, 39} and hamsters^{38, 39}.

Mice became the most convenient model system^{40, 41} with the creation of transgenic mice expressing a wide variety of PrP^C. For research purposes and ease of study, prions were adapted to infect mice in a more time efficient laboratory setting, such as scrapie⁴², TME⁴³, BSE⁴⁴, and CWD¹³⁷. Traditionally, mice that are inbred (WT), PrP^C over expressing mice, or mice that are transgenic (Tg)/Gene-targeted (Gt) for a heterologous PrP on a mouse-PrP null background are used. However, prion strain differentiation by bioassay remains time-consuming and financially costly, faster, higher throughput methods were needed.

The N2a⁴⁵, PK1⁴⁶, RK-PrP⁴⁷, NpL2⁴⁸, and HEK293⁴⁸ prion cell culture models, have been advantageous to examine a range of prion questions ranging from: prion adaption⁴⁹, spontaneous prion generation^{50, 51}, genetic variables that increase susceptibility^{52, 53}, the role of PrP^C in cellular function⁴⁸, modulators of infectivity (e.g. estrogen⁵⁴, siRNA⁵⁵, glycosides⁵⁶), to test anti-prion compounds^{57, 58, 59, 60, 61, 62, 63}, examine drug-induced prion evolution⁶⁴, and more. Prion cell culture models represented a new way to address questions about prion structure and characterize strains. Furthermore, new techniques, like the scrapie cell assay (SCA)⁶⁵, were generated specifically for use in prion cell culture models. The SCA was the first highly sensitive, reliable method to examine prion titre in cell culture; however, it had limited applications⁶⁶ due to a small subset of cell types⁶⁷ and laboratory-generated strains⁶⁸.

Unlike the cell lines used in the SCA, the rabbit kidney epithelial⁶⁹ (RK13) cell

culture model has vastly expanded the species and prion strains that could be examined. Specifically, RK13 cells transfected^{70,71} to stably express a pIRESpuro3 vector containing the PrP^C gene of choice⁷² and pcDNA3-gag expressing HIV-1 GAG precursor protein to enhance the release of PrP^C⁷³. This transfection paradigm works because RK13 cells do not endogenously express PrP^C⁷⁴ and rabbits are relatively resistant to prion disorders^{75,76,77,78}. RK-PrP cell lines have been useful to examine prion titre⁷⁹, anti-prion drug screening^{80,81}, and strain differentiation⁸². A significant advancement in the prion field^{83,84} was the ability to infect naïve cell culture models and perpetually propagate prion infection, also called “chronically infected” cell lines. These chronically infected lines effectively expanded the ability to address questions about prion structure and further characterize strains⁸⁵. Both naïve and chronically infected forms of the RK-PrP prion cell culture model was used in this dissertation.

The advancements in cell culture models allowed a more manageable prion conformational stability assays (CSA) to be created. Prion conformational stability assays use chaotropic agents to assess relative resistance of prions to protease degradation after partial denaturation to examine PrP^{Sc}. Chaotropic agents disturb the hydrogen bonding of water⁸⁶ around a protein, destabilizing the three-dimensional structure of a protein. This destabilization causes proteins to undergo a denaturation-renaturation event, where they unfold and re-fold. This denaturation and renaturation can be seen in Lysozyme^{87,88}, Bacteriorhodopsin⁸⁹, bacterial grown PrP⁹⁰, yeast prions⁹¹, mammalian prions²⁶, and PrP^{Sc}⁹². Hydrogen bonding of water is important to prion protein structural stability⁹³.

Although the use of chaotropic agents to indirectly study protein structure is not unique to the prion field^{94, 95, 96}, the prion field utilizes chaotropic agents via denaturation curves as a means to interrogate PrP^{Sc} structure and distinguish between different prion strains. Traditionally, CSAs depends on western blot⁴⁹, dot blot or enzyme linked immunosorbent assays (ELISA)⁹⁷ to visualize prion response to protease degradation after partial denaturation. The cell-based conformational stability assay⁷⁹ (C-CSA) utilizes GdnHCl in the RK-PrP cell system to examine differences between prion strains (Figure 2.2). The structure of guanidine is known^{98, 99} and as a chaotropic agent, GdnHCl, is a highly effective tool to denature proteins¹⁰⁰ via its interactions with water^{101, 102, 103}. Interestingly, GdnHCl stabilizes proteins during the transition period between the original form and renatured form¹⁰⁴ of the protein by pairing with positively charged Arginine side chains¹⁰⁵.

The specific conformational stability of prions has not been clarified because many of CSAs have focused on a single antibody^{106, 107} or a single strain¹⁰⁸. The knowledge garnered from interrogating a single antibody epitope is limited. Additionally, the precision of structural knowledge gained was lacking until the antibodies were epitope-mapped. Epitope-mapping an antibody is a process to identify the amino acids that the antibody Fab region binds^{109 110}. The use of denaturation, epitope-mapped antibodies, and conformational specific antibodies to probe protein structure is not unique to the prion protein, e.g. vitronectin¹¹¹, lysozyme¹¹², and neurofilament¹¹³. To expand understanding of the prion protein, a plethora of anti-prion

antibodies^{114, 115, 116, 117}, glycosylation specific antibodies¹¹⁸, and anti-amyloid antibodies¹¹⁹ have been generated.

Epitope mapping has been done with several anti-prion antibodies^{120, 121, 122, 123}, and, importantly, with antibodies our lab generated¹²⁴ (Figure 2.1B). Mapped antibodies have been explored for anti-prion qualities^{125, 126, 127}. In hopes of understanding more about the structure of both PrP^C and PrP^{Sc}, conformationally dependent antibodies¹²⁸ have been used to examine prion structure. Conformationally dependent antibodies require the protein to be in a specific conformation, as the epitope regions are discontinuous. Using a wide array of antibodies with varied epitopes clarifies subtle structural variation present between strains.

Although murine-adapted Rocky Mountain Laboratory (RML)¹²⁹ and 22L^{130, 131} scrapie strains have been around for over 50 years, the specific conformational differences between strains have not been clarified. As mentioned, most CSA focused on a single strain¹⁰⁸ or single antibody^{106, 107}. The two most detailed examinations of murine-adapted scrapie were (1) RML strain via conformational stability evaluated eight antibody epitopes via western blotting¹³² and (2), Chandler (RML), 22L, and Me7 were evaluated with twelve epitope-mapped antibodies via an ELISA system⁹⁷.

Chronic wasting disease strains have not been examined with conformational stability assays to the same extent as murine-adapted scrapie. CWD strains have been examined primarily with bioassay⁷. CWD bioassays have shown that the primary structure of PrP^C impacts susceptibility¹³³, and can generate multiple strains¹³⁴. Previous research focused on using western blot conformational stability to compare CWD to

emergent strains, different prion strains, or to compare CWD to prions in other species¹³⁵. However, an in-depth analysis of CWD conformational stability at multiple epitopes has not been performed to date. Additionally, unlike the early murine adaption of scrapie, CWD (cervid prion disease) has only recently been adapted into mice. Unfortunately the strain term “mCWD” encompasses 4 very distinct murine adaption events: deer CWD (isolate D10) into FVB inbred mice, then into C57BL/6 inbred mice¹³⁶, mule deer CWD isolate into Tg20¹³⁷, Elk CWD (brain pool E190Y+2229Y) into VM/Dk inbred mice¹³⁸, and white-tail deer CWD (Wisconsin isolate) into wild mice¹³⁹. Due to “mCWD” being a unified name for these recent multiple strain adaptations, the conformation and molecular characteristics of mouse-adapted CWD has not been well characterized. To strive for clarity, the mouse-adapted CWD strain that originated from isolate D10¹³⁶ will be referred to in this and subsequent chapters as “mD10” and not “mCWD.”

We have developed a more facile, expedient, and expanded cell-based conformational stability assay (C-CSA) combines methodology using chaotropic agents to probe epitope-mapped regions of the prion protein. The goal was to create a map of specific regional differences between strains and to help resolve how strains differ structurally. The C-CSA allows data to be gathered across multiple species, with multiple infectious prions, and more importantly provides a high-throughput method to examine the prion protein at multiple epitopes, simultaneously. Interrogation of the prion protein at multiple known epitopes can further delineate structural characteristics of PrP^{Sc}. Our expanded C-CSA recapitulates previous published data⁴⁷ showing

stability differences between CWD prions in deer (Q226) and elk (E226). Surprisingly, the C-CSA revealed a range of amyloid forms are present, which is seen in neuropathological analysis and amyloid detection with semi-denaturing detergent agarose gel electrophoresis (SDD-AGE). Additionally, the C-CSA is able to differentiate between three prion strains that contain the same mouse-PrP amino acid sequence: two classically murine-adapted scrapie RML and 22L strains and a more recent CWD murine-adapted prion strain (mD10). Specifically, the use of antibodies to probe multiple epitopes ranging from unstructured to globular regions revealed pronounced slope differences that further define these two classically used prions as being separate strains, and reinforced that mD10 contains a novel structure. Consequently, the C-CSA represents a new tool to reveal more details about prion strain structure in a facile and expedient process.

B. MATERIALS AND METHODOLOGY

Tissue Homogenization

Brains from sacrificed prion-infected, naïve (mock infected), and PrP-KO (null for prion cellular protein) mice were stored at -80°C. The brains passaged repeatedly through an 18-gauge, 23-gauge, and 26-gauge needle in cold sterile phosphate buffered saline (PBS) lacking Ca²⁺ and Mg²⁺ (Hyclone, Pittsburg, PA) to yield either 10% weight/volume (w/v) or 20%w/v brain homogenates. Brain homogenates were aliquoted and stored at -80°C until use.

Mouse Model

An inbred mouse line (C57BL/6) was purchased from Jackson Laboratories (Bar Harbor, ME). Transgenic mice (Tg(DeerPrP)1536^{+/-} and Tg(ElkPrP)5037^{+/-}) were generated as previously described^{140,141}; the transgenic mice used in experiments described in this dissertation only expressed a single allele of the prion cellular protein (i.e. heterologous expression of PrP^C). All mice were bred and maintained by Sehun Kim under protocols approved by the Institutional Animal Care and Use Committee (IACUC) at Colorado State University.

Mouse Infections

Inbred mouse line (C57BL/6) or transgenic mice (Tg(DeerPrP)1536^{+/-} and Tg(ElkPrP)5037^{+/-} mice) were anesthetized with isoflurane inhalation and intracerebrally inoculated. Specifically, 30 μ L of PBS lacking Ca²⁺ and Mg²⁺ (Hyclone, Pittsburg, PA) or infectious prion brain homogenate (1% w/v brain homogenate in PBS) was intracerebral inoculated through the coronal suture. Mice were monitored for clinical signs weekly; disease diagnosis was based off of identification of at least three clinical signs (e.g. truncal ataxia, loss of extensor reflex, hunched posture, difficulty righting, loss of tail pinch response, limb paralysis, circling, weight loss, tail rigidity, etc.). When mice presented increasingly poor health (nearing death) they were considered terminally ill and euthanized. Specifically, the mice were suffocated with CO₂ according to established Institutional Animal Care and Use Committee (IACUC) protocols. The organs (brain, spleen, etc.) were harvested, frozen and stored at -80°C until use.

Cell Model

Rabbit Kidney Epithelial (RK13)¹⁴² cells, lacking endogenous expression of the prion cellular protein²⁷, were purchased from the American Type Culture Collection (ATCC, Manassas, VA). RK13 cells were transfected to stably express a pIRESpuro3 vector (Clontech, Mountain View, CA) and pcDNA3-gag expressing HIV-1 GAG precursor protein as described previously^{70, 71, 79}. In brief, RK13 cells were maintained in Dulbecco's Modified Eagle's Medium (DMEM) high glucose (Invitrogen, Carlsbad, CA), supplemented with 10% Fetal Bovine Serum (FBS) (Gibco Life Technologies, Grand Island, NY), and 1% Penicillin/Streptomycin (P/S) (Gibco Life Technologies, Grand Island, NY), under saturated humidity and 5% CO₂ conditions at 37°C. RK13 cells grow to confluency as a single monolayer in cell culture. The prion protein (PrP) coding sequence for mouse, deer and elk were PCR amplified with primers containing *AflI* and *EcoRI* restriction sites; digested amplicons were inserted into the pIRESpuro3 vector (Clontech, Mountain View, CA). The resulting recombinant vector was transfected using Lipofectamine (Invitrogen, Carlsbad, CA) and Opti-MEM (Gibco Life Technologies, Grand Island, NY) into RK13 cells. RK13 cells transfected with an empty vector (pIRESpuro3 without PrP) produced RKV cells that are used as negative controls. Cells were then subjected selection pressure via 2.5 µg/mL puromycin (Sigma-Aldrich, St. Louis, MO) in media. Bulk transfected cell lines were maintained by splitting dilution 1:10 every five days after trypsin disassociation, stabilized, and screened for prion protein expression (via western blotting cell lysate). Cells were then challenged with prions from brain homogenate from mice diagnosed terminally ill with prion disease. Prion infected cells were then single cell cloned, saving highly infected cells.

Highly prion infected clones were then single cell cloned; cured (cell lines that no longer show prion infection) clones were segregated from chronically infected (cell lines that propagate prion infection). Cured clones were then split into two plates, one to passage and one as a repeated prion challenge. Cured clones that were able to be re-infected were considered prion sensitive, and cured clones that were not able to be re-infected were considered prion resistant. For prion infection paradigms, prion sensitive cells were utilized. Cell stocks were frozen at ~1 million cells per vial in media containing 10%DMSO, in liquid nitrogen, at every stage of cell line development.

Cell Culture

Highly prion sensitive cell lines, RK13 cells expressing the puromycin-PrP^C vector (developed as described previously^{70, 71}), were removed from liquid nitrogen storage for use. Cells were grown on 10-cm cell culture plates (BD Falcon, Franklin Lakes, NJ) in Dulbecco's Modified Eagle's Medium (DMEM) high glucose (Invitrogen, Carlsbad, CA), supplemented with 10% fetal bovine serum (FBS) (Gibco Life Technologies, Grand Island, NY) or* 10% calf newborn serum (Peak Serum, Wellington, CO), 1% penicillin/streptomycin (P/S) (Gibco Life Technologies, Grand Island, NY), and 0.01% puromycin (Sigma-Aldrich, St. Louis, MO), under saturated humidity and 5% CO₂ conditions at 37°C. After thawing, cell lines prion protein expression was verified via western blotting. Cell lines were maintained by splitting dilution 1:10 every five days after trypsin [Trypsin, 0.05% 1X, with 0.5 g porcine trypsin (1:250/L gamma irradiated) in HBSS with 0.2 g/L EDTA,] (Sigma-Aldrich, St. Louis, MO) disassociation. *Note: The supply of FBS ended and calf newborn serum was used as a replacement after several

alternatives were tested; calf newborn serum (Peak Serum, Wellington, CO) did not alter cell morphology, growth rate, prion protein expression, or other factors tested.

Prion Infection of Cell Culture

Highly prion sensitive cell lines, RK13 cells expressing the puromycin-PrP^C vector (developed as described previously^{70, 71}), were infected through coating prions on plastic cell culture dish prior to seeding cells, adapted from previously described techniques¹⁴³. Specifically, 0.1% w/v brain homogenate (in PBS) from prion-infected terminally diagnosed mice was added to 10-cm cell culture plates (BD Falcon, Franklin Lakes, NJ) and allowed to incubate at room temperature inside the cell culture hood for two hours to allow the prions to stick to the plastic. After incubation, the plates were rinsed three times with sterile phosphate buffered saline lacking Ca²⁺ and Mg²⁺ (PBS) (Hyclone, Pittsburg, PA) to remove brain material. Plates were then left uncovered in the cell culture hood for 2 - 4 hours to allow them to completely dry. Prion-coated dried plates were covered, wrapped in plastic wrap, and stored at 4°C until use. RK13 cells^{70, 71} expressing the puromycin-PrP^C vector and RK13 cells with an empty vector (pIRESpuro3 without PrP) were seeded onto the prion-coated plates at 1.6 million cells per plate. Cells were maintained at confluency (in a single cell monolayer) without splitting for 4 weeks; cell culture media was replaced every 5 days. Upon completion of the 4 weeks, cells were harvested for analysis via trypsin [Trypsin, 0.05% 1X, with 0.5 g porcine trypsin (1:250/L gamma irradiated) in HBSS with 0.2 g/L EDTA,] (Sigma-Aldrich, St. Louis, MO) disassociation.

Cell-Based Conformational Stability Assay (C-CSA)

Prion infected cells were assessed for prion conformational stability (Figure 2.2) as previously described⁴⁷. Specifically, after a 4-week incubation on a prion-coated plate, RK13 cells expressing the puromycin-PrP^C vector^{70, 71, 79} and RK13 cells with an empty vector (pIRESpuro3 without PrP) were harvested via trypsin (Sigma-Aldrich, St. Louis, MO) disassociation. Cells were seeded (20,000 cells per well) onto 70% Ethanol, molecular grade (Sigma- Aldrich, St. Louis, MO) activated Multiscreen IP 96-well 0.45- μ m ELISpot plates (Millipore, Billerica, MA), and rinsed three times with 200 μ L per well phosphate buffered saline lacking Ca²⁺ and Mg²⁺ (PBS) (Hyclone, Pittsburg, PA). The cells were fixed onto the ELISpot membrane at 50°C for 2 - 4 hours (until the membrane dries), and stored at -20°C until use. ELISpot plates with fixed cells were allowed to thaw for one hour at room temperature. ELISpot plates were stacked with lids on, in a humidity chamber (plastic container with ¼ inch dH₂O and 2 empty pipet tip rack tops in bottom) to maintain moisture throughout the following steps. The ELISpot wells were treated for one hour at room temperature with a solution of guanidine hydrochloride (GdnHCl) (Sigma-Aldrich, St. Louis, MO) in 10 mM Tris-HCl (Sigma-Aldrich, St. Louis, MO) at 100 μ L per well; the GdnHCl dilution series varied from 0M to 5.5M in 0.5M increments. The GdnHCl dilution series allowed the infectious prion protein (PrP^{Sc}) to denature, followed by three 200 μ L per well PBS washes to allow PrP^{Sc} to renature in a PrP^C-like conformation. The plates were treated with 100 μ L per well 5 μ g/mL proteinase K (PK) (Pierce Biotechnology Inc., Rockford, IL) in cold cell lysis buffer (50 mM Tris (Sigma-Aldrich, St. Louis, MO), pH 8.0; 150 mM NaCl (Sigma-Aldrich, St. Louis, MO); 0.5% sodium deoxycholate (Sigma-Aldrich, St. Louis, MO);

0.5% Igepal (Sigma-Aldrich, St. Louis, MO)) for one hour at 37°C to ablate PrP^C and denatured-renatured PrP^{Sc} signal. The PK was quenched by 150µL per well 2mM phenylmethylsulfonyl fluoride (PMSF) (Sigma-Aldrich, St. Louis, MO) in PBS for twenty minutes at room temperature, and then rinsed once with 200µL per well PBS. Plates were then be treated with 120µL per well 3M guanidine thiocyanate (Sigma-Aldrich, St. Louis, MO) in 10 mM Tris-HCl (Sigma-Aldrich, St. Louis, MO) for ten minutes and immediately washed four times with 200µL per well PBS to allow for denaturation and renaturation of the prion protein which exposes the epitopes for antibody probing. The samples were then given 150µl per well of 5% superbloc (Pierce, Rockford, IL) in ultrapure water for one hour at room temperature to reduce background signal. Following removal of superbloc, immunodetection began. 60µl per well of primary anti-PrP antibody in fresh, filtered Tris Buffered Saline – Tween (TBS-T) was added per well and incubated at 4°C overnight. Primary anti-PrP mAb Epitopes^{144, 145} (Figure 2.1B) used: PRC1 (Telling Lab, Fort Collins, CO) 1:5000 dilution, PRC5 (Telling Lab, Fort Collins, CO) 1:5000 dilution, PRC7 (Telling Lab, Fort Collins, CO) 1:5000 dilution, 6H4 (Prionics, Invitrogen Life Technologies, CA) 1:20000 dilution, D13 (Telling Lab, Fort Collins, CO) 1:5000 dilution, and D18 (Telling Lab, Fort Collins, CO) 1:5000 dilution. The following day, the wells were rinsed three times with 200µl per well TBS-T. 60µl per well of Alkaline Phosphatase-conjugated secondary antibodies in fresh, filtered TBS-T was added per well and incubated at room temperature for one hour. Secondary mAb used: AP-α-Mouse IgG (Southern Biotechnology Associates, Birmingham, AL) 1:5000 dilution for PRC1, PRC5, PRC7, and 6H4; AP Goat-α-Human

IgG (Southern Biotechnology Associates, Birmingham, AL) 1:5000 dilution for D13 and D18. The wells were rinsed three times with 200µl per well TBS-T; a final 200µl per well rinse with PBS removed the trace amounts of detergent left by the TBS-T. The plastic backing was removed from the bottom of the membrane-attached wells, then rinsed twice with flowing distilled Millipore water at the sink. Finally, the plates were allowed to dry for four hours. After the membranes fully dried, the wells were developed with a solution of nitro-blue tetrazolium chloride/ 5-bromo-4-chloro-3'-indolyphosphate p-toluidine salt (NBT/BCIP) (Roche, Basel, Switzerland) in ultrapure water. The development process was quenched with two rinses of filtered water. The plates were allowed to dry overnight at 4°C, and then at room temperature the following day for one hour. The plates were imaged with ImmunoSpot S6-V analyzer (Cellular Technology Ltd, Shaker Heights, OH), and spot numbers were determined using ImmunoSpot5 software (Cellular Technology Ltd, Shaker Heights, OH).

Semi-Denaturing Detergent Agarose Gel Electrophoresis (SDD-AGE)

Brain homogenates were treated according to previous protocol¹⁴⁶. In brief, the brain homogenates from chronic wasting disease (isolate D10) infected Tg(DeerPrP)1536+/- and Tg(ElkPrP)5037+/-, Uninfected Tg(DeerPrP)1536+/-, and PrP-KO (prion protein null mice) were treated with 2% Sodium Dodecyl Sulfate (SDS) in water at room temperature for five minutes, separated on 1.5% Agarose (Sigma-Aldrich, St. Louis, MO)/0.5% SDS gel, transferred to nitrocellulose membrane (VWR, Radnor, PA) with Southern blotting procedure followed by 3M guanidine thiocyanate (Sigma-Aldrich, St.

Louis, MO) in 10 mM Tris-HCl (Sigma-Aldrich, St. Louis, MO) denaturation and probed with PRC5 anti-prion monoclonal antibody.

Immunohistochemistry

Formalin-fixed brain samples were treated according to previous protocol¹⁴⁷. In brief, 8µm sections of paraffin embedded brain material were deparaffinized. Then, PrP^{Sc} visualized with a biotinylated secondary antibody in conjunction with 3,3'-diaminobenzidine in conjunction with anti-prion mAb 6H4 following hydrolytic autoclaving for fifteen minutes in 10mM HCl.

Statistical Analysis

Statistical significance was assessed using GraphPad Prism 8.0 for Mac OS X software

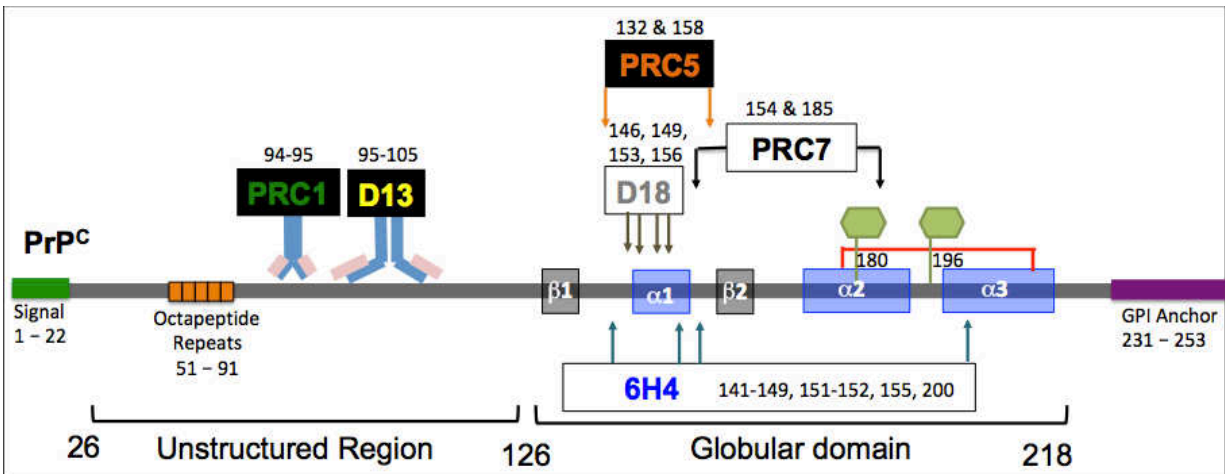


FIGURE 2.1: Schematic representation of the mouse cellular prion protein (PrP^c) and Epitopes of Anti-Prion Antibodies. (A) The mouse prion protein (PrP^c) is shown as a grey line with distinct areas indicated; the numbers shown represent amino acid locations along the molecule. An N-terminal target sequence (green box) is cleaved during protein processing prior to insertion into the plasma membrane. The remaining N-terminus is charged, primarily unstructured, and contains the copper octapeptide repeat binding motif (orange boxes). The C-terminal domain is structured with three alpha helices (blue boxes), two beta sheet motifs (grey boxes) and post-translational glycosylation at asparagine residues (green hexagons). A stabilizing disulfide bridge forms between alpha helix 2 and alpha helix 3 (red line). Finally, there is a Glycosylphosphatidylinositol (GPI) anchor attached at the C-terminus (purple box) which anchors the protein to the cellular plasma membrane. (B) Primary anti-PrP antibodies aligned to mouse PrP^c. Antibody epitopes have been mapped previously^{144, 145} and amino acid residues included in the binding epitope of each antibody is indicated numerically. Two antibodies recognize linear epitopes (PRC1 and D13) are shown with representative antibody images. Four antibodies recognizing discontinuous epitopes (PRC5, D18, 6H4, and PRC7) are shown with arrows indicating discontinuous amino acid residues included in binding epitope.

Cell based - Conformational Stability Assay

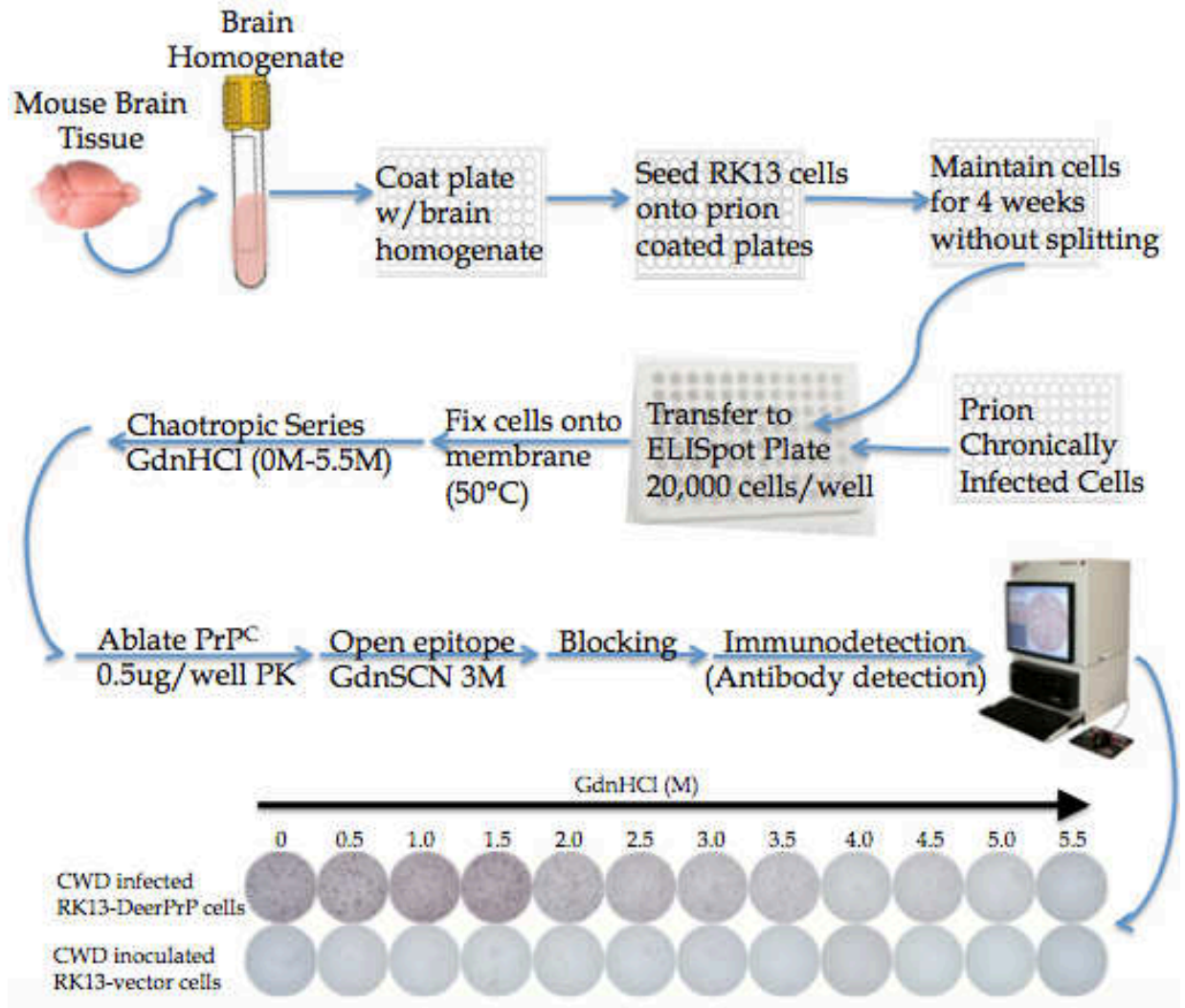


FIGURE 2.2: Schematic representation of the Cell-Based Conformational Stability Assay with representative example of data garnered. In brief, prion infected brains are homogenized and used to coat plates. Rabbit Kidney Epithelial cells (RK13) that are inducibly (via puromycin) transgenic for the prion protein (RK-mouse, RK-deer, or RK-elk) and RK13 cells containing an empty vector (RKV) and do not express the cellular prion protein (PrP^C) are seeded onto the coated plates. The culture lasts four weeks without splitting, but with a change in media once every five days. At the end of the infection, cells are transferred to the ELISpot plates (20,000 cells per well), fixed at 50°C. Samples are exposed to guanidine hydrochloride (GdnHCl) varied from 0M to 5.5M in 0.5M increments to allow the infectious prion protein (PrP^{Sc}) to denature and renature in a PrP^C-like conformation. PrP^C and PrP^C-like PrP^{Sc} is ablated by proteinase K (PK) treatment. Guanidine thiocyanate (GdnSCN) is used to open remaining PrP^{Sc} epitopes for immunodetection. The samples are exposed to blocking, and immunodetection with

anti-prion antibodies: PRC1, D13, PRC5, D18, 6H4, PRC7 (Figure 2.2). Resulting data is imaged with ImmunoSpot S6-V analyzer and spot numbers determined using ImmunoSpot5 software. A representative image of the resultant data is shown; dark spots within wells are PrP^{Sc} positive (anti-prion antibody 6H4). Cells (RK13-DeerPrP and RK13-vector) were plated on chronic wasting disease (CWD) coated plates, as indicated in the schematic. Data can be used quantitatively to evaluate PrP^{Sc}.

C. RESULTS

Freshly CWD prion infected RK-PrP cells recapitulate the conformational stability of chronically CWD prion infected cells

We previously developed⁴⁷ a prion cell-based conformational stability assay (C-CSA) using a cell model expressing PrP^C gene of choice in rabbit kidney epithelial (RK13) cells⁷⁰ as a tool to assess how strains differ (Figure 2.2). This technique was specifically developed as a quantitative measure of prions. We quantified changes in conformational stability due to quinacrine treatment in chronically prion-infected RK13 cells expressing either elk (RK-Elk) or deer (RK-Deer) PrP^C⁴⁷. Chronically infected RK-Deer (RK-Deer+) and RK-Elk (RK-Elk+) cell lines perpetually propagate CWD prion infection were developed previously⁷¹. In brief, CWD isolate (012-09442) was passaged into Tg(ElkPrP)5037^{+/-} and Tg(DeerPrP)1536^{+/-} mice, and the mice were sacrificed when terminally ill with CWD. Their prion-infected brains were homogenized in PBS, and 0.1% weight/volume brain homogenate was used to coat cell culture dishes (Figure 2.2). The plates were seeded with naïve RK-PrP cell lines, RK-Elk and RK-Deer, respectively. The cell lines were maintained without passaging for 4 weeks. Upon splitting, CWD prion infection was verified. The cells were maintained through multiple passages, and single cell cloned. Ultimately, this process created two stable prion infected cell lines, RK-Deer+ and RK-Elk+, which perpetually propagate CWD infection.

This study began by using the C-CSA to validate the significant ($p < 0.001$) difference (Figure 2.3A) due to the different amino acid at position 226 [deer (Q), elk (E)] has on the stability of chronic wasting disease (CWD)⁴⁷ in chronically infected cell

lines. The C-CSA gauges the relative resistance to protease cleavage after exposure to varying levels of a chaotropic agent. The resultant denaturation curve and guanidine hydrochloride midpoint of the sigmoidal transition ($GdHCl_{1/2}$) values are used to derive statistical significance. In brief, RK-Deer+ and RK-Elk+ cell lines were grown to confluency, maintained, and split onto ELISpot plates at 20,000 cells per well (Figure 2.2). The cells were fixed onto the membrane via drying at 50°C, and stored at -20°C until use. The following day, plates were allowed to thaw to room temperature. The cells were then treated with guanidine hydrochloride (GdnHCl) in a stepwise increasing molar concentration, i.e. 0M – 5.5M GdnHCl. This allowed PrP^{Sc} to denature and following washes allowed PrP^{Sc} to renature into a PrP^C / PrP^C – like conformation. Treatment with proteinase K (PK) in cell lysis buffer was done to lyse the cells while ablating PrP^C and the denatured-renatured fraction of PrP^{Sc} that resembled PrP^C. PMSF was used to quench the PK reaction. The prions were then exposed to guanidine thiocyanate to expose antibody epitopes, via denaturing PrP^{Sc} and following washes allowed PrP^{Sc} to renature into a PrP^C / PrP^C – like conformation. Blocking and immunodetection was then done. To recapitulate the previous study⁴⁷, anti-prion antibody 6H4 was used (Figure 2.1B).

The results recapitulated previous conclusions^{7, 47} that a single amino acid change to the PrP^C can have an intense impact on PrP^{Sc}. However, a C-CSA limited to chronically infected cell lines limits strains and species to the few established lines. We then developed the C-CSA to examine freshly infected cells in order to overcome that limitation (Figure 2.2). To test the application of C-CSA on freshly infected cells, prion-

infected brain homogenate (n=3) from terminally ill Tg(ElkPrP)5037^{+/-} and Tg(DeerPrP)1536^{+/-} mice infected with elk CWD isolate Bala05 were used to infect RK-Elk and RK-Deer cell lines, respectively, along with the RK-V(vector only, PrP^C null) cell line. They were then interrogated via C-CSA with anti-prion antibody (6H4) (Figure 2.2). The prion stability difference seen between CWD chronically infected RK-Deer and RK-Elk (p<0.001) was recapitulated in freshly infected cells (p<0.001) (Figure 2.3). However, the GdHCl_{1/2} value for chronically infected and freshly infected was not identical. A possible cause for the difference is that the CWD used to derive the chronically infected cell line and freshly infected cell line were different isolates, 012-9442 and Bala05 respectively.

The C-CSA is not limited to CWD PrP^{Sc}, chronically infected and freshly infected murine-adapted prion strains are detectable.

Our goal was to create a more universal C-CSA capable of differentiating subtle differences between strains in multiple species, especially in strains with the same host PrP^C background. To that endeavor, both chronically prion infected RK-mouse cell lines (Figure 2.4A) and freshly infected RK-mouse cell lines (Figure 2.4B) were examined with the C-CSA (Figure 2.2). RML and 22L are murine-adapted scrapie prion strains that share the same amino acid sequence, yet, ultimately produces unique diseases (Table 2.1). Freshly infected RK-mouse cell lines were derived from prion-infected brain homogenate (n=3) from terminally ill C57Bl/6 mice infected with classically defined murine-adapted scrapie strains (RML and 22L) were used to infect murine-PrP^C expressing RK13 (RK-Mouse) cells along with the RK-V (vector only, PrP^C null)

cell line. All cell lines underwent the C-CSA (Figure 2.2) and were interrogated with 6H4.

RML and 22L prion strains were significantly different ($p=0.0197$) in chronically infected cell lines (Figure 2.4A) and not significantly different ($p=0.6570$) in freshly infected cells. These differences that occur between freshly prion infected and chronically prion infected will be further explored in Chapter 4 of this dissertation. Although the difference between RML and 22L was not significantly different in freshly infected cells, the C-CSA showed that it could be used to detect the conformational stability of murine-adapted strains. Furthermore, Figures 2.3 and 2.4 demonstrate the C-CSA is not limited to established chronically infected cell lines; it can be used in freshly infected paradigms.

CWD PrP^{Sc} does not have a unified conformational stability to an expanded anti-prion epitope panel, emphasizing subtle variation across the molecule

The C-CSA was then expanded to interrogate a prion at multiple known epitopes to create a map of specific regional differences between prion strains and help resolve how strains differ. There has been a recent push to derive accurate epitope locations for anti-prion antibodies^{144, 145}. The amino acid residues included in the binding of each anti-prion antibody (PRC1, D13, PRC5, D18, 6H4, and PRC7) epitope is indicated (Figure 2.1B). PRC1¹⁴⁴ and D13¹⁴⁵ recognize linear epitopes located in the unstructured N-terminal region near the PK cleavage site. PRC5¹⁴⁴, D18¹⁴⁵, 6H4¹⁴⁵, and PRC7¹⁴⁴ recognize discontinuous epitopes located in the globular C-terminal region. Additionally, PRC7 is glycosylation specific and only binds to unglycosylated, and

monoglycosylated (residue 196) species of the prion protein. If the chaotropic agent denatures the molecule evenly, an identical $GdHCl_{1/2}$ value would be revealed at each antibody probed; however, if the $GdHCl_{1/2}$ value were not identical across antibodies it would imply that prion molecular micro-regions have a discreet denaturation response.

To test the application of the C-CSA with an expanded antibody panel on freshly infected cells, prion-infected brain homogenate (n=3) from terminally ill Tg(ElkPrP)5037^{+/-} and Tg(DeerPrP)1536^{+/-} mice infected with elk CWD isolate Bala05 were used to infect RK-Elk and RK-Deer cell lines, respectively, along with the RK-V(vector only, PrP^C null) cell line. For simplicity, RK-Elk infected with CWD from Tg(ElkPrP)5037^{+/-} brain homogenate will be referred to as Elk-CWD and RK-Deer infected with CWD from Tg(DeerPrP)1536^{+/-} brain homogenate will be referred to as Deer-CWD. Deer-CWD and Elk-CWD were interrogated via the C-CSA (Figure 2.2) with epitope-mapped (Figure 2.1B) anti-prion antibodies (PRC1, D13, PRC5, 6H4, D18, and PRC7). The significant difference between Elk-CWD and Deer-CWD resides in the single amino acid difference Q/E at residue 226.

The $GdHCl_{1/2}$ value of CWD was not identical across all antibodies within a species (Figure 2.5A-C). This implies CWD micro-regions have a discreet denaturation response. Elk-CWD presents tightly grouped with low (13%) heterogeneity, and with lower resistance to denaturation at all antibodies used. Whereas, Deer-CWD presents with a broad (60%) heterogeneity to denaturation and overall significantly ($p = 0.0015$) higher resistance to denaturation at all antibodies used (Figure 2.5D). There were more significant differences (Figure 2.5C) between epitopes in Deer-CWD than Elk-CWD.

Deer-CWD showed significant differences at 9 antibody comparisons (PRC1:D18, PRC1:PRC5, PRC1:6H4, PRC1:PRC7, D13:PRC5, D13:6H4, D18:PRC5, D18:6H4, and PRC7:6H4) as opposed to only 2 antibody comparisons (PRC1:PRC5, and PRC1:6H4) being significantly different with Elk-CWD (Figure 2.5C).

The heterogeneity of CWD due to the primary structural (Deer-Q226/Elk-E226) difference of the prion protein can be seen in amyloid detection with semi-denaturing detergent agarose gel electrophoresis (SDD-AGE) (Figure 2.5E) and neuropathological analysis (Figure 2.5F-G). The SDS semi-denaturation assay (SDD-AGE) allows for qualitative quantification of amyloid or monomer status of prions. SDD-AGE was done on brain homogenate from terminally ill Tg(ElkPrP)5037^{+/-} and Tg(DeerPrP)1536^{+/-} mice infected with deer CWD isolate D10, uninfected Tg(DeerPrP)1536^{+/-} mice, and prion knockout mice (Figure 2.5E). The data show a higher array of amyloid in the Tg(DeerPrP)1536^{+/-} mice as opposed to the Tg(ElkPrP)5037^{+/-} mice.

The C-CSA evidence that CWD prions have different structures due to being passaged into a deer or elk background (Figure 2.3, 2.5, 2.6) is further supported by presentation of brain deposition in prion-infected mice (Figure 2.5F-G).

Immunohistochemical analysis on brain cortex from terminally ill Tg(ElkPrP)5037^{+/-} and Tg(DeerPrP)1536^{+/-} mice infected with deer CWD isolate D10 shows granular deposits of PrP, microvacuolation and extensive PrP^{Sc} deposition coupled with very fewer cerebellar granular cells in Tg(ElkPrP)5037^{+/-} (Figure 2.4F) as opposed to florid cortical plaques and minimal cerebellar pathology in Tg(DeerPrP)1536^{+/-} mice (Figure 2.5G). The dissimilar presentation of elk-CWD and deer-CWD in amyloid detection

with semi-denaturing detergent agarose gel electrophoresis (Figure 2.5E) and neuropathological analysis (Figure 2.5F-G) further support the validity of the C-CSA data.

The expanded anti-prion epitope panel reinforces conformational stability differences due to cervid-PrP at residue 226

To compare Deer-CWD and Elk-CWD by individual epitope responses the C-CSA data derived for Figure 2.5 was further segregated by antibody (Figure 2.6). In line with previous observations, Deer-CWD show a higher resistance to denaturation, i.e. more stable conformation, than Elk-CWD. Overall, prion stability difference between Deer-CWD and Elk-CWD was significant at all epitopes examined (Figure 2.3B, 2.6).

At PRC1, a linear epitope in the unstructured region, Deer-CWD has a significantly different ($p = 0.0162$) $GdHCl_{1/2}$ value (2.263 M) than Elk-CWD (1.879 M). Similarly at the other linear epitope in the unstructured region, D13, Deer-CWD has a significantly different ($p = 0.0006$) $GdHCl_{1/2}$ value (2.600 M) than Elk-CWD (2.011 M). This difference was continued with discontinuous epitopes in the globular region. At D18, Deer-CWD has a significantly different ($p = 0.0007$) $GdHCl_{1/2}$ value (2.779 M) than Elk-CWD (2.261 M). Similarly at PRC5, a discontinuous epitope that straddles α -helix 1, Deer-CWD has a significantly different ($p < 0.0001$) $GdHCl_{1/2}$ value (3.427 M) than Elk-CWD (2.461 M). This difference was seen with 6H4, a discontinuous epitope that ranges from before α -helix 1 to inside α -helix 3, Deer-CWD has a significantly different ($p < 0.0001$) $GdHCl_{1/2}$ value (3.583 M) than Elk-CWD (2.400 M). The difference occurred with a glycosylation specific antibody, PRC7, Deer-CWD has a significantly different (p

< 0.0001) $GdHCl_{1/2}$ value (3.063 M) than Elk-CWD (2.000 M). The overall $GdHCl_{1/2}$ value primarily increased from the linear epitopes in the unstructured region into the discontinuous epitopes in the globular region, with Deer-CWD being significantly higher than Elk-CWD at all epitopes examined (Figure 2.6F).

Subtle PrP^{Sc} variations within three murine-adapted prion strains were revealed with the expanded conformational stability anti-prion epitope panel.

The significant difference caused by the single amino acid difference in Deer-CWD and Elk-CWD is evident (Figure 2.3, 2.5, 2.6). However, the goal was to create a more universal C-CSA capable of differentiating subtle differences between strains in multiple species, especially in strains with the same host PrP^C background. To that endeavor, prion-infected brain homogenate (n=3) from terminally ill C57Bl/6 mice infected with classically defined murine-adapted scrapie strains (RML and 22L) and recently murine-adapted CWD strain¹³⁶ (mD10) were used to infect murine- PrP^C expressing RK13 (RK-Mouse) cells along with the RK-V (vector only, PrP^C null) cell line. All three murine-adapted prion strains (RML, 22L, and mD10) share the same amino acid sequence, yet, produces different diseases (Table 2.1). The conformational stability of three murine-adapted prion strains (RML, 22L, and mD10) was compared via the C-CSA with five epitope-mapped (Figure 2.1B) anti-prion antibodies: D13, D18, PRC5, 6H4 and PRC7. PRC1 is not a murine-specific anti-prion antibody and was, therefore, not used. D13¹⁴⁵ recognizes a linear epitope located in the unstructured N-terminal region near the PK cleavage site. PRC5¹⁴⁴, D18¹⁴⁵, 6H4¹⁴⁵, and PRC7¹⁴⁴ recognize discontinuous epitopes located in the globular C-terminal region. Additionally, PRC7 is

glycosylation specific and only binds to unglycosylated, and monoglycosylated (residue 196) species of the prion protein.

Since the $GdHCl_{1/2}$ value of CWD was not identical across all antibodies within a species (Figure 2.5A-C), the differences present between murine-adapted prion strains (Figure 2.7A-E) further verified that prion micro-regions have a discrete denaturation response. All murine-adapted prions presented with similar high broad heterogeneity (60% RML; 70% 22L; 60% mD10). Every antibody comparison was significantly different in at least one mouse-adapted strain and the D13:6H4 and D18:PRC7 comparison was significant for all three mouse-adapted strains (Figure 2.7D-E). There were 7 significantly different antibody comparisons for 22L (Figure 2.7A, 2.7D): D13 was significantly different than PRC5 ($p = 0.0174$), 6H4 ($p = 0.0003$), and PRC7 ($p = 0.0224$), D18 was significantly different than PRC7 ($p = 0.0013$), PRC5 was significantly different than 6H4 ($p = 0.0132$) and PRC7 ($p = 0.0006$), and, lastly, 6H4 was significantly different from PRC7 ($p = 0.0018$). There were 6 significantly different antibody comparisons for RML (Figure 2.7B, 2.7D): D13 was significantly different than D18 ($p = 0.0054$), and 6H4 ($p = 0.0239$), D18 was significantly different than PRC5 ($p = 0.0283$), 6H4 ($p = 0.0203$), and PRC7 ($p = 0.0062$), and, lastly, 6H4 was significantly different from PRC7 ($p = 0.032$). There were 6 significantly different antibody comparisons for mD10 (Figure 2.7C, 2.7E): D13 was significantly different than D18 ($p = 0.0089$), PRC5 ($p = 0.0146$) and 6H4 ($p = 0.0044$), D18 was significantly different than PRC5 ($p = 0.0091$), and PRC7 ($p = 0.0254$), and, lastly, 6H4 was significantly different from PRC5 ($p =$

0.0031). This indicates that RML and mD10 share similar responses if not similar GdnHCl $\frac{1}{2}$ values to denaturation.

Unexpectedly, when grouping 22L by all antibodies (Figure 2.7A, 2.7F) the slope appeared steeper than RML (Figure 2.7B) and mD10 (Figure 2.7C). Slope analysis (Figure 2.7G), revealed 22L contains the steepest slopes at all discontinuous epitopes when compared to RML and mD10. Surprisingly, 22L has the most gradual slope in the linear unstructured epitope. The slope for RML and 22L differs at every epitope examined. The slope of mD10 and 22L differ in the discontinuous epitope regions but not at the linear epitope. While, the slope of mD10 and RML only differ at PRC7 (the glycosylation specific antibody).

Unlike the significant ($p = 0.0015$) difference between Deer-CWD and Elk-CWD (Figure 2.5D), mouse-adapted prions summed by antibody and segregated by strain (Figure 2.7F) show no significance differences between 22L:RML ($p = 0.6341$), 22L:mD10 ($p = 0.4863$) and RML:mD10 ($p = 0.9881$). This lack of significance when grouping data shows that to truly evaluate subtle differences in strains with identical amino acid composition, one must rely on individual epitopes (Figure 2.8).

Murine-adapted PrP^{Sc} strains containing the same amino acid sequence reveal strain-based variation with the expanded conformational stability anti-prion epitope panel

To compare RML, 22L, and mD10 by individual epitope responses the C-CSA data derived for Figure 2.7 was further segregated by antibody (Figure 2.8). The murine-adapted strains differed at multiple epitopes (Figure 2.8F). However, murine-adapted prion strains (Figure 2.8A-F) did not have a trend of increasing the GdnHCl $\frac{1}{2}$

value from the linear epitopes in the unstructured region into the discontinuous epitopes in the globular region like CWD (Figure 2.6F).

We compared two classical murine-adapted scrapie strains, RML and 22L. These strains had significantly different conformational stabilities at 3 of the 5 antibodies examined (Figure 2.5A-F). The $GdHCl_{1/2}$ value of 22L, 2.233 M, significantly differed ($p = 0.0003$) from RML, 2.059 M, at the D13 linear epitope examined. RML and 22L had significantly different $GdHCl_{1/2}$ values at the discontinuous epitopes around α helix-1, D18 ($p < 0.0001$) and PRC5 ($p = 0.0002$). However, 22L and RML were not significantly different at the glycosylation specific discontinuous epitope (PRC7) or a discontinuous epitope (6H4) ranging from before α helix-1 to inside α helix-3. RML and 22L share a scrapie origin and the cell lines share the same PrP^C amino acid sequence, yet propagate different diseases due to subtle variation in the tertiary structure of PrP^{Sc}. The subtle variation and similarities are detectable with the C-CSA.

We compared a classically murine-adapted 22L scrapie strain and recently murine-adapted CWD (mD10). These strains had significantly different conformational stabilities at 4 of the 5 antibodies examined (Figure 2.5A-F). The $GdHCl_{1/2}$ value of 22L, 2.233 M, significantly differed ($p < 0.0001$) from mD10, 1.94 M, at the D13 linear epitope examined. The discontinuous epitope discontinuous epitope ranging before α helix-1 to α helix-3, 6H4, had significantly different ($p < 0.0001$) $GdHCl_{1/2}$ values between 22L, 2.526 M, and mD10, 2.778 M. There is subtle variation in α helix-1 between mD10 and 22L. 22L, 2.347 M, and mD10, 2.811 M, had significantly different ($p < 0.0001$) $GdHCl_{1/2}$ values at the discontinuous epitope embedded in the α helix-1, D18. However, the

discontinuous epitope straddling α helix-1, PRC5, was not significantly different ($p = 0.0615$). PRC7, the glycosylation specific epitope which binds to aglycosylated, and monoglycosylated (at residue 196) PrP, had significantly different ($p < 0.0001$) $GdHCl_{1/2}$ values between 22L, 1.974 M, and mD10, 2.246 M. RML and mD10 cell lines share the same PrP^C amino acid sequence, yet propagate different diseases due to subtle variation in the tertiary structure of PrP^{Sc}. They do not share a scrapie origin, so more differences could be expected. The subtle variation and similarities between 22L and RML are detectable with the C-CSA.

We compared a classically murine-adapted RML scrapie strain and recently murine-adapted CWD (mD10). These strains had significantly different conformational stabilities at 3 of the 5 antibodies examined (Figure 2.5A-F). The $GdHCl_{1/2}$ value of RML, 2.059 M, significantly differed ($p = 0.016$) from mD10, 1.94 M, at the D13 linear epitope examined. The discontinuous epitope discontinuous epitope ranging before α helix-1 to α helix-3, 6H4, had significantly different ($p < 0.0001$) $GdHCl_{1/2}$ values between RML, 2.504 M, and mD10, 2.778 M. PRC7, the glycosylation specific epitope which binds to aglycosylated, and monoglycosylated (at residue 196) PrP, had significantly different ($p < 0.0001$) $GdHCl_{1/2}$ values between RML, 2.033 M, and mD10, 2.246 M. However, RML and mD10 were not significantly different at the D18 discontinuous epitope embedded in the α helix-1 or the PRC5 discontinuous epitope which straddles α helix-1. RML and mD10 cell lines share the same PrP^C amino acid sequence, yet propagate different diseases due to subtle variation in the tertiary structure of PrP^{Sc}. They do not share a scrapie origin, so more differences could be

expected. The subtle variation and similarities between 22L and RML are detectable with the C-CSA. Overall, the murine-adapted C-CSA data reinforces the need to examine multiple epitopes individually (Figure 2.8), and not just sum them (Figure 2.7), to evaluate subtle variations in prion strain conformational stability.

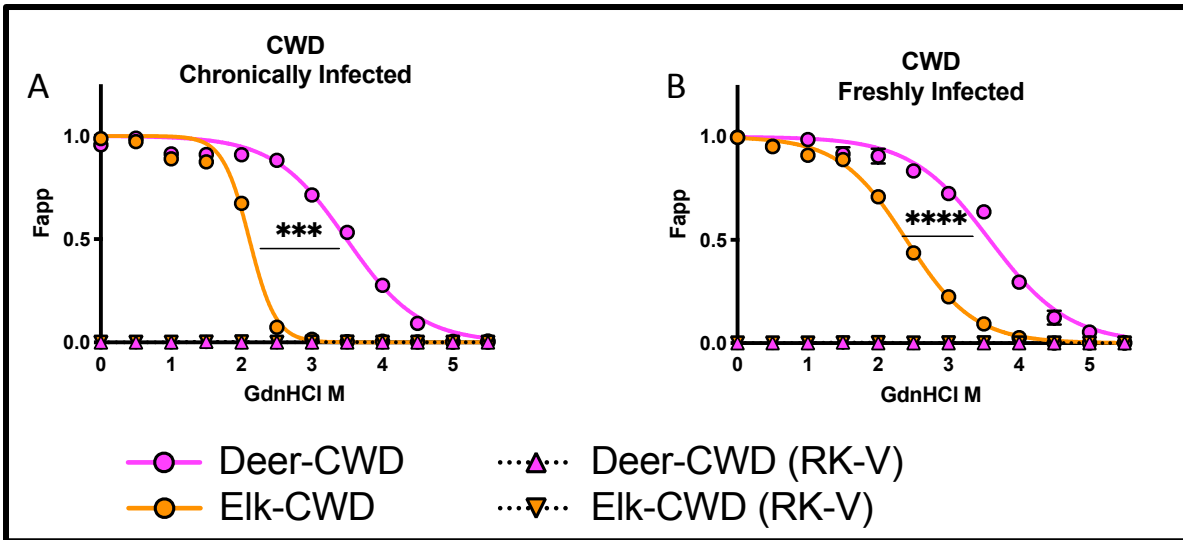
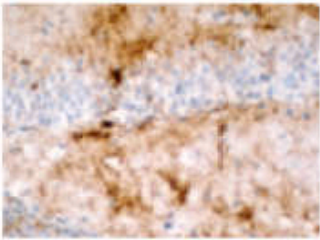
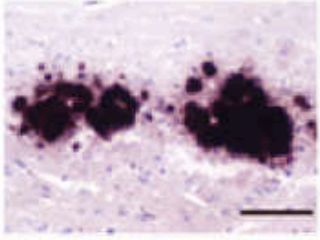
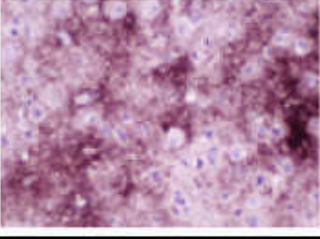


FIGURE 2.3: C-CSA method can differentiate CWD strains in both chronically infected and freshly infected cell lines. (A) Validation of the significant ($p < 0.001$) difference due to the different amino acid at position 226 [deer (Q), elk (E)] has on the stability of chronic wasting disease (CWD). Cell-based Conformational Stability Assay (C-CSA) examining CWD chronically infected RK-Deer (magenta) and RK-Elk (orange) ($n=4$) cell lines, interrogated with anti-prion antibody (6H4). The chronically infected cell lines were derived from CWD isolate (012-09442); cell lines are considered chronically infected if they stably propagate prion infection through cell culture passages. **(B)** CWD stability pattern seen in chronically infected RK-Deer and RK-Elk was recapitulated in freshly infected cells; RK-Deer passaged CWD is more resistant to denaturation compared to RK-Elk passaged CWD. Brains ($n=3$) from terminally ill Tg(ElkPrP)5037^{+/-} and Tg(DeerPrP)1536^{+/-} mice infected with elk CWD isolate Bala05 were used to infect RK-Elk and RK-Deer cell lines, respectively, along with the RK-V(vector only, PrP^C null) cell line. The resultant CWD prions were interrogated with the C-CSA using anti-prion antibody 6H4.

F_{app}, fraction of apparent signal. The sigmoidal dose-response curve was plotted using a four parameter algorithm and nonlinear least-squares fit; with curve comparison. Error bars, SD from $n=4$ chronic cell lines per group (A), and $n=3$ animals per group (B-H). Statistical significance: * $p \leq 0.05$; ** $p \leq 0.01$; *** $p \leq 0.001$; **** $p \leq 0.0001$. Statistical differences from the GdnHCl_{1/2} values between matched, best fit curves were calculated via unpaired t-test.

TABLE 2.1: Murine-adapted prion strains properties. Strains name is listed. Origin indicates the original prion and species of the material adapted into murine model. All three strains have a similar terminally ill (days post inoculation) within the same species (C57Bl/6). Unique clinical signs are specific disease phenotypes exhibited by C57Bl/6 mice terminally diagnosed with prion disease. Neuroinvasion and pathology data was adapted from Bett et al. 2012 ²².

Strain Name	Origin	Terminally Ill, Days Post Inoculation	Unique Clinical Signs	Neuroinvasion/ pathology
RML	Sheep Scrapie	142.5 ± 2.1	Hunched Posture	Weak 
mD10	Deer Chronic Wasting Disease	144.8 ± 3.0	Loss of Extensor Reflexes	Strong 
22L	Sheep Scrapie	131.2 ± 2.66	Plastic Tail, Loss of Extensor reflexes, & Difficulty Righting	Strong 

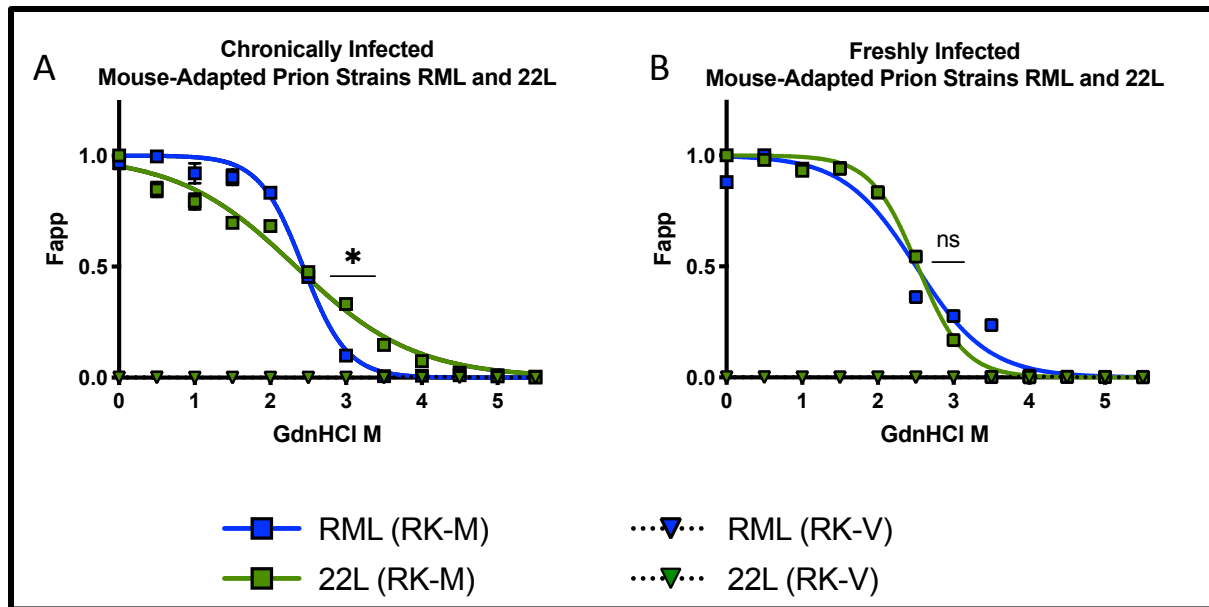


FIGURE 2.4: C-CSA method can detect murine-adapted prion strains, RML and 22L. (A) Further validation of the Cell-based Conformational Stability Assay (C-CSA) examining RML (blue) and 22L (green) chronically infected RK-Mouse (n=4) cell lines, interrogated with anti-prion antibody (6H4). Cell lines are considered chronically infected if they stably propagate prion infection through multiple cell culture passages. (B) Brains (n=3) from terminally ill C57Bl/6 mice infected with RML (blue) and 22L (green) were used to infect the RK-Mouse cell line, with the RK-V(vector only, PrP^C null) cell line. The resultant murine-adapted scrapie prions were interrogated with the C-CSA using anti-prion antibody 6H4.

Fapp, fraction of apparent signal. The sigmoidal dose-response curve was plotted using a four parameter algorithm and nonlinear least-squares fit; with curve comparison. Error bars, SD n=3 animals per group (A-F). Statistical significance: ns $p \geq 0.05$; * $p \leq 0.05$; ** $p \leq 0.01$; *** $p \leq 0.001$; **** $p \leq 0.0001$. Statistical differences from the GdnHCl_{1/2} values between matched, best fit curves were calculated via ANOVA.

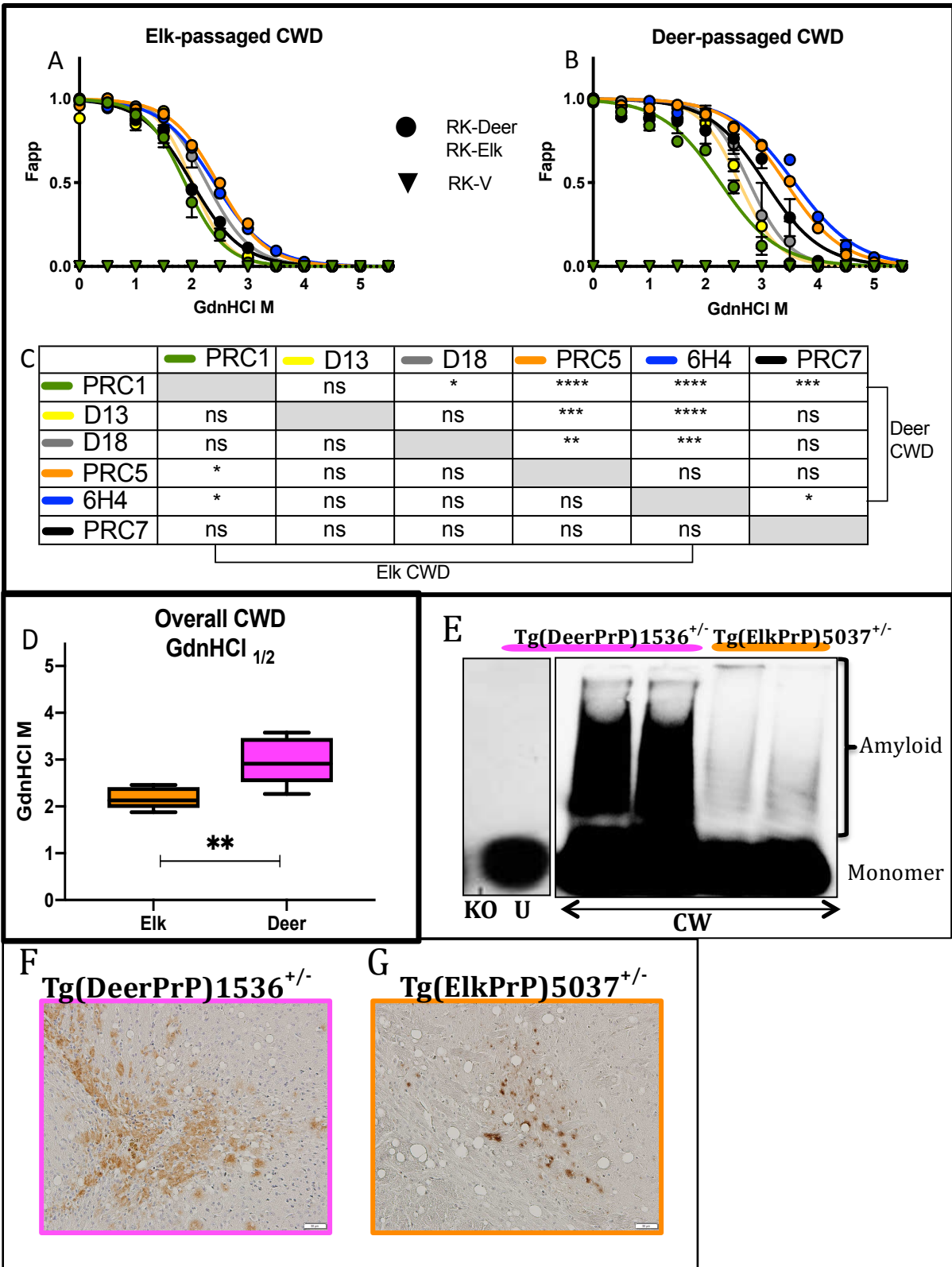


FIGURE 2.5: Overall reaction to denaturation, protease resistance, and amyloid deposition is more heterogeneous in Deer passed CWD compared to Elk passed

CWD (A-B) CWD Guanidine Hydrochloride_{1/2} (GdHCl_{1/2}) value within deer and elk were not identical across all antibodies, CWD contains micro-regions with discreet denaturation responses. C-CSA data are shown segregated by host PrP^C, i.e. grouped by the primary structural (Deer-Q226/Elk-E226) difference of the prion protein. mAbs: PRC1, D13, D18, PRC5, 6H4, and PRC7. The RK-Deer passaged CWD prion displays a wider array of amyloids than those passaged through RK-Elk. **(C)** Statistical comparison (ANOVA) of graphical representations (A & B) with significance for each antibody within a species, i.e. Deer passaged CWD mAbs PRC1 compared to deer passaged CWD mAbs PRC5. There is more evidence of epitope heterogeneity in deer passaged CWD. **(D)** Overall, RK-Elk passaged CWD presents a tightly grouped GdHCl_{1/2} value with lower resistance to denaturation; whereas, RK-Deer passaged CWD presents with a broad heterogeneity to denaturation (GdHCl_{1/2} value) and overall higher resistance to denaturation. Grouping data by all antibodies and host PrP^C, a general significance (p = 0.0015) is revealed. **(E)** CWD prions passaged through Tg(DeerPrP)1536+/- displays higher resistance to denaturation and wider array of amyloids than Tg(ElkPrP)5037+/- to the SDS semi-denaturation assayed with SDD-AGE. U= Uninfected mice, KO = PrP^{0/0} Knockout mice **(F-G)** Neuropathology of CWD infected Tg(DeerPrP)1536+/- and Tg(ElkPrP)5037+/- showing greater range of aggregates in Tg(DeerPrP)1536+/- . Immunohistochemistry assay reveals different neuropathology changes in brains of diseased Tg(DeerPrP)1536+/- and Tg(ElkPrP)5037+/- . Tg(ElkPrP)5037+/- mice displayed granular deposits of PrP, microvacuolation and extensive PrP^{Sc} deposition coupled with very fewer cerebellar granular cells. Conversely, Tg(DeerPrP)1536+/- mice are characterized by florid cortical plaques and minimal cerebellar pathology.

F_{app}, fraction of apparent signal. The sigmoidal dose-response curve was plotted using a four parameter algorithm and nonlinear least-squares fit; with curve comparison. Error bars, SD from n=3 animals per group (A-D). Statistical significance: ns p ≥ 0.05; * p ≤ 0.05; ** p ≤ 0.01; *** p ≤ 0.001; **** p ≤ 0.0001. Statistical differences from the GdHCl_{1/2} values between matched, best fit curves were calculated via unpaired t-test. Statistical differences comparing antibodies within deer and elk were calculated via an ANOVA. **Note:** Data in (Figure 2.4 E-G) was collected by Dr. Jifang Bian.

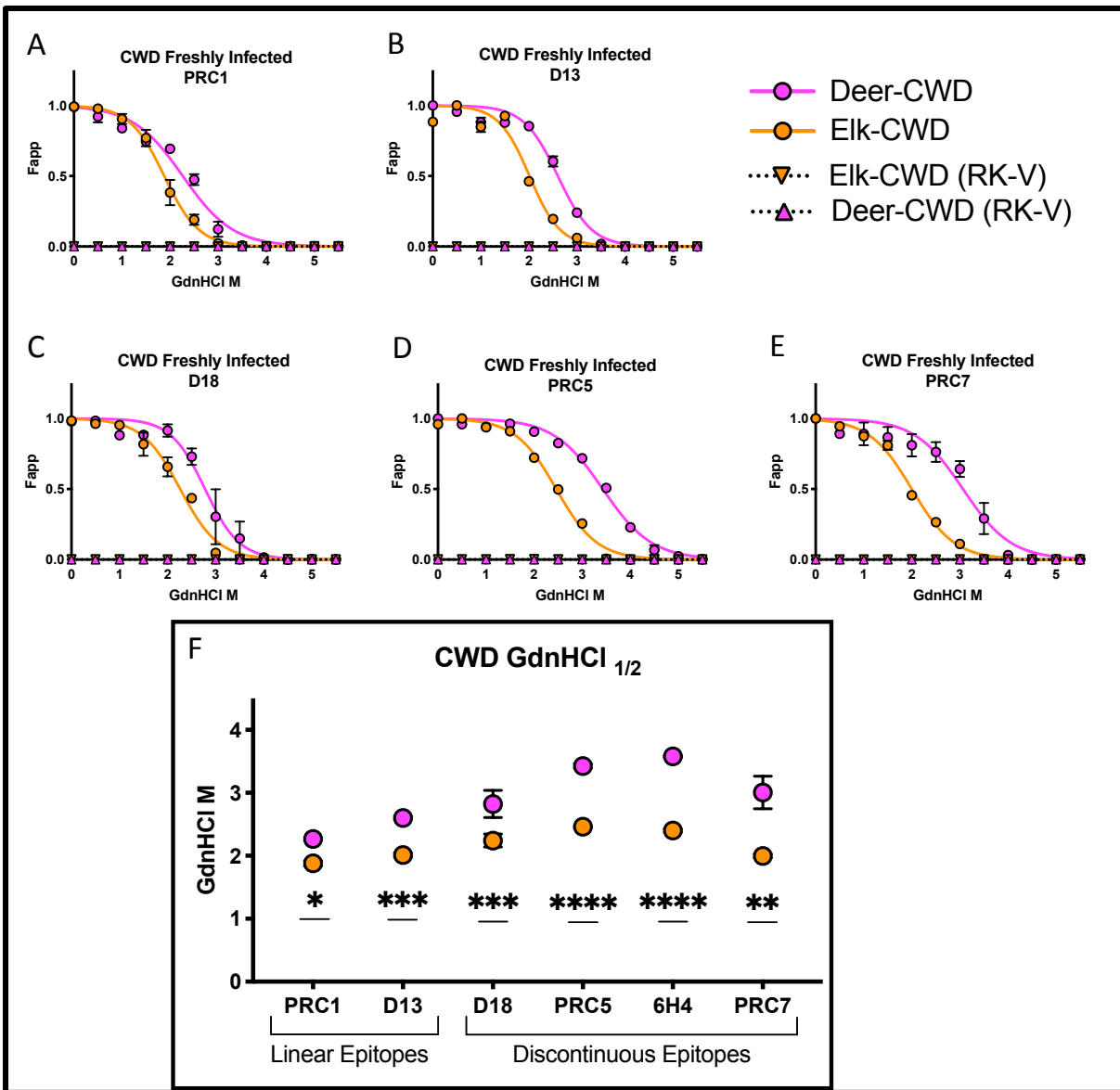


FIGURE 2.6: C-CSA method can differentiate CWD strains at multiple epitopes.

CWD stability pattern seen in chronically infected RK-Deer and RK-Elk was recapitulated in freshly infected cells at multiple epitopes. RK-Deer passaged CWD is more resistant to denaturation at all epitopes examined compared to RK-Elk passaged CWD. Brains (n=3) from terminally ill Tg(ElkPrP)5037^{+/-} and Tg(DeerPrP)1536^{+/-} mice infected with elk CWD isolate Bala05 were used to infect RK-Elk and RK-Deer cell lines, respectively, along with the RK-V(vector only, PrP^C null) cell line. The resultant CWD prions were interrogated with the C-CSA using anti-prion antibody: (A) PRC1 (B) D13 (C) D18 (D) PRC5 (E) PRC7. All sigmoidal dose-response curves of RK-Elk passaged CWD to RK-Deer passaged CWD were significantly different (p<0.001).

(H) When comparing RK-Elk passaged CWD to RK-Deer passaged CWD, each antibody presented statistical differences between the GdnHCl_{1/2} values.

F_{app}, fraction of apparent signal. The sigmoidal dose-response curve was plotted using a four parameter algorithm and nonlinear least-squares fit; with curve comparison. Error bars, SD from n=4 chronic cell lines per group (A), and n=3 animals per group (B-H). Statistical significance: * p ≤ 0.05; ** p ≤ 0.01; *** p ≤ 0.001; **** p ≤ 0.0001. Statistical differences from the GdHCl_{1/2} values between matched, best-fit curves were calculated via unpaired t-test.

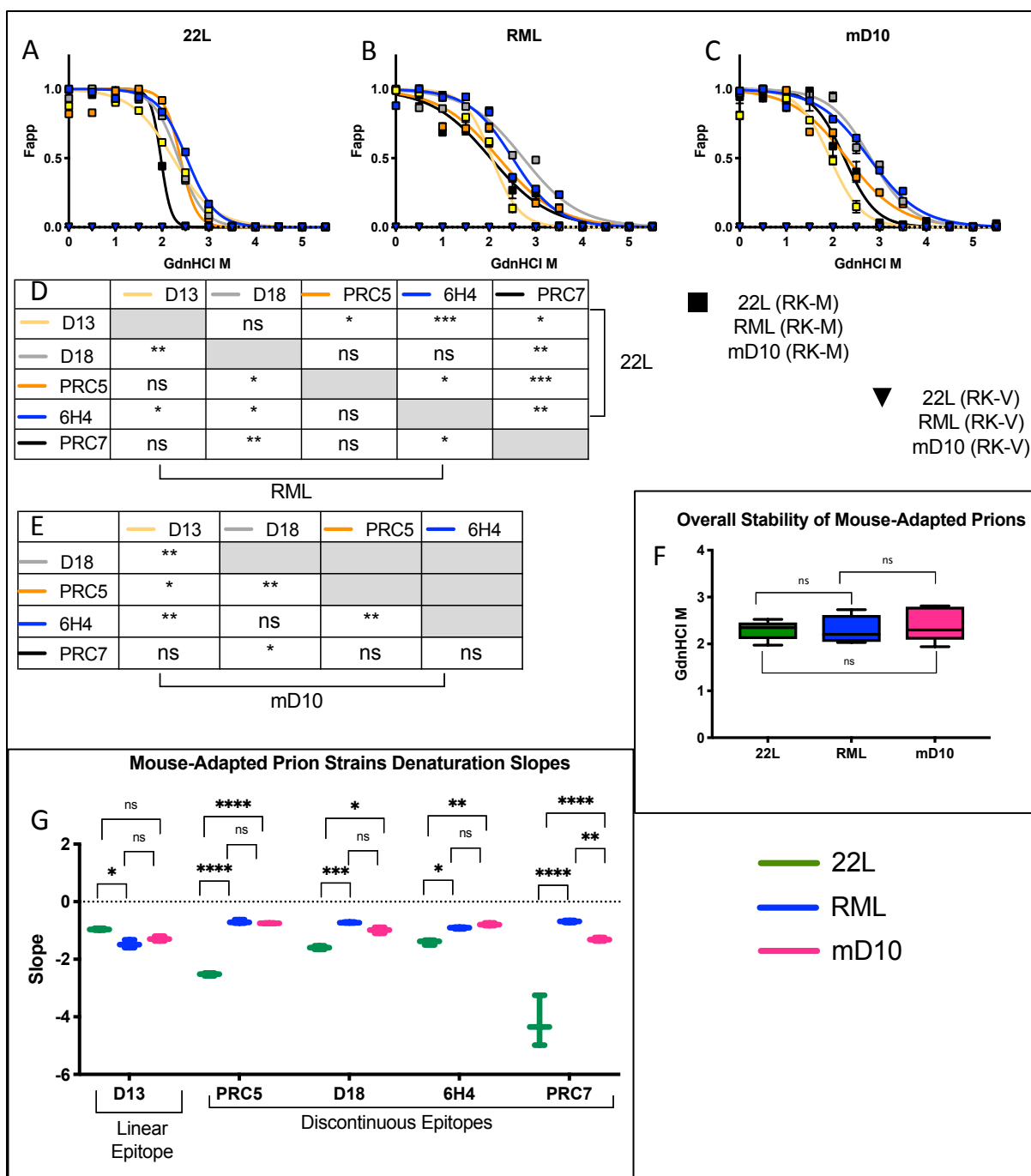


FIGURE 2.7: Subtle structural micro-regions responses to denaturation and protease cleavage define murine-adapted prion strains (A-C) The Guanidine Hydrochloride_{1/2} (GdHCl_{1/2}) value within each murine-adapted strain is not unified, further supporting that prion structure contains micro-regions with discrete denaturation responses. Brains (n=3) from terminally ill C57Bl/6 inbred mice infected with 22L RML, and mD10 were used to infect the RK-Murine cell line along with the RK-V(vector only, PrP^C null) cell line. The resultant murine-adapted prions were interrogated with the C-CSA using anti-prion antibodies (Figure 2.2). Data are shown segregated by PrP^{Sc}, i.e. grouped by

the prion strain. mAbs: D13, D18, PRC5, 6H4, and PRC7. Murine-adapted prion strain stability patterns are complexly different and similar. **(D-E)** Statistical comparison (ANOVA) of each antibody within each prion strain, i.e. RML mAbs PRC5 compared to RML mAbs PRC7. **(F)** Overall, when grouping data by all antibodies and PrP^{Sc}, a general significance is not apparent. This lack of significance when grouping data indicates that to truly evaluate subtle differences in strains with identical amino acid composition, one must rely on individual epitopes **(G)** 22L shows the steepest slope in the discontinuous epitope regions, but surprisingly has the least steep slope in the linear (unstructured) epitope. The slope for RML and 22L differs at every epitope examined; mD10 and 22L differ in the discontinuous epitope regions; finally, mD10 and RML only differ at PRC7 (the glycosylation specific antibody). This indicates that RML and mD10 share similar responses if not similar GdnHCl $\frac{1}{2}$ values to denaturation.

F_{app}, fraction of apparent signal. The sigmoidal dose-response curve was plotted using a four parameter algorithm and nonlinear least-squares fit; with curve comparison. Error bars, SD n=3 animals per group. Statistical significance: ns p \geq 0.05; * p \leq 0.05; ** p \leq 0.01; *** p \leq 0.001; **** p \leq 0.0001. Statistical differences from the GdnHCl_{1/2} values between matched, best fit curves were calculated via ANOVA.

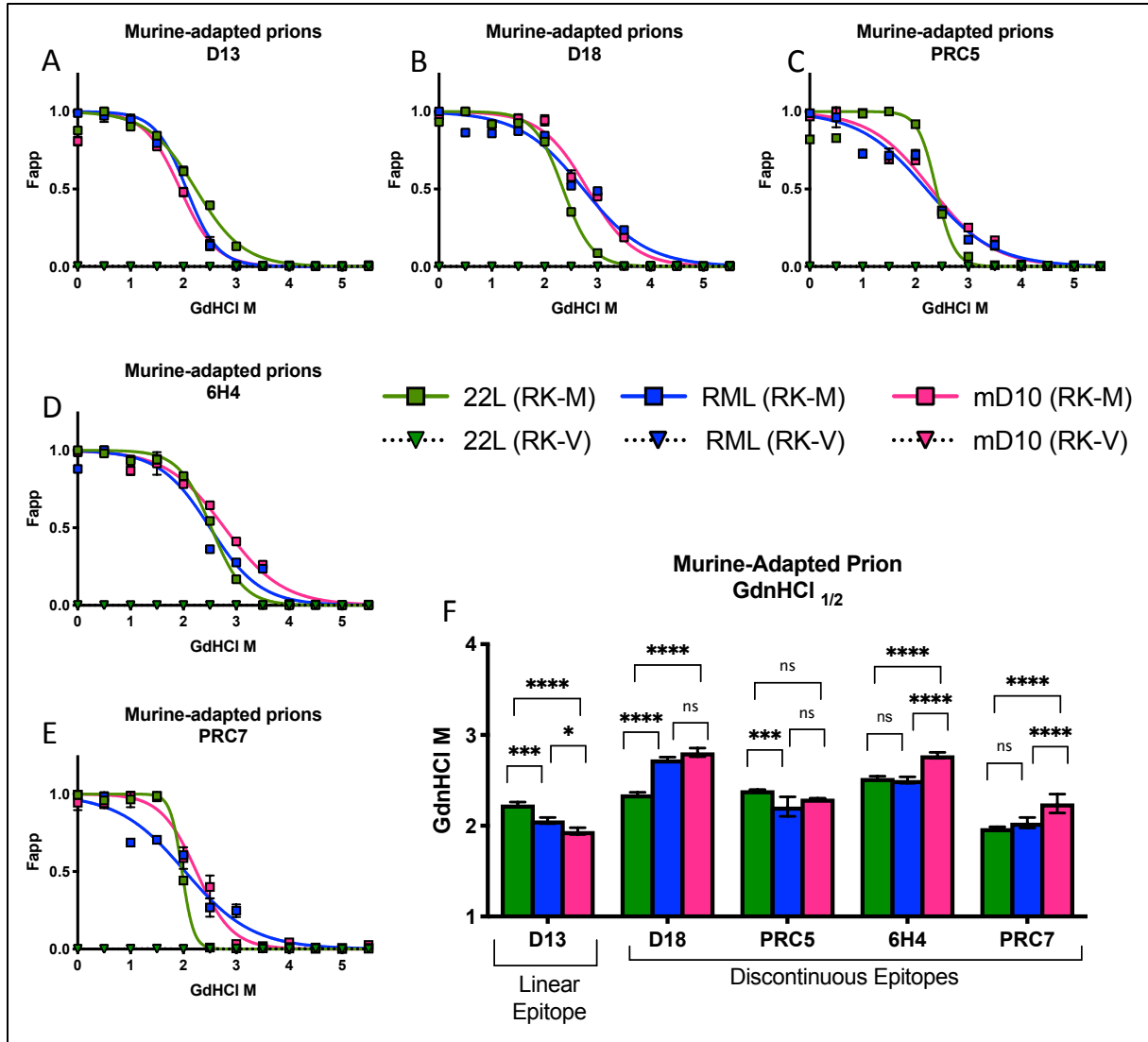


FIGURE 2.8: C-CSA method can differentiate between subtle differences in murine-adapted prion strains (A-E) Murine-adapted prion strain stability patterns are complexly different and similar. Brains (n=3) from terminally ill C57Bl/6 inbred mice infected with 22L (green), RML (blue), and mD10 (pink) were used to infect the RK-Murine cell line along with the RK-V(vector only, PrP^C null) cell line. The resultant murine-adapted prions were interrogated with the C-CSA using anti-prion antibody: (A) D13 (B) D18 (C) PRC5 (D) 6H4 (E) PRC7. (F) Due to identical amino acid sequence, the statistical differences between the GdnHCl_{1/2} values ranged; e.g. some epitopes were more heterogeneous (D13) compared to others (PRC5, and 6H4)

F_{app}, fraction of apparent signal. The sigmoidal dose-response curve was plotted using a four parameter algorithm and nonlinear least-squares fit; with curve comparison. Error bars, SD n=3 animals per group (A-F). Statistical significance: ns p ≥ 0.05; * p ≤

0.05; ** $p \leq 0.01$; *** $p \leq 0.001$; **** $p \leq 0.0001$. Statistical differences from the $GdHCl_{1/2}$ values between matched, best fit curves were calculated via ANOVA.

D. DISCUSSION

The results can be summarized into two components: (i) C-CSA technique, and (ii) further delineation of strain properties of Elk-CWD, Deer-CWD, mouse-adapted scrapie (22L), mouse-adapted scrapie (RML), and mouse adapted deer CWD (mD10).

C-CSA technique

Research becomes stymied by current technological tools and the confounding complexity found in natural systems; the answer is to find novel, innovative techniques that can expand our ability to ask important questions. Consequently, the C-CSA (Figure 2.2) represents a new tool to reveal more details about prion strain structure in a facile and expedient process. The C-CSA allows data to be gathered across multiple species, with multiple infectious prions, in both chronically infected and freshly infected paradigms (Figure 2.3, 2.4) and more importantly provides a high-throughput method to examine the prion protein at multiple epitopes (Figure 2.5-2.8). The C-CSA combined with an array of epitope-mapped antibodies provides a new means to differentiate prion strains in murine-adapted scrapie and chronic wasting disease strains and chronic wasting disease in both deer and elk. This technique could be expanded in the future for use with other prions; i.e. scrapie (sheep/goats), CJD (humans), TME (mink), etc. Only a researcher's imagination, finances, and cell susceptibility to the chosen prion limit the possibilities inherent in the C-CSA. The C-CSA could be a truly useful tool to reliably show strain differences in multiple strains and species. A limitation of the C-CSA is the required usage of PK. Any PK-sensitive PrP^{Sc} fraction will not be examined

with this technique. Additionally, this technique is limited to transfected cell lines available and infectious material that can infect said cell lines.

Establishing subtle conformational differences between prion strains

Like the artistic complexity that can turn a piece of paper into an origami masterpiece, the primary structure of the prion cellular protein is bent and folded into multiple forms. The folding differences of these forms of the prion protein are fundamental to the ability to cause and propagate disease. It is crucial for the overall survival of cervids and protection of humans that we understand CWD and the structure of the cervid prion protein better. Human risk due to exposure to animal prion diseased tissues is a prevailing concern. The CWD prion has a resoundingly different structure and resistance to denaturation due to the single amino acid difference in the substrate (PrP^C) of infected species, i.e. Deer-Q226/Elk-E226.

Overall, the C-CSA recapitulates previous differences between Elk and Deer CWD, Deer-CWD show a higher resistance to denaturation, i.e. more stable conformation, than Elk-CWD. The first unexpected but added bonus of the C-CSA was the disparity between the GdHCl_{1/2} value for chronically CWD infected and freshly CWD infected RK-Deer and RK-Elk (Figure 2.3A-B), and chronically and freshly infected murine-adapted scrapie (Figure 2.4A-B). The comparison between chronically infected and freshly infected cells is further examined in Chapter 4.

Freshly infected Deer-CWD and Elk-CWD were significantly different when the epitopes were summed (Figure 2.5D) and at each epitope (Figure 2.6F) examined. As expected, the murine-adapted strains were not as resoundingly different as the cervid

CWD data. The murine-adapted strains were not significantly different when summed (Figure 2.7F), but were different at multiple epitopes (Figure 2.8F). Unlike the CWD data (Figure 2.6F), murine-adapted prion strains (Figure 2.8F) did not have a trend of increasing the $GdHCl_{1/2}$ value from the unstructured region (linear epitope) into the globular region (discontinuous epitopes).

The heterogeneity within a single strains response to denaturation and protease cleavage was unexpected. The premise that the prion molecule denatures at all epitopes equally and therefore responds to protease cleavage identically did not hold out (Figures 2.5, 2.7). The least heterogeneous was Elk-CWD (13%), Deer-CWD, mouse-adapted scrapie 22L strain, and mouse-adapted CWD mD10 strain were (60%) heterogeneous and the most heterogeneous was mouse-adapted scrapie RML strain (70%) (Figure 2.5C, 2.7D-E).

Mouse-adapted prion strain structural differences further delineate classically defined and newly adapted prions (Figure 2.7, 2.8). First, structural differences between classically defined mouse-adapted scrapie 22L and RML strains range between the N-terminal unstructured region and α helix-1 region. Whereas, the glycosylation specific epitope (aglycosylated, and monoglycosylated at residue 196), and α helix-3 are similar between these two strains. A further consequence of these subtle differences between two murine-adapted sheep scrapie strains is that each adaption of CWD into mice has the potential to be a unique "mCWD" and contain as many differences as RML and 22L have to each other. The structural differences between a classically defined mouse-adapted scrapie 22L strain and newly adapted CWD mD10 strain range through the

entire molecule with an exception on the region straddling α helix-1. Overall, mD10 contains a unique structure, distinct to 22L. The structural differences between a classically defined mouse-adapted scrapie RML strain and newly adapted CWD mD10 strain range between the N-terminal unstructured region with a brief similarity at α helix-1, then differentiate again between α helix-1 and α helix-3. Overall, mD10 has a distinctly different structure than RML, and similar the α helix-1 region, this is trend is similar to the α helix-1 region comparison of mD10 and 22L.

The abrupt slope seen in the discontinuous region of 22L might originate from the serially cloning of this mouse-adapted scrapie strain. Serial cloning a prion promotes selection of a single prion conformer in the quasi-species paradigm of the conformational selection model¹⁴⁸. This model tries to reconcile why a copious possible prion protein conformational structures exist; yet, a specific strain can be both faithfully propagated via bioassay in the same species and produce a completely different adaptive disease in a new species. The selection model proposes that there are quasi-species, which can be defined as different tertiary conformers of the same primary amino acid sequence. Moreover, this model proposes that the interaction between PrP^{Sc} and PrP^C structures selects a specific PrP^{Sc} conformation to be propagated. Strain diversity undergoes strain-dependent or species-dependent selection that resolves a preferred PrP^{Sc} conformation¹⁴⁹. In line with previous CSA observations¹⁵⁰, RML contains a more gradual slope at all discontinuous epitopes examined which could indicate the presence of quasispecies or simply a higher complexity in the RML amyloid fibrils compared to 22L.

Overall, subtle but insidious conformational variations of the misfolded prion protein at epitope-mapped micro-regions ultimately convey prion strain properties. The multiple epitope-mapped antibody C-CSA expands the ability to elucidate subtle variation between prion strains. Ultimately, human desire to prevent lethal disease in other humans and animals is often stymied by the complexities nature imbues in pathogens. Until recently, the concept of a protein folding into a pathological conformation and propagating the misfolded form to cause disease was limited to prion diseases; however, other devastating neurodegenerative diseases (e.g. Alzheimer's¹⁵¹, Parkinson's¹⁵², etc.) share similar etiology¹⁵³. Understanding prion diseases may further our ability to understand other neurodegenerative diseases¹⁵⁴. This allows the prion protein to serve as a model for these human diseases and increases the need for stringent well-designed prion protein experiments.

BIBLIOGRAPHY

-
- ¹ Sigurðsson, B. (1954). *Rida, a chronic encephalitis of sheep: with general remarks on infections which develop slowly and some of their special characteristics.*
 - ² Stockman, S (1913, November 8) "Scrapie." *The Scottish Farmer*,¹ vol. xxi., No. 1088, p. 1059: Glasgow
 - ³ Prusiner SB (1982) Novel proteinaceous infectious particles cause scrapie. *Science* 216: 136-144
 - ⁴ Oesch, B., Teplow, D. B., Stahl, N., Serban, D., Hood, L. E., & Prusiner, S. B. (1990). Identification of cellular proteins binding to the scrapie prion protein. *Biochemistry*, 29(24), 5848-5855.
 - ⁵ Basler, K., Oesch, B., Scott, M., Westaway, D., Wälchli, M., Groth, D. F., & Weissmann, C. (1986). Scrapie and cellular PrP isoforms are encoded by the same chromosomal gene. *Cell*, 46(3), 417-428.
 - ⁶ Belt, P. B., Muileman, I. H., Schreuder, B. E., Bos-de Ruijter, J., Gielkens, A. L., & Smits, M. A. (1995). Identification of five allelic variants of the sheep PrP gene and their association with natural scrapie. *Journal of General Virology*, 76(3), 509-517.
 - ⁷ Angers, R. C., H. E. Kang, D. Napier, S. Browning, T. Seward, C. Mathiason, A. Balachandran, D. McKenzie, J. Castilla, C. Soto, J. Jewell, C. Graham, E. A. Hoover, and G. C. Telling. 2010. Prion strain mutation determined by prion protein conformational compatibility and primary structure. *Science* 328:1154-1158.
 - ⁸ Pan, K. M., Baldwin, M., Nguyen, J., Gasset, M., Serban, A. N. A., Groth, D., & Cohen, F. E. (1993). Conversion of alpha-helices into beta-sheets features in the formation of the scrapie prion proteins. *Proceedings of the National Academy of Sciences*, 90(23), 10962-10966.
 - ⁹ Prusiner, S. B., Groth, D. F., Bolton, D. C., Kent, S. B., & Hood, L. E. (1984). Purification and structural studies of a major scrapie prion protein. *Cell*, 38(1), 127-134.
 - ¹⁰ Prusiner, S. B., Groth, D. F., Bildstein, C., Masiarz, F. R., McKinley, M. P., & Cochran, S. P. (1980). Electrophoretic properties of the scrapie agent in agarose gels. *Proceedings of the National Academy of Sciences*, 77(5), 2984-2988.
 - ¹¹ Alper T, Cramp WA, Haig DA, *et al.* Does the agent of scrapie replicate without nucleic acid? *Nature* 1967;**214**:764-6.
 - ¹² Gibbs, C. J., Gajdusek, D. C., & Latarjet, R. (1978). Unusual resistance to ionizing radiation of the viruses of kuru, Creutzfeldt-Jakob disease, and scrapie. *Proceedings of the National Academy of Sciences*, 75(12), 6268-6270.
 - ¹³ Pattison IH. Resistance of the scrapie agent to formalin. *J Comp Pathol* 1965;**75**:159-64.
 - ¹⁴ Yuan Q, Eckland T, Telling G, Bartz J, Bartelt-Hunt S (2015) Mitigation of Prion Infectivity and Conversion Capacity by a Simulated Natural Process – Repeated Cycles of Drying and Wetting. *PLoS Pathog* 11(2)
 - ¹⁵ Seidel, B., Thomzig, A., Buschmann, A., Groschup, M. H., Peters, R., Beekes, M., & Terytze, K. (2007). Scrapie agent (strain 263K) can transmit disease via the oral route after persistence in soil over years. *PLoS One*, 2(5), e435.

-
- ¹⁶ Nichols, T. A., Pulford, B., Wyckoff, A. C., Meyerett, C., Michel, B., Gertig, K., & Zabel, M. D. (2009). Detection of protease-resistant cervid prion protein in water from a CWD-endemic area. *Prion*, 3(3), 171-183.
- ¹⁷ Pritzkow, S., Morales, R., Moda, F., Khan, U., Telling, G. C., Hoover, E., & Soto, C. (2015). Grass Plants Bind, Retain, Uptake, and Transport Infectious Prions. *Cell reports*, 11(8), 1168-1175.
- ¹⁸ Vázquez-Fernández, E., Alonso, J., Pastrana, M. A., Ramos, A., Stitz, L., Vidal, E., & Requena, J. R. (2012). Structural organization of mammalian prions as probed by limited proteolysis. *PLoS One*, 7(11), e50111.
- ¹⁹ Dron, M., Moudjou, M., Chapuis, J., Salamat, M. K. F., Bernard, J., Cronier, S., & Laude, H. (2010). Endogenous proteolytic cleavage of disease-associated prion protein to produce C2 fragments is strongly cell-and tissue-dependent. *Journal of Biological Chemistry*, 285(14), 10252-10264.
- ²⁰ Nicot, S., & Baron, T. G. (2010). Strain-specific proteolytic processing of the prion protein in prion diseases of ruminants transmitted in ovine transgenic mice. *Journal of general virology*, 91(2), 570-574.
- ²¹ Requena, J. R., & Wille, H. (2014). The structure of the infectious prion protein: experimental data and molecular models. *Prion*, 8(1), 60-66.
- ²² Bett C, Joshi-Barr S, Lucero M, Trejo M, Liberski P, et al. (2012) Biochemical Properties of Highly Neuroinvasive Prion Strains. *PLoS Pathog* 8(2)
- ²³ Tanaka, M., Collins, S. R., Toyama, B. H., & Weissman, J. S. (2006). The physical basis of how prion conformations determine strain phenotypes. *Nature*, 442(7102), 585-589.
- ²⁴ Telling, G. C., Parchi, P., DeArmond, S. J., Cortelli, P., Montagna, P., Gabizon, R., & Prusiner, S. B. (1996). Evidence for the conformation of the pathologic isoform of the prion protein enciphering and propagating prion diversity. *Science*, 274(5295), 2079-2082.
- ²⁵ Colby, D. W., Giles, K., Legname, G., Wille, H., Baskakov, I. V., DeArmond, S. J., & Prusiner, S. B. (2009). Design and construction of diverse mammalian prion strains. *Proceedings of the National Academy of Sciences*, 106(48), 20417-20422.
- ²⁶ Peretz, D., Scott, M. R., Groth, D., Williamson, R. A., Burton, D. R., Cohen, F. E., & Prusiner, S. B. (2001). Strain-specified relative conformational stability of the scrapie prion protein. *Protein Science*, 10(4), 854-863.
- ²⁷ Collinge, J., Sidle, K. C., Meads, J., Ironside, J., & Hill, A. F. (1996). Molecular analysis of prion strain variation and the aetiology of 'new variant' CJD. *Nature*, 383(6602), 685.
- ²⁸ Comber, T. (1772). *Real improvements in agriculture:(on the principles of A. Young, Esq. :) recommended to accompany improvements of rents; in a letter to Reade Peacock, esq; alderman of Huntingdon. To which is added, a letter to Dr. Hunter, physician in York. Concerning the rickets in sheep.* Printed for W. Nicoll.
- ²⁹ Cuillé, J. & Chelle, P. L. (1936). La maladie dite tremblante du mouton est-elle inoculable. *CR Acad Sci* 203, 1552-1554

-
- ³⁰ Pattison, I. H., Gordon, W. S., & Millson, G. C. (1959). Experimental production of scrapie in goats. *Journal of Comparative Pathology and Therapeutics*, 69, 300-312.
- ³¹ Autenried, P., Ague&, M., Weissmann, C., Zentraliabor, S., & Zurich, U. (2004). Mice Devoid of PrP Are Resistant to Scrapie. *Cell*, 116(116), 1339-1347.
- ³² Sailer, A., Büeler, H., Fischer, M., Aguzzi, A., & Weissmann, C. (1994). No propagation of prions in mice devoid of PrP. *Cell*, 77(7), 967-968.
- ³³ Büeler, H., Aguzzi, A., Sailer, A., Greiner, R. A., Autenried, P., Aguet, M., & Weissmann, C. (1993). Mice devoid of PrP are resistant to scrapie. *Cell*, 73(7), 1339-1347.
- ³⁴ Chandler, R. (1961). Encephalopathy in mice produced by inoculation with scrapie brain material. *The Lancet*, 1(7191), 1378-1379.
- ³⁵ Darcel, C. L. Q., Merriman, M., Beauregard, M., Avery, R. J., & Kasting, R. (1963). Scrapie I. Transmission and Pathogenesis. *Canadian journal of comparative medicine and veterinary science*, 27(4), 81.
- ³⁶ Fraser, H., & Dickinson, A. G. (1973). Scrapie in mice: agent-strain differences in the distribution and intensity of grey matter vacuolation. *Journal of comparative pathology*, 83(1), 29-40.
- ³⁷ Eklund, C. M., Hadlow, W. J., & Kennedy, R. C. (1963). Some properties of the scrapie agent and its behavior in mice. *Experimental Biology and Medicine*, 112(4), 974-979.
- ³⁸ Kimberlin, R. H., Cole, S., & Walker, C. A. (1987). Temporary and permanent modifications to a single strain of mouse scrapie on transmission to rats and hamsters. *Journal of General Virology*, 68(7), 1875-1881.
- ³⁹ Zlotnik, I., & Rennie, J. C. (1965). Experimental transmission of mouse passaged scrapie to goats, sheep, rats and hamsters. *Journal of comparative pathology*, 75(2), 147IN3157-156IN6.
- ⁴⁰ Mould, D. L., Dawson, A. M., Slater, J. S., & Zlotnik, I. (1967). Relationships between chemical changes and histological damage in the brains of scrapie affected mice. *Journal of comparative pathology*, 77(4), 393IN5403-402IN6.
- ⁴¹ Kim, Y. S., Carp, R. I., Callahan, S. M., Natelli, M., & Wisniewski, H. M. (1990). Vacuolization, incubation period and survival time analyses in three mouse genotypes injected stereotactically in three brain regions with the 22L scrapie strain. *Journal of Neuropathology & Experimental Neurology*, 49(2), 106-113.
- ⁴² Chandler, R. (1961). Encephalopathy in mice produced by inoculation with scrapie brain material. *The Lancet*, 1(7191), 1378-1379.
- ⁴³ Marsh, R. F., Burger, D., Eckroade, R., Rhein, G. Z., & Hanson, R. P. (1969). A preliminary report on the experimental host range of the transmissible mink encephalopathy agent. *The Journal of infectious diseases*, 713-719.
- ⁴⁴ Bruce, M. E., Will, R. G., Ironside, J. W., McConnell, I., Drummond, D., Suttie, A., & Cousens, S. (1997). Transmissions to mice indicate that 'new variant' CJD is caused by the BSE agent. *Nature*, 389(6650), 498-501.
- ⁴⁵ Bosque, P. J., & Prusiner, S. B. (2000). Cultured cell sublines highly susceptible to prion infection. *Journal of virology*, 74(9), 4377-4386.

-
- ⁴⁶ Marbiah, M. M., Harvey, A., West, B. T., Louzolo, A., Banerjee, P., Alden, J., & Bloom, G. S. (2014). Identification of a gene regulatory network associated with prion replication. *The EMBO journal*, e201387150.
- ⁴⁷ Bian, J., Kang, H. E., & Telling, G. C. (2014). Quinacrine promotes replication and conformational mutation of chronic wasting disease prions. *Proceedings of the National Academy of Sciences*, 111(16), 6028-6033.
- ⁴⁸ Ramljak, S., Asif, A. R., Armstrong, V. W., Wrede, A., Groschup, M. H., Buschmann, A., & Zerr, I. (2008). Physiological role of the cellular prion protein (PrP_C): protein profiling study in two cell culture systems. *Journal of proteome research*, 7(7), 2681-2695.
- ⁴⁹ Oelschlegel, A. M., Fallahi, M., Ortiz-Umpierre, S., & Weissmann, C. (2012). The Extended Cell Panel Assay (ECPA) characterizes the relationship of RML, 79A and 139A prion strains and reveals conversion of 139A to 79A-like prions in cell culture. *Journal of virology*, JVI-00181.
- ⁵⁰ Zou, R. S., Fujioka, H., Guo, J. P., Xiao, X., Shimoji, M., Kong, C., & Moudjou, M. (2011). Characterization of spontaneously generated prion-like conformers in cultured cells. *Aging (Albany NY)*, 3(10), 968-984.
- ⁵¹ Edgeworth, J. A., Gros, N., Alden, J., Joiner, S., Wadsworth, J. D., Linehan, J., & Collinge, J. (2010). Spontaneous generation of mammalian prions. *Proceedings of the National Academy of Sciences*, 107(32), 14402-14406.
- ⁵² Brown, C. A., Schmidt, C., Poulter, M., Hummerich, H., Klöhn, P. C., Jat, P., & Lloyd, S. E. (2014). In vitro screen of prion disease susceptibility genes using the scrapie cell assay. *Human molecular genetics*, 23(19), 5102-5108.
- ⁵³ Marbiah, M. M., Harvey, A., West, B. T., Louzolo, A., Banerjee, P., Alden, J., & Bloom, G. S. (2014). Identification of a gene regulatory network associated with prion replication. *The EMBO journal*, e201387150.
- ⁵⁴ Molloy, B., & McMahon, H. E. (2014). A cell-biased effect of estrogen in prion infection. *Journal of virology*, 88(2), 1342-1353.
- ⁵⁵ Pulford, B., Reim, N., Bell, A., Veatch, J., Forster, G., Bender, H., & Wyckoff, A. C. (2010). Liposome-siRNA-peptide complexes cross the blood-brain barrier and significantly decrease PrP^C on neuronal cells and PrP^{RES} in infected cell cultures. *PloS one*, 5(6), e11085.
- ⁵⁶ Nishizawa, K., Oguma, A., Kawata, M., Sakasegawa, Y., Teruya, K., & Doh-ura, K. (2014). Efficacy and mechanism of a glycoside compound inhibiting abnormal prion protein formation in prion-infected cells: implications of interferon and phosphodiesterase 4D-interacting protein. *Journal of virology*, 88(8), 4083-4099.
- ⁵⁷ Lu D, et al. (2013) Biaryl amides and hydrazones as therapeutics for prion disease in transgenic mice. *J Pharmacol Exp Ther* 347(2):325-338.
- ⁵⁸ Li Z, et al. (2013) Discovery and preliminary SAR of arylpiperazines as novel, brain-penetrant antiprion compounds. *ACS Med Chem Letters* 4(4):397-401.
- ⁵⁹ Kimata A, et al. (2007) New series of antiprion compounds: Pyrazolone derivatives have the potent activity of inhibiting protease-resistant prion protein accumulation. *J Med Chem* 50(21):5053-5056.

-
- ⁶⁰ Geissen M, et al. (2011) From high-throughput cell culture screening to mouse model: Identification of new inhibitor classes against prion disease. *ChemMedChem* 6(10): 1928–1937.
- ⁶¹ Ghaemmaghami S, May BC, Renslo AR, Prusiner SB (2010) Discovery of 2-aminothiazoles as potent anti-prion compounds. *J Virol* 84(7):3408–3412.
- ⁶² Bate, C., Salmona, M., Diomedea, L., & Williams, A. (2004). Squalastatin cures prion-infected neurons and protects against prion neurotoxicity. *Journal of Biological Chemistry*, 279(15), 14983-14990.
- ⁶³ Kocisko, D. A., & Caughey, B. (2006). Searching for Anti-Prion Compounds: Cell-Based High-Throughput In Vitro Assays and Animal Testing Strategies. *Methods in enzymology*, 412, 223-234.
- ⁶⁴ Li, J., Browning, S., Mahal, S. P., Oelschlegel, A. M., & Weissmann, C. (2010). Darwinian evolution of prions in cell culture. *Science*, 327(5967), 869-872.
- ⁶⁵ Klohn, P. C., L. Stoltze, E. Flechsig, M. Enari, and C. Weissmann. 2003. A quantitative, highly sensitive cell-based infectivity assay for mouse scrapie prions. *Proc Natl Acad Sci U S A* 100:11666-71.
- ⁶⁶ van Der Merwe, J., Aiken, J., Westaway, D., & McKenzie, D. (2015). The standard scrapie cell assay: development, utility and prospects. *Viruses*, 7(1), 180-198.
- ⁶⁷ Bosque, P. J., and S. B. Prusiner. 2000. Cultured cell sublines highly susceptible to prion infection. *J. Virol.* 74:4377–4386.
- ⁶⁸ Mahal, S. P., C. A. Demczyk, E. W. Smith, Jr., P. C. Klohn, and C. Weissmann. 2008. Assaying prions in cell culture: the standard scrapie cell assay (SSCA) and the scrapie cell assay in end point format (SCEPA). *Methods Mol. Biol.* 459:49–68.
- ⁶⁹ Christofinis, G. J., & Beale, A. J. (1968). Some biological characters of cell lines derived from normal rabbit kidney. *The Journal of Pathology*, 95(2), 377-381.
- ⁷⁰ Bian, J., Napier, D., Khaychuck, V., Angers, R., Graham, C., & Telling, G. (2010). Cell-based quantification of chronic wasting disease prions. *Journal of virology*, 84(16), 8322-8326.
- ⁷¹ Khaychuk, V. (2012). Prion Characterization Using Cell Based Approaches. Doctoral Dissertation, University of Kentucky
- ⁷² Arellano-Anaya, Z. E., Savistchenko, J., Mathey, J., Huor, A., Lacroux, C., Andréoletti, O., & Vilette, D. (2011). A simple, versatile and sensitive cell-based assay for prions from various species. *PLoS One*, 6(5), e20563.
- ⁷³ Leblanc, P., S. Alais, I. Porto-Carreiro, S. Lehmann, J. Grassi, G. Raposo, and J. L. Darlix. 2006. Retrovirus infection strongly enhances scrapie infectivity release in cell culture. *EMBO J.* 25:2674–2685.
- ⁷⁴ Vilette, D., O. Andreoletti, F. Archer, M. F. Madelaine, J. L. Vilotte, S. Lehmann, and H. Laude. 2001. Ex vivo propagation of infectious sheep scrapie agent in heterologous epithelial cells expressing ovine prion protein. *Proc. Natl. Acad. Sci. U. S. A.* 98:4055–4059
- ⁷⁵ Sweeting B., Brown, E., Chakrabarty, A., & Pai, E. F. (2009). The structure of rabbit PrPC: clues into species barrier and prion disease susceptibility. *Canadian Light Source*, 28.

-
- ⁷⁶ Sweeting, B, Brown E, Khan MQ, Chakrabartty A, Pai EF (2013) N-Terminal Helix-Cap in α -Helix 2 Modulates β -State Misfolding in Rabbit and Hamster Prion Proteins. *PLoS ONE* 8(5)
- ⁷⁷ Chianini, F., Fernández-Borges, N., Vidal, E., Gibbard, L., Pintado, B., de Castro, J., & Pang, Y. (2012). Rabbits are not resistant to prion infection. *Proceedings of the National Academy of Sciences*, 109(13), 5080-5085.
- ⁷⁸ Moore, R. A., Vorberg, I., & Priola, S. A. (2005). Species barriers in prion diseases – brief review. In *Infectious Diseases from Nature: Mechanisms of Viral Emergence and Persistence* (pp. 187-202). Springer Vienna.
- ⁷⁹ Bian, J., Napier, D., Khaychuck, V., Angers, R., Graham, C., & Telling, G. (2010). Cell-based quantification of chronic wasting disease prions. *Journal of virology*, 84(16), 8322-8326.
- ⁸⁰ Kocisko, D. A., & Caughey, B. (2006). Searching for Anti-Prion Compounds: Cell-Based High-Throughput In Vitro Assays and Animal Testing Strategies. *Methods in enzymology*, 412, 223-234.
- ⁸¹ Korth, C., May, B. C., Cohen, F. E., & Prusiner, S. B. (2001). Acridine and phenothiazine derivatives as pharmacotherapeutics for prion disease. *Proceedings of the National Academy of Sciences*, 98(17), 9836-9841.
- ⁸² Oelschlegel, A. M., Fallahi, M., Ortiz-Umpierre, S., & Weissmann, C. (2012). The Extended Cell Panel Assay (ECPA) characterizes the relationship of RML, 79A and 139A prion strains and reveals conversion of 139A to 79A-like prions in cell culture. *Journal of virology*, JVI-00181.
- ⁸³ Lawson, V. A., L. J. Vella, J. D. Stewart, R. A. Sharples, H. Klemm, D. M. Machalek, C. L. Masters, R. Cappai, S. J. Collins, and A. F. Hill. 2008. Mouse-adapted sporadic human Creutzfeldt-Jakob disease prions propagate in cell culture. *Int. J. Biochem. Cell Biol.* 40:2793–2801.
- ⁸⁴ Courageot, M. P., N. Daude, R. Nonno, S. Paquet, M. A. Di Bari, A. Le Dur, J. Chapuis, A. F. Hill, U. Agrimi, H. Laude, and D. Vilette. 2008. A cell line infectible by prion strains from different species. *J. Gen. Virol.* 89:341–347.
- ⁸⁵ Oelschlegel, A. M., Fallahi, M., Ortiz-Umpierre, S., & Weissmann, C. (2012). The Extended Cell Panel Assay (ECPA) characterizes the relationship of RML, 79A and 139A prion strains and reveals conversion of 139A to 79A-like prions in cell culture. *Journal of virology*, JVI-00181.
- ⁸⁶ Pace, C. N., Fu, H., Fryar, K., Landua, J., Trevino, S. R., Schell, D., & Sevcik, J. (2014). Contribution of hydrogen bonds to protein stability. *Protein Science*, 23(5), 652-661.
- ⁸⁷ Goldberg, M. E., Rudolph, R., & Jaenicke, R. (1991). A kinetic study of the competition between renaturation and aggregation during the refolding of denatured-reduced egg white lysozyme. *Biochemistry*, 30(11), 2790-2797.
- ⁸⁸ Ohkuri, T., Nagatomo, S., Oda, K., So, T., Imoto, T., & Ueda, T. (2010). A protein's conformational stability is an immunologically dominant factor: evidence that free-energy barriers for protein unfolding limit the immunogenicity of foreign proteins. *The Journal of Immunology*, 185(7), 4199-4205.

-
- ⁸⁹ Huang, K. S., Bayley, H., Liao, M. J., London, E., & Khorana, H. G. (1981). Refolding of an integral membrane protein. Denaturation, renaturation, and reconstitution of intact bacteriorhodopsin and two proteolytic fragments. *Journal of Biological Chemistry*, 256(8), 3802-3809.
- ⁹⁰ Swietnicki, W., Petersen, R. B., Gambetti, P., & Surewicz, W. K. (1998). Familial mutations and the thermodynamic stability of the recombinant human prion protein. *Journal of Biological Chemistry*, 273(47), 31048-31052.
- ⁹¹ Yeh, V., Broering, J. M., Romanyuk, A., Chen, B., Chernoff, Y. O., & Bommarius, A. S. (2010). The Hofmeister effect on amyloid formation using yeast prion protein. *Protein Science*, 19(1), 47-56.
- ⁹² O'Brien, E. P., Dima, R. I., Brooks, B., & Thirumalai, D. (2007). Interactions between hydrophobic and ionic solutes in aqueous guanidinium chloride and urea solutions: lessons for protein denaturation mechanism. *Journal of the American Chemical Society*, 129(23), 7346-7353.
- ⁹³ De Simone, A., Dodson, G. G., Verma, C. S., Zagari, A., & Fraternali, F. (2005). Prion and water: tight and dynamical hydration sites have a key role in structural stability. *Proceedings of the National Academy of Sciences of the United States of America*, 102(21), 7535-7540.
- ⁹⁴ Hatefi, Y., & Hanstein, W. G. (1969). Solubilization of particulate proteins and nonelectrolytes by chaotropic agents. *Proceedings of the National Academy of Sciences*, 62(4), 1129-1136.
- ⁹⁵ Salvi, G., De Los Rios, P., & Vendruscolo, M. (2005). Effective interactions between chaotropic agents and proteins. *Proteins: Structure, Function, and Bioinformatics*, 61(3), 492-499.
- ⁹⁶ Sawyer, W. H., & Puckridge, J. (1973). The dissociation of proteins by chaotropic salts. *Journal of Biological Chemistry*, 248(24), 8429-8433.
- ⁹⁷ Saijo E, Hughson AG, Raymond GJ, Suzuki A, Horiuchi M, Caughey B. 2016. PrPSc-specific antibody reveals C-terminal conformational differences between prion strains. *J Virol* 90:4905-4913.
- ⁹⁸ Yamada, T., Liu, X., Englert, U., Yamane, H., & Dronskowski, R. (2009). Solid-State Structure of Free Base Guanidine Achieved at Last. *Chemistry—A European Journal*, 15(23), 5651-5655.
- ⁹⁹ Mason, P. E., Neilson, G. W., Enderby, J. E., Saboungi, M. L., Dempsey, C. E., MacKerell, A. D., & Brady, J. W. (2004). The structure of aqueous guanidinium chloride solutions. *Journal of the American Chemical Society*, 126(37), 11462-11470.
- ¹⁰⁰ Makhatadze, G. I., & Privalov, P. L. (1992). Protein interactions with urea and guanidinium chloride: a calorimetric study. *Journal of molecular biology*, 226(2), 491-505.
- ¹⁰¹ Shih, O., England, A. H., Dallinger, G. C., Smith, J. W., Duffey, K. C., Cohen, R. C., & Saykally, R. J. (2013). Cation-cation contact pairing in water: Guanidinium. *The Journal of chemical physics*, 139(3), 07B616_1.

-
- ¹⁰² Cooper, R. J., Heiles, S., DiTucci, M. J., & Williams, E. R. (2014). Hydration of guanidinium: second shell formation at small cluster size. *The Journal of Physical Chemistry A*, 118(30), 5657-5666.
- ¹⁰³ Ball, P., & Hallsworth, J. E. (2015). Water structure and chaotropicity: their uses, abuses and biological implications. *Physical Chemistry Chemical Physics*, 17(13), 8297-8305.
- ¹⁰⁴ Graziano, G. (2011). Contrasting the denaturing effect of guanidinium chloride with the stabilizing effect of guanidinium sulfate. *Physical Chemistry Chemical Physics*, 13(25), 12008-12014.
- ¹⁰⁵ Kubíčková, A., Krížek, T., Coufal, P., Wernersson, E., Heyda, J., & Jungwirth, P. (2011). Guanidinium cations pair with positively charged arginine side chains in water. *The Journal of Physical Chemistry Letters*, 2(12), 1387-1389.
- ¹⁰⁶ Safar, J., Wille, H., Itri, V., Groth, D., Serban, H., Torchia, M., & Prusiner, S. B. (1998). Eight prion strains have PrP Sc molecules with different conformations. *Nature medicine*, 4(10), 1157.
- ¹⁰⁷ Peretz, D., Scott, M. R., Groth, D., Williamson, R. A., Burton, D. R., Cohen, F. E., & Prusiner, S. B. (2001). Strain-specified relative conformational stability of the scrapie prion protein. *Protein Science*, 10(4), 854-863.
- ¹⁰⁸ Novitskaya, V., Makarava, N., Bellon, A., Bocharova, O. V., Bronstein, I. B., Williamson, R. A., & Baskakov, I. V. (2006). Probing the conformation of the prion protein within a single amyloid fibril using a novel immunoconformational assay. *Journal of Biological Chemistry*, 281(22), 15536-15545.
- ¹⁰⁹ Kunik, V., Peters, B., & Ofran, Y. (2012). Structural consensus among antibodies defines the antigen binding site. *PLoS Comput Biol*, 8(2), e1002388.
- ¹¹⁰ Scarabelli, G., Morra, G., & Colombo, G. (2010). Predicting interaction sites from the energetics of isolated proteins: a new approach to epitope mapping. *Biophysical journal*, 98(9), 1966-1975.
- ¹¹¹ Stockmann, A., Hess, S., Declerck, P., Timpl, R., & Preissner, K. T. (1993). Multimeric vitronectin. Identification and characterization of conformation-dependent self-association of the adhesive protein. *Journal of Biological Chemistry*, 268(30), 22874-22882.
- ¹¹² Amit, A. G., Mariuzza, R. A., Phillips, S. E. V., & Poljak, R. J. (1986). Three-dimensional structure of an antigen-antibody complex at 2.8 Å resolution. *Science*, 233, 747-754.
- ¹¹³ Schmidt, M. L., Murray, J., Lee, V. M., Hill, W. D., Wertkin, A., & Trojanowski, J. Q. (1991). Epitope map of neurofilament protein domains in cortical and peripheral nervous system Lewy bodies. *The American journal of pathology*, 139(1), 53.
- ¹¹⁴ McCutcheon S, Langeveld JPM, Tan BC, Gill AC, de Wolf C, et al. (2014) Prion Protein-Specific Antibodies That Detect Multiple TSE Agents with High Sensitivity. *PLoS ONE* 9(3)
- ¹¹⁵ Williamson, R. A., Peretz, D., Smorodinsky, N., Bastidas, R., Serban, H., Mehlhorn, I., & Burton, D. R. (1996). Circumventing tolerance to generate autologous

-
- monoclonal antibodies to the prion protein. *Proceedings of the national Academy of Sciences*, 93(14), 7279-7282.
- ¹¹⁶ Cordes, H., Bergström, A. L., Ohm, J., Laursen, H., & Heegaard, P. M. (2008). Characterisation of new monoclonal antibodies reacting with prions from both human and animal brain tissues. *Journal of immunological methods*, 337(2), 106-120.
- ¹¹⁷ Yuan, F. F., Biffin, S., Brazier, M. W., Suarez, M., Cappai, R., Hill, A. F., & Geczy, A. F. (2005). Detection of prion epitopes on PrP^C and PrP^{Sc} of transmissible spongiform encephalopathies using specific monoclonal antibodies to PrP. *Immunology and cell biology*, 83(6), 632-637.
- ¹¹⁸ Moudjou, M., Treguer, E., Rezaei, H., Sabuncu, E., Neuendorf, E., Groschup, M. H., & Laude, H. (2004). Glycan-controlled epitopes of prion protein include a major determinant of susceptibility to sheep scrapie. *Journal of virology*, 78(17), 9270-9276.
- ¹¹⁹ Brannstrom K, Lindhagen-Persson M, Gharibyan AL, Iakovleva I, Vestling M, et al. (2014) A Generic Method for Design of Oligomer-Specific Antibodies. *PLoS ONE* 9(3)
- ¹²⁰ Polymenidou, M., Moos, R., Scott, M., Sigurdson, C., Shi, Y. Z., Yajima, B., & Bellon, A. (2008). The POM monoclonals: a comprehensive set of antibodies to non-overlapping prion protein epitopes. *PLoS One*, 3(12), e3872.
- ¹²¹ Doolan, K. M., & Colby, D. W. (2015). Conformation-dependent epitopes recognized by prion protein antibodies probed using mutational scanning and deep sequencing. *Journal of molecular biology*, 427(2), 328-340.
- ¹²² Williamson, R. A., Peretz, D., Pinilla, C., Ball, H., Bastidas, R. B., Rozenshteyn, R., & Burton, D. R. (1998). Mapping the prion protein using recombinant antibodies. *Journal of Virology*, 72(11), 9413-9418.
- ¹²³ Pan, T., Li, R., Kang, S. C., Wong, B. S., Wisniewski, T., & Sy, M. S. (2004). Epitope scanning reveals gain and loss of strain specific antibody binding epitopes associated with the conversion of normal cellular prion to scrapie prion. *Journal of neurochemistry*, 90(5), 1205-1217.
- ¹²⁴ Kang, H. E., Weng, C. C., Saijo, E., Saylor, V., Bian, J., Kim, S., & Telling, G. C. (2012). Characterization of conformation-dependent prion protein epitopes. *Journal of Biological Chemistry*, 287(44), 37219-37232.
- ¹²⁵ Sonati, T., Reimann, R. R., Falsig, J., Baral, P. K., O'Connor, T., Hornemann, S., & Swayampakula, M. (2013). The toxicity of anti-prion antibodies is mediated by the flexible tail of the prion protein. *Nature*, 501(7465), 102-106.
- ¹²⁶ Klöhn, P. C., Farmer, M., Linehan, J. M., O'malley, C., de Marco, M. F., Taylor, W., & Collinge, J. (2012). PrP antibodies do not trigger mouse hippocampal neuron apoptosis. *Science*, 335(6064), 52-52.
- ¹²⁷ Reimann, R. R., Sonati, T., Hornemann, S., Herrmann, U. S., Arand, M., Hawke, S., & Aguzzi, A. (2016). Differential toxicity of antibodies to the prion protein. *PLoS Pathog*, 12(1), e1005401.

-
- ¹²⁸ Stanker, L. H., Serban, A. V., Cleveland, E., Hnasko, R., Lemus, A., Safar, J., & Prusiner, S. B. (2010). Conformation-dependent high-affinity monoclonal antibodies to prion proteins. *The Journal of Immunology*, 185(1), 729-737.
- ¹²⁹ Chandler, R. (1961). Encephalopathy in mice produced by inoculation with scrapie brain material. *The Lancet*, 1(7191), 1378-1379.
- ¹³⁰ Darcel, C. L. Q., Merriman, M., Beauregard, M., Avery, R. J., & Kasting, R. (1963). Scrapie I. Transmission and Pathogenesis. *Canadian journal of comparative medicine and veterinary science*, 27(4), 81.
- ¹³¹ Kim, Y. S., Carp, R. I., Callahan, S. M., Natelli, M., & Wisniewski, H. M. (1990). Vacuolization, incubation period and survival time analyses in three mouse genotypes injected stereotactically in three brain regions with the 22L scrapie strain. *Journal of Neuropathology & Experimental Neurology*, 49(2), 106-113.
- ¹³² Shindoh, R., Kim, C. L., Song, C. H., Hasebe, R., & Horiuchi, M. (2009). The region approximately between amino acids 81 and 137 of proteinase K-resistant PrP^{Sc} is critical for the infectivity of the Chandler prion strain. *Journal of virology*, 83(8), 3852-3860.
- ¹³³ Johnson, C., Johnson, J., Vanderloo, J. P., Keane, D., Aiken, J. M., & McKenzie, D. (2006). Prion protein polymorphisms in white-tailed deer influence susceptibility to chronic wasting disease. *Journal of General Virology*, 87(7), 2109-2114.
- ¹³⁴ Johnson, C. J., Herbst, A., Duque-Velasquez, C., Vanderloo, J. P., Bochsler, P., Chappell, R., & McKenzie, D. (2011). Prion protein polymorphisms affect chronic wasting disease progression. *PLoS One*, 6(3), e17450.
- ¹³⁵ Xie, Z., O'Rourke, K. I., Dong, Z., Jenny, A. L., Langenberg, J. A., Belay, E. D., ... & Gambetti, P. (2006). Chronic Wasting Disease of Elk and Deer and Creutzfeldt-Jakob Disease COMPARATIVE ANALYSIS OF THE SCRAPIE PRION PROTEIN. *Journal of biological chemistry*, 281(7), 4199-4206.
- ¹³⁶ Reid, C. M. (2014). *Prion strain adaptation: breaking and building species barriers* (Doctoral dissertation, Colorado State University. Libraries).
- ¹³⁷ Sigurdson, C. J., Manco, G., Schwarz, P., Liberski, P., Hoover, E. A., Hornemann, S., & Aguzzi, A. (2006). Strain fidelity of chronic wasting disease upon murine adaptation. *Journal of virology*, 80(24), 12303-12311.
- ¹³⁸ Lee, Y. H., Sohn, H. J., Kim, M. J., Kim, H. J., Park, K. J., Lee, W. Y., & Balachandran, A. (2013). Experimental chronic wasting disease in wild type VM mice. *Journal of Veterinary Medical Science*, 75(8), 1107-1110.
- ¹³⁹ Heisey, D. M., Mickelsen, N. A., Schneider, J. R., Johnson, C. J., Johnson, C. J., Langenberg, J. A., & Barr, D. J. (2010). Chronic wasting disease (CWD) susceptibility of several North American rodents that are sympatric with cervid CWD epidemics. *Journal of virology*, 84(1), 210-215.
- ¹⁴⁰ Browning SR, et al.(2004) Transmission of prions from mule deer and elk with chronic wasting disease to transgenic mice expressing cervid PrP. *J Virol*78(23):13345-13350.
- ¹⁴¹ Angers RC, et al.(2009) Chronic wasting disease prions in elk antler velvet. *Emerg Infect Dis*15(5):696-703.

-
- ¹⁴² Christofinis, G. J., & Beale, A. J. (1968). Some biological characters of cell lines derived from normal rabbit kidney. *The Journal of pathology and bacteriology*, 95(2), 377-381.
- ¹⁴³ Arellano-Anaya ZE, Savistchenko J, Mathey J, Huor A, Lacroux C, et al. (2011) A Simple, Versatile and Sensitive Cell-Based Assay for Prions from Various Species. *PLoS ONE* 6(5)
- ¹⁴⁴ Kang, H. E., Weng, C. C., Saijo, E., Saylor, V., Bian, J., Kim, S., Ramos, L., Angers, R., Langenfeld, K., Khaychuk, V., & Calvi, C. (2012). Characterization of conformation-dependent prion protein epitopes. *Journal of Biological Chemistry*, jbc-M112.
- ¹⁴⁵ Doolan, K. M., & Colby, D. W. (2015). Conformation-dependent epitopes recognized by prion protein antibodies probed using mutational scanning and deep sequencing. *Journal of molecular biology*, 427(2), 328-340.
- ¹⁴⁶ Halfmann, R., & Lindquist, S. (2008). Screening for amyloid aggregation by semi-denaturing detergent-agarose gel electrophoresis. *J Vis Exp*, 17.
- ¹⁴⁷ Muramoto, T., DeArmond, S. J., Scott, M., Telling, G. C., Cohen, F. E., & Prusiner, S. B. (1997). Heritable disorder resembling neuronal storage disease in mice expressing prion protein with deletion of an α -helix. *Nature medicine*, 3(7), 750-755.
- ¹⁴⁸ Collinge, J., & Clarke, A. R. (2007). A general model of prion strains and their pathogenicity. *Science*, 318(5852), 930-936.
- ¹⁴⁹ Tixador, P., Herzog, L., Reine, F., Jaumain, E., Chapuis, J., Le Dur, A., & Beringue, V. (2010). The physical relationship between infectivity and prion protein aggregates is strain-dependent. *PLoS Pathog*, 6(4), e1000859.
- ¹⁵⁰ Shindoh, R., Kim, C. L., Song, C. H., Hasebe, R., & Horiuchi, M. (2009). The region approximately between amino acids 81 and 137 of proteinase K-resistant PrP^{Sc} is critical for the infectivity of the Chandler prion strain. *Journal of virology*, 83(8), 3852-3860.
- ¹⁵¹ Bernstein, S. L., Dupuis, N. F., Lazo, N. D., Wyttenbach, T., Condrón, M. M., Bitan, G., & Bowers, M. T. (2009). Amyloid- β protein oligomerization and the importance of tetramers and dodecamers in the aetiology of Alzheimer's disease. *Nature chemistry*, 1(4), 326-331.
- ¹⁵² Cremades, N., Cohen, S. I., Deas, E., Abramov, A. Y., Chen, A. Y., Orte, A., & Bertonecini, C. W. (2012). Direct observation of the interconversion of normal and toxic forms of α -synuclein. *Cell*, 149(5), 1048-1059.
- ¹⁵³ Soto, C. (2012). Transmissible proteins: Expanding the prion heresy. *Cell*, 149(5), 968-977.
- ¹⁵⁴ Aguzzi, A., & O'Connor, T. (2010). Protein aggregation diseases: Pathogenicity and therapeutic perspectives. *Nature Reviews Drug Discovery*, 9(3), 237-248

CHAPTER 3 – A NOVEL EPITOPE ACCESSIBILITY ASSAY REVEALS STRAIN DIFFERENCES AND NATIVE PrP^{Sc} STRUCTURAL INFORMATION

A. INTRODUCTION

Prion neurodegenerative diseases are invariably fatal and there exists no effective treatment or cure for these diseases¹. A unique pathway is involved in prion diseases: conformational corruption of cellular prion protein (PrP^C) by the pathogenic form (PrP^{Sc})². The knowledge regarding the structure of PrP^{Sc} is still unresolved³. The very nature of the prion hypothesis is at the crux of a conundrum: How do you accurately resolve the structure of a misfolded protein?

There are two aspects to this question: the tertiary structure of PrP^{Sc} and structural differences encoding prion strains⁴. Prion strains defy the conventional genetic-based definition that is applied to strains of viruses, bacteria, and fungi. Instead, prion strains properties rely on specific prion protein tertiary conformations⁵. Some prion strains contain the same amino acid sequence yet produce different disease phenotypes⁶. Some prion strains are generated due to genetic polymorphisms in the prion protein (*PRPN*)^{7,8} (Figure 1.1). Single amino acid changes to the prion protein can have intense impact on transmission and susceptibility⁹. For example, a difference in amino acid at position 226 [deer (Q), elk (E)] has profound effects on the presentation of chronic wasting disease¹⁰. Considering both origins of prion strains, a prion strain is defined as an infectious prion protein particle with a specific tertiary conformation¹¹ that produces a specific neurodegenerative phenotype¹². Specifically, a prion strain can

be considered to have a strain-specific¹³ disease phenotype¹⁴ based on the prion's ability to be stably propagated, fidelity to neuropathology, disease length, glycosylation profile, molecular weight of PK-resistant PrP^{Sc}, resistance to denaturation, amyloid seeding potential and other molecular characteristics.

Bioassay, the passing of infectious material in living animals^{15, 16}, allowed researchers to develop tools to identify prions with neuropathology, disease length, and glycosylation profile, molecular weight of PK-resistant PrP^{Sc}, resistance to denaturation, and other molecular characteristics. Mice became the most convenient model system^{17, 18} with the creation of transgenic mice expressing a wide variety of PrP^C. For research purposes and ease of study, prions were adapted to infect mice in a more time efficient laboratory setting, such as scrapie¹⁹, TME²⁰, BSE²¹, and CWD²². However, prion strain differentiation by bioassay remains time-consuming and financially costly, faster, higher throughput methods were needed.

Prion cell culture models represented a new way to examine prion questions ranging from: prion adaption²³, spontaneous prion generation^{24, 25}, genetic variables that increase susceptibility^{26, 27}, the role of PrP^C in cellular function^{28, 28}, modulators of infectivity^{29, 30, 31}, to test anti-prion compounds^{32, 33, 34, 35, 36, 37, 38}, examine drug-induced prion evolution³⁹, and more. The rabbit kidney epithelial⁴⁰ (RK13) cell culture model has vastly expanded the species and prion strains that could be examined. Specifically, RK13 cells transfected^{41, 42} to stably express a pIRESpuro3 vector containing the PrP^C gene of choice⁴³ and pcDNA3-gag expressing HIV-1 GAG precursor protein to enhance the release of PrP^C⁴⁴. RK-PrP cell lines have been useful to examine prion titre⁴⁵, anti-

prion drug screening^{46, 47}, and strain differentiation⁴⁸. The advancements in cell culture models allowed a more manageable prion conformational stability assays (CSA) to be created.

Prion conformational stability assays use chaotropic agents to assess relative resistance of prions to protease degradation after partial denaturation to examine PrP^{Sc}. Chaotropic agents disturb the hydrogen bonding of water⁴⁹ around a protein, destabilizing the three-dimensional structure of a protein. This destabilization causes proteins to undergo a denaturation-renaturation event, where they unfold and re-fold^{50, 51, 52, 53, 54, 55}. Hydrogen bonding of water is important to prion protein structural stability⁵⁶. Although the use of chaotropic agents to indirectly study protein structure is not unique to the prion field^{57, 58, 59}, the prion field utilizes chaotropic agents via denaturation curves as a means to interrogate PrP^{Sc} structure and distinguish between different prion strains. CSAs depends on western blot²³, dot blot, enzyme linked immunosorbent assays (ELISA)⁶⁰, or cell-based systems [Chapter 2] to examine prion response to protease degradation after partial denaturation.

The specific conformational stability of prions has not been clarified because many of CSAs have focused on a single antibody^{61, 62} or a single strain⁶³. The knowledge garnered from interrogating a single antibody epitope is limited. Additionally, the precision of structural knowledge gained was lacking until the antibodies were epitope-mapped. Epitope-mapping an antibody is a process to identify the amino acids that the antibody Fab region binds^{64 65}. The use of denaturation, epitope-mapped antibodies, and conformational specific antibodies to probe protein structure is not unique to the

prion protein, e.g. vitronectin⁶⁶, lysozyme⁶⁷, and neurofilament⁶⁸. To expand understanding of the prion protein, a plethora of anti-prion antibodies^{69, 70, 71 72}, glycosylation specific antibodies⁷³, and anti-amyloid antibodies⁷⁴ have been generated.

Epitope mapping has been done with several anti-prion antibodies^{75 76, 77, 78}, and, importantly, with antibodies our lab generated⁷⁹ (Figure 3.1B). In hopes of understanding more about the structure of both PrP^C and PrP^{Sc}, conformationally dependent antibodies⁸⁰ have been used to examine prion structure. Conformationally dependent antibodies require the protein to be in a specific conformation, as the epitope regions are discontinuous. Using a wide array of antibodies with varied epitopes clarifies subtle structural variation present between strains.

We have developed a conformational stability assay sandwich ELISA using two in-house generated conformationally dependent antibodies (7-5 ELISA-CSA). Unlike more traditional CSA's, the 7-5 ELISA-CSA interrogates the epitope accessibility of PrP^{Sc} under different denaturing (GdnHCl) conditions rather than interrogating the PK sensitivity of PrP^C and PrP^{Sc} that has been exposed to different denaturing conditions (GdnHCl and GdnTh). The 7-5 ELISA has the profound advantage of preferentially detecting PrP^{Sc} in the absence of Proteinase K (PK).

We developed a facile, expedient, and novel cell-based epitope stability assay (ESA) from conceptually merging the 7-5 ELISA-CSA and a previously developed⁸¹ C-CSA [Chapter 2] to provide previously inaccessible structural information about the prion protein. The ESA (Figure 3.2) uses chaotropic agents to probe epitope-mapped regions of the prion protein. The ESA allows data to be gathered across multiple

species, with multiple infectious prions, and more importantly provides a high-throughput method to examine the prion protein at multiple epitopes, simultaneously. Interrogation of the prion protein at multiple known epitopes can further delineate structural characteristics of PrP^{Sc}. The ESA recapitulates⁸¹ the difference between CWD prions in deer (Q226) and elk (E226). The ESA is not limited to natural prion infections, mouse-adapted scrapie prions, RML, that were newly adapted into cervid (cerRML) transgenic mice showed pronounced differences due to deer (Q226) and elk (E226) sequence differences. Additionally, the ESA is able to differentiate between four prion strains that contain the same mouse-PrP amino acid sequence: three classically murine-adapted scrapie RML, 22L, and 139A strains and a more recent CWD murine-adapted prion strain (mD10). Specifically, the use of antibodies to probe multiple epitopes (ranging from unstructured to globular regions) further defines these classically used prions as being separate strains, and reinforced that mD10 contains a novel structure. Consequently, the ESA represents a new tool to reveal more details about prion strain structure in a facile and expedient process. Detailed information about the infectious form of the prion protein has been insufficient to serve as a template for treatment options. The research contained in this chapter will further our knowledge of the structure of PrP^{Sc}.

B. MATERIALS AND METHODOLOGY

Tissue Homogenization

The brains were homogenized in one of two ways. The (2) bead homogenization methodology used as a safer replacement of the (1) needle homogenization methodology when the FastPrep-24 Classic Grinder (MP Biomedical) was purchased.

(1) Needle homogenization: See Chapter 2 – B. Tissue Homogenization

(2) Bead Homogenization: The brains and cold sterile phosphate buffered saline (PBS) lacking Ca^{2+} and Mg^{2+} (Hyclone, Pittsburg, PA) were added to 4.5 mL Tallprep Tubes (MP Biomedical) to yield either 10% weight/volume (w/v) or 20%w/v brain homogenates. The brain-PBS mixture was bead homogenized in the FastPrep-24 Classic Grinder (MP Biomedical) in three rounds of 15 seconds followed by 5 minute rest on ice. Brain homogenates were aliquoted and stored at -80°C until use.

Mouse Model

See Chapter 2 – B. Mouse Model

Mouse Infections

See Chapter 2 – B. Mouse Infections

Cell Model

See Chapter 2 – B. Cell Model

Cell Culture

See Chapter 2 – B. Cell Culture

Prion Infection of Cell Culture

See Chapter 2 – B. Prion Infection of Cell Culture

7-5 Sandwich ELISA-CSA

Brain homogenates were assessed for prion conformational stability via a novel sandwich Enzyme-Linked Immunosorbent Assay (ELISA) using in-house created epitope-mapped⁸² anti-PrP antibodies: PRC5 and PRC7. Specifically, 100µL per well of 10µg/mL capture antibody PRC7 (Telling Lab, Fort Collins, CO) in Carbonate-Bicarbonate (Sigma-Aldrich, St. Louis, MO) was used to coat 96-well ELISA Nunc Maxisorp (Thermo Fisher Scientific, Waltham, MA). Plates were sealed to prevent evaporation and stored at 4°C until use. Upon use, capture antibody was flicked out of plates, and blocked with 3% Bovine Serum Album (BSA) (Sigma-Aldrich, St. Louis, MO) in PBS at 200µL per well for 1 hour at 37°C on a rotational shaker. Plates were then rinsed 3 times with fresh, filtered Tris Buffered Saline – Tween (TBS-T) at 200µL per well. 100µL of prepared samples were then added per well, in triplicate.

Sample preparation (7-5 Sandwich ELISA-CSA)

1% Triton X-100 (Sigma-Aldrich, St. Louis, MO) in PBS and equivalent protein concentrations of brain homogenate in PBS were incubated for 1 hour in the thermomixer at 37°C at 1000 rpm. Note, if proteinase K (PK) (Pierce Biotechnology Inc., Rockford, IL) treatment was desired to ablate the cellular prion protein (PrP^C), then 1µg PK was added to this step. After incubation, PK containing mixtures were quenched with 2mM phenylmethylsulfonyl fluoride (PMSF) (Sigma-Aldrich, St. Louis, MO). 12.5µL of each brain mixture was aliquoted into 12 wells of a deep well dish to facilitate the chaotropic denaturation step. A dilution series of the chaotropic agent, guanidine hydrochloride (GdnHCl) (Sigma-Aldrich, St. Louis, MO) in 50 mM Tris-HCl

(Sigma-Aldrich, St. Louis, MO), varied from 0M to 5.5M, in step-wise 0.5M increments, was added to the wells. The GdnHCl and brain homogenate mixtures were incubated for 15 minutes in the thermomixer at 37°C at 1000 rpm to allowed the infectious prion protein (PrP^{Sc}) to denature. Following the incubation, 1% BSE/PBS and 8M GdnHCl/Tris-HCl was used to quench the reaction and yield equivalent total GdnHCl in each reaction.

Plates were sealed and incubated overnight at 4°C on the rotational shaker.

Immunodetection followed the next day. The prepared sample mixture was removed, and plate washed 3 times with fresh, filtered TBS-T at 200µL per well. The detecting anti-PrP antibody PRC5 (Telling Lab, Fort Collins, CO) 1:5000 dilution in 1% BSA/PBS at 100µL per well was added, plates sealed, and then incubated 1 hour at 37°C on a rotational shaker. Plates were washed 3 times with fresh, filtered TBS-T at 200µL per well. Then, a developing antibody anti-mouse IgG2a-HRP conjugate (Alpha Diagnostic Intl. Inc., San Antonio, TX) 1:5000 dilution in 1% BSA/PBS at 100µL per well was added, plates sealed, and then incubated 1 hour at 37°C on a rotational shaker. Plates were then washed seven times with fresh, filtered TBS-T at 200µL per well. The plates were developed with 100µl per well room temperature ABTS 2-component microwell peroxidase substrate (SeraCare, Milford, MA); plates were maintained in a dark environment during the 12-20 minutes developing time. Finally, 100µl per well 1X ABTS Peroxidase Stop Solution (SeraCare, Milford, MA) in ultrapure water was added to the plates. The plates were immediately imaged with FLUOstar Omega at 405nm, and statistical analysis performed.

Cell-Based Epitope Stability Assay (ESA)

Prion infected cells were assessed for prion epitope stability (Figure 3.2) via a novel modification to previously described⁸¹ methods. Specifically, after a 4-week incubation on a prion-coated plate, RK13 cells expressing the puromycin-PrP^C vector^{83, 84} and RK13 cells with an empty vector (pIRESpuro3 without PrP) were harvested via trypsin (Sigma-Aldrich, St. Louis, MO) disassociation. Cells were seeded (20,000 cells per well) onto 70% Ethanol, molecular grade (Sigma- Aldrich, St. Louis, MO) activated Multiscreen IP 96-well 0.45- μ m ELISpot plates (Millipore, Billerica, MA), and rinsed three times with 200 μ L per well phosphate buffered saline lacking Ca²⁺ and Mg²⁺ (PBS) (Hyclone, Pittsburg, PA). The cells were fixed onto the ELISpot membrane at 50°C for 2 – 4 hours (until the membrane dries), and stored at -20°C until use. ELISpot plates with fixed cells were allowed to thaw for one hour at room temperature. ELISpot plates were stacked with lids on, in a humidity chamber (plastic container with ¼ inch dH₂O and 2 empty pipet tip rack tops in bottom) to maintain moisture throughout the following steps. The plates were treated with 100 μ L per well 5 μ g/mL proteinase K (PK) (Pierce Biotechnology Inc., Rockford, IL) in cell lysis buffer (50 mM Tris (Sigma-Aldrich, St. Louis, MO), pH 8.0; 150 mM NaCl (Sigma-Aldrich, St. Louis, MO); 0.5% sodium deoxycholate (Sigma-Aldrich, St. Louis, MO); 0.5% Igepal (Sigma-Aldrich, St. Louis, MO)) for ninety minutes at 37°C to ablate PrP^C. The PK was quenched by 150 μ L per well 2mM phenylmethylsulfonyl fluoride (PMSF) (Sigma-Aldrich, St. Louis, MO) in PBS for twenty minutes at room temperature, and then rinsed once with 200 μ L per well PBS. Then, ELISpot wells were treated for one hour at room temperature with a solution of

guanidine hydrochloride (GdnHCl) (Sigma-Aldrich, St. Louis, MO) in 10 mM Tris-HCl (Sigma-Aldrich, St. Louis, MO) at 100 μ L per well; the GdnHCl dilution series varied from 0M to 5.5M in 0.5M increments. The GdnHCl dilution series allowed denaturation of the infectious prion protein (PrP^{Sc}) to exposes the epitopes for antibody probing. Plates were then washed three times with 200 μ L per well PBS to allow PrP^{Sc} to renature in a PrP^C-like conformation. The samples were then given 150 μ l per well of 5% superbloc (Pierce, Rockford, IL) in ultrapure water for one hour at room temperature to reduce background signal. Following removal of superbloc, immunodetection began. 60 μ l per well of primary anti-PrP antibody in fresh, filtered TBS-T was added per well and incubated at 4°C overnight. Primary anti-PrP mAb Epitopes^{82, 85} (Figure 3.1B) used: PRC1 (Telling Lab, Fort Collins, CO) 1:5000 dilution, PRC5 (Telling Lab, Fort Collins, CO) 1:5000 dilution, PRC7 (Telling Lab, Fort Collins, CO) 1:5000 dilution, 6H4 (Prionics, Invitrogen Life Technologies, CA) 1:20000 dilution, D13 (Telling Lab, Fort Collins, CO) 1:5000 dilution, and D18 (Telling Lab, Fort Collins, CO) 1:5000 dilution. The following day, the wells were rinsed three times with 200 μ l per well TBS-T. 60 μ l per well of Alkaline Phosphatase-conjugated secondary antibodies in fresh, filtered TBS-T was added per well and incubated at room temperature for one hour. Secondary mAb used: AP- α -Mouse IgG (Southern Biotechnology Associates, Birmingham, AL) 1:5000 dilution for PRC1, PRC5, PRC7, and 6H4; AP Goat- α -Human IgG (Southern Biotechnology Associates, Birmingham, AL) 1:5000 dilution for D13 and D18. The wells were rinsed three times with 200 μ l per well TBS-T; a final 200 μ l per well rinse with PBS removed the trace amounts of detergent left by the TBS-T. The plastic backing was

removed from the bottom of the membrane-attached wells, then rinsed twice with flowing distilled Millipore water at the sink. Finally, the plates were allowed to dry for four hours. After the membranes fully dried, the wells were developed with a solution of nitro-blue tetrazolium chloride/ 5-bromo-4-chloro-3'-indolyphosphate p-toluidine salt (NBT/BCIP) (Roche, Basel, Switzerland) in ultrapure water. The development process was quenched with two rinses of filtered water. The plates were allowed to dry overnight at 4°C, and then at room temperature the following day for one hour. The plates were imaged with ImmunoSpot S6-V analyzer (Cellular Technology Ltd, Shaker Heights, OH), and spot numbers were determined using ImmunoSpot5 software (Cellular Technology Ltd, Shaker Heights, OH).

Proteinase K (PK) ablation of PrP^C

Procedure to establish the concentration of PK necessary to ablate PrP^C signal in the RK13-PrP^C cell model (Figure 3.4A-B), modification of the ESA protocol (above), specifically changes:

(1) Uninfected RK13 cells expressing the puromycin-PrP^C vector^{83, 84}, RK13 cells with an empty vector (pIRESpuro3 without PrP), and chronically prion infected cell lines (see Chapter 2) were not maintained for 4 weeks. They were thawed, verified by western blot, passaged twice, and used.

(3) A dilution series of PK to ablate the PrP^C signal was used, instead of just the standard operating protocol [100µL per well 5µg/mL PK] to examine PrP^{Sc} in RK13-PrP^C cell models. The samples were treated with 100µL per well of PK (range 0µg/mL - 20µg/mL) in cell lysis buffer for ninety minutes at 37°C.

(4) Only 5.5 M GdnHCl in 10 mM Tris-HCl was used for one hour at room temperature; this was to allow full denaturation and renaturation of the infectious prion protein (PrP^{Sc}) to expose the epitopes for antibody probing.

PrP^C Guanidine Hydrochloride Sensitivity

Procedure to examine the interaction between PrP^C and guanidine hydrochloride in the RK13-PrP^C cell model (Figure 3.4C-D), modification of the ESA protocol (above), specifically changes:

(1) Uninfected RK13 cells expressing the puromycin-PrP^C vector^{83, 84} and RK13 cells with an empty vector (pIRESpuro3 without PrP) were not maintained for 4 weeks. They were thawed, verified by western blot, passaged twice, and used.

(2) Previous (unpublished) work by Dr. Hae-Eun Kang showed [5,000 cells seeded per well] to be optimal when examining PrP^C in RK13-PrP^C cell models. The standard operating protocol to examine PrP^{Sc} in RK13-PrP^C cell models, [20,000 cells seeded per well] overwhelms maximal detectable signals when examining PrP^C.

(3) Use of PK would ablate the desired PrP^C signal; the plates were treated with cell lysis buffer for ninety minutes at 37°C without 100µL per well 5µg/mL PK. To remove additional variables, plates were still treated with 150µL per well 2mM PMSF in PBS for twenty minutes at room temperature.

Statistical Analysis

Statistical significance was assessed using GraphPad Prism 8.0 for Mac OS X software.

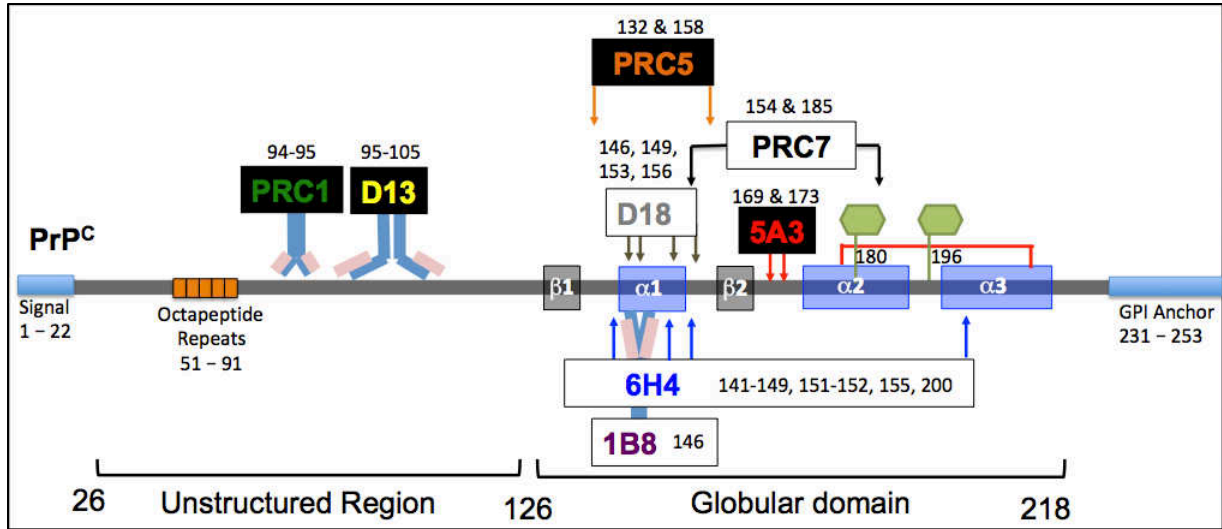


FIGURE 3.1: Schematic representation of the mouse cellular prion protein (PrP^c) and Epitopes of Anti-Prion Antibodies. (A) The mouse prion protein (PrP^c) is shown as a grey line with distinct areas indicated; the numbers shown represent amino acid locations along the molecule. An N-terminal target sequence (green box) is cleaved during protein processing prior to insertion into the plasma membrane. The remaining N-terminus is charged, primarily unstructured, and contains the copper octapeptide repeat binding motif (orange boxes). The C-terminal domain is structured with three alpha helices (blue boxes), two beta sheet motifs (grey boxes) and post-translational glycosylation at asparagine residues (green hexagons). A stabilizing disulfide bridge forms between alpha helix 2 and alpha helix 3 (red line). Finally, there is a Glycosylphosphatidylinositol (GPI) anchor attached at the C-terminus (purple box) which anchors the protein to the cellular plasma membrane. (B) Primary anti-PrP antibodies aligned to mouse PrP^c. Antibody epitopes have been mapped previously and amino acid residues included in the binding epitope of each antibody is indicated numerically. Three antibodies recognize linear epitopes (PRC1, D13, and 1B8) are shown with representative antibody images. Five antibodies recognizing discontinuous epitopes (PRC5, D18, 6H4, 5A3 and PRC7) are shown with arrows indicating discontinuous amino acid residues included in binding epitope.

cell based - Epitope Stability Assay

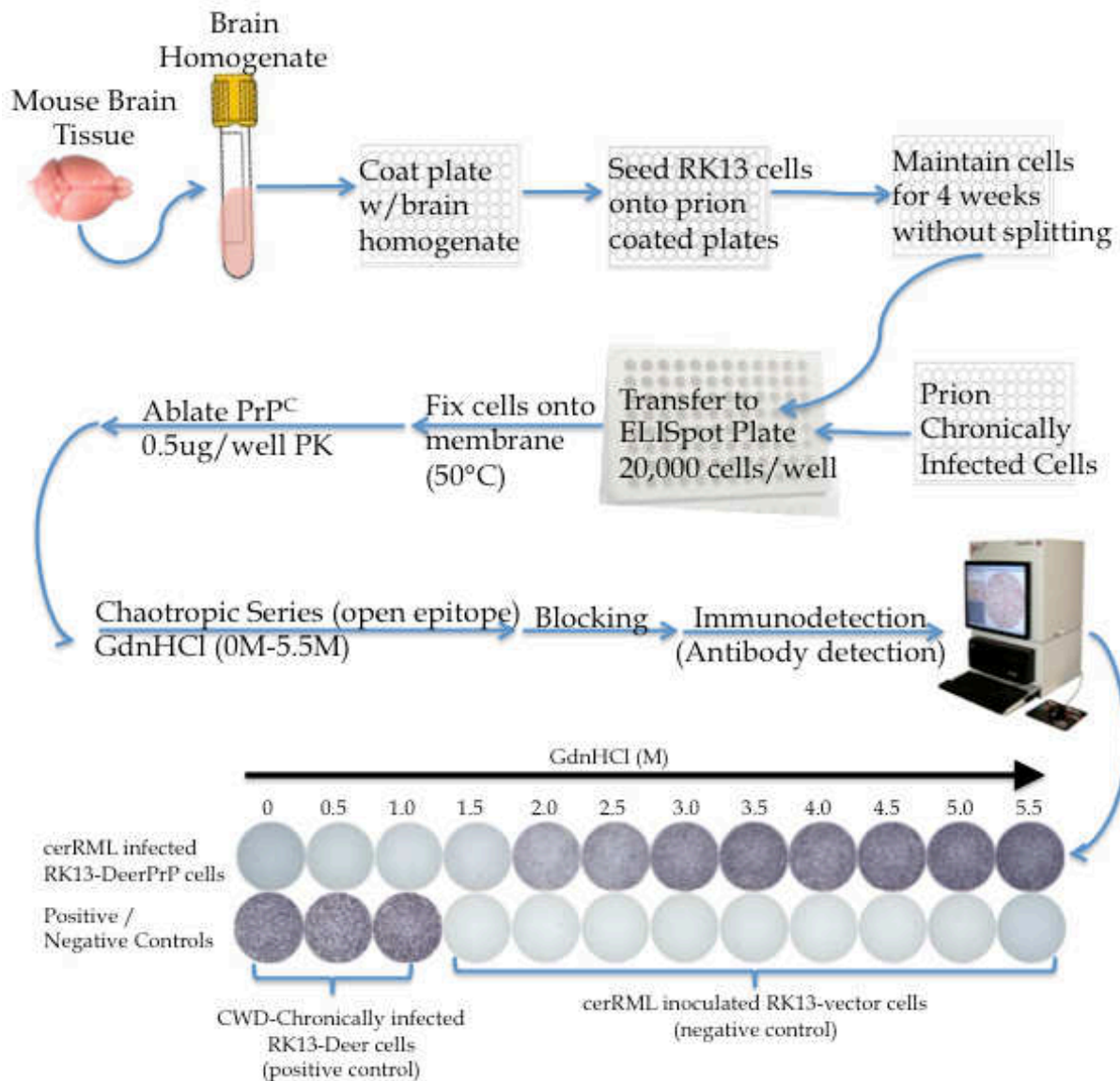


FIGURE 3.2: Schematic representation of the Epitope Stability Assay with representative example of data garnered. In brief, prion infected brains are homogenized and used to coat plates. Rabbit Kidney Epithelial cells (RK13) that are inducibly (via puromycin) transgenic for the prion protein (RK-mouse, RK-Deer, or RK-Elk) and RK13 cells containing an empty vector (RK-V) and do not express the cellular prion protein (PrP^C) are seeded onto the coated plates. The culture lasts four weeks without splitting, but with a change in media once every five days. At the end of the infection, cells are transferred to the ELISpot plates (20,000 cells per well), fixed at 50°C. PrP^C is ablated by proteinase K (PK) treatment. Samples are then exposed to guanidine hydrochloride (GdnHCl) varied from 0M to 5.5M in 0.5M increments to allow the

infectious prion protein (PrP^{Sc}) to denature and renature in a PrP^C-like conformation for immunodetection. The samples are exposed to blocking, and immunodetection with anti-prion antibodies: PRC1, D13, D18, 1B8, PRC5, 6H4, 5A3, and PRC7 (Figure 3.1B). Resulting data is imaged with ImmunoSpot S6-V analyzer and spot numbers determined using ImmunoSpot5 software. A representative image of the resultant data is shown; dark spots within wells are PrP^{Sc} positive (anti-prion antibody 6H4). Cells (RK13-DeerPrP and RK13-vector) were plated on cervid-adapted RML (cerRML) coated plates, as indicated in the schematic, a positive control (CWD-chronically infected Deer cell line) was included.

TABLE 3.1: Prion strain properties and infection paradigm. Strains name is listed. Origin indicates the original prion and species of the inoculum. Primary adaption indicates the original host the inoculum was adapted into; i.e. hamster, murine, or transgenic murine model. Secondary adaption indicates a secondary adaption of the inoculum to a new host (PrP^C). Brain Homogenate Host - PrP^C indicates the PrP^C of the animal host that was infected; note, this also indicates the PrP^{Sc} species that was used to infect the RK-PrP cell culture system. Lastly, cell line - PrP^C indicates which RK-PrP cell lines were infected with the material, and their respective PrP^C primary structure; note, null indicates the RK-V (vector and PrP-null) cell line that is used as a negative control.

Strain Name	Origin	Primary Adaption	Secondary Adaption	Brain Homogenate Host - PrP^C	Cell line - PrP^C
<u>22L</u>	Sheep Scrapie	Inbred Mice		Mouse	Mouse, null
<u>139A</u>	Sheep Scrapie	Hamsters	Inbred Mice	Mouse	Mouse, null
<u>mD10</u>	Deer D10 Chronic Wasting Disease	Tg(Deer) Mice	Inbred Mice	Mouse	Mouse, null
<u>RML</u>	Sheep Scrapie	Inbred Mice		Mouse	Mouse, null
<u>Deer-RML</u>	Sheep Scrapie	Inbred Mice	Tg(Deer) Mice	Deer	Deer, Elk, null
<u>Elk-RML</u>	Sheep Scrapie	Inbred Mice	Tg(Elk) Mice	Elk	Deer, Elk, null
<u>Deer-CWD</u>	Elk Bala05 Chronic Wasting Disease	Tg(Deer) Mice		Deer	Deer, Elk, null
<u>Elk-CWD</u>	Elk Bala05 Chronic Wasting Disease	Tg(Elk) Mice		Elk	Deer, Elk, null

C. RESULTS

The ultimate goal of analyzing the epitope availability of PrP^{Sc} after exposure to varying levels of a chaotropic agent is to better understand the subtle structural differences between prion strains. Prion strains were subjected to a stepwise increasing molar gradation, i.e. 0M – 5.5M of guanidine hydrochloride (GdnHCl). The resultant denaturation curve and guanidine hydrochloride midpoint of the sigmoidal transition (GdnHCl_{1/2}) value are used to derive statistical significance.

Infection specific, 7-5 ELISA-CSA, is able to differentiate between prion strains via differences in epitope binding without requiring PK ablation of PrP^C.

We previously developed⁸² epitope-mapped anti-prion antibodies (Figure 3.1B) that were applied in a 7-5 sandwich ELISA format: PRC7 anti-prion antibody is the capture antibody, and PRC5 anti-prion antibody is the detecting antibody. PRC7 is glycosylation specific and only binds to unglycosylated, and monoglycosylated (residue 196) species of the prion protein. Whereas, PRC5 is not glycosylation specific, it binds to residues (132 and 158) on either side of α helix-1⁷⁹. To establish the use of the 7-5 ELISA, brains (n=3) from terminally ill C57Bl/6 inbred mice infected with RML (blue), age-matched PBS-mock infected C57Bl/6 (grey), and PrP-KO (PrP^C null) mice (brown) were interrogated with the 7-5 ELISA without (Figure 3.3A) and with (Figure 3.3B) a chaotropic agent, GdnHCl. Prion protein detection by the 7-5 ELISA highly preferentially detects denatured PrP^{Sc} over denatured PrP^C (Figure 3.3A-B) and requires denaturation of PrP^{Sc} to access the epitope because PRC7 preferentially binds the infection specific fraction of PrP.

To examine if proteinase K (PK) will alter the fraction being detected with the 7-5 ELISA, brains (n=3) from terminally ill Tg(ElkPrP)5037^{+/-} mice infected with elk CWD isolate Bala05, PBS-mock infected Tg(ElkPrP)5037^{+/-} and PrP-KO (PrP^C null) mice (Figure 3.3C) and terminally ill Tg(DeerPrP)1536^{+/-} mice infected with elk CWD isolate Bala05, PBS-mock infected Tg(DeerPrP)1536^{+/-} mice, and PrP-KO (PrP^C null) mice (Figure 3.3D) were interrogated with the 7-5 ELISA-CSA. The use of PK does not alter the signal of PrP^{Sc} detected (Figure 3.3C-D); specifically, there was no significance (p=0.9367) between PK treated (black) and untreated (orange) Elk-CWD prions and no significance (p=0.1442) between PK treated (black) and untreated (orange) Deer-CWD prions. There was nearly undetectable signal from PBS-mock infected Tg(ElkPrP)5037^{+/-} and Tg(DeerPrP)1536^{+/-} (grey) and PrP-KO (PrP^C null) mice (brown). We determined the 7-5 ELISA does not require the traditionally required use of PK to differentiate between PrP^{Sc} over PrP^C.

We next tested the ability of the 7-5 ELISA-CSA to differentiate between prion strains based on each strain's response to denaturation (Figure 3.3E-F). Chronic wasting disease (CWD) passaged through Tg(Deer) and Tg(Elk) mice differ in their primary structure by a single amino acid (Q/E) at residue 226. This amino acid difference conveys conformational differences between Deer-CWD and Elk-CWD^{10, 81}. We assessed the capability of the 7-5-ELISA-CSA to discern conformational differences between Deer-CWD and Elk-CWD. We compared (Figure 3.3E) terminally ill Tg(ElkPrP)5037^{+/-} mice (orange) and Tg(DeerPrP)1536^{+/-} (pink) infected with CWD isolate Bala05, revealing strain differences (p ≤ 0.0001). PBS-mock infected

Tg(ElkPrP)5037^{+/-} and Tg(DeerPrP)1536^{+/-} (grey) and PrP-KO (PrP^C null) mice (brown) do not show detectable differences. The 7-5 ELSA-CSA was able to detect conformational differences between Deer-CWD and Elk-CWD.

Given the ability for the 7-5 ELSA-CSA to detect conformational differences between CWD which contain a single residue difference, we tested if the technique could detect conformational differences between well characterized mouse prion strains containing the same amino acid sequence. The conformational stability differences occur between strains containing the same primary structure (Figure 3.3F). Comparing brains (n=3) from terminally ill C57Bl/6 mice infected with classically defined murine-adapted scrapie strains RML (blue) and 22L (green) and recently murine-adapted CWD strain⁸⁶ mD10 (pink) reveals strain differences (RML:22L p = 0.0001; RML-mD10 p=0.0053; 22L:mD10 p=0.007). PBS-mock infected C57Bl/6 (grey) and PrP-KO (PrP^C null) mice (brown) do not show detectable differences. We can conclude that the 7-5 ELISA-CSA (Figure 3.3) is able to detect conformational differences between strains that share or differ in their amino acid composition. The 7-5 ELISA has the profound advantage of preferentially detecting PrP^{Sc} in the absence of Proteinase K (PK).

Developing a new technique: Epitope Stability Assay (ESA)

The 7-5 ELISA-CSA interrogates the epitope accessibility of PrP^{Sc} under different denaturing (GdnHCl) conditions. Unlike the ELISA, the C-CSA interrogates the PK sensitivity of PrP^C and PrP^{Sc} that has been exposed to different denaturing conditions (GdnHCl and GdnTh). The C-CSA was developed using a cell model^{83, 84} expressing PrP^C gene of choice in rabbit kidney epithelial (RK13) cells as a tool to assess prion

strains. Using this RK-PrP cell model, we quantified changes in conformational stability⁸¹ in chronically prion-infected RK13 cells expressing either elk (RK-Elk) or deer (RK-Deer) PrP^C. The C-CSA assay was expanded [Chapter 2] to assess how prion strains differ at multiple mapped epitopes. The premise was to create an assay with benefits from both original assays

The goal was to create a cell-based assay that interrogated the epitope accessibility of PrP^{Sc} under different denaturing (GdnHCl) conditions, akin to the ELISA, rather than interrogating the PK sensitivity of PrP^C and PrP^{Sc} that has been exposed to different denaturing conditions (GdnHCl and GdnTh), akin to the C-CSA. We developed a facile, expedient, and novel cell-based epitope stability assay (ESA) from conceptually merging the 7-5 ELISA-CSA and a previously developed⁸¹ C-CSA [Chapter 2] to provide previously inaccessible structural information about the prion protein. The ESA (Figure 3.2) uses chaotropic agents (GdnHCl) to probe epitope-mapped regions of the prion protein.

Establishing the concentration of Proteinase K sufficient to ablate PrP^C signal

To develop the ESA to reveal the epitope accessibility of PrP^{Sc}, we first examined the concentration of PK required to fully ablate PrP^C signal in the transgenic RK13-PrP cell model (Figure 3.4A-B). Uninfected PrP^C expressing cell lines (RK-Mouse, and RK-Deer), chronically infected cell lines that perpetually propagate prion infection (RML/RK-Mouse, and CWD/RK-Deer), and PrP^C a null cell line (RK-V) were exposed to an array of PK concentrations (0µg/mL - 20µg/mL) for 90 minutes, and then interrogated with anti-prion antibody (6H4). The PrP^C signal (pink) was reduced to

PrP^C-null signal (black dashed line) by 2.5µg/mL – RK-Deer, and 5µg/mL – RK-Mouse; whereas, PrP^{Sc} signal (maroon) was detectable at all PK concentrations, although a slow reduction of signal did occur at higher PK concentrations. This indicates that the standard operating protocol of 100µL per well 5µg/mL PK will guarantee detectable signal is PrP^{Sc} and not PrP^C.

Denaturation with a chaotropic agent alters epitope accessibility of PrP^{Sc} but not PrP^C.

Once PK levels were established, the ESA was then expanded to interrogate a prion at multiple known epitopes to be able to create a map of specific regional differences between prion strains and help resolve how strains differ. Deriving an accurate epitope location for anti-prion antibodies is recent^{82, 85}. The amino acid residues included in the binding of each anti-prion antibody (PRC1, D13, D18, 1B8, PRC5, 6H4, 5A3 and PRC7) epitope is indicated (Figure 3.1B). PRC1⁸² and D13⁸⁵ recognize linear epitopes located in the unstructured N-terminal region near the PK cleavage site. 1B8 recognizes a linear epitope located in the globular C-terminal region. PRC5⁸², D18⁸⁵, 6H4⁸⁵, 5A3 and PRC7⁸² recognize discontinuous epitopes located in the globular C-terminal region. Additionally, PRC7 is glycosylation specific and only binds to unglycosylated, and monoglycosylated (residue 196) species of the prion protein. Of note, PRC1 is cervid specific and 5A3 is murine specific.

We proceeded to determine if denaturation by a chaotropic agent (GdnHCl) would alter PrP^C (Figure 3.4C-D) and PrP^{Sc} (Figure 3.4E-F) epitope accessibility. The PrP^C signals in the RK13-PrP^C cell models (RK-Deer and RK-Mouse) are unaffected by denaturation (Figure 3.4C-D) at epitopes of anti-prion antibodies: PRC1 (green), D13

(yellow), D18 (grey), 1B8 (purple), PRC5 (orange) 6H4 (blue), and 5A3 (red). PRC7 (black) signal was low/non-existent, and presented qualitatively different (light shadow versus punctate spots); the data indicate a variation in the amount of underglycosylated PrP^C (aglycosylated and monoglycosylated at residue 196) in the cells. However, the PrP^{Sc} signals in chronically infected cell lines that perpetually propagate prion infection (RML/RK-Mouse, and CWD/RK-Deer) are affected by denaturation after PK treatment at all epitopes queried (Figure 3.4E-F). Surprisingly, there was PrP^{Sc} signal without denaturation at some linear and discontinuous epitopes (RML/RK-Mouse - 1B8, PRC5, and 6H4).

PrP^{Sc} epitope accessibility can be used to differentiate between Elk-CWD and Deer CWD.

To examine strain differences with the ESA, we began by validating the significant differences (Figure 2.3) due to the different amino acid at position 226 [deer (Q), elk (E)] has on the stability of CWD of freshly infected cells. Brains (n=3) from terminally ill Tg(ElkPrP)5037^{+/-} and Tg(DeerPrP)1536^{+/-} mice infected with elk CWD isolate Bala05 were used to infect RK-Elk and RK-Deer cell lines, respectively, along with the RK-V(vector only, PrP^C null) cell line. They were then interrogated via ESA with epitope-mapped anti-prion antibodies (Figure 3.5); like the C-CSA [Chapter 2], we expanded the assay to query multiple antibodies to examine epitopes across the molecule. The GdnHCl_{1/2} value represents the midway point of the linear denaturation until the entire molecule is accessible and the curve fit value represents the strains responds to denaturation by GdnHCl. As such, the GdnHCl_{1/2} and curve fit have been

indicated. The sigmoidal curve fit for all pairs (Elk-CWD and Deer-CWD) were significantly different ($p < 0.0001$) at all epitopes. When Comparing $GdnHCl_{1/2}$ value, the unstructured N-terminal region, showed a significant difference between Elk-CWD and Deer-CWD at both PRC1 ($p = 0.0005$) and D13 ($p = 0.0003$) linear epitopes. The globular domain of Elk-CWD and Deer-CWD were significantly different at all discontinuous epitopes ($p < 0.0001$) D18 and PRC7, ($p = 0.0477$) PRC5, and ($p = 0.0057$) 6H4. Since the CWD originated from a single sample (Bala05 isolate) that was passaged between Tg(Deer) and Tg(Elk) mice into RK-Deer and RK-Elk cells, respectively, the expectation is that there would be similarities in structure, and differences due to the single amino acid residue difference (226 Q/E) between Deer and Elk, respectively.

PrP^{Sc} epitope accessibility can be used to differentiate between classically defined murine-adapted scrapie RML and 22L strains.

The significant difference caused by the single amino acid difference in deer passaged CWD and elk passaged CWD cannot be denied; however, the goal was to create a more universal ESA capable of differentiating subtle differences between strains in multiple species, especially in strains with the same host PrP^C background. To that endeavor, brains ($n = 3$) from terminally ill C57Bl/6 mice infected with classically defined murine-adapted scrapie strains (RML and 22L) were used to infect murine-PrP^C expressing RK13 (RK-Mouse) cells along with the RK-V (vector only, PrP^C null) cell line. Both murine-adapted prion strains (RML, and 22L) share the same amino acid sequence; yet, each ultimately produces a different disease (Table 3.1). Epitope accessibility was compared via the ESA (Figure 3.2) with anti-prion antibodies (Figure

3.1B) ranging the unstructured region and globular domain; PRC1 is not a murine-specific anti-prion antibody and was, therefore, not used. The GdnHCl_{1/2} value represents the midway point of the linear denaturation until the entire molecule is accessible and the curve fit value represents the strains responds to denaturation by GdnHCl. As such, the GdnHCl_{1/2} and curve fit have been indicated. Figure 3.6, the sigmoidal curve fit for 6H4, D18, and PRC7 were (p<0.0001), 1B8 (p=0.0001), 5A3 (p=0.0174), D13 (p=0.01), and PRC5 was non-significant (p=0.1304); this implies that the overall response to GdnHCl was different for all antibodies, except for PRC5. When comparing the GdnHCl_{1/2} value via t-test, two epitopes were not significantly different (PRC5 p=0.1024; and 5A3 p=0.3322) where the other epitopes were significantly different at D13 (p=0.0331), 6H4 (p=0.0090), D18 (p<0.0001), 1B8 (p=0.0003), and PRC7 (p=0.0059). Overall, this implies that RML and 22L are similar in their response to GdnHCl and at their GdnHCl $\frac{1}{2}$ value around the first alpha helix, although the area within the helix is different. Similarly, the response to GdnHCl and GdnHCl $\frac{1}{2}$ value in RML and 22L is similar at the unstructured loop between beta sheet-2 and alpha helix 3, but differs more broadly at discontinuous epitopes surrounding the area.

PK-treated, non-denatured PrP^{Sc} epitopes are accessible and create strain and host-PrP^C specific patterns.

Interestingly, some prion strains did not require denaturation to reveal signal at discontinuous PrP^{Sc} epitopes (Figure 3.4F). To this end, we examined an array of cervid and murine-adapted strains (Table 3.1) with ESA. Brains (n=3) from terminally ill C57Bl/6 mice infected with murine-adapted scrapie strains (RML, 22L, and 139A) and

recently murine-adapted CWD strain⁸⁶ (mD10) were used to infect murine- PrP^C expressing RK13 (RK-Mouse) cells along with the RK-V (vector only, PrP^C null) cell line. All four murine-adapted prion strains (RML, 22L, 139A and mD10) share the same amino acid sequence; yet, each ultimately produces a different disease (Table 3.1). Brains (n=3) from terminally ill Tg(DeerPrP)1536^{+/-} and Tg(ElkPrP)5037^{+/-} mice infected with elk CWD isolate Bala05 were used to infect RK-Elk and RK-Deer cell lines, respectively, along with the RK-V(vector only, PrP^C null) cell line; this was to validate a mismatch PrP^{Sc}-PrP^C paradigm. Additionally, brains (n=3) from terminally ill Tg(ElkPrP)5037^{+/-} and Tg(DeerPrP)1536^{+/-} mice infected with mouse-adapted RML were used to infect RK-Elk and RK-Deer cell lines, respectively, along with the RK-V(vector only, PrP^C null) cell line; this was to examine species adaption and prion evolution. All strains were examined with epitope-mapped antibodies (Figure 3.1B) via the ESA (Figure 3.2); however, 5A3 is murine-specific and not used to detect cervid prion strains, and PRC1 is cervid-specific and not used to detect murine-adapted prion strains. The noticeable signal without denaturation offered additional insight into prion structure (Figure 3.7). The non-denatured prions produced strain specific fingerprints; each prion strain showing signal produced a unique pattern of epitope availability.

Overall, RK-Deer passaged prions (Elk-CWD, Deer-CWD, Elk-RML, and Deer-RML) were inaccessible without denaturation (Figure 3.7A); only one comparison between RK-Deer passaged prions was significant, all others were non-significant. The only prominent epitope available in folded (non-denatured) Deer PrP^{Sc} was within

Deer-RML at PRC5; which significantly differed from all other RK-Deer passaged prions ($p < 0.0001$). This is the only point where cervid-adapted RML passaged into RK-Deer somewhat mirror the original murine-adapted RML pattern (Figure 3.7C). The species barrier between murine-adapted and cervidized RML on a deer-PrP^C host background significantly alters the structure of RML.

Overall, RK-Elk passaged elk-adapted prion strains (Elk-CWD and Elk-RML) were accessible without denaturation (Figure 3.7B); whereas Deer-CWD was inaccessible without denaturation. Deer-adapted RML did not successfully infect RK-Elk. Within RK-Elk passaged elk-adapted prion strains (Elk-CWD and Elk-RML), there is a significant segregation into two very different forms ($p < 0.0001$, at all epitopes). In the N-terminal unstructured region (PRC1 and D13), Elk-RML is more structurally available than Elk-CWD. Moreover, epitopes embedded in α -helix 1 (1B8 and D18) are available in Elk-RML but not Elk-CWD; although, the discontinuous epitope ranging around the α -helix 1 region (PRC5) is accessible in Elk-CWD and not in Elk-RML. The other discontinuous epitope (6H4) that ranges from α -helix 1 to α -helix 3 is accessible in PK treated, non-denatured PrP^{Sc} more in Elk-CWD than Elk-RML. Glycosylation occupancy at residue 180 prohibits PRC7 binding; as such, Elk-RML contains more 180-glycosylation than Elk-CWD.

When comparing cervid strains, elk PrP^{Sc} was overall more accessible than deer PrP^{Sc}. Deer-CWD remained inaccessible without denaturation regardless of the host PrP^C, i.e. deer or elk (Figure 3.7A-B). Unlike Elk-CWD in RK-Deer, Elk-CWD in RK-Elk was accessible without denaturation at multiple epitopes PRC1, D13, PRC5, 6H4, PRC7;

the difference was significantly ($p < 0.0001$) more accessible at D13, PRC5, 6H4, PRC7 and not significantly different at PRC1 ($p = 0.2667$). Unlike Elk-RML PrP^{Sc} in RK-Deer, Elk-RML PrP^{Sc} in RK-Elk was highly accessible in the unstructured C-terminus region PRC1 ($p < 0.0001$) and D13 ($p < 0.0001$), and within α -helix 1, but similar Elk-RML PrP^{Sc} in RK-Deer is inaccessible at discontinuous N-terminus epitopes PRC5 (ns, $p = 0.998$), 6H4 (ns, $p = 0.1836$), and PRC7 (ns, $p = 0.9999$). This pattern is a dramatic shift from the original murine-adapted RML strain; resembling an entirely new structure for RML (Figure 3.7B-C).

PK treated, non-denatured PrP^{Sc} of murine-adapted prion strains (Figure 3.7C) structurally resemble PrP^C around the first α -helix; specifically, α -helix 1 is detectable by a discontinuous antibodies (PRC5 and 6H4) but, PrP^{Sc} is in a conformation where portions of the α -helix 1 are buried (1B8, and D18). Although detectable signal in the folded (non-denatured) state is profound, when murine-adapted prion strains were compared the epitopes D13, D18, 5A3, and PRC7 were non-significantly different between strains. There were significant differences between strains at the linear epitope 1B8, and discontinuous epitopes PRC5 and 6H4. The linear 1B8 epitope buried in α -helix 1 showed significant differences when comparing mD10 to all other murine-adapted strains: RML ($p < 0.0001$), 22L ($p < 0.0001$) and 139A ($p < 0.0001$); this implies that murine-adapted CWD varies significantly from murine-adapted scrapie within α -helix 1. Additionally, 22L and 139A were significantly different ($p = 0.01$) at the linear 1B8 epitope buried in α -helix 1; strain comparisons (RML:22L and RML:139A) were not significantly different. The highest variability between strains occurred at PRC5 and

6H4, which span the area from before α -helix 1 to α -helix 3. With one exception, all discontinuous PRC5 epitope comparisons between murine-adapted prion strains were significant ($p \leq 0.0001$), with the exception of 22L:mD10 (ns, $p = 0.0599$); the variation of the structure on either side of α -helix 1 is an important difference between these strains. Every discontinuous 6H4 epitope comparisons between murine-adapted prion strains were significant ($p \leq 0.0002$); the variation in the globular region spanning α -helix 1 to α -helix 3 reinforces that the difference between prion strains resides in how PrP^{Sc} is folded. Lastly, there was a trend (ns, $p = 0.12$) of glycosylation state of murine-adapted PrP^{Sc} segregated into two states with PRC7; PRC7 is glycosylation specific and only binds to unglycosylated, and monoglycosylated (residue 196) species of the prion protein. Glycosylation occupancy at residue 180 prohibits PRC7 binding; as such, RML and 22L contain more 180-glycosylation than 139A and mD10. The PRC7 trend along with strain differences with PRC5 may factor into the difference seen in the 7-5 ELISA-CSA (Figure 3.3F).

PrP^{Sc} epitope GdnHCl_{1/2} values and curve fits further delineate the structural difference a single amino acid can make on the tertiary shape of Chronic Wasting Disease PrP^{Sc}

Conformational stability assays traditionally rely on the GdnHCl_{1/2} value to differentiate strains and provide further information about the relative stability of the molecule and how available or resistant the epitope is to detection. To that end, all strains (Table 3.1) examined (Figure 3.7) were compared for the GdnHCl_{1/2} value of each antibody probed (Figure 3.8-3.11). As mentioned, the GdnHCl_{1/2} value represents the midway point of the linear denaturation until the entire molecule is accessible and

the curve fit value represents how the strains are responding to denaturation by GdnHCl. As such, the $GdnHCl_{1/2}$ and curve fit have been indicated. Using both points is an important distinction, allowing a more nuanced evaluation of prion strain structure. For example, if the $GdnHCl_{1/2}$ value is similar but the strains arrive at that point differently; it implies that although the epitope is available at roughly the same molarity, the process of denaturation varies. Another possible response is if the $GdnHCl_{1/2}$ value is different and the curve fit is the same; it implies that the difference only represents a shift in mirrored response to denaturation by GdnHCl. Some strains did not fit the best-fit curves parameters, were unable to be resolved at a specific epitope, or were otherwise unable to provide a $GdnHCl_{1/2}$ value; those that lack a $GdnHCl_{1/2}$ value are noted on graphs with an “x” at the antibody along the $GdnHCl_{1/2}$ value line.

To verify and expand on how the single amino acid difference at position 226 [deer (Q), elk (E)] effects the structure of Chronic Wasting Disease (CWD) brains (n=3) from terminally ill Tg(ElkPrP)5037^{+/-} and Tg(DeerPrP)1536^{+/-} mice infected with elk CWD isolate Bala05 were used to infect RK-Elk and RK-Deer cell lines, along with the RK-V(vector only, PrP^C null) cell line. The resultant CWD prions were interrogated with the ESA (Figure 3.2) using anti-prion antibodies (Figure 3.1B): PRC1, D13, D18, PRC5, 6H4, and PRC7. This represented six infection groups, four experimental and two control (Figure 3.8); terminology: RK-Deer passaged deer-CWD (Deer-CWD>Deer) pink solid line; RK-Deer passaged elk-CWD (Elk-CWD>Deer) orange dashed line; RK-Elk passaged deer-CWD (Deer-CWD>Elk) pink dashed line; and RK-Elk passaged elk-

CWD (Elk-CWD>Elk) orange solid line. Since the CWD originated from a single sample (Bala05 isolate) that was passaged between Tg(Deer) and Tg(Elk) mice into RK-Deer and RK-Elk cells, the expectation is that there would be similarities in structure, and differences due to the single amino acid residue difference (226 Q/E) between Deer and Elk. Figure 3.8A contains all four experimental groups, the control groups were completely negative, and left off Figure 3.8 to aid interpretability. The data was then segregated into all possible comparisons: matching PrP^C-PrP^{Sc} (Figure 3.8B), mismatching PrP^C-PrP^{Sc} (Figure 3.8C), Tg(Deer) passaged CWD (Figure 3.8D), Tg(Elk) passaged CWD (Figure 3.8E), CWD infected RK-Deer (Figure 3.8F), and CWD infected RK-Elk (Figure 3.8G). Each pair allows for a different comparison of structure.

As seen in Figures 3.5 and 3.8B matching PrP^C-PrP^{Sc} [Deer-CWD>Deer and Elk-CWD>Elk] had significantly different curve fits ($p < 0.0001$) at all epitopes and significantly different GdnHCl_{1/2} values at all epitopes examined: PRC1 ($p = 0.0005$), D13 ($p = 0.0003$), D18 ($p < 0.0001$), PRC5 ($p = 0.0477$), and 6H4 ($p = 0.0057$), and PRC7 ($p < 0.0001$). When there was a mismatching PrP^C-PrP^{Sc} [Elk-CWD>Deer and Deer-CWD>Elk] there was a loss of GdnHCl_{1/2} value via curve fit for Elk-CWD>Deer at D13 and D18, and for Deer-CWD>Elk at PRC1, D13, and D18. The curves were significantly different at PRC1 ($p < 0.0001$), PRC5 ($p < 0.0001$), 1B8 ($p = 0.0013$), and 6H4 ($p = 0.0002$), and not significantly different at D13 ($p = 0.9134$), D18 ($p = 0.9134$), and PRC7 ($p = 0.3253$). Overall, when there is a mismatching of host and infectious material, CWD unifies into a more homogenous structure based off of GdnHCl_{1/2} value at PRC5, 6H4, and PRC7. The only significant difference between GdnHCl_{1/2} values was at 1B8 ($p = 0.0104$); the other available

comparisons were not significant PRC5 ($p=0.0594$), 6H4 ($p=0.0850$), and PRC7 ($p=0.5537$). Overall, it implies that mismatching causes $GdnHCl_{1/2}$ values to be similar although the response to GdnHCl denaturation is different.

To show that the amino acid composition of the host PrP^C causes changes in prion strain structure (Figure 3.8D-E), comparisons were made between Deer CWD PrP^{Sc} going into different host PrP^C (RK-Deer vs. RK-Elk) and Elk CWD PrP^{Sc} going into different host PrP^C (RK-Deer vs. RK-Elk). Deer CWD PrP^{Sc} presents as two different structures based on host PrP^C. Deer CWD PrP^{Sc} is overall more inaccessible in RK-Elk than RK-Deer. There were significant differences in curve fit at PRC1 ($p<0.0001$), D13 ($p=0.0014$), D18 ($p<0.0001$), PRC5 ($p<0.0001$), 6H4 ($p<0.0001$), and PRC7 ($p=0.0004$). For available comparisons of $GdnHCl_{1/2}$ value there were significant differences in the $GdnHCl_{1/2}$ value at PRC5 ($p<0.0001$) and 6H4 ($p=0.0063$) and no significant difference at PRC7 ($p=0.0945$). Elk CWD PrP^{Sc} presents as two different structures based on host PrP^C with overall more constant variation than Deer CWD PrP^{Sc} in different host PrP^Cs. Elk CWD PrP^{Sc} is overall more inaccessible in RK-Deer than RK-Elk. There were significant differences between Elk CWD PrP^{Sc} in RK-Deer than RK-Elk in the curve fit at PRC1 ($p=0.0009$), D13 ($p<0.0001$), D18 ($p<0.0001$), PRC5 ($p<0.0001$), 6H4 ($p<0.0001$), and PRC7 ($p=0.0048$). For available comparisons of $GdnHCl_{1/2}$ value there were significant differences at PRC1 ($p<0.0001$), PRC5 ($p<0.0001$), 6H4 ($p=0.0002$) and PRC7 ($p=0.0033$). This implies that the response and $GdnHCl_{1/2}$ value are both changing. Overall, it implies that the amino acid composition of the infectious material, CWD PrP^{Sc}, can cause changes in both $GdnHCl_{1/2}$ values and the response to GdnHCl

denaturation; specifically that a mismatched to host PrP^C causes the structure to become more inaccessible.

To show that the amino acid composition of the infectious PrP^{Sc} causes changes in prion strain structure (Figure 3.8F-G), comparisons were made between RK-Deer infected with Deer and Elk CWD PrP^{Sc} and RK-Elk infected with Deer and Elk CWD PrP^{Sc}. Deer PrP^C causes significant differences between Deer and Elk CWD PrP^{Sc} curve fit at all epitopes: PRC1 (p=0.0003), D13 (p<0.0001), D18 (p<0.0001), PRC5 (p<0.0001), 6H4 (p<0.0001), and PRC7 (p = 0.0002). For available comparisons of GdnHCl_{1/2} value there were significant differences at PRC1 (p=0.0060), PRC5 (p<0.0001), 6H4 (p=0.0041), and no significant difference at PRC7 (p=0.1158). Elk PrP^C causes significant differences between Deer and Elk CWD PrP^{Sc} curve fit at all epitopes: PRC1 (p<0.0001), D13 (p=0.0007), D18 (p<0.0001), PRC5 (p<0.0001), 6H4 (p<0.0001), and PRC7 (p<0.0001). For available comparisons of GdnHCl_{1/2} value there were significant differences at PRC5 (p<0.0001), 6H4 (p=0.0002), and PRC7 (p=0.0200). Overall, it implies that final PrP^{Sc} structure varies dependent on the CWD PrP^{Sc} amino acid composition. Figure 3.8, overall, verifies that single amino acid differences between the infectious material and host substrate cause significant difference in PrP^{Sc} structure.

PrP^{Sc} epitope GdnHCl_{1/2} values and curve fits delineate the structural difference a single amino acid can make on the tertiary shape of recently adapted cervidized-RML

PrP^{Sc}

Chronic Wasting Disease is native to cervids, but prions are ever evolving: new prions are being discovered in camelids, CWD is now in Europe. As such,

understanding prion adaption across the species barrier is crucial. RML is a classically defined murine-adapted scrapie strain that our lab then adapted into Tg(ElkPrP)5037^{+/-} and Tg(DeerPrP)1536^{+/-} mice. This new cervidized-RML, cerRML, presents differently than CWD (Table 1). CWD and RML passaged through Tg(DeerPrP)1536^{+/-} mice and CWD and RML passaged through Tg(ElkPrP)5037^{+/-} mice represent a prion that is native to the host and a newly adapted prion with similar or varying PrP^C-PrP^{Sc} sequences. To better understand the structural changes that occurred as part of species adaption, brains (n=3) from terminally ill Tg(ElkPrP)5037^{+/-} and Tg(DeerPrP)1536^{+/-} mice infected with mouse-adapted RML were used to infect RK-Deer and RK-Elk cell lines, along with the RK-V(vector only, PrP^C null) cell line. The resultant cervidized-RML prions were interrogated with the ESA (Figure 3.2) using anti-prion antibodies (Figure 3.1B): PRC1, D13, D18, PRC5, 6H4, and PRC7. This initially represented six infection groups: four experimental and two control (Figure 3.9); however, Deer-RML did not successfully infect RK-Elk cells.

The remaining three experimental groups were: RK-Deer passaged Deer-RML (Deer-RML>Deer) light blue solid line; RK-Deer passaged Elk-RML (Elk-RML>Deer) dark blue dashed line; and RK-Elk passaged Elk-RML (Elk-RML>Elk) dark blue solid line. Since the RML originated from a single sample that was passaged between Tg(Deer) and Tg(Elk) mice into RK-Deer and RK-Elk cells, the expectation is that there would be similarities in structure, and differences due to the single amino acid residue difference (226 Q/E) between Deer and Elk. Figure 3.9A contains all three experimental group, the control groups were completely negative, and left off Figure 3.9 to aid

interpretability. The data was then segregated into all possible comparisons: Tg(Elk) passaged RML in RK-Deer and RK-Elk (Figure 3.9B), CerRML infected RK-Deer (Figure 3.9C), and matching PrP^C-PrP^{Sc} (Figure 3.9D). Each pair allows for a different comparison of structure.

To show that the amino acid composition of the host PrP^C causes changes in prion strain structure (Figure 3.9B), comparisons were made between Elk-RML PrP^{Sc} going into different host PrP^C (RK-Deer vs. RK-Elk). Elk-RML PrP^{Sc} presents as two different structures based on host PrP^C with Elk-RML>Deer being less accessible at linear epitopes and at the glycosylation-specific epitope, more accessible along alpha helix 1-2 and identical to Elk-RML>Elk on either side of the alpha helix-1. There were significant differences between Elk-RML PrP^{Sc} in RK-Deer than RK-Elk in the curve fit at PRC1 (p<0.0001), D13 (p<0.0001), 1B8 (p<0.0001), D18 (p<0.0001), PRC5 (p= 0.0207), 6H4 (p<0.0001), and PRC7 (p<0.0001). For available comparisons of GdnHCl_{1/2} value there were significant differences at D13 (p=0.0051), 1B8 (p<0.0001), 6H4 (p<0.0001), and PRC7 (p<0.0001) and no significant differences at D18 (p=0.1451) and PRC5 (p=0.2066). Overall, it implies that the amino acid composition of the infectious material, RML PrP^{Sc}, causes changes in both GdnHCl_{1/2} values and the response to GdnHCl denaturation.

To show that the amino acid composition of the infectious PrP^{Sc} causes changes in prion strain structure, comparisons were made between RK-Deer infected with Deer-RML and Elk-RML (Figure 3.9C). Deer PrP^C causes significant differences between Deer-RML and Elk-RML in the curve fit at PRC1 (p<0.0001), D13 (p<0.0001), D18

($p < 0.0001$), PRC5 ($p = 0.0322$), 6H4 ($p = 0.0170$), and PRC7 ($p < 0.0001$) and not significantly different at 1B8 ($p = 0.6515$). GdnHCl_{1/2} value comparisons showed significant differences at PRC1 ($p < 0.0001$), D13 ($p < 0.0001$), D18 ($p < 0.0001$), 6H4 ($p = 0.0478$), and PRC7 ($p < 0.0001$) and not significantly different at 1B8 ($p = 0.3712$) and PRC5 ($p = 0.1170$). Overall, it implies that final PrP^{Sc} structure varies dependent on the cerRML PrP^{Sc} amino acid composition.

To show that even matching PrP^C-PrP^{Sc} amino acid composition causes changes in prion strain structure, comparisons were made between RK-Deer infected with Deer-RML and RK-Elk infected with Elk-RML (Figure 3.9D). Deer-RML>Deer and Elk-RML>Elk had significantly different curve fits at PRC1 ($p < 0.0001$), D13 ($p < 0.0001$), 1B8 ($p < 0.0001$), D18 ($p < 0.0001$), 6H4 ($p < 0.0001$), and PRC7 ($p < 0.0001$) and were not significantly different PRC5 ($p = 0.2238$). For available comparisons of GdnHCl_{1/2} value there were significant differences at 1B8 ($p < 0.0001$), PRC5 ($p = 0.0063$), 6H4 ($p < 0.0001$), and PRC7 ($p = 0.0005$) and were not significantly different at D13 ($p = 0.1270$) and D18 ($p = 0.8302$). Overall, even when the host and infectious material match, cerRML structure is not unified; although the PRC5 epitope seems unified in all three forms.

In parallel to CWD in Figure 3.8, cerRML in Figure 3.9 further supports that a single amino acid differences between the infectious material and host substrate cause significant difference in PrP^{Sc} structure. Chronic Wasting Disease is native to deer and elk; whereas, RML originated from sheep scrapie that was adapted into inbred mice and then was adapted into deer and elk transgenic mice. Furthermore, when CWD (Figure 3.8) and cerRML (Figure 3.9) are compared (Figure 3.10), species-adapted strains have

different tertiary structures than those passaged within their native host PrP^C. There is a striking difference between prion epitope accessibility of the native prions compared to recently adapted prions across all comparisons, along the range of epitopes examined.

The curve fit comparisons between CWD and cerRML were overall significantly different at every comparison except: (1) curves that didn't produce a GdnHCl_{1/2} value and (2) at PRC7 in Deer-CWD>Deer: Elk-RML>Deer (p= 0.1836) and Elk-CWD>Elk : Elk-RML>Elk (p= 0.1860). When comparing GdnHCl_{1/2} values between CWD and cerRML an overall pattern emerged: (1) specific epitopes were not significantly different, (2) GdnHCl_{1/2} values were similar but significantly different (3) GdnHCl_{1/2} values were pronouncedly different and significantly different, and (4) a lack of GdnHCl_{1/2} values at some epitopes. These indicate that each prion contains a unique tertiary structure.

The overall pattern of GdnHCl_{1/2} values is the most similar between Deer-CWD>Deer compared to Elk-RML>Elk (Figure 3.10C) in relation to other comparisons (Figure 3.10 A-B, D-L). Deer-CWD>Deer compared to Elk-RML>Elk are non-significantly different at D13 (p=0.2973), D18 (p=0.4808), and 6H4 (p=0.4940). The similarity between the GdnHCl_{1/2} value at PRC5 of Deer-CWD>Deer (2.00M) and Elk-RML>Elk (1.74M) doesn't preclude a significant difference (p=0.0002). The greatest difference between the GdnHCl_{1/2} value of Deer-CWD>Deer (3.46M) and Elk-RML>Elk (2.01M) occurred at PRC7 (p<0.0001). This implies that species adaption can alter the previously seen (Figure 3.8-3.9) interaction between PrP^C and PrP^{Sc} amino acid composition.

The pattern of $GdnHCl_{1/2}$ values in the unstructured region is overall the most similar between Deer-CWD>Deer compared to Deer-RML>Deer (Figure 3.10A) in relation to other comparisons (Figure 3.10 B-L). They contain significantly different ($p<0.0001$) curve fits at every epitope examined (Figure 3.10A) Deer-CWD>Deer compared to Deer-RML>Deer are non-significantly different at PRC1 ($p=0.2351$). The similarity between the $GdnHCl_{1/2}$ value at D13 of Deer-CWD (2.59 M) and Deer-RML (2.76 M) doesn't preclude a significant difference ($p=0.0015$). This overall similarity in pattern but significant difference occurs at D18 ($p=0.0123$) with Deer-CWD (2.92 M) and Deer-RML (3.09 M). However, Deer-CWD and Deer-RML differ at the remaining discontinuous epitopes in the globular region: PRC5 ($p=0.0002$), 6H4 ($p=0.0015$), and PRC7 ($p<0.0001$). This implies that adapting RML into deer creates a prion that resembles native prions at the unstructured region and overall perturbs the $GdnHCl_{1/2}$ values the least of all comparisons. Deer-RML>Deer and Deer-CWD>Deer contain the same amino acid sequence yet produce different diseases (Table 1), further verifying that prions propagate strain properties via subtle differences in their tertiary structure. PrP^{Sc} epitope $GdnHCl_{1/2}$ values and curve fits delineate the subtle structural differences between murine-adapted prions that share the same host PrP^C

There is an expectation of PrP^{Sc} structural variation between strains that do not share an identical amino acid sequence, i.e. Deer-CWD and Elk-CWD. However, all four murine-adapted prion strains (RML, 22L, 139A and mD10) share the same amino acid sequence; yet, each ultimately produces a different disease (Table 1). Brains (n=3) from terminally ill C57Bl/6 mice infected with murine-adapted scrapie strains RML,

22L, and 139A and recently murine-adapted CWD strain⁸⁶ mD10 were used to infect murine- PrP^C expressing RK13 (RK-Mouse) cells along with the RK-V (vector only, PrP^C null) cell line. All resultant prions were interrogated with the ESA (Figure 3.2) using anti-prion antibodies (Figure 3.1B): D13, 1B8, D18, PRC5, 6H4, 5A3, and PRC7.

Figure 3.11A contains all murine-adapted strains are included to visualize the similarity/ difference in overall pattern: RML (blue), 22L (green), 139A (grey) and mD10 (pink); the control groups were completely negative, and left off Figure 11 to aid interpretability. The data was then segregated into all possible comparisons: RML:22L (Figure 3.11B), 22L:139A (Figure 3.11C), RML:mD10 (Figure 3.11D), 22L:mD10 (Figure 3.11E), RML:139A (Figure 3.11F), and 139A:mD10 (Figure 3.11G). Each pair allows for a different comparison of structure.

As seen in Figure 3.6, Figure 3.11B shows a comparison of two classically defined murine-adapted scrapie strains: RML and 22L. Overall, RML and 22L have significantly different sigmoidal curve fits at D13 ($p=0.01$), 1B8 ($p=0.0001$), D18 ($p<0.0001$), 6H4 ($p<0.0001$), 5A3 ($p=0.0174$), and PRC7 ($p<0.0001$). PRC5 showed no significant differences between RML and 22L for curve fit ($p=0.1304$) or comparing GdnHCl_{1/2} value ($p=0.1024$). Unlike the curve fit, when comparing the GdnHCl_{1/2} value for RML and 22L, 5A3 was also non-significant ($p=0.3322$); whereas, D13 ($p=0.0331$), 1B8 ($p=0.0003$), D18 ($p<0.0001$), 6H4 ($p=0.0090$), and PRC7 ($p=0.0059$) were significantly different. Overall, this implies that RML and 22L are similar in their response to GdnHCl and at their GdnHCl $\frac{1}{2}$ value around the first alpha helix, although the area within the helix is different. Similarly, the response to GdnHCl and GdnHCl $\frac{1}{2}$ value in

RML and 22L is similar at the unstructured loop between beta sheet-2 and alpha helix 3, but differs more broadly at discontinuous epitopes surrounding the area.

Figure 3.11C shows a comparison of two murine-adapted scrapie strains: 22L and 139A. Overall, 22L and 139A have significantly different sigmoidal curve fits at D13 ($p < 0.0001$), D18 ($p = 0.0003$), 6H4 ($p < 0.0001$), 5A3 ($p < 0.0001$), and PRC7 ($p < 0.0001$). Two epitopes did not yield significantly different curve fits: 1B8 ($p = 0.0513$) and PRC5 ($p = 0.1474$). Although 1B8 did not have a significantly different curve fit, the $GdnHCl_{1/2}$ value was significantly different ($p = 0.0333$); this means that the response to GdnHCl was identical but subtly shifted to yield a different $GdnHCl_{1/2}$ value. Like RML:22L, PRC5 was not significantly different for 22L:139A for either curve fit, or $GdnHCl_{1/2}$ value ($p = 0.6636$). The other significantly different $GdnHCl_{1/2}$ values were D13 ($p = 0.0036$), D18 ($p = 0.0364$), 6H4 ($p = 0.0073$), 5A3 ($p = 0.0001$) and PRC7 ($p < 0.0001$). Overall, this implies that 22L and 139A are more similar around alpha helix-1 and diverge at either end of the molecule.

Figure 3.11D shows a comparison of murine-adapted scrapie RML and murine-adapted CWD mD10. Overall, RML and mD10 are the most divergent in structure with every sigmoidal curve fit and every $GdnHCl_{1/2}$ value being significantly different. The sigmoidal curve fits were significantly different at D13 ($p < 0.0001$), 1B8 ($p = 0.0359$), D18 ($p < 0.0001$), PRC5 ($p = 0.0043$), 6H4 ($p < 0.0001$), 5A3 ($p < 0.0001$), and PRC7 ($p < 0.0001$). The $GdnHCl_{1/2}$ values were significantly different at D13 ($p = 0.0026$), 1B8 ($p = 0.0037$), D18 ($p = 0.0003$), PRC5 ($p = 0.0036$), 6H4 ($p = 0.0009$), 5A3 ($p = 0.0085$), and PRC7 ($p < 0.0001$). The closest similarity between the two strains was at the linear epitope 1B8 in the globular

region. This striking difference shows that murine-adaptation of scrapie and CWD can create pronouncedly different structures.

Figure 3.11E shows a comparison of murine-adapted scrapie 22L and murine-adapted CWD mD10. Unlike RML:mD10, 22L and mD10 share some similarities in response to GdnHCl and GdnHCl_{1/2} value. 22L and mD10 have significantly different sigmoidal curve fits at D13 (p<0.0001), 1B8 (p=0.0263), D18 (p<0.0001), 6H4 (p<0.0001), 5A3 (p=0.0174), and PRC7 (p<0.0001). Although PRC5 did not have a significantly different curve fit (p=0.0630), the GdnHCl_{1/2} value was significantly different (p=0.0082); this means that the response to GdnHCl was identical but subtly shifted to yield a different GdnHCl_{1/2} value. Unlike the curve fit, when comparing the GdnHCl_{1/2} value for 22L and mD10, 6H4 was non-significant (p=0.0814). The other epitopes compared showed a significant difference in GdnHCl_{1/2} value for 22L and mD10 at D13 (p=0.0013), 1B8 (p=0.0086), D18 (p=0.0094), 5A3 (p=0.0028), and PRC7 (p<0.0001) were significantly different. This implies that murine-adapted CWD is more like 22L than RML.

Figure 3.11F shows a comparison of two murine-adapted scrapie strains, RML and 139A. Like RML and 22L, 139A shares a scrapie origin. RML and 139A have single overlapping epitope at 6H4, curve fit (p=0.5679) and GdnHCl_{1/2} value (p=0.0530). PRC5 had a significantly different sigmoidal curve fit (p<0.0001) but not significantly different GdnHCl_{1/2} value (p=0.0980); this implies that although the GdnHCl_{1/2} value is the same, the way that each arrive to it varies. All other epitope curve fit comparisons were all highly significantly different (p<0.0001). When comparing the remaining GdnHCl_{1/2}

values, each comparison was significantly different: D13 ($p=0.0085$), 1B8 ($p=0.0004$), D18 ($p<0.0001$), 5A3 ($p=0.0070$), and PRC7 ($p=0.0002$). Overall, this implies that RML and 139A share similarities but remain distinctly different.

Figure 3.11G shows a comparison of murine-adapted scrapie 139A and murine-adapted CWD mD10. mD10 is the most similar structurally to 139A, as compared to RML (Figure 3.11D) and 22L (Figure 3.11E). 139A and mD10 have single overlapping epitope at 5A3, curve fit ($p=0.3075$) and $GdnHCl_{1/2}$ value ($p=0.3779$). Additionally, D13 does not have a significantly different $GdnHCl_{1/2}$ value ($p=0.0622$) and PRC7 does not have a significantly different curve fit ($p=0.2386$). The curve fits were significantly different at D13 ($p=0.0001$), 1B8 ($p=0.0169$), D18 ($p<0.0001$), PRC5 ($p=0.0233$) and 6H4 ($p<0.0001$). The overall significance and difference is to a lesser degree at 1B8 and PRC5, implying that the curves still resemble each other to a greater extent than those with higher significance. The $GdnHCl_{1/2}$ values were significantly different at 1B8 ($p=0.0045$), D18 ($p=0.0017$), PRC5 ($p=0.0180$), 6H4 ($p=0.0007$) and PRC7 ($p=0.0426$). The overall significance and difference is to a lesser degree at PRC5 and PRC7, implying that the $GdnHCl_{1/2}$ value still resemble each other to a greater extent than those with higher significance. Overall, of all murine-adapted scrapie strains, 139A has the highest resemblance to murine-adapted CWD.

Overall, each murine adapted prion strain contained similarities and differences in structure to each other strain it was compared to. This further validates the technique and reinforces that prions propagate strain information via subtle variations in their PrP^{Sc} folded state.

The ESA and C-CSA are distinctively different tools for measuring PrP^{Sc} structure: prion resistance to protease degradation after partial denaturation (C-CSA) is not equivalent to epitope accessibility (ESA)

The epitope stability assay was created from conceptually merging the 7-5 ELISA-CSA (Figure 3.3) and the previously developed⁸¹ prion cell-based conformational stability assay (Figure 2.2). The C-CSA derives the GdnHCl_{1/2} value from the prions relative resistance to Proteinase K after stepwise denaturation; whereas the ESA derives the GdnHCl_{1/2} value from the accessibility of an epitope after stepwise denaturation. As such, the two assays are interrogating the prion molecule differently. If C-CSA [Chapter 2] GdnHCl_{1/2} values were not significantly different from the ESA GdnHCl_{1/2} values, that implies that epitope accessibility is equivalent to resistance to protease degradation; however, significant differences implies that these two molecular characteristics are independent.

To test this, the C-CSA GdnHCl_{1/2} values for Deer-CWD, Elk-CWD, mD10, RML, and 22L (Figure 2.5-2.8) were compared to ESA GdnHCl_{1/2} values (Figure 3.8 & 3.11). The resultant comparison (Figure 3.12) compares C-CSA GdnHCl_{1/2} values (dashed line) and ESA GdnHCl_{1/2} values (solid line). Curve fits were not calculated since the curves were opposite in direction. Overall, prion resistance to protease degradation after partial denaturation (C-CSA) is not equivalent to epitope accessibility (ESA). The most dissimilar GdnHCl_{1/2} values occurred with mD10 and RML; while, Elk-CWD had the most similar GdnHCl_{1/2} values.

For comparison of mouse-adapted prions strains mD10, RML, and 22L; 22L contained the most similarities. Comparing mD10 C-CSA to ESA (Figure 3.12A) showed significant differences at D13 ($p < 0.0001$), PRC5 ($p = 0.0002$), 6H4 ($p = 0.0002$), and PRC7 ($p = 0.0025$), and not significant difference at D18 ($p = 0.2813$). This implies that at the D18 epitope, epitope accessibility is equivalent to resistance to protease degradation. For the other epitopes, the epitope accessibility is not equivalent to resistance to protease degradation. Comparing RML C-CSA to ESA (Figure 3.12C) showed significant differences at D13 ($p = 0.0041$), D18 ($p < 0.0001$), PRC5 ($p = 0.0125$), and PRC7 ($p = 0.0009$), and not significant difference at 6H4 ($p = 0.4624$). This implies that at the 6H4 epitope, epitope accessibility is equivalent to resistance to protease degradation. For the other epitopes, the epitope accessibility is not equivalent to resistance to protease degradation. Comparing 22L C-CSA to ESA (Figure 3.12E) showed significant differences at PRC5 ($p = 0.0002$), 6H4 ($p = 0.0090$) and PRC7 ($p < 0.0001$), and no significant differences at D13 ($p = 0.0548$) and D18 ($p = 0.3697$). This implies that for both the D13 and D18 epitope, epitope accessibility is equivalent to resistance to protease degradation. For the other epitopes, the epitope accessibility is not equivalent to resistance to protease degradation.

For comparisons of cervid prion strains Deer-CWD and Elk-CWD; both showed more similarities than murine strains with Elk-CWD having the most similarities of all strains examined. Comparing Deer-CWD C-CSA to ESA (Figure 3.12B) showed significant differences at PRC1 ($p = 0.0273$), PRC5 ($p < 0.0001$) and 6H4 ($p = 0.0014$), and no significant differences at D13 ($p = 0.7138$), D18 ($p = 0.6729$) and PRC7 ($p = 0.1552$). This

implies that at D13, D18, and PRC7, epitope accessibility is equivalent to resistance to protease degradation. For the PRC1, PRC5 and 6H4 epitopes, the epitope accessibility is not equivalent to resistance to protease degradation. Comparing Elk-CWD C-CSA to ESA (Figure 3.12D) showed significant differences at only two epitopes: PRC5 ($p=0.0001$) and 6H4 ($p=0.0005$). The other epitopes were all not significantly different: PRC1 ($p=0.9826$), D13 ($p=0.2157$), D18 ($p=0.2035$) and PRC7 ($p=0.1366$). This implies that at PRC1, D13, D18, and PRC7, epitope accessibility is equivalent to resistance to protease degradation. For the PRC5 and 6H4 epitopes, the epitope accessibility is not equivalent to resistance to protease degradation. Overall, this indicates that the ESA is an independent molecular tool that is capable of examining prion structure in a new way.

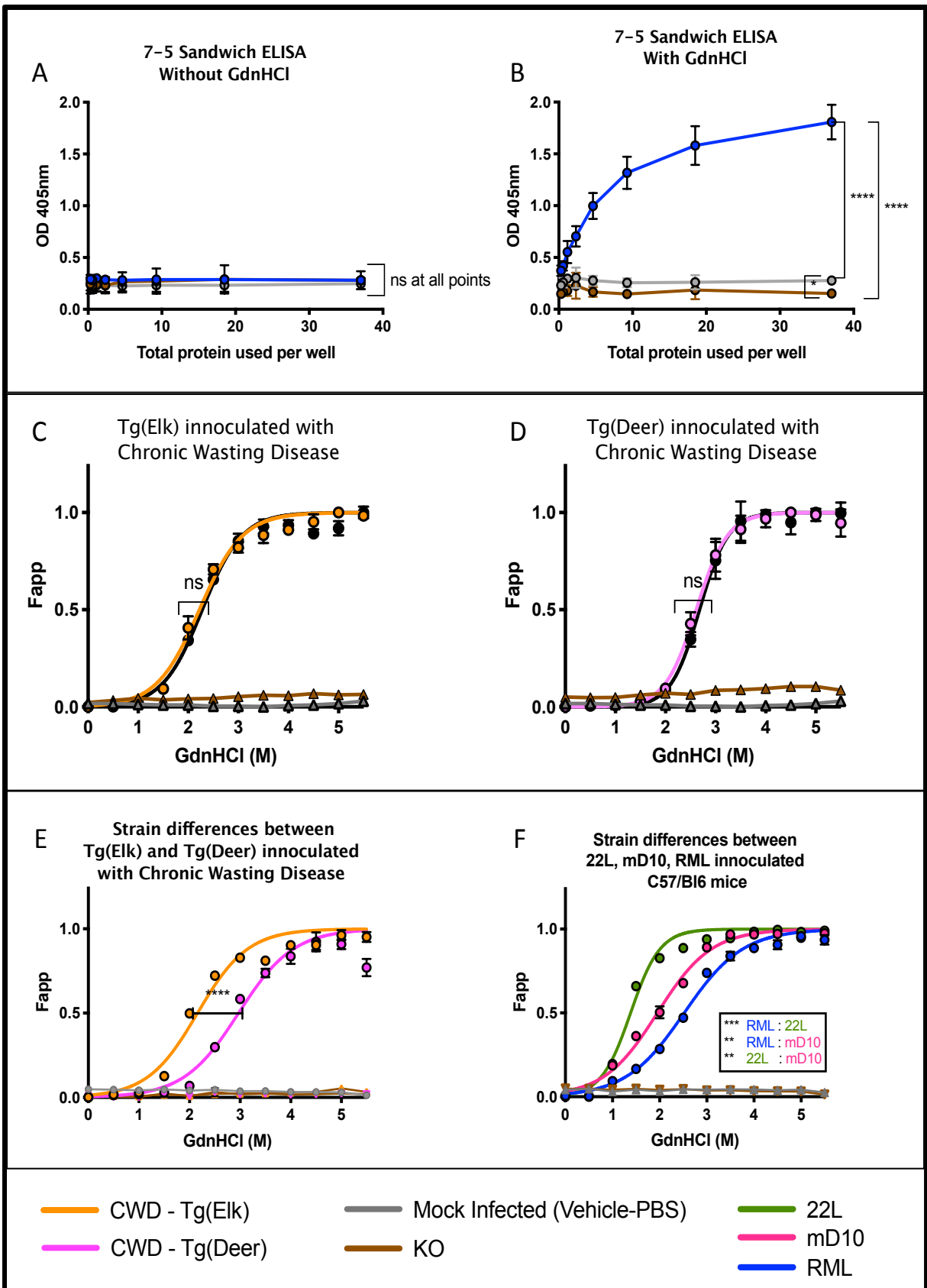


FIGURE 3.3: Infection specific, 7-5 ELISA-CSA, is able to differentiate between prion strains via differences in epitope binding without requiring PK ablation of PrP^C. (A-B) Brains (n=3) from terminally ill C57Bl/6 inbred mice infected with RML (blue), age-matched PBS-mock infected C57Bl/6 (grey), and PrP-KO (PrP^C null) mice (brown) were interrogated with the 7-5 ELISA without (A) and with (B) a chaotropic agent, GdnHCl. The prion protein is detectable in GdnHCl treated, infected brains. (C) Brains (n=3) from terminally ill Tg(ElkPrP)5037^{+/-} mice infected with elk CWD isolate Bala05, PBS-mock infected Tg(ElkPrP)5037^{+/-} and PrP-KO (PrP^C null) mice were interrogated with the 7-5 ELISA. There was no significance (p= 0.9367) between PK treated (black) and untreated (orange) Elk-CWD prions. There was no detectable signal from PBS-mock infected Tg(ElkPrP)5037^{+/-} (grey) and PrP-KO (PrP^C null) mice (brown). (D) Brains (n=3) from terminally ill Tg(DeerPrP)1536^{+/-} mice infected with elk CWD isolate Bala05, PBS-mock infected Tg(DeerPrP)1536^{+/-} mice, and PrP-KO (PrP^C null) mice were interrogated with the 7-5 ELISA. There was no significance (p=0.1442) between PK treated (black) and untreated (orange) Deer-CWD prions. There was no detectable signal from PBS-mock infected Tg(DeerPrP)1536^{+/-} (grey) and PrP-KO (PrP^C null) mice (brown). (E) Comparing terminally ill Tg(ElkPrP)5037^{+/-} mice (orange) and Tg(DeerPrP)1536^{+/-} (pink) infected with elk CWD isolate Bala05 reveals strain differences (p ≤ 0.0001). PBS-mock infected (grey) and PrP-KO (PrP^C null) mice (brown) do not show detectable differences. (F) Comparing terminally ill C57Bl/6 mice infected with RML (blue), 22L (green), and mD10 (pink) reveals strain differences (RML:22L p = 0.0001; RML-mD10 p=0.0053; 22L:mD10 p=0.007). PBS-mock infected C57Bl/6 (grey) and PrP-KO (PrP^C null) mice (brown) do not show detectable differences.

OD_{405nm}, the detectable signal was at optical density 405nm. F_{app}, fraction of apparent signal. The sigmoidal dose-response curve was plotted using a four parameter algorithm and nonlinear least-squares fit; with curve comparison. Error bars, SD from n=3 animals per group. Statistical significance: ns p > 0.05; * p ≤ 0.05; ** p ≤ 0.01; *** p ≤ 0.001; **** p ≤ 0.0001. Statistical differences from the GdnHCl_{1/2} values between matched, curves were calculated by curve fit parameters and via t-test (means)

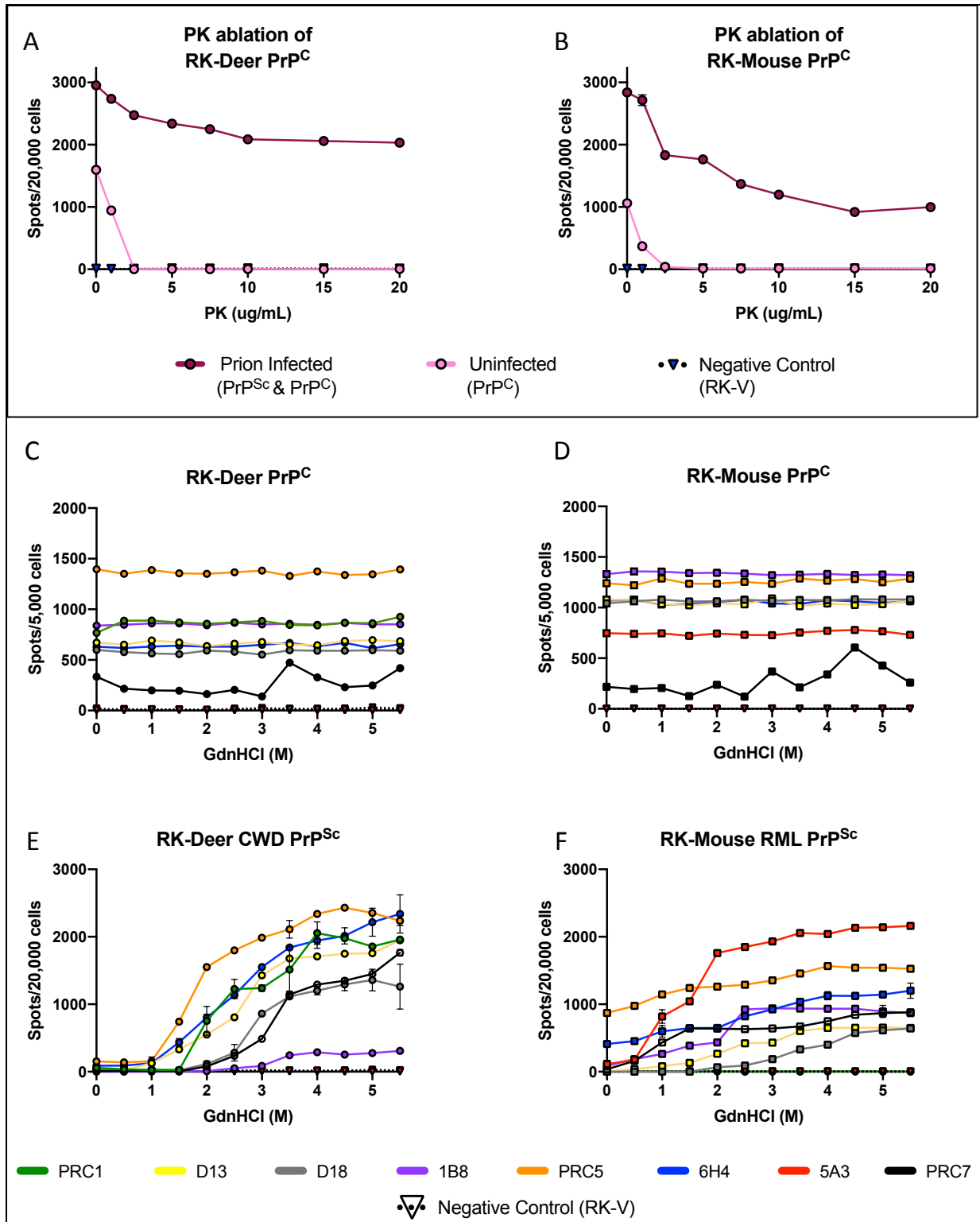


FIGURE 3.4: Ablating PrP^C signal with Proteinase K and denaturation with a chaotropic agent alters epitope accessibility of PrP^{Sc} but not PrP^C at most epitopes. (A-B) Standard operating protocol [100µL per well 5µg/mL PK] is sufficient to ablate PrP^C

signal in the RK13-PrP^C cell model. Uninfected (pink line) RK13-PrP^C cell signal is reduced to RK-V (PrP^C null) cell signal (black dashed line) by (2.5µg/mL - RK-Deer, and 5µg/mL - RK-Mouse). Chronically prion infected (RML/RK-Mouse, and CWD/RK-Deer) cell signal (maroon) is detectable at all PK concentrations. **(C-D)** PrP^C signal in the RK13-PrP^C cell models are unaffected by denaturation with GdnHCl at epitopes of anti-prion antibodies: PRC1 (green), D13 (yellow), D18 (grey), 1B8 (purple), PRC5 (orange) 6H4 (blue), and 5A3 (red). PRC7 (black) signal is low/non-existent, qualitatively different (light shadow versus punctate spots); since PRC7 is a glycosylation specific epitope (aglycosylated, and monoglycosylated at residue 196), the data indicates a variation in the amount of underglycosylated PrP^C in the cells. **(E-F)** PrP^{Sc} signal in the RK13-PrP^C cell models are affected by denaturation with GdnHCl at all epitopes. Additionally, there is PrP^{Sc} signal without denaturation at some epitopes (RML/RK-Mouse - 1B8, PRC5, and 6H4).

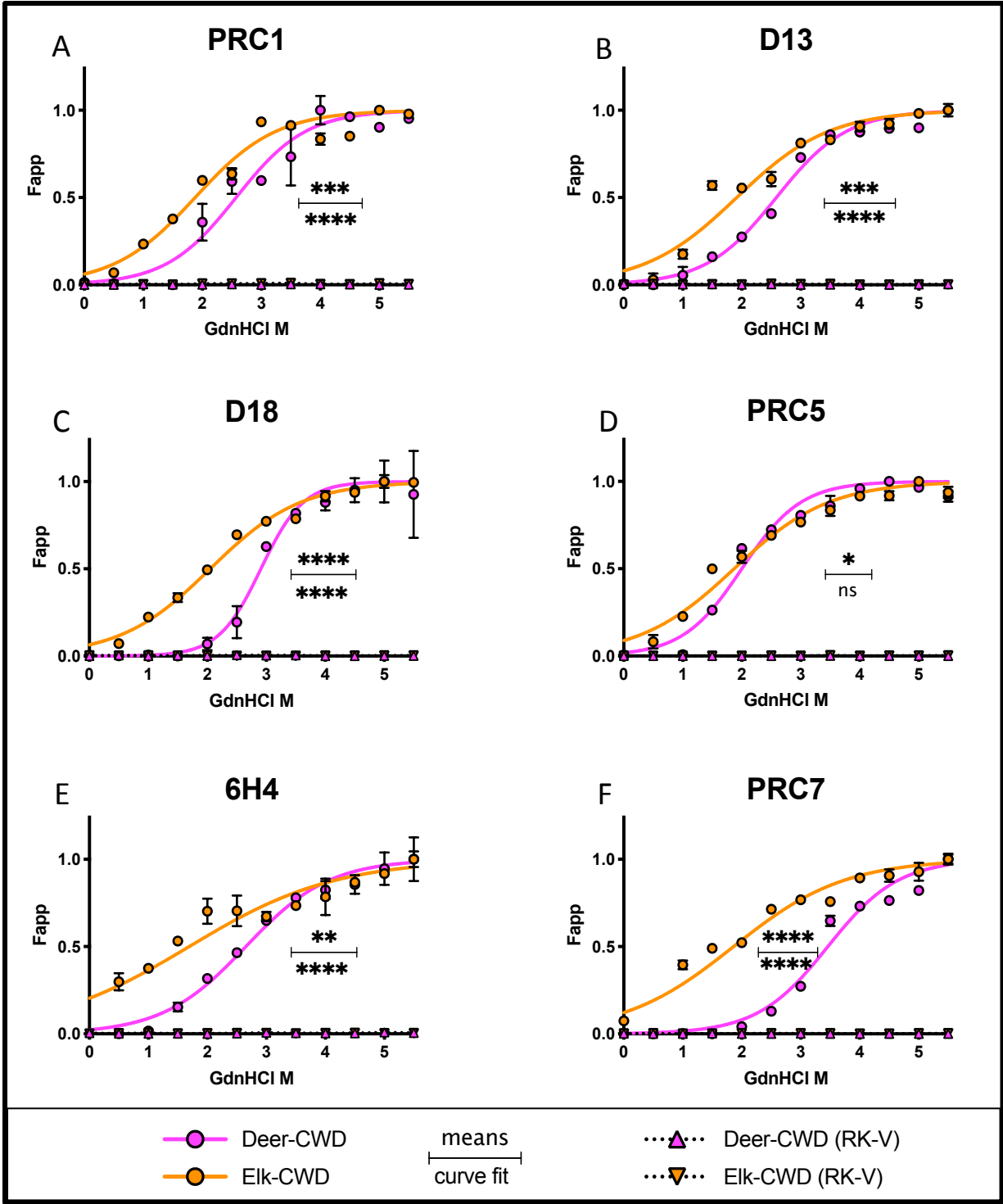


FIGURE 3.5: PrP^{Sc} epitope accessibility can be used to differentiate between Elk-CWD and Deer-CWD. The ESA validates the difference due to the different amino acid at position 226 [deer (Q), elk (E)] has on the stability of Chronic Wasting Disease (CWD). Brains (n=3) from terminally ill Tg(ElkPrP)5037^{+/-} and Tg(DeerPrP)1536^{+/-} mice infected with elk CWD isolate Bala05 were used to infect RK-Elk and RK-Deer cell lines,

respectively, along with the RK-V(vector only, PrP^C null) cell line. The resultant CWD prions were interrogated with the ESA (Figure 3.2) using anti-prion antibodies (Figure 3.1B): **(A)** PRC1 **(B)** D13 **(C)** D18 **(D)** PRC5 **(E)** 6H4 **(F)** PRC7. All antibodies showed significantly different ($p < 0.0001$) curves, by curve comparison. When means were compared via t-test, except for PRC5 ($p = ns$), RK-Elk passaged CWD to RK-Deer passaged CWD were significantly different ($p < 0.0001$) for all other antibodies tested.

F_{app}, fraction of apparent signal. The sigmoidal dose-response curve was plotted using a four parameter algorithm and nonlinear least-squares fit; with curve comparison. Error bars, SD from $n=3$ animals per group. Statistical significance: ns $p > 0.05$; * $p \leq 0.05$, ** $p \leq 0.01$; *** $p \leq 0.001$; **** $p \leq 0.0001$. Statistical differences from the GdnHCl_{1/2} values between matched, curves were calculated by curve fit parameters and via t-test (means)

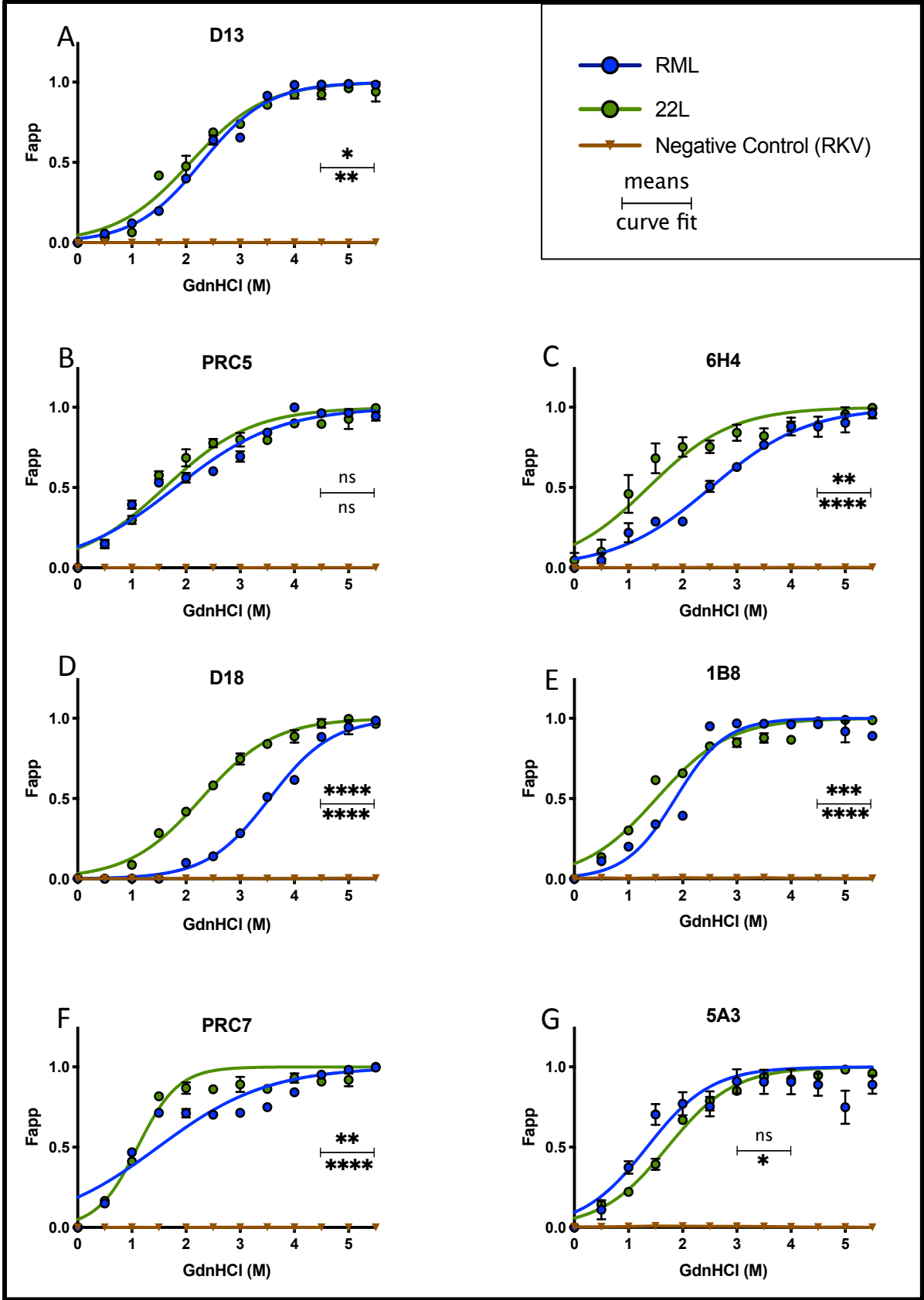


FIGURE 3.6: PrP^{Sc} epitope accessibility can be used to differentiate between classically defined murine-adapted scrapie strains (RML and 22L). Brains (n=3) from terminally ill C57Bl/6 inbred mice infected with 22L (green) and RML (blue) were used to infect the RK-Murine cell line along with the RK-V(vector only, PrP^C null) cell line (brown). The resultant murine-adapted prions were interrogated with the ESA using anti-prion antibody: **(A)** D13 **(B)** PRC5 **(C)** 6H4 **(D)** D18 **(E)** 1B8 **(F)** PRC7 and **(G)** 5A3.

F_{app}, fraction of apparent signal. The sigmoidal dose-response curve was plotted using a four parameter algorithm and nonlinear least-squares fit; with curve comparison. Error bars, SD n=3 animals per group. Statistical significance: ns p > 0.05; * p ≤ 0.05, ** p ≤ 0.01; *** p ≤ 0.001; **** p ≤ 0.0001. Statistical differences from the GdnHCl_{1/2} values between matched, curves were calculated by curve fit parameters and via t-test (means)

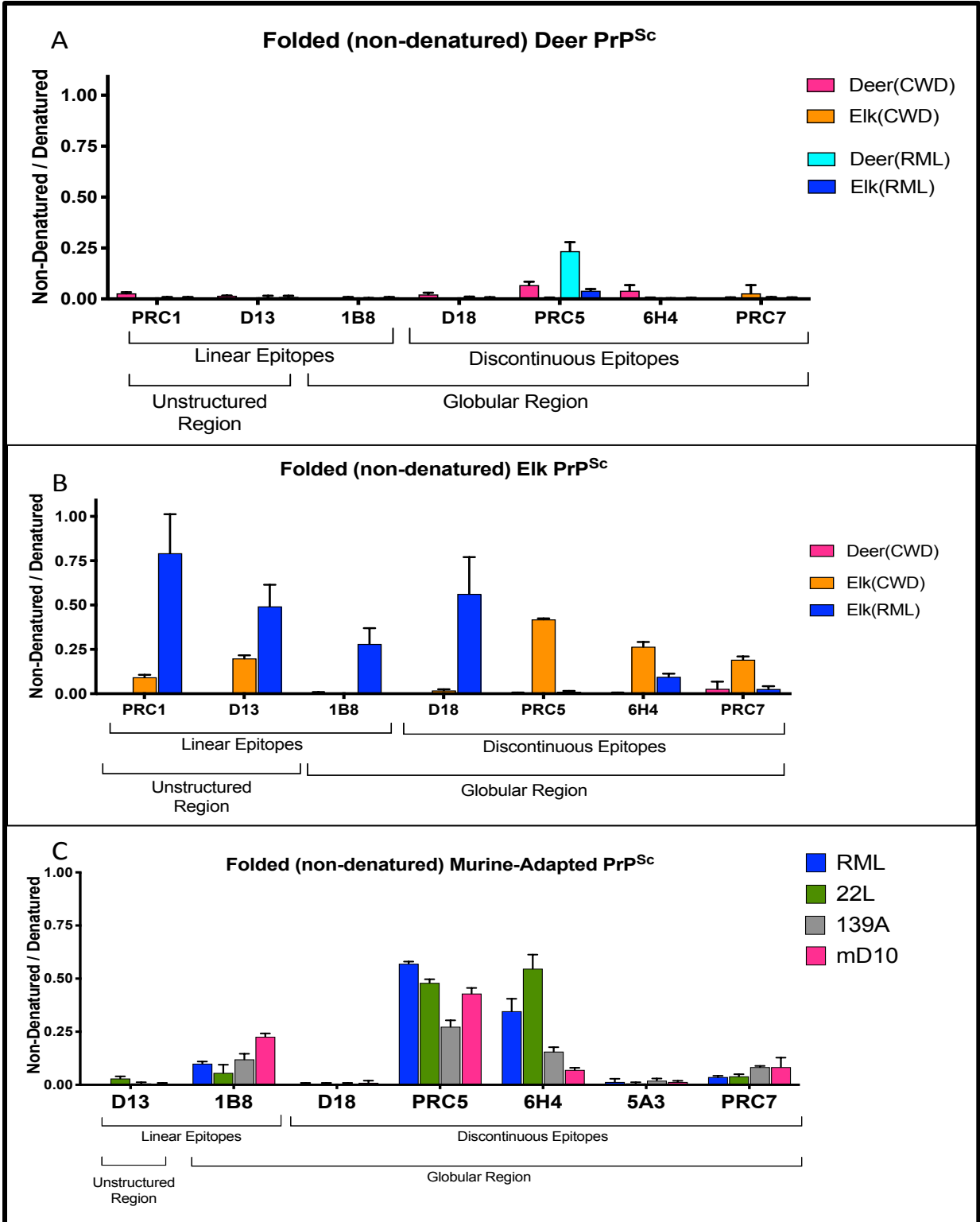


FIGURE 3.7: PK-treated, non-denatured PrP^{Sc} epitopes are accessible and create strain and host-PrP^C specific patterns. All prion strains were examined with an array of epitope-mapped antibodies (Figure 3.1B) via the ESA (Figure 3.2); however, antibody

5A3 is murine-specific and not used to detect cervid prion strains, and PRC1 is cervid-specific and not used to detect murine-adapted prion strains. **(A)** Brains (n=3) from terminally ill Tg(DeerPrP)1536^{+/-} and Tg(ElkPrP)5037^{+/-} mice infected with elk CWD isolate Bala05 were used to infect RK-Deer cell lines, respectively, along with the RK-V(vector only, PrP^C null) cell line. Brains (n=3) from terminally ill Tg(ElkPrP)5037^{+/-} and Tg(DeerPrP)1536^{+/-} mice infected with mouse-adapted RML were used to infect RK-Deer cell lines, respectively, along with the RK-V(vector only, PrP^C null) cell line. Overall, RK-Deer passaged prions were inaccessible without denaturation. **(B)** Brains (n=3) from terminally ill Tg(DeerPrP)1536^{+/-} and Tg(ElkPrP)5037^{+/-} mice infected with elk CWD isolate Bala05 were used to infect RK-Elk cell lines, respectively, along with the RK-V(vector only, PrP^C null) cell line. Brains (n=3) from terminally ill Tg(ElkPrP)5037^{+/-} and Tg(DeerPrP)1536^{+/-} mice infected with mouse-adapted RML were used to infect RK-Elk cell lines, respectively, along with the RK-V(vector only, PrP^C null) cell line. Elk-passaged prions were more accessible than deer-passaged prions and exhibit a switch of PrP^{Sc} epitope availability based on the origin of the inoculum. **(C)** Brains (n=3) from terminally ill C57Bl/6 mice infected with murine-adapted scrapie strains (RML, 22L, and 139A) and recently murine-adapted CWD strain⁸⁶ (mD10) were used to infect murine- PrP^C expressing RK13 (RK-Mouse) cells along with the RK-V (vector only, PrP^C null) cell line. PK treated, non-denatured PrP^{Sc} of murine-adapted prion strains structurally resemble PrP^C around the first α -helix but PrP^{Sc} is in a conformation where portions of the α -helix 1 are buried.

Y-axis: Ratio of non-denatured (GdnHCl 0M) signal by fully denatured (GdnHCl 5.5M) signal. X-axis: anti-prion antibodies used. Error bars SD n=3 animals per group. Statistical differences were calculated by t-test (means) of the ratio of non-denatured (GdnHCl 0M) signal by fully denatured (GdnHCl 5.5M) signal.

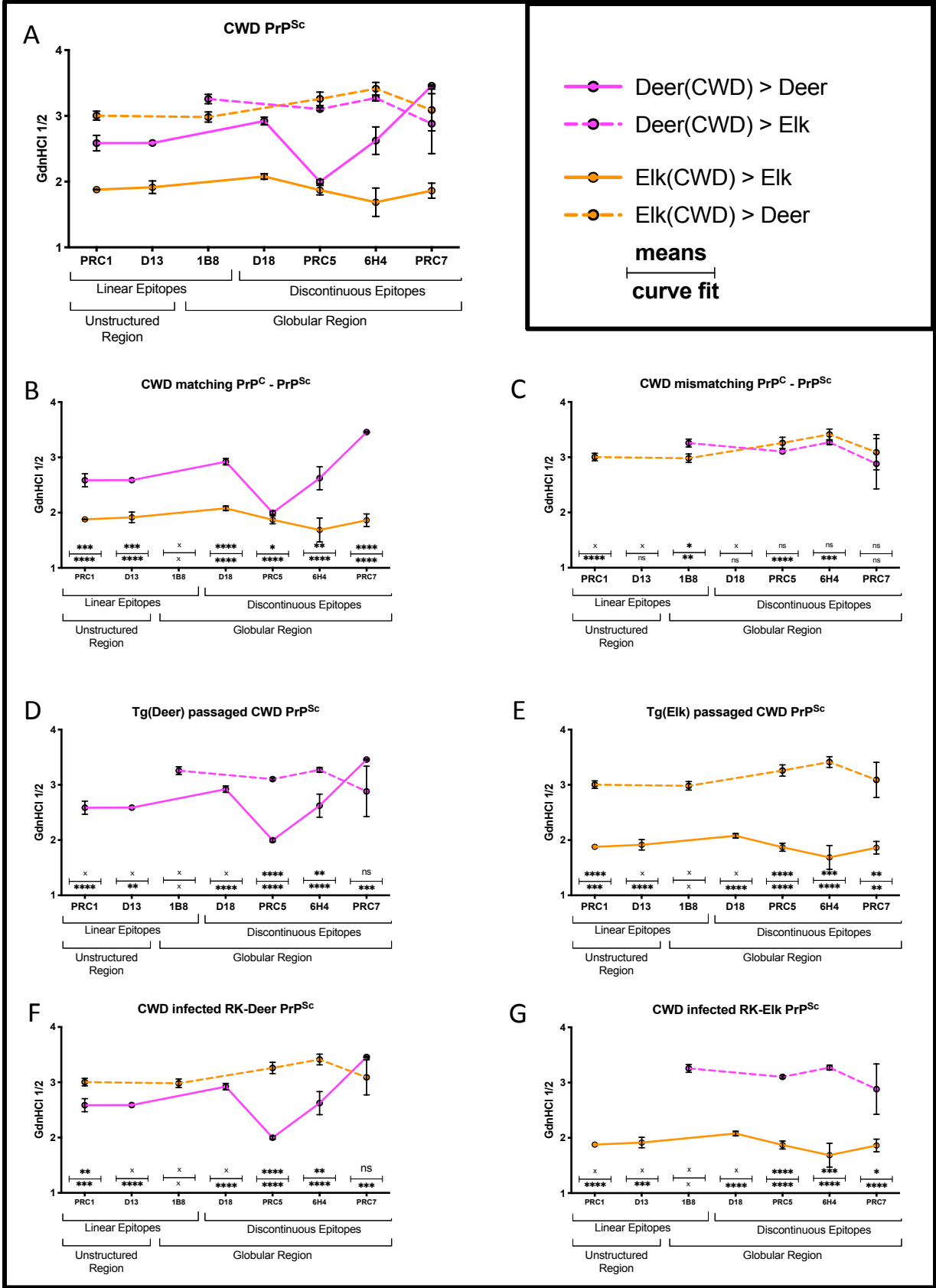


FIGURE 3.8: A single amino acid difference in the inoculum and/or the substrate make drastic differences on the tertiary shape of PrP^{Sc} The ESA validates the difference due to the different amino acid at position 226 [deer (Q), elk (E)] has on the stability of Chronic Wasting Disease (CWD). Brains (n=3) from terminally ill Tg(ElkPrP)5037^{+/-} and Tg(DeerPrP)1536^{+/-} mice infected with elk CWD isolate Bala05 were used to infect RK-Elk and RK-Deer cell lines, along with the RK-V(vector only, PrP^C null) cell line. The resultant CWD prions were interrogated with the ESA (Figure 3.2) using anti-prion antibodies (Figure 3.1B): PRC1, D13, D18, PRC5, 6H4, and PRC7. **(A)** All 4 experimental groups included to show general trends: RK-Deer passaged deer-CWD (Deer-CWD>Deer) pink solid line; RK-Deer passaged elk-CWD (Elk-CWD>Deer) orange dashed line; RK-Elk passaged deer-CWD (Deer-CWD>Elk) pink dashed line; and RK-Elk passaged elk-CWD (Elk-CWD>Elk) orange solid line. **(B)** Comparison of PrP^{Sc} GdnHCl 1/2 values where the inoculum, CWD PrP^{Sc}, matched the substrate, PrP^C: RK-Deer passaged deer-CWD and RK-Elk passaged elk-CWD. **(C)** Comparison of PrP^{Sc} GdnHCl 1/2 values where the inoculum, CWD PrP^{Sc}, is mismatched with the substrate, PrP^C: RK-Deer passaged elk-CWD and RK-Elk passaged deer-CWD. **(D)** Comparison of PrP^{Sc} GdnHCl 1/2 values where Deer-CWD was passaged into RK-Deer and RK-Elk **(E)** Comparison of PrP^{Sc} GdnHCl 1/2 values where Elk-CWD was passaged into RK-Deer and RK-Elk **(F)** Comparison of PrP^{Sc} GdnHCl 1/2 values where Deer-CWD and Elk-CWD were passaged into RK-Deer. **(G)** Comparison of PrP^{Sc} GdnHCl 1/2 values where Deer-CWD and Elk-CWD were passaged into RK-Elk.

The sigmoidal dose-response curve was plotted using a four parameter algorithm and nonlinear least-squares fit; with best fit curve comparison. Error bars, SD from n=3 animals per group. Statistical significance: ns p > 0.05; * p ≤ 0.05, ** p ≤ 0.01; *** p ≤ 0.001; **** p ≤ 0.0001. Statistical differences from the GdnHCl_{1/2} values between matched, curves were calculated by curve fit parameters and via t-test (means)

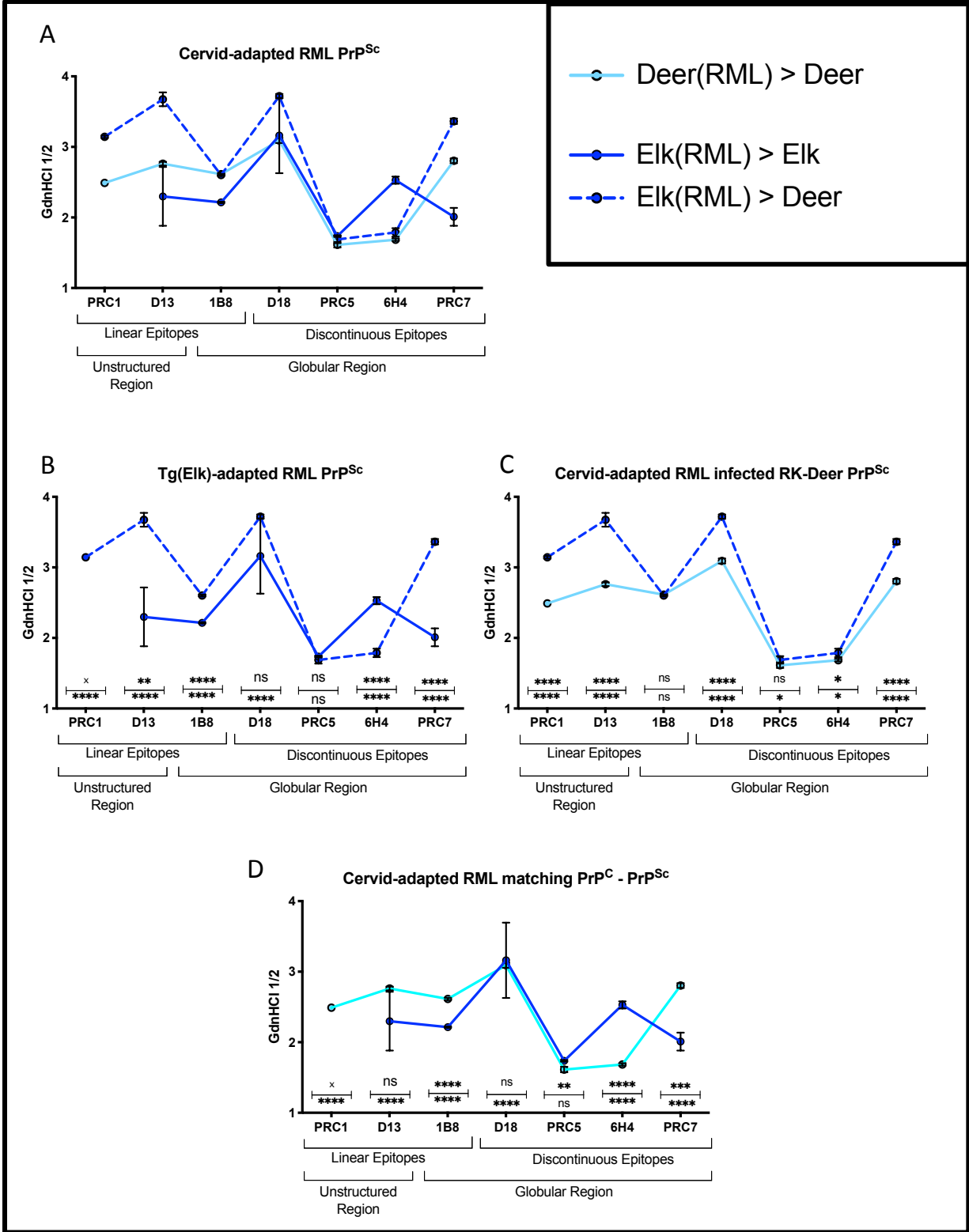


FIGURE 3.9: A single amino acid difference in the inoculum and/or the substrate can cause differences in the tertiary shape of PrP^{Sc} in newly adapted strains.

Brains (n=3) from terminally ill Tg(ElkPrP)5037^{+/-} and Tg(DeerPrP)1536^{+/-} mice infected with mouse-adapted RML were used to infect RK-Deer and RK-Elk cell lines, along with the RK-V(vector only, PrP^C null) cell line. The Deer-RML did not successfully infect RK-Elk cells. The resultant cervidized-RML prions were interrogated with the ESA (Figure 3.2) using anti-prion antibodies (Figure 3.1B): PRC1, D13, D18, PRC5, 6H4, and PRC7. **(A)** All 3 experimental groups included to show general trends: RK-Deer passaged Deer-RML (Deer-RML>Deer) light blue solid line; RK-Deer passaged Elk-RML (Elk-RML>Deer) dark blue dashed line; and RK-Elk passaged Elk-RML (Elk-RML>Elk) dark blue solid line. **(B)** Comparison of PrP^{Sc} GdnHCl^{1/2} values where Elk-RML was passaged into RK-Deer and RK-Elk **(C)** Comparison of PrP^{Sc} GdnHCl^{1/2} values where Deer-RML and Elk-RML were passaged into RK-Deer. **(D)** Comparison of PrP^{Sc} GdnHCl^{1/2} values where the inoculum, Cervidized-RML PrP^{Sc}, matched the substrate, PrP^C: RK-Deer passaged Deer-RML and RK-Elk passaged Elk-RML.

The sigmoidal dose-response curve was plotted using a four parameter algorithm and nonlinear least-squares fit; with best fit curve comparison. Error bars, SD from n=3 animals per group. Statistical significance: ns p > 0.05; * p ≤ 0.05, ** p ≤ 0.01; *** p ≤ 0.001; **** p ≤ 0.0001. Statistical differences from the GdnHCl^{1/2} values between matched, curves were calculated by curve fit parameters and via t-test (means)

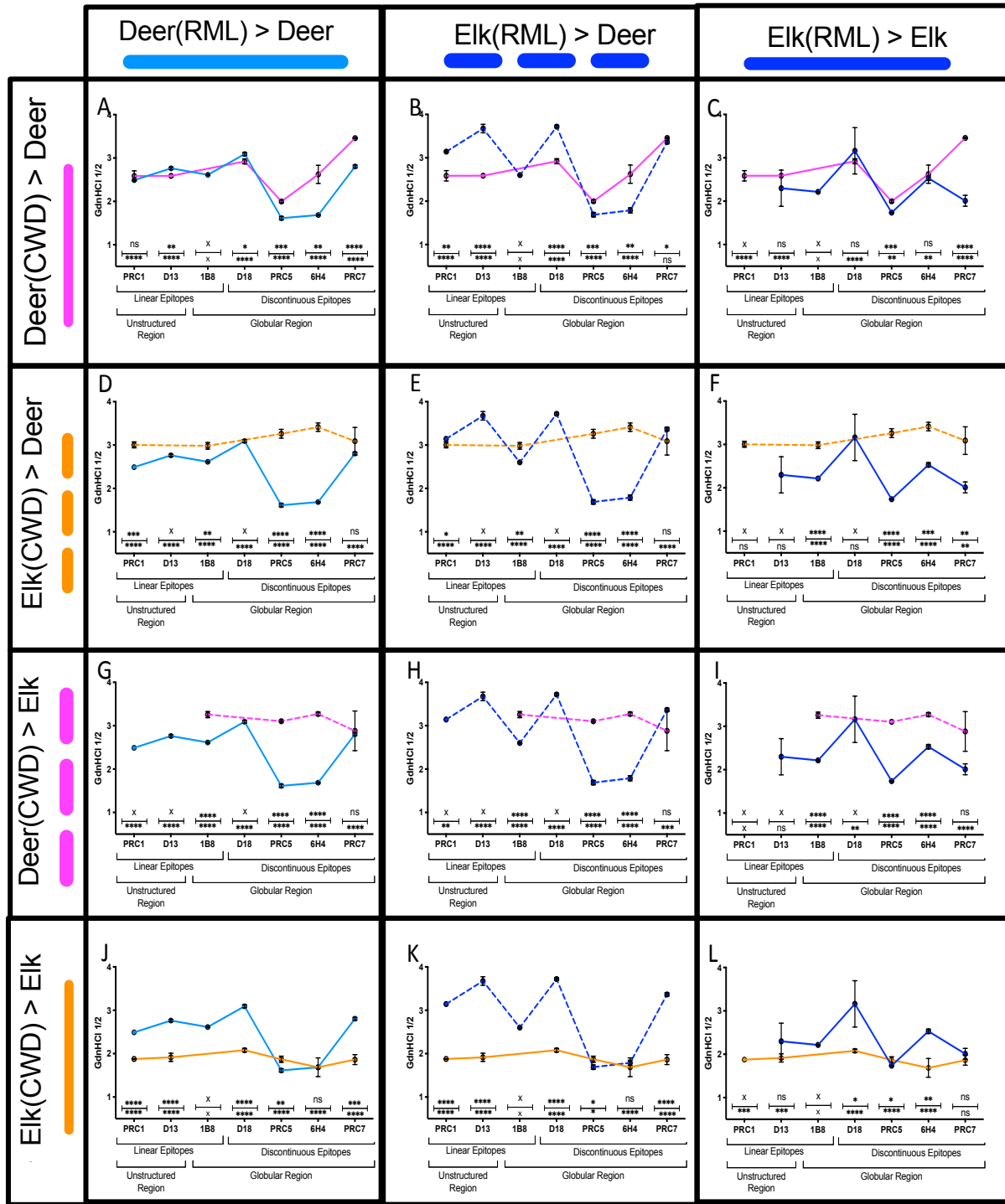


FIGURE 3.10: Species-adapted strains have different tertiary structures than those passed within their native host PrP^C. Brains (n=3) from terminally ill Tg(ElkPrP)5037^{+/-} and Tg(DeerPrP)1536^{+/-} mice infected with elk CWD isolate Bala05 were used to infect RK-Elk and RK-Deer cell lines, along with the RK-V(vector only, PrP^C null) cell line. CWD experimental groups: RK-Deer passaged deer-CWD (Deer-CWD>Deer) pink solid line; RK-Deer passaged elk-CWD (Elk-CWD>Deer) orange

dashed line; RK-Elk passaged deer-CWD (Deer-CWD>Elk) pink dashed line; and RK-Elk passaged elk-CWD (Elk-CWD>Elk) orange solid line. Brains (n=3) from terminally ill Tg(ElkPrP)5037^{+/-} and Tg(DeerPrP)1536^{+/-} mice infected with mouse-adapted RML were used to infect RK-Deer and RK-Elk cell lines, along with the RK-V(vector only, PrP^C null) cell line. The Deer-RML did not successfully infect RK-Elk cells. Cervidized RML experimental groups: RK-Deer passaged Deer-RML (Deer-RML>Deer) light blue solid line; RK-Deer passaged Elk-RML (Elk-RML>Deer) dark blue dashed line; and RK-Elk passaged Elk-RML (Elk-RML>Elk) dark blue solid line. All resultant prions were interrogated with the ESA (Figure 3.2) using anti-prion antibodies (Figure 3.1B): PRC1, D13, D18, PRC5, 6H4, and PRC7. Comparisons show Deer-CWD>Deer (**A, B, C**), Elk-CWD>Deer (**D, E, F**), Deer-CWD>Elk (**G, H, I**), Elk-CWD>Elk (**J, K, L**) with Deer-RML>Deer (**A, D, G, J**), Elk-RML>Deer (**B, E, H, K**), Elk-RML>Elk (**C, F, I, L**).

The sigmoidal dose-response curve was plotted using a four parameter algorithm and nonlinear least-squares fit; with best fit curve comparison. Error bars, SD from n=3 animals per group. Statistical significance: ns $p > 0.05$; * $p \leq 0.05$, ** $p \leq 0.01$; *** $p \leq 0.001$; **** $p \leq 0.0001$. Statistical differences from the GdnHCl_{1/2} values between matched, curves were calculated by curve fit parameters and via t-test (means)

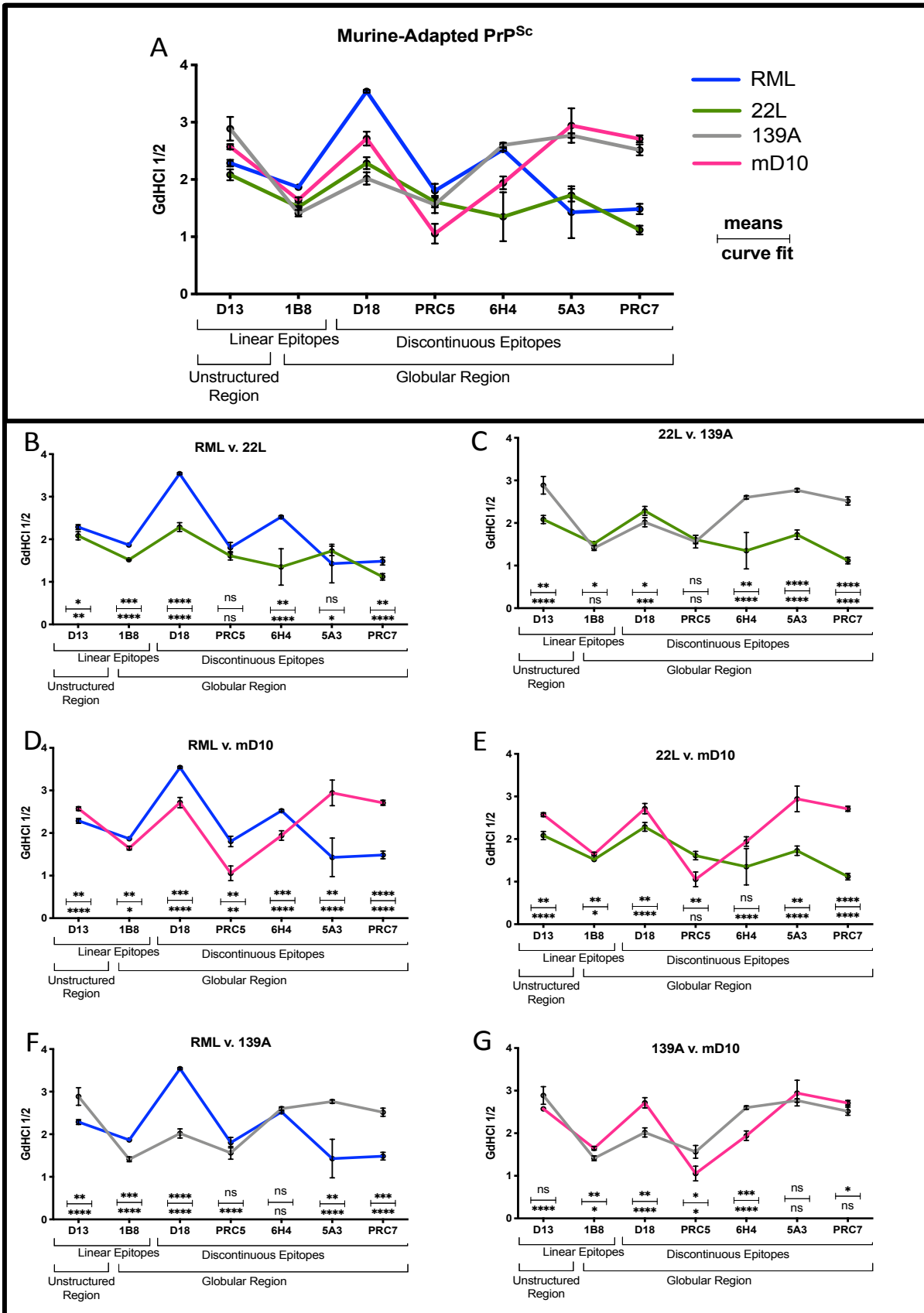


FIGURE 3.11: The tertiary structure of PrP^{Sc} is different at multiple epitopes along the molecule even in prion strains sharing the same PrP^C substrate. Brains (n=3) from terminally ill C57Bl/6 mice infected with murine-adapted scrapie strains RML (blue), 22L (green), and 139A (grey) and recently murine-adapted CWD strain⁸⁶ mD10 (pink) were used to infect murine- PrP^C expressing RK13 (RK-Mouse) cells along with the RK-V (vector only, PrP^C null) cell line. All resultant prions were interrogated with the ESA (Figure 3.2) using anti-prion antibodies (Figure 3.1B): D13, 1B8, D18, PRC5, 6H4, 5A3, and PRC7. **(A)** All murine-adapted strains are included to see the pattern: RML (blue), 22L (green), 139A (grey) and mD10 (pink); the control groups were completely negative, and left off Figure 3.11 to aid interpretability. **(B)** Comparison of RML and 22L, **(C)** Comparison of 22L and 139A, **(D)** Comparison of RML and mD10, **(E)** Comparison of 22L and mD10, **(F)** Comparison of RML and 139A, and **(G)** Comparison of 139A and mD10. Each pair allows for a different comparison of structure.

The sigmoidal dose-response curve was plotted using a four parameter algorithm and nonlinear least-squares fit; with curve comparison. Error bars, SD n=3 animals per group. Statistical significance: ns p > 0.05; * p ≤ 0.05, ** p ≤ 0.01; *** p ≤ 0.001; **** p ≤ 0.0001. Statistical differences from the GdnHCl_{1/2} values between matched, curves were calculated by curve fit parameters and via t-test (means)

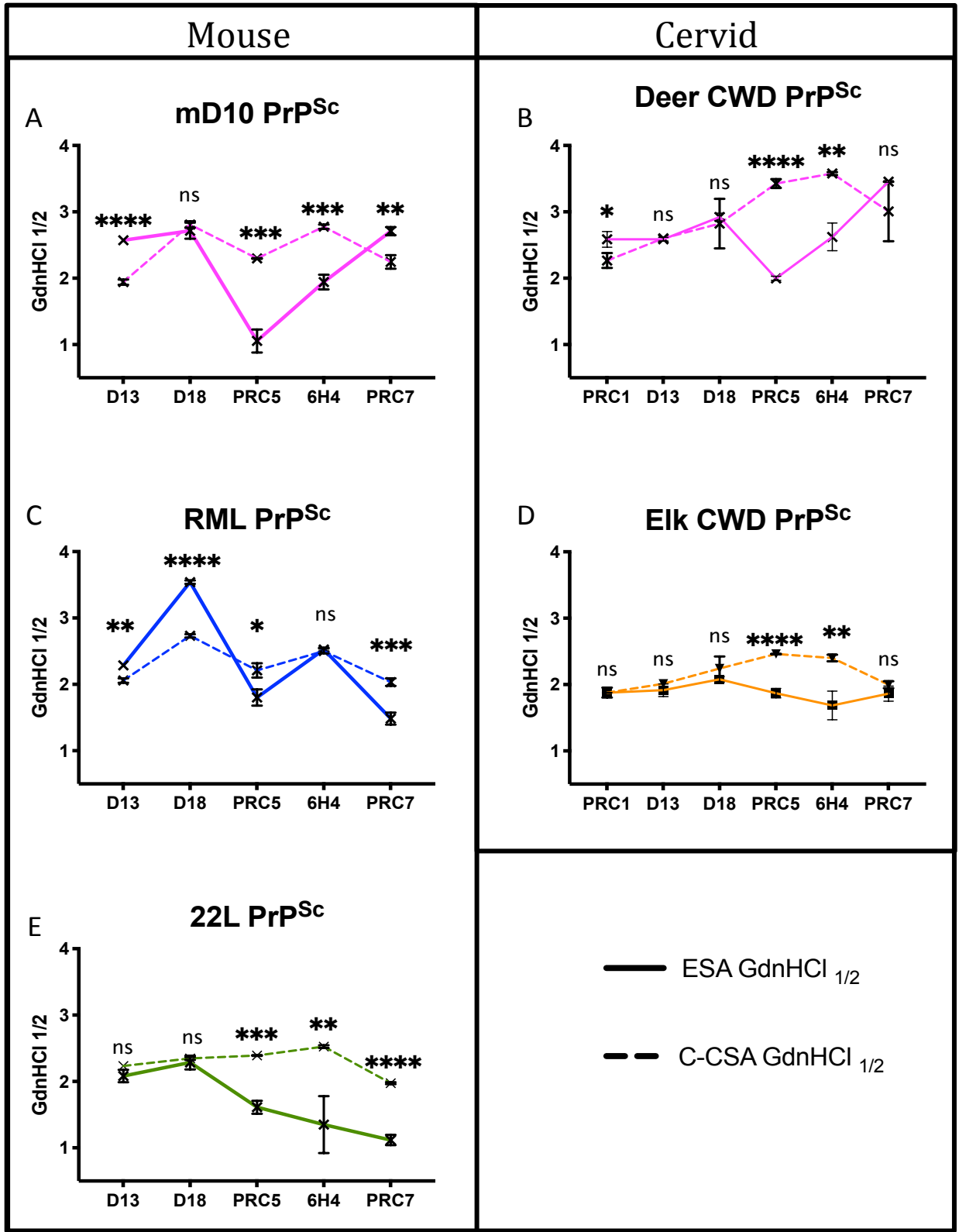


Figure 3.12: Prion resistance to protease degradation after partial denaturation (C-CSA) is not equivalent to epitope accessibility (ESA). The epitope stability assay was

created from conceptually marrying the 7-5 ELISA-CSA (Figure 3.3) and the previously developed⁸¹ prion cell-based conformational stability assay [Chapter 2]. The C-CSA derives the GdnHCl_{1/2} value from the prions relative resistance to Proteinase K after stepwise denaturation; whereas the ESA derives the GdnHCl_{1/2} value from the accessibility of an epitope after stepwise denaturation. The C-CSA GdnHCl_{1/2} values for Deer-CWD, Elk-CWD, mD10, RML, and 22L (Figure 2.5-2.8) were compared to ESA GdnHCl_{1/2} values (Figure 3.8 & 3.11). This graph compares C-CSA GdnHCl_{1/2} values (dashed line) and ESA GdnHCl_{1/2} values (solid line). Curve fits were not calculated since the curves were opposite in direction. The most dissimilar GdnHCl_{1/2} values occurred with mD10 and RML; while, Elk-CWD had the most similar GdnHCl_{1/2} values.

The sigmoidal dose-response curve was plotted using a four parameter algorithm and nonlinear least-squares fit; with curve comparison. Error bars, SD n=3 animals per group. Statistical significance: ns $p > 0.05$; * $p \leq 0.05$, ** $p \leq 0.01$; *** $p \leq 0.001$; **** $p \leq 0.0001$. Statistical differences from the GdnHCl_{1/2} values were calculated by t-test (means)

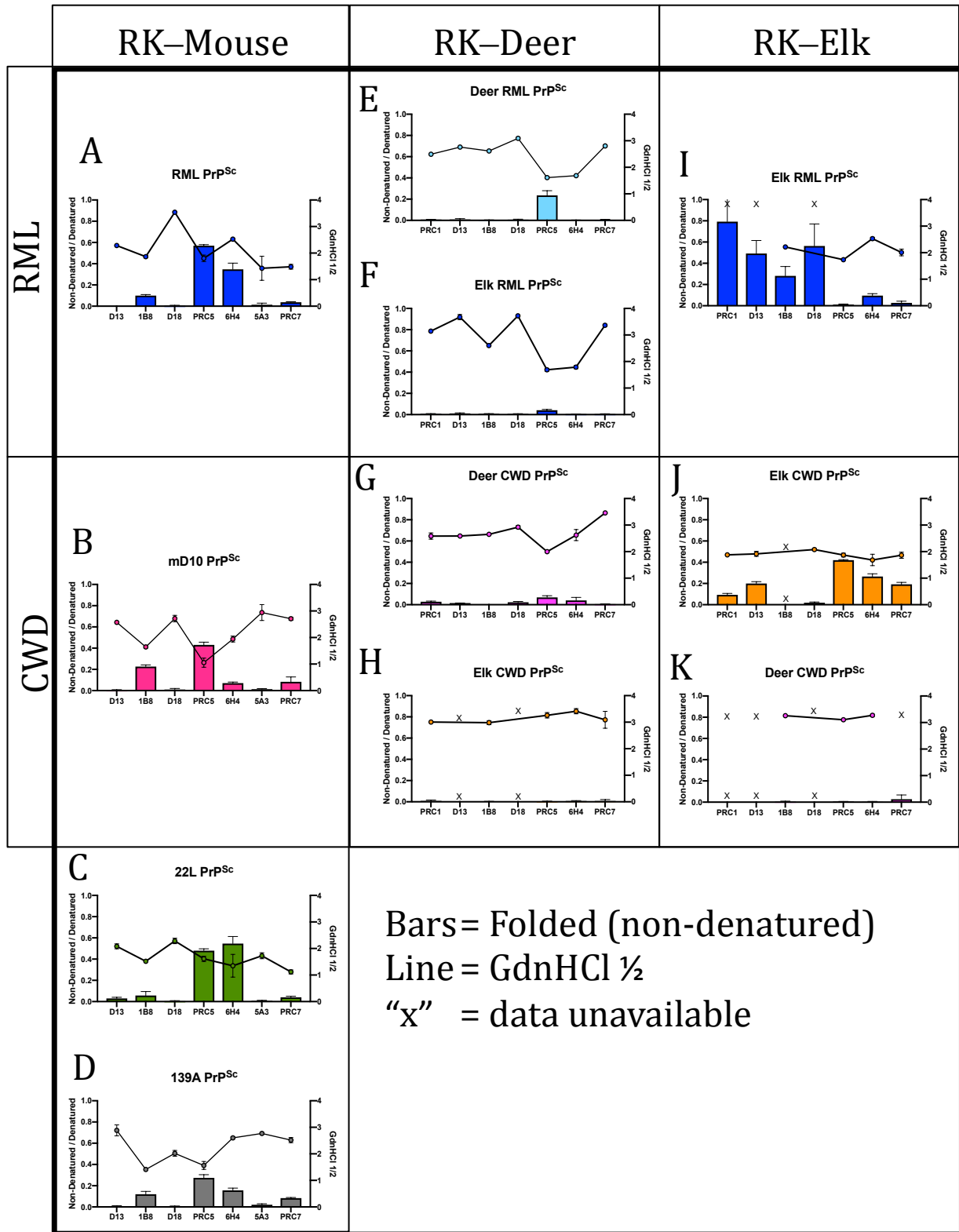


FIGURE 3.13: PrP^{Sc} epitope folded (non-denatured) and GdnHCl_{1/2} values create an individual fingerprint for each strain.

D. DISCUSSION

Ultimately, understanding the prion structure is vital to prion diseases⁸⁷, as well as other neurodegenerative disorders^{88, 89} like Alzheimer's, Parkinson's, and Huntington's. There is a link between amyloid structure and disease seen in prions, Hyp-FN protein⁹⁰, α -synuclein⁹¹, β -amyloid⁹², and other amyloidogenic diseases. The reliance on the primary sequence to dictate seeding potential is shared with other amyloidogenic proteins⁹³. As such, new techniques that capitalize on nuances of antibody epitope binding can further illuminate the complexities of PrP^{Sc} structure.

Current technological tools and the confounding complexity found in natural systems stymie research. The answer is to find novel, innovative techniques that can expand our ability to ask important questions. Consequently, the expanded C-CSA [Chapter 2], 7-5 ELISA-CSA (Figure 3.3) and ESA (Figures 3.5-3.13) represent new tools to reveal more details about prion strain structure in a facile and expedient process.

The 7-5 ELISA-CSA (Figure 3.3) represents a new tool that can be used without proteinase K. Although it is dependent on glycosylation differences, the capacity to examine PrP^{Sc} without requiring PK to ablate PrP^C is a necessary step in understanding PrP^{Sc}. This is because the term PrP^{Sc} encompasses various forms: single misfolded PrP^{Sc} monomers, small soluble PrP^{Sc} oligomers, and insoluble PrP^{Sc} amyloid fibrils⁹⁴. There is some debate in the field on whether the soluble oligomers or amyloid fibrils are the infectious fraction or toxic species of prion protein⁹⁵. As such, being able to detect the PK- sensitive but possibly toxic fraction of PrP^{Sc} is advantageous. A limitation to this technique is rooted in the antibodies used. PRC7 and PRC5 have species specific

binding, which limits the PrP^{Sc} available to examine. As such, other anti-prion antibodies have been tested in the sandwich ELISA format. The data is not included in this dissertation.

This new technique can differentiate between infected and uninfected samples, and between strains differing at one amino acid or having the same amino acid sequence. The ESA allows data to be gathered across multiple species, with multiple infectious prions, in both chronically infected and freshly infected paradigms and more importantly provides a high-throughput method to examine the prion protein at multiple epitopes (Figure 3.5-3.13). The ESA combined with an array of epitope-mapped antibodies provides a new means to differentiate prion strains in murine-adapted strains (scrapie and chronic wasting disease) and cervid prion strains (chronic wasting disease and cervidized-RML) in both deer and elk. This technique could be expanded in the future for use with other prions; i.e. scrapie (sheep/goats), CJD (humans), TME (mink), etc. Only a researcher's imagination, finances, and cell susceptibility to the chosen prion limit the possibilities inherent in the ESA.

The ESA was optimized for PK (Figure 3.4), denaturation (Figure 3.4), and anti-prion antibodies dilution (not shown). Surprisingly, the optimization rounds revealed that the ESA is capable of evaluating the folded (non-denatured) fraction of PrP^{Sc}. This folded (non-denatured) signal was prominent in murine-adapted and elk prion strains but not in deer prion strains. This may speak to overall permissibility in disease transmission and overall stability in environmental reservoirs. However, the necessity

of using PK is a limitation of this technique, as PK will degrade both PrP^C and any PrP^{Sc} that is sensitive to PK.

Overall comparisons between the GdnHCl $\frac{1}{2}$ value and curve fits of elk and deer CWD further supported previous work that the single amino acid difference between elk and deer PrP^C plays an important role in prion structure. When comparing CWD, in most cases Deer-CWD had a higher GdnHCl $\frac{1}{2}$ value than Elk-CWD. This implies that Deer-CWD is more resistant to PK degradation and its epitopes are more difficult to access than Elk-CWD. Although both Elk and Deer passaged CWD prion (Bala05) share the same initial inoculum, each ultimately produces a different disease phenotype (Table 1) dependent on the host PrP^C primary structure. The combination whether PrP^{Sc} – PrP^C contain matching amino acid sequences spawns new PrP^{Sc} structures. This will be important now that CWD is in Europe and there are camel prions. The differences and similarities between cerRML and CWD add to the concern that when adaption occurs, new prions emerge. Perhaps CWD or camel prions will make the zoonotic leap into humans and create an entirely new prion.

Similar to the 7-5 ELISA-CSA, the ESA (Figure 3.2) reveals the epitope accessibility of PrP^{Sc} under different denaturing conditions; this differs from the C-CSA [Chapter 2], which reveals PK sensitivity of PrP^C and PrP^{Sc} that has been exposed to different denaturing conditions. This was seen in Figure 3.12, prion resistance to protease degradation after partial denaturation (C-CSA) was not equivalent to epitope accessibility (ESA). Overall, Elk-CWD presented more similar C-CSA and ESA GdnHCl $\frac{1}{2}$ values than other compared prions and mouse-adapted CWD (mD10) had the least

similarities between C-CSA and ESA GdnHCl $\frac{1}{2}$ values. This could indicate that adaption drastically alters the original structure of the prion.

In summation, PrP^{Sc} epitope folded (non-denatured) and GdnHCl $\frac{1}{2}$ values create strain and host-PrP^C specific patterns, essentially creating an individual strain fingerprint (Figure 3.13). This pattern is altered by adaption into new species, i.e. RML (Figure 3.13A) into cervids (Figure 3.13E, F, I). It can also be altered by the amino acid composition of the host PrP^C substrate or the amino acid composition infectious PrP^{Sc}. Additionally, the folded (non-denatured) signal were not identical within each strain implying that the epitopes are not evenly available along a non-denatured prion. The GdnHCl $\frac{1}{2}$ values were, also, not identical within each strain implying that the prions have molecular micro-regions with discreet denaturation responses.

Using different techniques: e.g. C-CSA, 7-5 ELISA-CSA, and ESA, can further characterize the unique structure of a prion strain; data yielded from all three techniques showed similar trends with unique differences. The GdnHCl $\frac{1}{2}$ values for C-CSA, 7-5 ELISA-CSA, and ESA were not identical across the same epitopes examined, indicating that each methodology is interrogating PrP^{Sc} differently. Ideally, future prion researchers will use this data, generated by these three methodologies, to create more accurate molecular models of prion structure and better understand the subtle variation between prion strains.

BIBLIOGRAPHY

- ¹ Aguzzi, A., & O'Connor, T. (2010). Protein aggregation diseases: Pathogenicity and therapeutic perspectives. *Nature Reviews Drug Discovery*, 9(3), 237-248.
- ² Prusiner SB (1982) Novel proteinaceous infectious particles cause scrapie. *Science* 216: 136-144
- ³ Requena, J. R., & Wille, H. (2014). The structure of the infectious prion protein: experimental data and molecular models. *Prion*, 8(1), 60-66.
- ⁴ Falsig, J., Nilsson, K. P. R., Knowles, T. P., & Aguzzi, A. (2008). Chemical and biophysical insights into the propagation of prion strains. *HFSP journal*, 2(6), 332-341.
- ⁵ Tanaka, M., Collins, S. R., Toyama, B. H., & Weissman, J. S. (2006). The physical basis of how prion conformations determine strain phenotypes. *Nature*, 442(7102), 585-589.
- ⁶ Bessen, R. A., & Marsh, R. F. (1992). Biochemical and physical properties of the prion protein from two strains of the transmissible mink encephalopathy agent. *Journal of virology*, 66(4), 2096-2101.
- ⁷ Schoch G, Seeger H, Bogousslavsky J, Tolnay M, Janzer RC, et al. (2006) Analysis of prion strains by PrP^{Sc} profiling in sporadic Creutzfeldt-Jakob disease. *PLoS Med* 3(2): e14
- ⁸ Cracco, L., Notari, S., Cali, I., Sy, M. S., Chen, S. G., Cohen, M. L., & Safar, J. G. (2017). Novel strain properties distinguishing sporadic prion diseases sharing prion protein genotype and prion type. *Scientific Reports*, 7.
- ⁹ Belt, P. B., Muileman, I. H., Schreuder, B. E., Bos-de Ruijter, J., Gielkens, A. L., & Smits, M. A. (1995). Identification of five allelic variants of the sheep PrP gene and their association with natural scrapie. *Journal of General Virology*, 76(3), 509-517.
- ¹⁰ Angers, R. C., H. E. Kang, D. Napier, S. Browning, T. Seward, C. Mathiason, A. Balachandran, D. McKenzie, J. Castilla, C. Soto, J. Jewell, C. Graham, E. A. Hoover, and G. C. Telling. 2010. Prion strain mutation determined by prion protein conformational compatibility and primary structure. *Science* 328:1154-1158.
- ¹¹ Telling, G. C., Parchi, P., DeArmond, S. J., Cortelli, P., Montagna, P., Gabizon, R., & Prusiner, S. B. (1996). Evidence for the conformation of the pathologic isoform of the prion protein enciphering and propagating prion diversity. *Science*, 274(5295), 2079-2082.
- ¹² Colby, D. W., Giles, K., Legname, G., Wille, H., Baskakov, I. V., DeArmond, S. J., & Prusiner, S. B. (2009). Design and construction of diverse mammalian prion strains. *Proceedings of the National Academy of Sciences*, 106(48), 20417-20422.
- ¹³ Peretz, D., Scott, M. R., Groth, D., Williamson, R. A., Burton, D. R., Cohen, F. E., & Prusiner, S. B. (2001). Strain-specified relative conformational stability of the scrapie prion protein. *Protein Science*, 10(4), 854-863.
- ¹⁴ Collinge, J., Sidle, K. C., Meads, J., Ironside, J., & Hill, A. F. (1996). Molecular analysis of prion strain variation and the aetiology of new variant CJD. *Nature*, 383(6602), 685.
- ¹⁵ Cuillé, J. & Chelle, P. L. (1936). La maladie dite tremblante du mouton est-elle inoculable. *CR Acad Sci* 203, 1552-1554

-
- ¹⁶ Pattison, I. H., Gordon, W. S., & Millson, G. C. (1959). Experimental production of scrapie in goats. *Journal of Comparative Pathology and Therapeutics*, 69, 300-312.
- ¹⁷ Mould, D. L., Dawson, A. M., Slater, J. S., & Zlotnik, I. (1967). Relationships between chemical changes and histological damage in the brains of scrapie affected mice. *Journal of comparative pathology*, 77(4), 393IN5403-402IN6.
- ¹⁸ Kim, Y. S., Carp, R. I., Callahan, S. M., Natelli, M., & Wisniewski, H. M. (1990). Vacuolization, incubation period and survival time analyses in three mouse genotypes injected stereotactically in three brain regions with the 22L scrapie strain. *Journal of Neuropathology & Experimental Neurology*, 49(2), 106-113.
- ¹⁹ Chandler, R. (1961). Encephalopathy in mice produced by inoculation with scrapie brain material. *The Lancet*, 1(7191), 1378-1379.
- ²⁰ Marsh, R. F., Burger, D., Eckroade, R., Rhein, G. Z., & Hanson, R. P. (1969). A preliminary report on the experimental host range of the transmissible mink encephalopathy agent. *The Journal of infectious diseases*, 713-719.
- ²¹ Bruce, M. E., Will, R. G., Ironside, J. W., McConnell, I., Drummond, D., Suttie, A., & Cousens, S. (1997). Transmissions to mice indicate that 'new variant' CJD is caused by the BSE agent. *Nature*, 389(6650), 498-501.
- ²² Sigurdson, C. J., Manco, G., Schwarz, P., Liberski, P., Hoover, E. A., Hornemann, S., & Aguzzi, A. (2006). Strain fidelity of chronic wasting disease upon murine adaptation. *Journal of virology*, 80(24), 12303-12311.
- ²³ Oelschlegel, A. M., Fallahi, M., Ortiz-Umpierre, S., & Weissmann, C. (2012). The Extended Cell Panel Assay (ECPA) characterizes the relationship of RML, 79A and 139A prion strains and reveals conversion of 139A to 79A-like prions in cell culture. *Journal of virology*, JVI-00181.
- ²⁴ Zou, R. S., Fujioka, H., Guo, J. P., Xiao, X., Shimoji, M., Kong, C., & Moudjou, M. (2011). Characterization of spontaneously generated prion-like conformers in cultured cells. *Aging (Albany NY)*, 3(10), 968-984.
- ²⁵ Edgeworth, J. A., Gros, N., Alden, J., Joiner, S., Wadsworth, J. D., Linehan, J., & Collinge, J. (2010). Spontaneous generation of mammalian prions. *Proceedings of the National Academy of Sciences*, 107(32), 14402-14406.
- ²⁶ Brown, C. A., Schmidt, C., Poulter, M., Hummerich, H., Klöhn, P. C., Jat, P., & Lloyd, S. E. (2014). In vitro screen of prion disease susceptibility genes using the scrapie cell assay. *Human molecular genetics*, 23(19), 5102-5108.
- ²⁷ Marbiah, M. M., Harvey, A., West, B. T., Louzolo, A., Banerjee, P., Alden, J., & Bloom, G. S. (2014). Identification of a gene regulatory network associated with prion replication. *The EMBO journal*, e201387150.
- ²⁸ Ramljak, S., Asif, A. R., Armstrong, V. W., Wrede, A., Groschup, M. H., Buschmann, A., & Zerr, I. (2008). Physiological role of the cellular prion protein (PrP^c): protein profiling study in two cell culture systems. *Journal of proteome research*, 7(7), 2681-2695.
- ²⁹ Molloy, B., & McMahon, H. E. (2014). A cell-biased effect of estrogen in prion infection. *Journal of virology*, 88(2), 1342-1353.
- ³⁰ Pulford, B., Reim, N., Bell, A., Veatch, J., Forster, G., Bender, H., & Wyckoff, A. C. (2010). Liposome-siRNA-peptide complexes cross the blood-brain barrier and significantly decrease PrP^C on neuronal cells and PrP^{RES} in infected cell cultures. *PloS one*, 5(6), e11085.

-
- ³¹ Nishizawa, K., Oguma, A., Kawata, M., Sakasegawa, Y., Teruya, K., & Doh-ura, K. (2014). Efficacy and mechanism of a glycoside compound inhibiting abnormal prion protein formation in prion-infected cells: implications of interferon and phosphodiesterase 4D-interacting protein. *Journal of virology*, 88(8), 4083-4099.
- ³² Lu D, et al. (2013) Biaryl amides and hydrazones as therapeutics for prion disease in transgenic mice. *J Pharmacol Exp Ther* 347(2):325–338.
- ³³ Li Z, et al. (2013) Discovery and preliminary SAR of arylpiperazines as novel, brain-penetrant antiprion compounds. *ACS Med Chem Letters* 4(4):397–401.
- ³⁴ Kimata A, et al. (2007) New series of antiprion compounds: Pyrazolone derivatives have the potent activity of inhibiting protease-resistant prion protein accumulation. *J Med Chem* 50(21):5053–5056.
- ³⁵ Geissen M, et al. (2011) From high-throughput cell culture screening to mouse model: Identification of new inhibitor classes against prion disease. *ChemMedChem* 6(10): 1928–1937.
- ³⁶ Ghaemmaghami S, May BC, Renslo AR, Prusiner SB (2010) Discovery of 2-amino- thiazoles as potent antiprion compounds. *J Virol* 84(7):3408–3412.
- ³⁷ Bate, C., Salmona, M., Diomede, L., & Williams, A. (2004). Squalastatin cures prion-infected neurons and protects against prion neurotoxicity. *Journal of Biological Chemistry*, 279(15), 14983-14990.
- ³⁸ Kocisko, D. A., & Caughey, B. (2006). Searching for Anti-Prion Compounds: Cell-Based High-Throughput In Vitro Assays and Animal Testing Strategies. *Methods in enzymology*, 412, 223-234.
- ³⁹ Li, J., Browning, S., Mahal, S. P., Oelschlegel, A. M., & Weissmann, C. (2010). Darwinian evolution of prions in cell culture. *Science*, 327(5967), 869-872.
- ⁴⁰ Christofinis, G. J., & Beale, A. J. (1968). Some biological characters of cell lines derived from normal rabbit kidney. *The Journal of Pathology*, 95(2), 377-381.
- ⁴¹ Bian, J., Napier, D., Khaychuck, V., Angers, R., Graham, C., & Telling, G. (2010). Cell-based quantification of chronic wasting disease prions. *Journal of virology*, 84(16), 8322-8326.
- ⁴² Khaychuk, V. (2012). Prion Characterization Using Cell Based Approaches. Doctoral Dissertation, University of Kentucky
- ⁴³ Arellano-Anaya, Z. E., Savistchenko, J., Mathey, J., Huor, A., Lacroux, C., Andréoletti, O., & Vilette, D. (2011). A simple, versatile and sensitive cell-based assay for prions from various species. *PLoS One*, 6(5), e20563.
- ⁴⁴ Leblanc, P., S. Alais, I. Porto-Carreiro, S. Lehmann, J. Grassi, G. Raposo, and J. L. Darlix. 2006. Retrovirus infection strongly enhances scrapie infectivity release in cell culture. *EMBO J.* 25:2674–2685.
- ⁴⁵ Bian, J., Napier, D., Khaychuck, V., Angers, R., Graham, C., & Telling, G. (2010). Cell-based quantification of chronic wasting disease prions. *Journal of virology*, 84(16), 8322-8326.
- ⁴⁶ Kocisko, D. A., & Caughey, B. (2006). Searching for Anti-Prion Compounds: Cell-Based High-Throughput In Vitro Assays and Animal Testing Strategies. *Methods in enzymology*, 412, 223-234.

-
- ⁴⁷ Korth, C., May, B. C., Cohen, F. E., & Prusiner, S. B. (2001). Acridine and phenothiazine derivatives as pharmacotherapeutics for prion disease. *Proceedings of the National Academy of Sciences*, *98*(17), 9836-9841.
- ⁴⁸ Oelschlegel, A. M., Fallahi, M., Ortiz-Umpierre, S., & Weissmann, C. (2012). The Extended Cell Panel Assay (ECPA) characterizes the relationship of RML, 79A and 139A prion strains and reveals conversion of 139A to 79A-like prions in cell culture. *Journal of virology*, JVI-00181.
- ⁴⁹ Pace, C. N., Fu, H., Fryar, K., Landua, J., Trevino, S. R., Schell, D., & Sevcik, J. (2014). Contribution of hydrogen bonds to protein stability. *Protein Science*, *23*(5), 652-661.
- ⁵⁰ Goldberg, M. E., Rudolph, R., & Jaenicke, R. (1991). A kinetic study of the competition between renaturation and aggregation during the refolding of denatured-reduced egg white lysozyme. *Biochemistry*, *30*(11), 2790-2797.
- ⁵¹ Ohkuri, T., Nagatomo, S., Oda, K., So, T., Imoto, T., & Ueda, T. (2010). A protein's conformational stability is an immunologically dominant factor: evidence that free-energy barriers for protein unfolding limit the immunogenicity of foreign proteins. *The Journal of Immunology*, *185*(7), 4199-4205.
- ⁵² Huang, K. S., Bayley, H., Liao, M. J., London, E., & Khorana, H. G. (1981). Refolding of an integral membrane protein. Denaturation, renaturation, and reconstitution of intact bacteriorhodopsin and two proteolytic fragments. *Journal of Biological Chemistry*, *256*(8), 3802-3809.
- ⁵³ Swietnicki, W., Petersen, R. B., Gambetti, P., & Surewicz, W. K. (1998). Familial mutations and the thermodynamic stability of the recombinant human prion protein. *Journal of Biological Chemistry*, *273*(47), 31048-31052.
- ⁵⁴ Yeh, V., Broering, J. M., Romanyuk, A., Chen, B., Chernoff, Y. O., & Bommarius, A. S. (2010). The Hofmeister effect on amyloid formation using yeast prion protein. *Protein Science*, *19*(1), 47-56.
- ⁵⁵ O'Brien, E. P., Dima, R. I., Brooks, B., & Thirumalai, D. (2007). Interactions between hydrophobic and ionic solutes in aqueous guanidinium chloride and urea solutions: lessons for protein denaturation mechanism. *Journal of the American Chemical Society*, *129*(23), 7346-7353.
- ⁵⁶ De Simone, A., Dodson, G. G., Verma, C. S., Zagari, A., & Fraternali, F. (2005). Prion and water: tight and dynamical hydration sites have a key role in structural stability. *Proceedings of the National Academy of Sciences of the United States of America*, *102*(21), 7535-7540.
- ⁵⁷ Hatefi, Y., & Hanstein, W. G. (1969). Solubilization of particulate proteins and nonelectrolytes by chaotropic agents. *Proceedings of the National Academy of Sciences*, *62*(4), 1129-1136.
- ⁵⁸ Salvi, G., De Los Rios, P., & Vendruscolo, M. (2005). Effective interactions between chaotropic agents and proteins. *Proteins: Structure, Function, and Bioinformatics*, *61*(3), 492-499.
- ⁵⁹ Sawyer, W. H., & Puckridge, J. (1973). The dissociation of proteins by chaotropic salts. *Journal of Biological Chemistry*, *248*(24), 8429-8433.
- ⁶⁰ Saijo E, Hughson AG, Raymond GJ, Suzuki A, Horiuchi M, Caughey B. 2016. PrPSc-specific antibody reveals C-terminal conformational differences between prion strains. *J Virol* 90:4905-4913.

-
- ⁶¹ Safar, J., Wille, H., Itri, V., Groth, D., Serban, H., Torchia, M., & Prusiner, S. B. (1998). Eight prion strains have PrP Sc molecules with different conformations. *Nature medicine*, 4(10), 1157.
- ⁶² Peretz, D., Scott, M. R., Groth, D., Williamson, R. A., Burton, D. R., Cohen, F. E., & Prusiner, S. B. (2001). Strain-specified relative conformational stability of the scrapie prion protein. *Protein Science*, 10(4), 854-863.
- ⁶³ Novitskaya, V., Makarava, N., Bellon, A., Bocharova, O. V., Bronstein, I. B., Williamson, R. A., & Baskakov, I. V. (2006). Probing the conformation of the prion protein within a single amyloid fibril using a novel immunoconformational assay. *Journal of Biological Chemistry*, 281(22), 15536-15545.
- ⁶⁴ Kunik, V., Peters, B., & Ofra, Y. (2012). Structural consensus among antibodies defines the antigen binding site. *PLoS Comput Biol*, 8(2), e1002388.
- ⁶⁵ Scarabelli, G., Morra, G., & Colombo, G. (2010). Predicting interaction sites from the energetics of isolated proteins: a new approach to epitope mapping. *Biophysical journal*, 98(9), 1966-1975.
- ⁶⁶ Stockmann, A., Hess, S., Declerck, P., Timpl, R., & Preissner, K. T. (1993). Multimeric vitronectin. Identification and characterization of conformation-dependent self-association of the adhesive protein. *Journal of Biological Chemistry*, 268(30), 22874-22882.
- ⁶⁷ Amit, A. G., Mariuzza, R. A., Phillips, S. E. V., & Poljak, R. J. (1986). Three-dimensional structure of an antigen-antibody complex at 2.8 Å resolution. *Science*, 233, 747-754.
- ⁶⁸ Schmidt, M. L., Murray, J., Lee, V. M., Hill, W. D., Wertkin, A., & Trojanowski, J. Q. (1991). Epitope map of neurofilament protein domains in cortical and peripheral nervous system Lewy bodies. *The American journal of pathology*, 139(1), 53.
- ⁶⁹ McCutcheon S, Langeveld JPM, Tan BC, Gill AC, de Wolf C, et al. (2014) Prion Protein-Specific Antibodies That Detect Multiple TSE Agents with High Sensitivity. *PLoS ONE* 9(3)
- ⁷⁰ Williamson, R. A., Peretz, D., Smorodinsky, N., Bastidas, R., Serban, H., Mehlhorn, I., & Burton, D. R. (1996). Circumventing tolerance to generate autologous monoclonal antibodies to the prion protein. *Proceedings of the national Academy of Sciences*, 93(14), 7279-7282.
- ⁷¹ Cordes, H., Bergström, A. L., Ohm, J., Laursen, H., & Heegaard, P. M. (2008). Characterisation of new monoclonal antibodies reacting with prions from both human and animal brain tissues. *Journal of immunological methods*, 337(2), 106-120.
- ⁷² Yuan, F. F., Biffin, S., Brazier, M. W., Suarez, M., Cappai, R., Hill, A. F., & Geczy, A. F. (2005). Detection of prion epitopes on PrP^C and PrP^{Sc} of transmissible spongiform encephalopathies using specific monoclonal antibodies to PrP. *Immunology and cell biology*, 83(6), 632-637.
- ⁷³ Moudjou, M., Treguer, E., Rezaei, H., Sabuncu, E., Neuendorf, E., Groschup, M. H., & Laude, H. (2004). Glycan-controlled epitopes of prion protein include a major determinant of susceptibility to sheep scrapie. *Journal of virology*, 78(17), 9270-9276.
- ⁷⁴ Brannstrom K, Lindhagen-Persson M, Gharibyan AL, Iakovleva I, Vestling M, et al. (2014) A Generic Method for Design of Oligomer-Specific Antibodies. *PLoS ONE* 9(3)

-
- ⁷⁵ Polymenidou, M., Moos, R., Scott, M., Sigurdson, C., Shi, Y. Z., Yajima, B., & Bellon, A. (2008). The POM monoclonals: a comprehensive set of antibodies to non-overlapping prion protein epitopes. *PLoS One*, 3(12), e3872.
- ⁷⁶ Doolan, K. M., & Colby, D. W. (2015). Conformation-dependent epitopes recognized by prion protein antibodies probed using mutational scanning and deep sequencing. *Journal of molecular biology*, 427(2), 328-340.
- ⁷⁷ Williamson, R. A., Peretz, D., Pinilla, C., Ball, H., Bastidas, R. B., Rozenshteyn, R., & Burton, D. R. (1998). Mapping the prion protein using recombinant antibodies. *Journal of Virology*, 72(11), 9413-9418.
- ⁷⁸ Pan, T., Li, R., Kang, S. C., Wong, B. S., Wisniewski, T., & Sy, M. S. (2004). Epitope scanning reveals gain and loss of strain specific antibody binding epitopes associated with the conversion of normal cellular prion to scrapie prion. *Journal of neurochemistry*, 90(5), 1205-1217.
- ⁷⁹ Kang, H. E., Weng, C. C., Saijo, E., Saylor, V., Bian, J., Kim, S., & Telling, G. C. (2012). Characterization of conformation-dependent prion protein epitopes. *Journal of Biological Chemistry*, 287(44), 37219-37232.
- ⁸⁰ Stanker, L. H., Serban, A. V., Cleveland, E., Hnasko, R., Lemus, A., Safar, J., & Prusiner, S. B. (2010). Conformation-dependent high-affinity monoclonal antibodies to prion proteins. *The Journal of Immunology*, 185(1), 729-737.
- ⁸¹ Bian, J., Kang, H. E., & Telling, G. C. (2014). Quinacrine promotes replication and conformational mutation of chronic wasting disease prions. *Proceedings of the National Academy of Sciences*, 111(16), 6028-6033.
- ⁸² Kang, H. E., Weng, C. C., Saijo, E., Saylor, V., Bian, J., Kim, S., Ramos, L., Angers, R., Langenfeld, K., Khaychuk, V., & Calvi, C. (2012). Characterization of conformation-dependent prion protein epitopes. *Journal of Biological Chemistry*, jbc-M112.
- ⁸³ Bian, J., Napier, D., Khaychuck, V., Angers, R., Graham, C., & Telling, G. (2010). Cell-based quantification of chronic wasting disease prions. *Journal of virology*, 84(16), 8322-8326.
- ⁸⁴ Khaychuk, V. (2012). Prion Characterization Using Cell Based Approaches. Doctoral Dissertation, University of Kentucky
- ⁸⁵ Doolan, K. M., & Colby, D. W. (2015). Conformation-dependent epitopes recognized by prion protein antibodies probed using mutational scanning and deep sequencing. *Journal of molecular biology*, 427(2), 328-340.
- ⁸⁶ Reid, C. M. (2014). *Prion strain adaptation: breaking and building species barriers* (Doctoral dissertation, Colorado State University. Libraries).
- ⁸⁷ Gajdusek, D. C. (1972). Spongiform virus encephalopathies. *Journal of Clinical Pathology. Supplement (Royal College of Pathologists)*, 6, 78.
- ⁸⁸ Soto, C., Estrada, L., & Castilla, J. (2006). Amyloids, prions and the inherent infectious nature of misfolded protein aggregates. *Trends in Biochemical Sciences*, 31(3), 150-155.
- ⁸⁹ Soto, C. (2012). Transmissible proteins: Expanding the prion heresy. *Cell*, 149(5), 968-977.

-
- ⁹⁰ Campioni, S., Mannini, B., Zampagni, M., Pensalfini, A., Parrini, C., Evangelisti, E., & Chiti, F. (2010). A causative link between the structure of aberrant protein oligomers and their toxicity. *Nature chemical biology*, 6(2), 140.
- ⁹¹ Cremades, N., Cohen, S. I., Deas, E., Abramov, A. Y., Chen, A. Y., Orte, A., & Bertocchini, C. W. (2012). Direct observation of the interconversion of normal and toxic forms of α -synuclein. *Cell*, 149(5), 1048-1059.
- ⁹² Bernstein, S. L., Dupuis, N. F., Lazo, N. D., Wyttenbach, T., Condrón, M. M., Bitan, G., & Bowers, M. T. (2009). Amyloid- β protein oligomerization and the importance of tetramers and dodecamers in the aetiology of Alzheimer's disease. *Nature chemistry*, 1(4), 326-331.
- ⁹³ Krebs, M. R., Morozova-Roche, L. A., Daniel, K., Robinson, C. V., & Dobson, C. M. (2004). Observation of sequence specificity in the seeding of protein amyloid fibrils. *Protein Science*, 13(7), 1933-1938.
- ⁹⁴ Come, J. H., Fraser, P. E., & Lansbury, P. T. (1993). A kinetic model for amyloid formation in the prion diseases: importance of seeding. *Proceedings of the National Academy of Sciences*, 90(13), 5959-5963.
- ⁹⁵ Sandberg, M. K., Al-Doujaily, H., Sharps, B., Clarke, A. R., & Collinge, J. (2011). Prion propagation and toxicity in vivo occur in two distinct mechanistic phases. *Nature*, 470(7335), 540-542.

CHAPTER 4 - MONITORING PRION STRAIN EVOLUTION

A. INTRODUCTION

One fundamental aspect of biology is evolution; species, environments, and the world around us are in a constant state of growth and change. This constant must, therefore, apply to prion diseases. Prion diseases are irreversible, lethal, neurodegenerative diseases that originate from the corruption of the cellular prion protein (Pr^{PC}) into a pathogenic misfolded form (Pr^{Sc})^{1, 2, 3}. The existence of prion strains⁴ (multiple misfolded conformations of the prion protein) of gives rise to further complexities, i.e. becomes a confounding issue, in the structural understanding of Pr^{Sc}.

Although prion diseases depend on protein-templated misfolding and not informational nucleic acids to propagate disease, genetic variations (mutations and polymorphisms) in the prion protein gene can alter the amino acid composition of the mature protein. Single amino acid changes to the prion protein can have intense impact on transmission and susceptibility⁵; e.g. the difference amino acid at position 226 [deer (Q), elk (E)] has profound effects on the presentation of Chronic Wasting Disease⁶. Genetic mutations can predispose the prion protein to misfold and spontaneously cause disease (e.g. familial Creutzfeldt-Jakob Disease and Fatal Familial Insomnia⁷). The conventional genetic-based strain definition that is applied to viruses, bacteria, and fungi is insufficient to define prion strains. Prion strains defy genetic-based strain differentiation because prions containing the same amino acid sequence can produce different disease phenotypes. Instead, a prion strain is operationally defined as

infectious prion protein particles with a specific tertiary conformation that produces a specific phenotype^{8, 9, 10} based on the ability to be stably propagated, fidelity to specific neuropathology (e.g. vacuolation, reactive astrocyte gliosis, and amyloid deposition), disease length, and molecular characteristics (i.e. glycosylation profile, molecular weight of PK-resistant PrP^{Sc}, resistance to denaturation, etc.).

The primary structure of the prion protein has direct consequences on transmission¹¹, especially across the species barrier^{12, 13}. Specifically, the species barrier relates to the ability for PrP^{Sc} (containing the amino acid sequence of one species) to convert the PrP^C of a different species into the misfolded conformer¹⁴. This barrier has served, thus far, as an obstacle to zoonotic events with most known animal prions¹⁵. The only verified example of humans contracting an animal prion disease was the appearance of a new strain of Creutzfeldt-Jakob (vCJD) after exposure to BSE infected cattle¹⁶. The concern for future zoonotic events with other prion strains remains a prevailing issue in the prion field.

Propagation of specific diseases via subtle variations in tertiary folding is complex, and has led to the quasi-species paradigm of the conformational selection model¹⁷. This model tries to reconcile why a copious possible prion protein conformational structures exist; yet, a specific strain can be both faithfully propagated via bioassay (same species) and produce a completely different adaptive disease in a new species. The selection model proposes that there are quasi-species (different tertiary conformers of the same primary amino acid sequence) and the interaction between PrP^{Sc} and PrP^C structures selects a specific PrP^{Sc} conformation to be

propagated. Strain diversity undergoes strain-dependent or species-dependent selection that resolves a preferred PrP^{Sc} conformation¹⁸. Prion strains propagate via specific tertiary misfolded form of PrP^{Sc}. As such, prion protein evolution can cause changes in the tertiary structure of PrP^{Sc} or drive selection pressures that choose a specific PrP^{Sc} isoform from the available quasi-species. Selection pressures can come from mutations in PRNP (the gene encoding the PrP^C protein), or environmental stressors. Selection pressures in prion cell culture models can cause, also, cause prion structural evolution. Traditionally, cell culture prion evolution in one of two ways: (1) creation of cell lines containing a variety of PrP^C amino acid mutations, and then tested the permissibility to prion infection, and ability to maintain prion infection (2) drug-induced prion evolution.

Prion cell culture models represented a new way to address questions about prion structure and characterize strains. Cell culture models became the next frontier with the advent of scrapie cell assay¹⁹, i.e. the first highly sensitive, reliable method to examine prion titre in cell culture. However, the scrapie cell assay had limited applications²⁰ due to a small subset of cell types²¹ and laboratory-generated strains²². The rabbit kidney epithelial²³ (RK13) cell culture model vastly expanded the species and prion strains that could be examined and allowed for the creation of cell lines that perpetually propagate prion infection (i.e. chronically infected cell lines); as such it was a significant advancement in the prion field^{24, 25, 26}. RK13 cells do not endogenously express PrP^C²⁷ and rabbits are relatively immune to prion disorders^{28, 29, 30, 31}. RK13 cells transfected^{32, 33} to stably to express a pIRESpuro3 vector containing the PrP^C gene of

choice³⁴ and pcDNA3-gag expressing HIV-1 GAG precursor protein to enhance the release of PrP^C³⁵ create a cornucopia of available cellular tools (e.g. prion titre³², drug screening^{36, 37}, strain differentiation³⁸, etc.). This model provides advantages over cell-free systems (Protein Misfolding Cyclic Amplification^{39, 40} and Real Time-Quaking Induced Conversion⁴¹) that have been recently developed; as cell-free systems focus primarily on amyloidogenesis, whereas cell-based models can examine prion infection in living cells.

Cell lines have been advantageous to examine infectivity via fresh infection of naïve cell culture models; effectively expanding the prion fields' ability to address questions about prion structure and characterizing strains⁴². Examining how infectivity has been modulated in cell culture has been one avenue cell culture is used; i.e. estrogen⁴³, siRNA⁴⁴, glycosides⁴⁵. Additionally, there is a focus on chronically infected cell lines (N2a⁴⁶, PK1⁴⁷, RK-PrP⁴⁸) that perpetually propagate prion infection. We previously developed a cell model expressing PrP^C gene of choice in rabbit kidney epithelial cells as a tool to assess how strains differ; specifically, it has been used chronically prion-infected RK13 cells expressing either elk (RK-Elk) or deer (RK-Deer) PrP^C. Chronically infected (noted as "+") is defined as a population of naïve RK-PrP cells that became infected with a prion strain and then stably perpetually propagate prion infection through a minimum of 15 cell culture passages. More specifically, this Chapter will focus on chronic wasting disease chronically infected cell lines (RK-Deer+ and RK-Elk+), mouse-adapted scrapie (RML and 22L) infected cell lines (RK-RML+ and RK-22L+).

The first round of anti-prion therapeutic testing is often done in chronically infected cell culture systems^{49, 50, 51, 52, 53, 54, 55}. This strategy is problematic because drugs that work in cell culture lack efficacy in the targeted host, e.g. quinacrine. Drug-induced prion structural changes have been seen when anti-prion drug therapies were tested in cell culture: Swansonine⁵⁶, Chrysoidine⁵⁷, IND24 / IND81⁵⁸, Quinalone Compounds⁵⁹, Functionalized 9-aminoacridines⁶⁰, Quinacrine-like compounds⁶¹, Gly-9⁶², Melanin⁶³, Isoprenoid Compounds⁶⁴, etc. Some drug treatments produced positive anti-prion results in cell culture, but upon testing in higher organisms (mice, humans) the drugs failed. Quinacrine⁶⁵ was touted as anti-prion due to the anti-prion action in mouse cells and therefore a potential therapy³⁷. Since quinacrine was approved for use in humans in the 1930s as an anti-malarial drug for soldiers World War 2, and prion diseases are lethal without treatment options, quinacrine trials in humans to treat prion disease was approved rapidly when quinacrine looked promising in cell culture. However, all the human trials failed to show improvement^{66, 67, 68, 69, 70, 71} with quinacrine treatment. Our lab showed that quinacrine treatment of chronically infected cervid cells (RK-Elk+ and RK-Deer+), instead of chronically infected murine cells⁶⁵, increased prion load⁴⁸. This led us to the desire to attempt tracking prion drug-induced evolution as it happened.

Prion strain characteristics and the species barrier are dependent on the conformational structure of the misfolded prion protein (PrP^{Sc}). Understanding what prion structural changes occur during evolution and emergence will provide vital information for future emergent strains; for example, newly emergent chronic wasting disease in Europe and drug-induced evolution. We hypothesized that subtle tertiary

structural changes occurring as prions emerge/evolve can be tracked via chaotropic agents and epitope-mapped antibodies. To that end, we compared emerging and evolving strains to better understand the basis of strain/species adaptation and ultimately the species barrier. This chapter addresses prion evolution via two selection pressures with the techniques we created (Figure 2.2 & 3.2): (1) Drug-induced prion evolution, and (2) evolution in cell culture systems.

As stated, quinacrine was touted as an anti-prion potential therapy due to effectiveness in murine cell culture systems; however, it failed in human trials and was shown to increase prion load in a cervid-PrP transgenic cell culture system. Quinacrine perturbation of the prion protein was detectable in the cell culture system by day 6 (Bian et al 2014). We examined the daily effect on PrP^{Sc} due to quinacrine treatment over five days. Drug-induced prion evolution of PrP^{Sc} structure was subtle but detectable within 24 hours of treatment; additionally, the structural changes were not stable, but in daily flux. The quinacrine-induced evolution yields a more epitope-inaccessible protein.

Potential prion diseases therapeutic testing relies on the fundamental prion biology assumption that prion cell culture models recapitulate molecular characteristics of natural prion diseases in higher order animals (human, deer, elk, sheep, etc.). This assumption has not been reliable: i.e., quinacrine; so, to ensure scientific facts are accurate we must continually challenge our assumptions. To test the validity that prion strains are truly stable within cell culture, chaotropic agents and epitope-mapped antibodies (Figure 2.2, 3.2) were used to compare fresh prion infection to chronic (long-

term) prion infection in cell culture. Repeated passaging of a prion strain in cell culture selects for the most stable quasi-species, leading to a PrP^{Sc} native conformation that is inaccessible at some epitopes (without denaturation) unlike primarily infected cell material. Cell-induced selection of prion quasi-species potentially confounds current drug screening methodologies. Using chronically infected (repeatedly passaged) cell material as an infectious source yields different epitope accessibilities than either primarily infected or chronically infected materials. Overall, the prion fields' reliance on chronically infected cells needs to be re-evaluated. Prion strains evolve in cell culture through serial passaging; they do not recapitulate molecular characteristics of a biological prion infection.

B. MATERIALS AND METHODOLOGY

Tissue Homogenization

See Chapter 3 – B. Tissue Homogenization

Mouse Model

See Chapter 2 – B. Mouse Model

Mouse Infections

See Chapter 2 – B. Mouse Infections

Cell Model

See Chapter 2 – B. Cell Model

Cell Culture

See Chapter 2 – B. Cell Culture

Brain Homogenate Prion Infection of Cell Culture

See Chapter 2 – B. Prion Infection of Cell Culture

Cell Lysate Preparation

A confluent 10cm² plate of the desired cell line was collected. Media was removed, plates were then rinsed twice with 10mL of cold sterile phosphate buffered saline (PBS) lacking Ca²⁺ and Mg²⁺ (Hyclone, Pittsburg, PA). Plates were then exposed to 1mL cold cell lysis buffer (50 mM Tris (Sigma-Aldrich, St. Louis, MO), pH 8.0; 150 mM NaCl (Sigma-Aldrich, St. Louis, MO); 0.5% sodium deoxycholate (Sigma-Aldrich, St. Louis, MO); 0.5% Igepal (Sigma-Aldrich, St. Louis, MO)) on ice for 5-10 minutes; this was done to detach the cells from the plate. The resultant mixture was stored at -80°C until use.

Cell Lysate Prion Infection of Cell Culture

Three confluent 10cm² plates were grown of the desired chronically prion infected cell line, media was removed, plates were then rinsed twice with 10mL of cold sterile PBS. Plates were then exposed to 1mL cold cell lysis buffer on ice for 5-10 minutes; this was done to detach the cells from the plate. All three plates with cells in cell lysis buffer were collected in one tube. The tube was put through three cycles of freeze-thaw: freezing them overnight at -80°C and then rapid thaw at room temperature. At this point, cell lysates were prepared in one of two ways: (1) air-exposure methodology and (2) bead homogenization methodology. The bead homogenization method was used as more reliably repeatable replacement to the air-exposure method of the when the FastPrep-24 Classic Grinder (MP Biomedical) was purchased.

- (1) Air-Exposure Methodology: The 1mL of the freeze-thawed mixture was placed on a 10cm² plate (akin to Chapter 2 – B. Prion Infection of Cell Culture).

(2) Bead Homogenization: The 1mL of the freeze-thawed mixture was added to 4.5 mL Tallprep Tubes (MP Biomedical). The mixture was bead homogenized in the FastPrep-24 Classic Grinder (MP Biomedical) in three rounds of 15 seconds followed by 5 minute rest on ice. The mixture was then used to as infectious material; 1mL of the mixture was placed on a 10cm² plate (akin to Chapter 2 – B. Prion Infection of Cell Culture).

Quinacrine Treatment

Cells were treated with quinacrine in one of two ways: (1) As previously published⁴⁸, and (2) drug treatment after cell confluence. RK-PrP cell lines (see Chapter 2.B Cell Model) were grown (see Chapter 2.B Cell Culture) to confluence.

(1) As published⁴⁸, RK-Elk+, RK-Elk-, and RK-V cell lines were split onto new 10cm² cell culture plates. The following day, the media was removed and replaced with media containing 1µM quinacrine or an identical volume of vehicle (PBS); treatment lasted 24 hours (Day 1 samples). Treatment groups that were multiple days (Day 2, 3, 4, and 5) received fresh media with or without drug every day and were collected 24 hours after last treatment; i.e. 2-24 hour treatments (Day 2), 3-24 hour treatments (Day 3), 4-24 hour treatments (Day 4), and 5-24 hour treatments (Day 5). Cells were harvested via trypsin (Sigma-Aldrich, St. Louis, MO) disassociation and seeded (20,000 cells per well) onto 70% Ethanol, molecular grade (Sigma- Aldrich, St. Louis, MO) activated Multiscreen IP 96-well 0.45-µm ELISpot plates (Millipore, Billerica, MA). See Chapter 3.B Epitope Stability Assay, for further methods.

(2) Alternatively, to be able to reduce variability in control sample, cell lines were split onto new 10cm² cell culture plates and allowed to come to ~80% confluence before treatment. They were treated identically to (1) from that point onwards.

Western Blot Analysis of Pr^{PC} and Pr^{PSc}

Tissues were prepared (see Chapter 3 – B. Tissue Homogenization), and cell lysates were prepared (see above, Cell Lysate Preparation). Total protein concentration was determined by bicinchoninic acid (BCA) assay (Pierce Biotechnology Inc., Rockford, IL), and used to normalize the samples for comparison. Homogenized brains and cell lysates were either not treated or treated with 40 µg/ml proteinase K (PK) (Pierce Biotechnology Inc., Rockford, IL) in 2% sarkosyl in PBS for 1 hour at 50°C. The PK was quenched with 4 mM phenylmethylsulfonyl fluoride (PMSF) (Sigma-Aldrich, St. Louis, MO) in PBS for ten minutes at on ice. Samples designated for Pr^{PSc} detection that were treated with PK, were then purified by centrifugation for 1 hour at 100,000 X g at 4°C. The supernatant was removed and pellet suspended in in 2% sarkosyl in PBS. Loading dye was added, and proteins separated by SDS-PAGE using discontinuous 12% Tris-Glycine gels. Proteins were then transferred to PVDF-FL membranes (Millipore, Billerica, MA). Membranes exposed to Tris buffered saline, 0.05 % Tween (TBS-T) and 5% non-fat milk to block extraneous antibody reactions. The membrane was then incubated with primary anti-prion antibody (Figure 3.1B) PRC5 (Telling Lab, Fort Collins, CO) 1:5000 dilution overnight. The following day, the membrane was treated with HRP-conjugated sheep α-mouse IgG secondary antibody (Southern Biotechnology

Associates, Birmingham, AL) 1:5000 dilution for 1 hour at room temperature.

Membranes were then developed using ECL-plus (GE Healthcare Biosciences, Pittsburgh, PA) and analyzed by either a a FLA-5000 scanner (Fuji/ GE Healthcare Biosciences, Pittsburgh, PA) or LI-COR (LI-COR Biosciences, Lincoln, NE).

7-5 Sandwich ELISA-CSA

See Chapter 3 – B. 7-5 Sandwich ELISA-CSA

Cell-Based Conformational Stability Assay (C-CSA)

See Chapter 2 – B. Cell-Based Conformational Stability Assay (C-CSA)

Cell-Based Epitope Stability Assay (ESA)

See Chapter 3 – B. Cell-Based Epitope Stability Assay (ESA)

Statistical Analysis

Statistical significance was assessed using GraphPad Prism 8.0 for Mac OS X software.

C. RESULTS

Two forms of evolution were evaluated with the ESA [Chapter 3] and C-CSA [Chapter 2] methodologies: (1) drug-induced evolution, and (2) evolution within cell culture.

Quinacrine perturbs PrP^{Sc} epitopes, within 24 hours of use, causing new tertiary structures of PrP^{Sc} to emerge

As stated, quinacrine reduced prion load in chronically infected murine cells⁶⁵, but failed in human trials^{66, 67, 68, 69, 70, 71}. Our lab showed that quinacrine increases prion load in RK-Deer and RK-Elk cells and detectable structural changes, via C-CSA, occurred at a single epitope (6H4)⁴⁸. We hypothesized that ESA will uncover the subtle

structural changes to PrP^{Sc} caused by quinacrine over the first 5 days that the prion is exposed to the drug. RK-Elk chronically infected with CWD (RK-Elk+) showed a more rapid increase of PrP^{Sc} than RK-Deer chronically infected with CWD (RK-Deer+)⁴⁸; as such the experiment was designed to evaluate RK-Elk+ cells.

To track the changes to prion structure, we began with a pilot study (n=1) replicating the initial design used⁴⁸, Figure 4.1A, to assess if the ESA would replicate the difference due quinacrine treatment in chronically prion-infected RK-Elk with anti-prion antibody (6H4) and the viability of examining daily changes in PrP^{Sc}. The 6H4 epitope was used previously⁴⁸; it recognizes a discontinuous epitope ranging from before α helix-1 (amino acid residue 141) to α helix-3 (amino acid residue 200).⁷² 24 hours after being split onto new plates, RK-Elk+ and RK-Elk cells were treated with media laced with vehicle (PBS) or quinacrine (1 μ M); the effective, sub-lethal, dose of quinacrine was previously established⁴⁸. Cells were sampled daily, and treated (vehicle/quinacrine) media replaced daily for five days. The results (Figure 4.1B) recapitulated previous conclusions that quinacrine increases the GdnHCl $\frac{1}{2}$ value at 6H4 between quinacrine-treated and vehicle-treated RK-Elk+. However, comparing daily changes was problematic as daily sampling created an irregularity in the control (RK-Elk+/PBS) group, Figure 4.1C. This made comparisons to daily changes seen within the quinacrine-treated (Figure 4.1D) group difficult. Additionally, quinacrine slowed cellular growth, causing the cell count at harvesting to vary greatly between quinacrine-treated and vehicle-treated samples. These issues clouded ability to see stable structural differences between drug-treated and vehicle-treated groups.

To ameliorate these issues, the treatment paradigm was re-designed, Figure 4.2A. RK-Elk+ and RK-Elk cells were allowed to gain ~85% confluency prior to treatment with vehicle or quinacrine. The resultant second pilot study (data not shown) showed viability to scale up to a larger (n=3) design. Conformational stability assays and the ESA rely on the $GdnHCl_{1/2}$ value to differentiate strains and provide further information about the relative stability of the molecule and how available or resistant the epitope is to detection. To that end, all samples examined were compared for the $GdnHCl_{1/2}$ value of each antibody probed. The $GdnHCl_{1/2}$ value represents the midway point of the linear denaturation until the entire molecule is accessible and the curve fit value represents how the prion is responding to denaturation by GdnHCl. As such, the $GdnHCl_{1/2}$ and curve fit have been indicated. Using both points is an important distinction, allowing a more nuanced evaluation of prion structure. For example, if the $GdnHCl_{1/2}$ value is similar but the prions arrive at that point differently; it implies that although the epitope is available at roughly the same molarity, the process of denaturation varies. Another possible response is if the $GdnHCl_{1/2}$ value is different and the curve fit is the same; it implies that the difference only represents a shift in mirrored response to denaturation by GdnHCl.

The modified methodology created a more unified control (RK-Elk+/PBS) group ($p=0.4783$), Figure 4.2B as compared to Figure 4.1C. This facilitated daily comparisons (Figure 4.2C-G, 4.3D) to the treatment group (RK-Elk+/Quinacrine) and implies that changes in the epitope stability are directly due to quinacrine treatment. Although the first day showed no significance ($p=0.3615$) in how quinacrine-treatment

alters the curve fit of elk-CWD PrP^{Sc}, the following days showed significant difference: day 2 (p=0.0333), day 3 (p=0.0002), day 4 (p=0.0254), and day 5 (p=0.0003). This implies that it takes 2 consecutive days of quinacrine treatment to alter the response to GdnHCl, and quinacrine treatment does not yield a consistent curve fit (day1-5, p<0.0001). When the GdnHCl ½ values were compared, treatment caused significant differences starting from day 1 (p= 0.0463), this means that although the response to GdnHCl is the same, the 6H4 epitope is already responding to quinacrine treatment. The GdnHCl ½ values were significantly different due to quinacrine treatment at: day 2 (p<0.0001), day 3 (p=0.0002), and day 5 (p=0.0008). Day 4 had the most internal variation in quinacrine treated samples, and did not have a significantly different GdnHCl ½ values (p=0.4736) when compared to the vehicle treated samples. Overall, quinacrine impacts the elk-CWD PrP^{Sc} structure within 24 hours of treatment, and quinacrine changes are is not a single stable PrP^{Sc} isoform.

To address whether changes to the structure were occurring throughout the molecule, additional anti-prion antibodies PRC1, PRC5, and 1B8 (Figure 3.1B) were used via ESA to examine the daily changes in the epitope stability are directly due to quinacrine treatment of elk PrP^{Sc}. PRC1 recognizes recognize a linear epitope located in the unstructured N-terminal region (amino acid residues 94-95) near the PK cleavage site⁷³. PRC5 recognizes a discontinuous epitope located in the globular C-terminal region, straddling α helix-1 (amino acid residues 132 & 158)⁷³. 1B8, created recently by the Telling lab, recognizes recognize a linear epitope located within α helix-1 (amino acid residue 146). All control (RK-Elk+/PBS) groups were stable across the five days:

PRC1, 2.17M, $p=0.2024$; PRC5, 3.01M, $p=0.7599$; 1B8, 2.27M, $p=0.9589$, and 6H4, 1.54M, $p=0.4783$. This facilitated daily comparisons within antibodies (Figure 4.3) to the treatment group (RK-Elk+/Quinacrine) and implies that changes in the epitope stability are directly due to quinacrine treatment. 6H4 data (Figure 4.2C-G) was included (Figure 4.3D) to aid overall molecular comparison between antibodies.

The importance of the unstructured N-terminal region to PrP^{Sc} structure has been downplayed in prion research. Examining the PRC1 epitope implies that quinacrine makes the unstructured N-terminal region more accessible within 24 of treatment, and maintains the greater accessibility across all 5 days measured. The curve fit comparing quinacrine or vehicle-treated elk-CWD PrP^{Sc}, showed significant differences: day 1 ($p=0.0308$), day 2 ($p<0.0001$), day 3 ($p<0.0001$), day 4 ($p<0.0001$), and day 5 ($p<0.0001$). This means that the response to GdnHCl is altered by quinacrine treatment. The GdnHCl $\frac{1}{2}$ values were significantly different due to quinacrine treatment at: day 1 ($p=0.0389$), day 2 ($p=0.0239$), day 3 ($p<0.0001$), day 4 ($p<0.0001$), and day 5 ($p=0.0049$). The GdnHCl $\frac{1}{2}$ values further support the pronounced difference caused by quinacrine treatment at the unstructured N-terminal region of elk-CWD PrP^{Sc}.

The PRC5 discontinuous epitope straddles the α helix-1. Unlike all other epitopes examined, PRC5 begins with non-significant differences in GdnHCl $\frac{1}{2}$ value ($p=0.3957$) but significantly different curve fit ($p=0.304$) 24 hours after treatment; this implies that although the epitope maintained a stable GdnHCl $\frac{1}{2}$ value, the response to GdnHCl was already changing. After the first 24 hours, days 2-5, there were significant

differences between vehicle and quinacrine treated prions in both curve fit ($p < 0.0001$) and GdnHCl $\frac{1}{2}$ values ($p < 0.0001$). After the first 24 hours, quinacrine treatment altered the PrP^{Sc} tertiary structure, making the PRC5 epitope more accessible.

The 1B8 linear epitope is embedded within α helix-1. Unlike PRC1 but somewhat similar to PRC5, the 1B8 epitope does not have a consistent response to quinacrine treatment. Quinacrine treatment makes the 1B8 epitope progressively harder to access for the first two days and then, abruptly, the epitope becomes easier to access on the third day; this more available 1B8 epitope is relatively stable between days 3:5 (ns, $p = 0.1395$). Like 6H4, after 24 hours of quinacrine treatment, the curve fit of 1B8 is not significantly different ($p = 0.0738$) but the GdnHCl $\frac{1}{2}$ value is significantly different ($p = 0.0088$). Quinacrine-treatment alters the curve fit of elk-CWD PrP^{Sc}: day 2 ($p < 0.0001$), day 3 ($p < 0.0001$), day 4 ($p < 0.0001$), and day 5 ($p < 0.0001$). This implies that it takes 2 consecutive days of quinacrine treatment to alter the response to GdnHCl, and quinacrine treatment does not yield a consistent curve fit (day1-5, $p < 0.0001$). The GdnHCl $\frac{1}{2}$ values were significantly different due to quinacrine treatment at: day 1 ($p = 0.0010$), day 2 ($p < 0.0001$), day 3 ($p < 0.0001$), and day 5 ($p < 0.0001$). Overall, quinacrine impacts the elk-CWD PrP^{Sc} structure within 24 hours of treatment, and quinacrine changes go through several distinct PrP^{Sc} isoforms.

Evolution in cell culture

To examine prion evolution in cell culture, chronically infected cells were compared to freshly infected cells. To differentiate, original brain homogenate will be noted by the prion (e.g. Deer-CWD, Elk-CWD, RML, and 22L) freshly infected cells will

be noted with (prion>cell line) and chronically infected cells will be noted by (+). We used chronically prion-infected RK13 cells expressing either elk (RK-Elk), deer (RK-Deer), or mouse (RK-Mouse) PrP^C. CWD was used to chronically infected RK-Elk (RK-Elk+) and RK-Deer (RK-Deer+) cell lines; whereas, RML and 22L were used to chronically infect RK-Mouse (RK-RML+) and (RK-22L+), respectively, cell lines. Cells were considered chronically infected when they perpetually propagated detectable prion infection through a minimum of 15 passages.

First, we compared the initial infectious source (brain homogenate), freshly infected cells, and chronically infected cells using the prion field gold standard: detect and compare of PrP^{Sc} via proteinase K (PK) digestion and western blotting. Specifically, freshly infected RML>RK-Mouse, chronically infected RK- RML+, and the initial infection source (terminally ill C57BL/6 inbred mice infected with RML) were western blotted and interrogated with anti-prion antibody PRC5, Figure 4.4. Lack of PK usage reveals total PrP^C and PrP^{Sc} fraction; while, PK usage ablates PrP^C signals, allowing for detection of PrP^{Sc}. Included negative control for the brain homogenate was brain homogenate from a PrP-KO mouse, and negative control for the cell lines was cell lysate from RK-V(vector only, PrP^C null) cell line. Overall, the glycoform ratio is different when comparing the brain-PrP^{Sc} to cell-PrP^{Sc}; however there are no pronounced differences between RML>RK-Mouse and RK- RML+. This implies that chronically infected PrP^{Sc} resembles fresh infection, and the brain homogenate infectious source. We wanted to examine this presumption that the PrP^{Sc} in chronically infected cell lines resembles freshly infected cells with the C-CSA [Chapter 2] and ESA [Chapter 3].

To examine if serial passaging, i.e. creating a chronic line, would alter the tertiary structure of PrP^{Sc}, we compared the folded (non-denatured) PrP^{Sc} via ESA, Figure 4.5. The ESA [Chapter 3] showed that some prion strains did not require denaturation to reveal signal at linear or discontinuous PrP^{Sc} epitopes. We compared four pairs of prions: Deer-CWD (Figure 4.5A), Elk-CWD (Figure 4.5B), RML (Figure 4.5C), and 22L (Figure 4.5D). The results were resoundingly different in all four prions, creation of a chronic line altered PK-treated, non-denatured PrP^{Sc} epitope accessibility.

Deer-CWD>RK-Deer fresh infection [brains (n=3) from terminally ill Tg(DeerPrP)1536^{+/-} mice infected with elk CWD isolate Bala05 were used to infect RK-Deer] and chronically infected cell lines that perpetually propagate CWD prion infection (RK-Deer+) were compared. When comparing Deer-CWD (Figure 4.5A), in RK-Deer and RK-Deer+, there were significant differences in epitope accessibility at: PRC1 (p=0.0017), D18 (p=0.0498), PRC5 (p=0.0019), and 6H4 (p=0.0002). Although the accessibility changed at PRC1, it did not change at D13 (p=0.2338); this implies that the unstructured N-terminus linear epitopes are not equally accessible. Additionally PRC7, the discontinuous glycosylation-specific epitope, was not significantly different (p=0.1234); implying that the glycosylation state has not been drastically altered. The most drastic difference was a gain in accessibility (29.98%) at 6H4 in the chronically infected population.

Elk-CWD>RK-Elk fresh infection [brains (n=3) from terminally ill Tg(ElkPrP)5037^{+/-} mice infected with elk CWD isolate Bala05 were used to infect RK-Elk] and chronically infected cell lines that perpetually propagate CWD prion infection

(RK-Elk+) were compared. When comparing Elk-CWD (Figure 4.5B), in RK-Elk and RK-Elk+, there were significant differences in epitope accessibility at all epitopes examined: PRC1 ($p=0.0003$), D13 ($p<0.0001$), D18 ($p=0.0120$), PRC5 ($p<0.0001$), 6H4 ($p=0.0297$), and PRC7 ($p<0.0001$). Overall, the chronically infected line lost Elk-CWD PrP^{Sc} epitope accessibility at all epitopes, except 6H4. Like Deer-CWD, there was an increase (5.26%) in epitope accessibility at the 6H4 epitope.

RML>RK-Mouse fresh infection [brains ($n=3$) from terminally ill C57Bl/6 inbred mice infected with RML were used to infect RK-Mouse] and chronically infected cell lines that perpetually propagate RML prion infection (RK-RML+) were compared. When comparing RML (Figure 4.5C), in RK-Mouse and RK-RML+, there were significant differences in epitope accessibility at: 1B8 ($p<0.0001$), PRC5 ($p<0.0001$), 6H4 ($p=0.0005$), and PRC7 ($p=0.0021$). There were no significant differences at epitopes that had very low (<1.5%) detectable signal without denaturation: D13 ($p>0.9999$), D18 ($p=0.3739$), and 5A3 ($p=0.2051$). Like Elk-CWD, the chronically infected line lost RML PrP^{Sc} epitope accessibility at all epitopes that had (>1.5%) signal without denaturation. This implies that the chronically infected line is overall less accessible.

22L>RK-Mouse fresh infection [brains ($n=3$) from terminally ill C57Bl/6 inbred mice infected with 22L were used to infect RK-Mouse] and chronically infected cell lines that perpetually propagate 22L prion infection (RK-22L+) were compared. When comparing 22L (Figure 4.5D), in RK-Mouse and RK-22L+, there were significant differences in epitope accessibility at: PRC5 ($p<0.0001$), 6H4 ($p=0.0001$), and PRC7 ($p=0.0213$). PRC7, the discontinuous glycosylation-specific epitope, lost 3% accessibility

implying that the glycosylation state was not stable. Overall, 22L had the most similarity between fresh infection and chronic infection epitope accessibility: D13 ($p > 0.9999$), 1B8 ($p = 0.0605$), D18 ($p = 0.3739$), and 5A3 ($p = 0.1161$). With each prion pair, establishing a chronically infected line overall reduced epitope accessibility of PK-treated, folded/non-denatured PrP^{Sc}.

As mentioned, conformational stability assays and the ESA rely on the GdnHCl_{1/2} value to differentiate strains and provide further information about the relative stability of the molecule and how available or resistant the epitope is to detection. To that end, each prion pair (Figure 4.5) was compared for the GdnHCl_{1/2} value of each antibody probed. The GdnHCl_{1/2} value represents the midway point of the linear denaturation until the entire molecule is accessible and the curve fit value represents how the prion is responding to denaturation by GdnHCl. As such, the GdnHCl_{1/2} and curve fit have been indicated. Using both points is an important distinction, allowing a more nuanced evaluation of prion structure. Additionally, the prion pairs were examined with both the ESA [Chapter 3] and C-CSA [Chapter 2]. The use of both ESA (Figure 4.6 A, C, E, G) and C-CSA (Figure 4.6 B, D, F, H) techniques allows the strains to be compared for protease sensitivity after denaturation and epitope accessibility. The GdnHCl_{1/2} value and curve fit comparisons further supports that PrP^{Sc} structure in chronically infected lines is not identical to freshly infected lines in Deer-CWD (Figure 4.6A-B), Elk-CWD (Figure 4.6C-D), RML (Figure 4.6E-F), and 22L (Figure 4.6G-H).

Deer-CWD>RK-Deer fresh infection [brains (n=3) from terminally ill Tg(DeerPrP)1536^{+/-} mice infected with elk CWD isolate Bala05 were used to infect RK-Deer] and chronically infected cell lines that perpetually propagate CWD prion infection (RK-Deer+) were compared. Although the GdnHCl $\frac{1}{2}$ values from the ESA of Deer-CWD PrP^{Sc} (Figure 4.6A) in a chronic cell line closely resemble (≤ 0.62 M difference) fresh infection at multiple epitopes, it is misleading because only D13 is not significantly different ($p=0.8249$); the other epitopes are significantly different: PRC1 ($p=0.0062$), D18 ($p=0.0074$), PRC5 ($p=0.0001$), 6H4 ($p=0.0009$), and PRC7 ($p<0.0001$). The close resemblance of the GdnHCl $\frac{1}{2}$ values does not come from a similar response to denaturation, however, all the curve fits are significantly different: PRC1 ($p<0.0001$), D13 ($p<0.0001$), D18 ($p<0.0001$), PRC5 ($p=0.0041$), 6H4 ($p<0.0001$), and PRC7 ($p<0.0001$). When the same prion pair was examined via C-CSA (Figure 4.6B), a similar trend emerged. The curve fits are significantly different ($p<0.0001$) at all epitope examined: PRC1, D13, D18, PRC5, 6H4, and PRC7. The GdnHCl $\frac{1}{2}$ values were significantly different at PRC1 ($p<0.0001$), D13 ($p<0.0001$), PRC5 ($p<0.0001$), and 6H4 ($p=0.0006$); the D18 ($p=0.0520$) and PRC7 ($p=0.0640$) epitopes are trending but not significant. The C-CSA data implies that serial passaging Deer-CWD makes PrP^{Sc} more protease resistant after denaturation. Overall, this implies that the serially passaged Deer-CWD is similar but subtly different at multiple epitopes.

Elk-CWD>RK-Elk fresh infection [brains (n=3) from terminally ill Tg(ElkPrP)5037^{+/-} mice infected with elk CWD isolate Bala05 were used to infect RK-Elk] and chronically infected cell lines that perpetually propagate CWD prion infection

(RK-Elk+) were compared. Although the GdnHCl $\frac{1}{2}$ values from the ESA of Elk-CWD PrP^{Sc} (Figure 4.6C) in a chronic cell line closely resemble ($\leq 0.58M$ difference) fresh infection at multiple epitopes, the subtle difference is significant at PRC1 ($p < 0.0001$), PRC5 ($p = 0.0002$), 6H4 ($p = 0.0125$), and PRC7 ($p < 0.0001$); the difference is not significantly at D13 ($p = 0.2204$) and D18 ($p = 0.2581$). The close resemblance of the GdnHCl $\frac{1}{2}$ values does not come from a similar response to denaturation, however, because all the curve fits are significantly different: PRC1 ($p = 0.0067$), D13 ($p < 0.0001$), D18 ($p < 0.0001$), PRC5 ($p < 0.0001$), 6H4 ($p < 0.0001$), and PRC7 ($p < 0.0001$). When the same prion pair was examined via C-CSA (Figure 4.6D), a similar trend emerged. The curve fits are significantly different at all epitope examined: PRC1 ($p < 0.0001$), D13 ($p < 0.0001$), D18 ($p = 0.0046$), PRC5 ($p = 0.0219$), 6H4 ($p < 0.0001$), and PRC7 ($p < 0.0001$). The GdnHCl $\frac{1}{2}$ values were significantly different at PRC1 ($p = 0.0021$), D13 ($p = 0.0419$), PRC5 ($p = 0.0025$), 6H4 ($p = 0.0003$), and PRC7 ($p = 0.0004$); the D18 ($p = 0.0547$) epitope was trending but not significant. The C-CSA data implies that serial passaging Elk-CWD makes PrP^{Sc} more protease resistant after denaturation. Overall, this implies that the serially passaged Elk-CWD is similar but subtly different at multiple epitopes.

RML > RK-Mouse fresh infection [brains (n=3) from terminally ill C57Bl/6 inbred mice infected with RML were used to infect RK-Mouse] and chronically infected cell lines that perpetually propagate RML prion infection (RK-RML+) were compared. Surprisingly, the differences from serial passaging mouse-adapted scrapie strains RML (Figure 4.6E) and 22L (Figure 4.6G) are more pronounced with the ESA method than CWD in deer or elk. The GdnHCl $\frac{1}{2}$ values from the epitope accessibility assay (Figure

4.6E, G) are not identical to the GdnHCl $\frac{1}{2}$ values from the cell-based conformational stability assay (Figure 4.6F, H) for these strains. The ESA GdnHCl $\frac{1}{2}$ values comparing serial passaged RML and freshly infected RML (Figure 4.6E) are significantly different at every epitope examined: D13 ($p=0.0056$), 1B8 ($p=0.0001$), D18 ($p<0.0001$), PRC5 ($p=0.0014$), 6H4 ($p<0.0001$), 5A3 ($p=0.0004$), and PRC7 ($p<0.0001$); additionally, the ESA curve fits are significantly different at every epitope examined: D13 ($p=0.0014$), 1B8 ($p<0.0001$), D18 ($p<0.0001$), PRC5 ($p<0.0001$), 6H4 ($p<0.0001$), 5A3 ($p<0.0001$), and PRC7 ($p<0.0001$). When RML is compared via C-CSA (Figure 4.6F), the GdnHCl $\frac{1}{2}$ values remain significantly different at D13 ($p<0.0001$), PRC5 ($p=0.0008$), and 6H4 ($p=0.0160$); and the curve fits are significantly different ($p<0.0001$) at D13, PRC5, and 6H4. The significant differences between chronically infected RML and freshly infected RML ESA is not evident with the C-CSA at PRC7 GdnHCl $\frac{1}{2}$ ($p=0.5655$) and curve fit ($p=0.2399$) or at D18 GdnHCl $\frac{1}{2}$ ($p=0.4717$) and curve fit ($p=0.2159$). Overall, establishment of a chronic RML line made the RML PrP^{Sc} epitopes in the globular region less accessible while the becoming more resistant to protease degradation after denaturation.

22L>RK-Mouse fresh infection [brains ($n=3$) from terminally ill C57Bl/6 inbred mice infected with 22L were used to infect RK-Mouse] and chronically infected cell lines that perpetually propagate 22L prion infection (RK-22L+) were compared. 22L (Figure 4.6G) mirrors RML in having significantly different GdnHCl $\frac{1}{2}$ values when comparing serial passaged 22L and freshly infected 22L at every epitope examined via ESA: D13 ($p=0.0030$), 1B8 ($p<0.0001$), PRC5 ($p=0.0006$), 6H4 ($p=0.0007$), 5A3 ($p<0.0001$), and PRC7 ($p<0.0001$); additionally, the ESA curve fits are significantly different at every epitope

examined: D13 ($p=0.0045$), 1B8 ($p<0.0001$), PRC5 ($p<0.0001$), 6H4 ($p<0.0001$), 5A3 ($p<0.0001$), and PRC7 ($p<0.0001$). When 22L is compared via C-CSA (Figure 4.6H), it again mirrors RML in that the GdnHCl $\frac{1}{2}$ values remain significantly different at D13 ($p<0.0001$), D18 ($p<0.0001$), PRC5 ($p<0.0001$), and 6H4 ($p=0.0030$); and the curve fits are significantly different at D13 ($p<0.0001$), D18 ($p<0.0001$), PRC5 ($p<0.0001$), and 6H4 ($p=0.0004$). Unlike RML at PRC7 with the C-CSA, for 22L although the GdnHCl $\frac{1}{2}$ value was not significantly different ($p=0.0509$), the curve fit was significantly different ($p=0.0291$). Overall, establishment of a chronic 22L line made the 22L PrP^{Sc} epitopes less accessible at every epitope while maintaining or becoming more resistant to protease degradation after denaturation in the globular epitopes.

To ascertain if the PrP^{Sc} conformation of the chronic cell lines (Figure 4.6) would be maintained with passage back into the cell system, we infected naïve RK-PrP cells with lysate from chronically prion infected cell lines (Figure 4.7). The resultant prions were compared for GdnHCl $\frac{1}{2}$ values and curve fit across multiple antibodies (Figure 3.1B) with the ESA method [Chapter 3] and the C-CSA method [Chapter 2]. The new cell lysate infection was compared to fresh infection with brain homogenate and the chronically infected cells used for the lysate infection. The GdnHCl $_{1/2}$ value and curve fit comparisons further supports that PrP^{Sc} structure in chronically infected lines is not stable when passaged into naïve RK-PrP cells. Top statistics indicated in each graph are comparing (Freshly Infected : Chronic Cell Lysate Infected); and the bottom statistics indicated are comparing (Chronically Infected : Chronic Cell Lysate Infected). Both

statistical comparisons allow the PrP^{Sc} from chronic cell lysate infected to be compared to the brain homogenate PrP^{Sc}, and chronically prion infected cell PrP^{Sc}.

To that end, Deer-CWD>RK-Deer fresh infection [brains (n=3) from terminally ill Tg(DeerPrP)1536^{+/-} mice infected with elk CWD isolate Bala05 were used to infect RK-Deer], chronically infected cell lines that perpetually propagate CWD prion infection (RK-Deer+), and naïve RK-Deer cells infected with RK-Deer+ cell lysate (RK-Deer+>RK-Deer) were compared. RK-Deer+>RK-Deer (dotted line) and Deer-CWD>RK-Deer (solid line) were compared via ESA (Figure 4.7A) and C-CSA (Figure 4.7B). RK-Deer+>RK-Deer GdnHCl ½ derived from ESA does not resemble Deer-CWD>RK-Deer at three of the five epitopes examined: D13 (p=0.0066), PRC5 (p<0.0001), PRC7 (p<0.0001); they are non-significantly different at PRC1 (p=0.3715) and D18 (p=0.1287). However, GdnHCl ½ similarities do not imply that the response to denaturation is similar; the curve fits were significantly different at all epitopes examined: PRC1 (p=0.0455), D13 (p<0.0001), D18 (p=0.0120), PRC5 (p<0.0001), PRC7 (p<0.0001). When examining the same prion pair with C-CSA (Figure 4.7B), the curve fit remains significantly different at all epitopes examined: PRC1 (p<0.0001), PRC5 (p<0.0001), 6H4 (p=0.0033), and PRC7 (p<0.0001). The GdnHCl ½ is significantly different at all epitopes examined: PRC1 (p<0.0001), PRC5 (p=0.0007), 6H4 (p=0.0063), and PRC7 (p=0.0132). Overall, RK-Deer+>RK-Deer is more resistant to protease degradation after denaturation, and the epitopes are less accessible (D13 and PRC5) or more (PRC7) accessible compared to Deer-CWD>RK-Deer.

RK-Deer+ cell lysate (RK-Deer+>RK-Deer, dotted line) and RK-Deer+ (dashed line), were compared via ESA (Figure 4.7A) and C-CSA (Figure 4.7B). RK-Deer+>RK-Deer GdnHCl $\frac{1}{2}$ derived from ESA does not resemble RK-Deer+ at any of the epitopes examined: PRC1 (p=0.0026), D13 (p=0.0044), 1B8 (p<0.0001), D18 (p=0.0005), PRC5 (p<0.0001), and PRC7 (p<0.0001). The curve fits (response to denaturation) is significantly different (p<0.0001) at all epitopes examined: PRC1, D13, 1B8, D18, PRC5, and PRC7. When examining the same prion pair with C-CSA (Figure 4.7B), the curve fit remains significantly different (p<0.0001) at most epitopes examined: PRC5, 6H4, and PRC7. The curve fit is trending but not significantly different at PRC1 (p=0.518) although the GdnHCl $\frac{1}{2}$ is significantly different (p<0.0001); this implies that the curve is the same but subtly shifted enough to have different GdnHCl $\frac{1}{2}$ values. Like PRC1, all other GdnHCl $\frac{1}{2}$ values were significantly different at all epitopes compared with C-CSA: PRC5 (p<0.0001), 6H4 (p=0.0011), and PRC7 (p<0.0001). Overall, RK-Deer+>RK-Deer is more less resistant to protease degradation after denaturation (PRC5 and 6H4), more resistant to protease degradation after denaturation (PRC7) and the epitopes are less accessible (D13, 1B8 and PRC5) or more accessible (PRC1 and PRC7) compared to RK-Deer+.

Elk-CWD>RK-Elk fresh infection [brains (n=3) from terminally ill Tg(ElkPrP)5037^{+/-} mice infected with elk CWD isolate Bala05 were used to infect RK-Elk], chronically infected cell lines that perpetually propagate CWD prion infection (RK-Elk+), and naïve RK-Elk cells infected with RK-Elk+ cell lysate (RK-Elk+>RK-Elk) were compared. RK-Elk+>RK-Elk (dotted line) and Elk-CWD>RK-Elk (solid line) were compared via C-CSA

(Figure 4.7C). RK-Elk+>RK-Elk and Elk-CWD>RK-Elk have significantly different GdnHCl $\frac{1}{2}$ and curve fits at each epitope examined: PRC1 ($p=0.0012$, $p<0.0001$), PRC5 ($p<0.0001$, $p=0.0344$), 6H4 ($p=0.0091$, $p=0.0161$), and PRC7 ($p=0.0037$, $p=0.0002$). This difference extends to most epitopes when comparing RK-Elk+>RK-Elk and RK-Elk+ (dashed line). The curve fits were significantly different at all epitopes examined: PRC1 ($p=0.0065$), PRC5 ($p=0.0199$), 6H4 ($p=0.0153$), and PRC7 ($p=0.0005$). With PRC1, the GdnHCl $\frac{1}{2}$ is not significantly different ($p=0.2681$); this implies that the GdnHCl $\frac{1}{2}$ values is the same but how the denaturation curve arrives at that half value is different. The other GdnHCl $\frac{1}{2}$ comparisons are significantly different: PRC5 ($p<0.0001$), 6H4 ($p=0.0016$), and PRC7 ($p=0.0002$). Overall, the differences between RK-Elk+>RK-Elk, Elk-CWD>RK-Elk and RK-Elk+ are subtle but measurable with the C-CSA method.

We then compared murine-adapted scrapie RML strain in a mouse cell model. RML>RK-Mouse fresh infection [brains ($n=3$) from terminally ill C57Bl/6 inbred mice infected with RML were used to infect RK-Mouse], chronically infected cell lines that perpetually propagate RML prion infection (RK-RML+), and naïve RK-Mouse cells infected with RK-RML+ cell lysate (RK-RML+>RK-Mouse) were compared. RK-RML+>RK-Mouse (dotted line) and RML>RK-Mouse (solid line) were compared via ESA (Figure 4.7D) and C-CSA (Figure 4.7E). RK-RML+>RK-Mouse GdnHCl $\frac{1}{2}$ and curve fits derived from ESA do not resemble RML>RK-Mouse at the epitopes examined: 1B8 ($p=0.0189$, $p<0.0001$), D18 ($p=0.0009$, $p<0.0001$), and PRC7 ($p<0.0001$, $p<0.0001$). When examining the same prion pair with C-CSA (Figure 4.7E), the GdnHCl $\frac{1}{2}$ and curve fits remained significantly different at: D13 ($p<0.0001$, $p<0.0001$), D18

($p=0.0021$, $p<0.0001$), PRC5 ($p=0.0008$, $p<0.0001$), and 6H4 ($p=0.0002$, $p=0.0064$). The C-CSA examination of RML at the PRC7 epitope was the only entirely unified similarity between all three samples, i.e. freshly infected, chronically infected, and cell lysate infected, across all methods and prions examined; specifically, freshly RML infected: cell lysate infected GdnHCl $\frac{1}{2}$ ($p=0.1152$), and curve fit ($p=0.6760$), and chronically RML infected: cell lysate infected GdnHCl $\frac{1}{2}$ ($p=0.4764$), and curve fit ($p=0.6760$). Overall, RK-RML+>RK-Mouse is more resistant to protease degradation after denaturation (D13, D18, PRC5, and 6H4) and the epitopes are less accessible (1B8, and PRC7) or more accessible (D18) compared to RML>RK-Mouse.

RK-RML+ cell lysate (RK-RML+>RK-Mouse, dotted line) and RK-RML+ (dashed line) were compared via ESA (Figure 4.7D) and C-CSA (Figure 4.7E). RK-RML+>RK-Mouse GdnHCl $\frac{1}{2}$ and curve fits derived from ESA do not resemble RK-RML+ at: D18 ($p=0.0001$, $p<0.0001$), and PRC7 ($p<0.0001$, $p<0.0001$). The 1B8 epitope has a significantly different ($p<0.0001$) curve but not significantly different GdnHCl $\frac{1}{2}$ values ($p=0.7033$). When examining the same prion pair with C-CSA (Figure 4.7E), the GdnHCl $\frac{1}{2}$ and curve fits remained significantly different at: D18 ($p=0.0072$, $p<0.0001$), PRC5 ($p=0.0497$, $p<0.0001$), and 6H4 ($p=0.0235$, $p=0.0064$). As mentioned, PRC7 is not significantly different at GdnHCl $\frac{1}{2}$ and curve fits; likewise, D13 has non-significant GdnHCl $\frac{1}{2}$ ($p=0.9999$), and curve fit ($p=0.9999$). Overall, RK-RML+>RK-Mouse is more resistant to protease degradation after denaturation (D18, PRC5, and 6H4) and the epitopes are less accessible (1B8, D18 and PRC7) compared to RK-RML+.

22L>RK-Mouse fresh infection [brains (n=3) from terminally ill C57Bl/6 inbred mice infected with 22L were used to infect RK-Mouse], chronically infected cell lines that perpetually propagate 22L prion infection (RK-22L+), and naïve RK-Mouse cells infected with RK-22L+ cell lysate (RK-22L+>RK-Mouse) were compared. RK-22L+>RK-Mouse (dotted line) and 22L>RK-Mouse (solid line) were compared via C-CSA (Figure 4.7F). RK-22L+>RK-Mouse and 22L>RK-Mouse have significantly different GdnHCl $\frac{1}{2}$ at D18 ($p<0.0001$), PRC5 ($p<0.0001$), and 6H4 ($p=0.0007$). The GdnHCl $\frac{1}{2}$ values were not significantly different at D13 ($p=0.0952$), but it had significantly different curve fits ($p<0.0001$). All the epitopes examined had significantly different ($p<0.0001$) curve fits: D13, D18, PRC5, and 6H4. This difference is lost somewhat when comparing RK-22L+>RK-Mouse and RK-22L+ (dashed line). The curve fit was only significantly different at D18 ($p=0.0108$) and 6H4 ($p<0.0001$); and GdnHCl $\frac{1}{2}$ values significantly different at D18 ($p=0.0068$) and 6H4 ($p=0.0004$). The GdnHCl $\frac{1}{2}$ values and curve fits were not significantly different at both D13 ($p=0.3565$, $p=0.2279$) and PRC5 ($p=0.9999$, $p=0.9999$). RK-22L+>RK-Mouse is more similar to the chronic RK-22L+ origin than freshly infected 22L PrP^{Sc}; RK-22L+>RK-Mouse is more resistant to protease degradation after denaturation (D18, PRC5, and 6H4) than freshly infected 22L PrP^{Sc}.

Ultimately, PrP^{Sc} structure from chronically infected cell lysate does not recapitulate the PrP^{Sc} structure from brain source material or the PrP^{Sc} structure from the chronically prion infected cells that the lysate was derived from. Moreover, the PrP^{Sc} structure in chronically infected cells is not stable, and undergoes changes when it is passaged. Chronically passaged murine adapted scrapie (22L and RML) is more similar to its

chronic cell origin than chronically passaged CWD in deer or elk. However, Figure 4.7 further emphasizes the subtle variations that the C-CSA and ESA methods can uncover.

Given the instability of the prion conformation in chronically infected lines, we then examined the extent the conformation of the chronic cell lines would be maintained or altered with passage back into a mouse model (Figure 4.8). To that end, brains (n=3) from terminally ill Tg(DeerPrP)1536^{+/-} mice infected with cell lysate from chronically prion infected RK-Elk⁺ cells were used to infect RK-Deer cells; noted as RK-Elk⁺>Tg(Deer)>RK-Deer. This bioassay material was compared to fresh infections: brains (n=3) from terminally ill Tg(ElkPrP)5037^{+/-} and Tg(DeerPrP)1536^{+/-} mice infected with elk CWD isolate Bala05 were used to infect RK-Elk and RK-Deer, respectively; noted as Elk-CWD>RK-Elk and Deer-CWD>RK-Deer. This bioassay material was additionally compared to chronically infected cell lines that perpetually propagate CWD prion infection; noted as RK-Deer⁺, RK-Elk⁺. Resultant prions were analyzed with the multiple antibodies (Figure 3.1B) via the ESA (Figure 3.2).

Epitope accessibility of PK-treated, non-denatured RK-Elk⁺>Tg(Deer)>RK-Deer PrP^{Sc} is unlike freshly infected (Deer-CWD>RK-Deer) or chronically infected RK-Deer⁺ at most epitopes compared (Figure 4.8A). When comparing the epitope accessibility of RK-Elk⁺>Tg(Deer)>RK-Deer PrP^{Sc} to freshly infected Deer-CWD>RK-Deer PrP^{Sc} is significantly different at all epitopes examined: PRC1 (p=0.0009), D13 (p<0.0001), D18 (p=0.0110), PRC5 (p<0.0001), 6H4 (p=0.0229), and PRC7 (p=0.0381). RK-Elk⁺>Tg(Deer)>RK-Deer PrP^{Sc} is more like chronically infected RK-Deer⁺; there are no significant differences at PRC1 (p=0.1788), D13 (p=0.1367), and D18 (p=0.1296).

However, there are significant differences at 1B8 ($p=0.0005$), PRC5 ($p<0.0001$), 6H4 ($p<0.0001$), and PRC7 ($p=0.0044$). The epitope accessibility of PK-treated, non-denatured RK-Elk+>Tg(Deer)>RK-Deer PrP^{Sc} is unlike freshly infected (Elk-CWD>RK-Elk) or chronically infected RK-Elk+ at most epitopes compared (Figure 4.8B). When comparing the epitope accessibility of RK-Elk+>Tg(Deer)>RK-Deer PrP^{Sc} to freshly infected Elk-CWD>RK-Elk PrP^{Sc} is significantly different at all epitopes examined: PRC1 ($p=0.0003$), D13 ($p<0.0001$), D18 ($p=0.0117$), PRC5 ($p<0.0001$), 6H4 ($p=0.0005$), and PRC7 ($p<0.0001$). RK-Elk+>Tg(Deer)>RK-Deer PrP^{Sc} is more like chronically infected RK-Elk+; there are no significant differences at PRC1 ($p=0.8647$), D13 ($p=0.1587$), and D18 ($p=0.9425$). However, there are significant differences at 1B8 ($p=0.0002$), PRC5 ($p<0.0001$), 6H4 ($p<0.0001$), and PRC7 ($p=0.0137$). Overall, RK-Elk+>Tg(Deer)>RK-Deer PrP^{Sc} is more like chronically infected (RK-Deer+ and RK-Elk+) than freshly infected even though the material was passaged back through Tg(DeerPrP)1536^{+/-} mice.

As mentioned, conformational stability assays and the ESA rely on the GdnHCl_{1/2} value to differentiate strains and provide further information about the relative stability of the molecule and how available or resistant the epitope is to detection. To that end, each prion pair (Figure 4.8A-B) was compared for the GdnHCl_{1/2} value of each antibody probed that yielded a GdnHCl 1/2 value (Figure 4.8 C-F). The GdnHCl 1/2 value represents the midway point of the linear denaturation until the entire molecule is accessible and the curve fit value represents how the prion is responding to denaturation by GdnHCl. As such, the GdnHCl_{1/2} and curve fit have been indicated.

Using both points is an important distinction, allowing a more nuanced evaluation of prion structure.

The trend of RK-Elk+>Tg(Deer)>RK-Deer PrP^{Sc} resembling RK-Deer+ more than Deer-CWD>RK-Deer in the PK-treated, non-denatured epitope accessibility (Figure 4.8A) is not recapitulated with the GdnHCl $\frac{1}{2}$ and curve fit data (Figure 4.8 C, E); although, the overall pattern of epitope accessibility is shifted to be more accessible in RK-Elk+>Tg(Deer)>RK-Deer PrP^{Sc} compared to Deer-CWD>RK-Deer. The GdnHCl $\frac{1}{2}$ values and curve fit values for RK-Elk+>Tg(Deer)>RK-Deer PrP^{Sc} and Deer-CWD>RK-Deer are significantly different ($p<0.0001$) at every epitope examined: PRC1, D13, D18, PRC5, 6H4, and PRC7. The GdnHCl $\frac{1}{2}$ values of RK-Elk+>Tg(Deer)>RK-Deer PrP^{Sc} and RK-Deer+ are significantly different at every epitope examined: PRC1 ($p=0.0012$), D13 ($p<0.0001$), 1B8 ($p<0.0001$), D18 ($p<0.0001$), PRC5 ($p=0.0010$), 6H4 ($p=0.0017$), and PRC7 ($p<0.0001$). The curve fit for the pair is also significantly different at every epitope examined: PRC1 ($p<0.0001$), D13 ($p<0.0001$), 1B8 ($p<0.0001$), D18 ($p<0.0001$), PRC5 ($p<0.0001$), 6H4 ($p=0.0009$), and PRC7 ($p<0.0001$). Overall, the patterns are similar, but subtle differences between structures are evident.

The trend of RK-Elk+>Tg(Deer)>RK-Deer PrP^{Sc} resembling RK-Elk+ more than Elk-CWD>RK-Elk in the PK-treated, non-denatured epitope accessibility (Figure 4.8A) is recapitulated with the GdnHCl $\frac{1}{2}$ and curve fit data (Figure 4.8 D, F); the overall pattern of epitope accessibility is shifted to be less accessible in RK-Elk+>Tg(Deer)>RK-Deer PrP^{Sc} compared to RK-Elk+. The GdnHCl $\frac{1}{2}$ values of RK-Elk+>Tg(Deer)>RK-Deer PrP^{Sc} and Elk-CWD>RK-Elk are significantly different at every epitope examined:

PRC1 ($p=0.0001$), D13 ($p=0.0306$), D18 ($p<0.0001$), PRC5 ($p=0.0002$), 6H4 ($p=0.0026$), and PRC7 ($p=0.0001$). The curve fit for the pair is also significantly different ($p<0.0001$) at almost every epitope examined: D13, D18, PRC5, 6H4, and PRC7. PRC1 does not have a significantly different curve fit ($p=0.0672$) although the GdnHCl $\frac{1}{2}$ is significantly different; implying that the curve is the same for both, but shifted to produce different GdnHCl $\frac{1}{2}$ values. The GdnHCl $\frac{1}{2}$ values of RK-Elk+>Tg(Deer)>RK-Deer PrP^{Sc} and RK-Elk+ are significantly different at some epitopes examined: PRC1 ($p<0.0001$), D18 ($p<0.0001$), PRC5 ($p=0.0008$), 6H4 ($p=0.0065$), and PRC7 ($p<0.0001$). Two epitopes did not have significantly different GdnHCl $\frac{1}{2}$ values: D13 ($p=0.4924$) and 1B8 ($p=0.9244$). The curve fit for the pair is also significantly different at almost every epitope examined: PRC1 ($p<0.0001$), D13 ($p=0.0068$), D18 ($p<0.0001$), PRC5 ($p<0.0001$), 6H4 ($p<0.0001$), and PRC7 ($p<0.0001$). 1B8 does not have a significantly different curve fit ($p=0.1391$) or GdnHCl $\frac{1}{2}$ value; implying that they share this epitope exactly. Overall, the expectation RK-Elk+>Tg(Deer)>RK-Deer PrP^{Sc} retains the tertiary structure of the original RK-Elk+ or Elk-CWD PrP^{Sc} is not statistically apparent throughout the molecule.

Overall, chronically infected cell material passaged through Tg(DeerPrP)^{1536+/-} mice does not recapitulate the brain source material or the chronically infected cells they were derived from. PrP^{Sc} is altered in PK-treated, non-denatured PrP^{Sc} epitopes accessibility and causes PrP^{Sc} structural differences in response to GdnHCl $\frac{1}{2}$ and curve fit. The pattern does retain a similarity to other CWD PrP^{Sc} examined, but subtle differences between structures are evident.

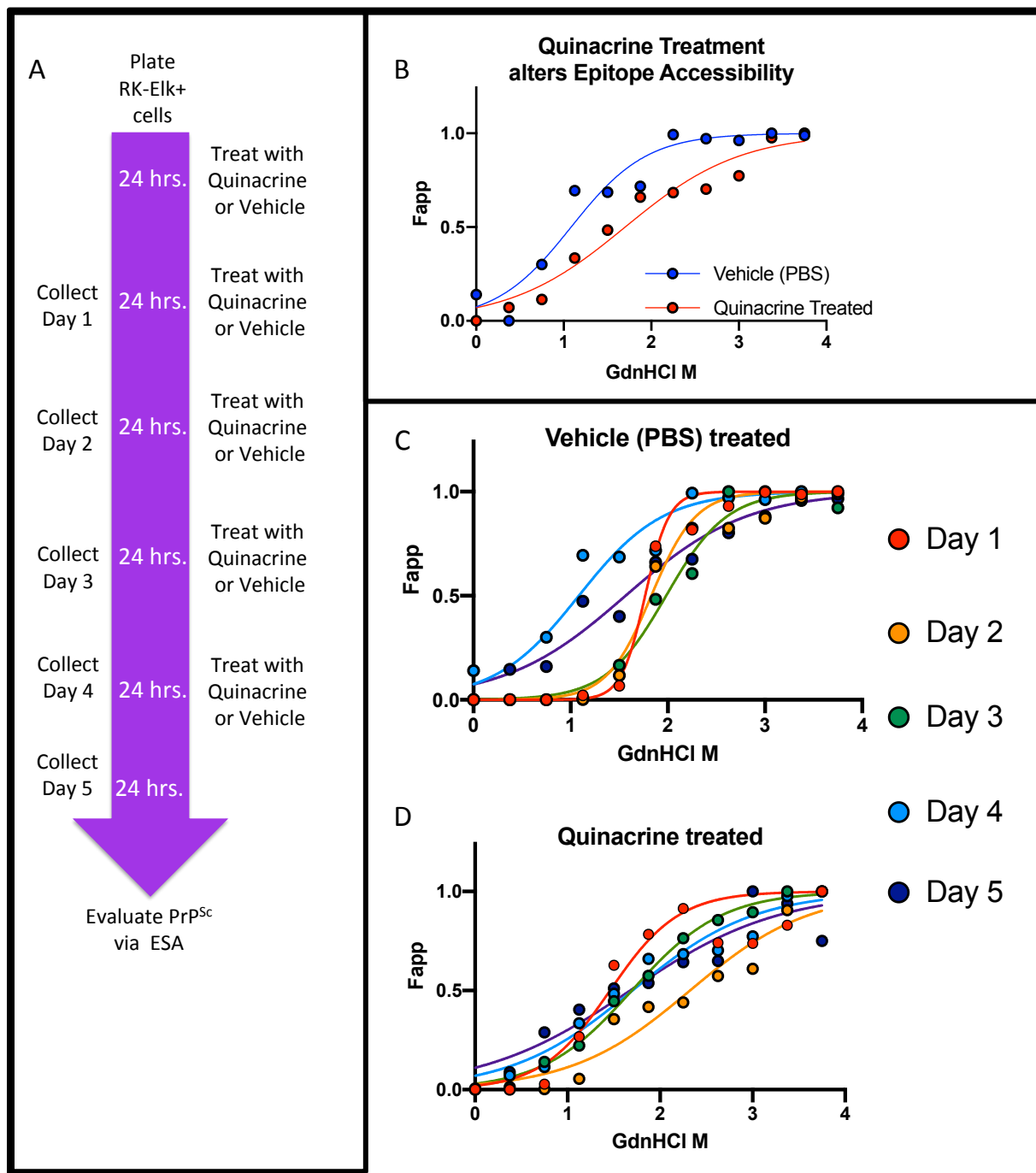


FIGURE 4.1: Pilot study, ESA can be used to examine changes due to quinacrine but published methodology⁴⁸ is insufficient to gauge daily changes (A) Treatment methodology used RK-Elk+, CWD chronically infected rabbit kidney epithelial cells expressing elk PrP^C, were treated for 5 days following splitting onto a new plate with media containing vehicle (PBS) or quinacrine (1 μ M). Resultant prions were examined interrogated with anti-prion antibody (6H4) via the ESA (Figure 3.2). (B) ESA is able to differentiate between quinacrine-treated and vehicle-treated elk PrP^{Sc}; quinacrine

treatment increases the GdnHCl $\frac{1}{2}$ value. Shown: Day 4 data (C) Vehicle-treated RK-Elk+, Day 1-5, contains no consistency. Without a stable control, daily comparisons to (D) Quinacrine-treated RK-Elk+, Day 1-5, becomes problematic.

Fapp, fraction of apparent signal. The sigmoidal dose-response curve was plotted using a four parameter algorithm and nonlinear least-squares fit; with curve comparison. Pilot study (n=1), chronic cell lines per group. Statistical comparisons unavailable.

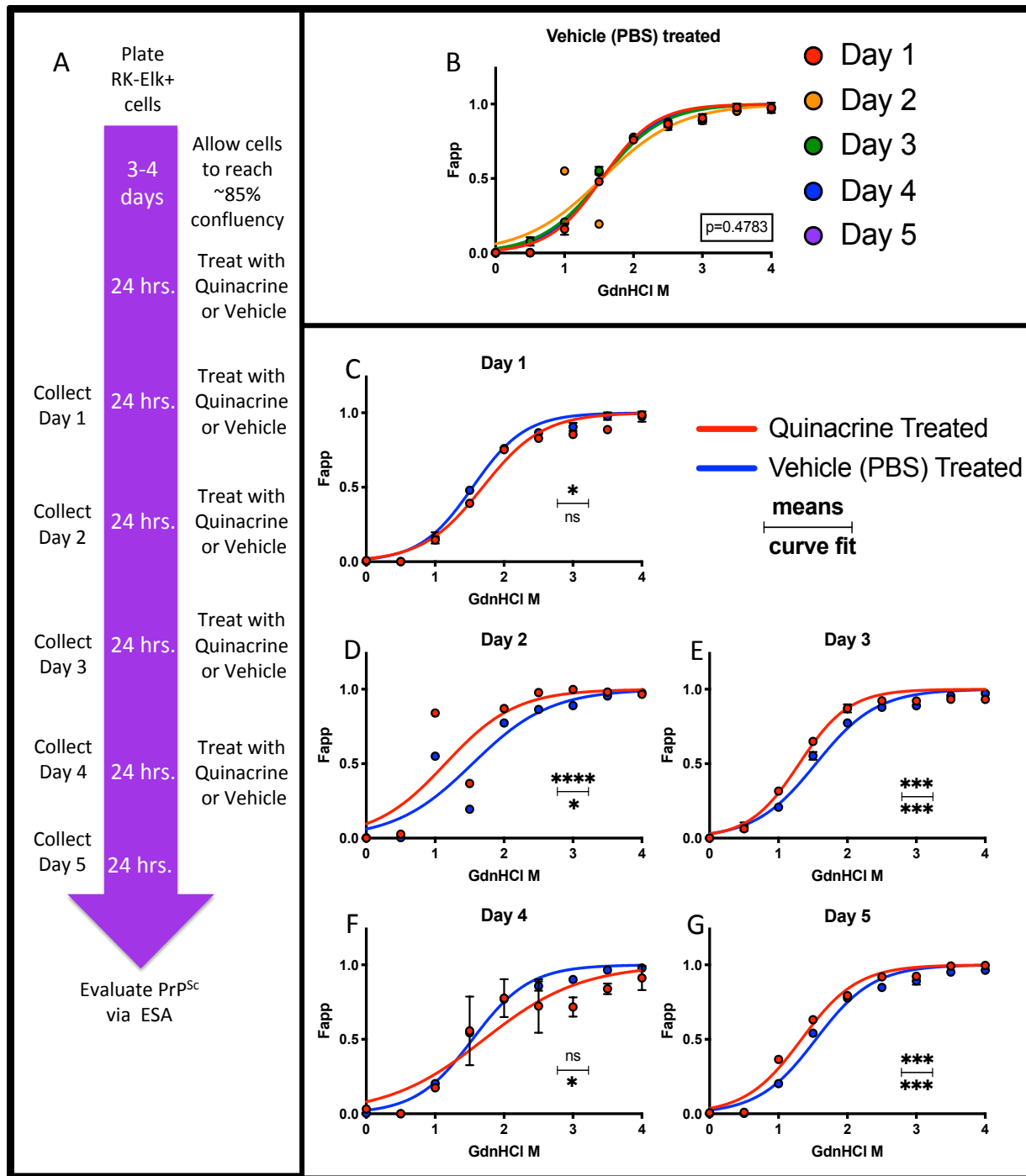


FIGURE 4.2 ESA can uncover subtle conformational changes to PrP^{Sc} over the first 5 days that the prion is exposed to quinacrine at the 6H4 epitope. Quinacrine-treated elk PrP^{Sc} is continuously changing at epitope 6H4 over 5 days, implying that quinacrine destabilizes the structure of elk PrP^{Sc} continuously. (A) Treatment methodology used: RK-Elk+, CWD chronically infected rabbit kidney epithelial cells expressing elk PrP^C, were treated for 5 days following growth to ~85% confluency with media containing vehicle (PBS) or quinacrine (1 μ M). Resultant prions were interrogated with anti-prion

antibody (6H4) via the ESA (Figure 3.2). **(B)** Vehicle-treated RK-Elk+, Day 1-5, are not significantly different ($p=0.4783$). This implies that daily changes are due to quinacrine treatment; comparisons are made at **(C)** 24 hours post treatment, **(D)** 2 days post treatment, **(E)** 3 days post treatment, **(F)** 4 days post treatment, and **(G)** 5 days post treatment.

Fapp, fraction of apparent signal. The sigmoidal dose-response curve was plotted using a four parameter algorithm and nonlinear least-squares fit; with curve comparison. Error bars, SD from $n=3$ per group. Statistical significance: ns $p > 0.05$; * $p \leq 0.05$; ** $p \leq 0.01$; *** $p \leq 0.001$; **** $p \leq 0.0001$. Statistical differences from the $GdnHCl_{1/2}$ values between matched, curves were calculated by curve fit parameters and via t-test (means)

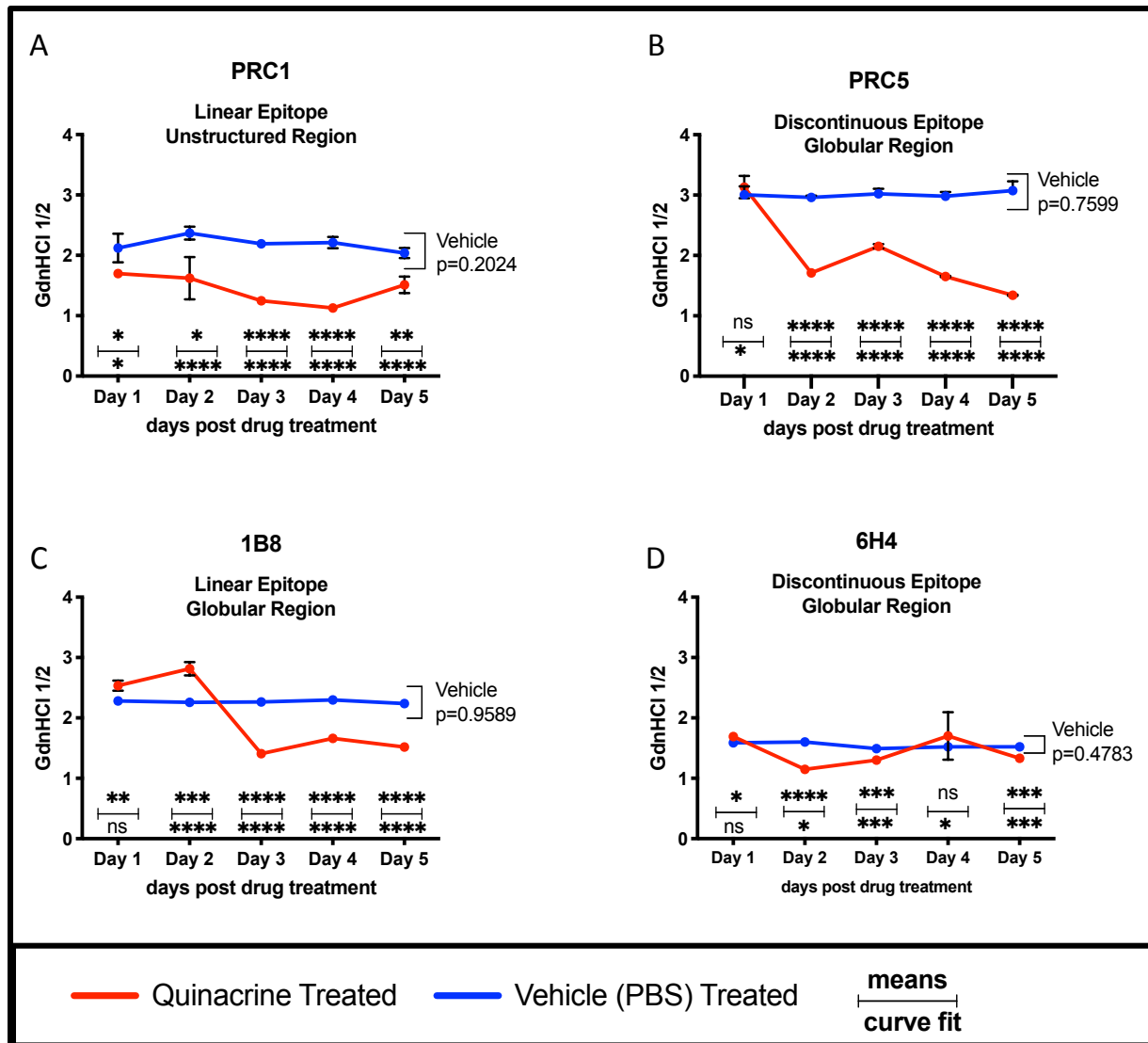


FIGURE 4.3: ESA can uncover subtle conformational changes to PrP^{Sc} over the first 5 days that the prion is exposed to quinacrine at multiple epitopes. CWD chronically infected RK-Elk+ cell lines were treated with media containing vehicle (PBS) or quinacrine (1 μ M) for 5 consecutive days (Figure 4.2A). Resultant prions were interrogated with anti-prion antibodies (A) PRC1, (B) PRC5, (C) 1B8, and (D) 6H4 (Figure 3.1B) via the ESA (Figure 3.2). Vehicle-treated RK-Elk+, Day 1-5, are not significantly different at epitopes: PRC1 ($p=0.2024$), PRC5 ($p=0.7599$), 1B8 ($p=0.9589$), and 6H4 ($p=0.4783$).

The sigmoidal dose-response curve was plotted using a four parameter algorithm and nonlinear least-squares fit; with best fit curve comparison. Error bars, SD from $n=3$ per group. Statistical significance: ns $p > 0.05$; * $p \leq 0.05$, ** $p \leq 0.01$; *** $p \leq 0.001$; **** $p \leq 0.0001$. Statistical differences from the GdnHCl_{1/2} values between matched, curves were calculated by curve fit parameters and via t-test (means)

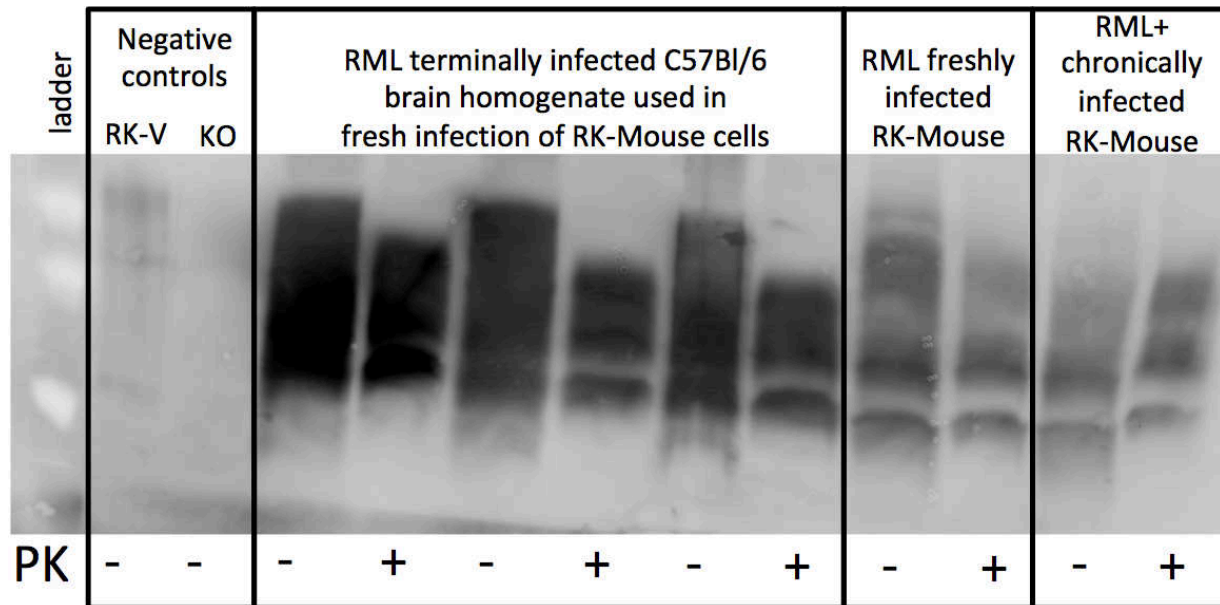


FIGURE 4.4: Traditional techniques do not adequately distinguish fresh and chronically infected cells. Cell lysate from RK-V (vector only, PrP^C null) cell line, brain homogenate from a PrP-KO (PrP^C null) mouse (KO), brain homogenate from terminally ill C57BL/6 inbred mice infected with RML (n=3), cell lysate from RML infected RK-Mouse cell line, and cell lysate from RML chronically infected RK-Mouse cells line (RK-RML+) were interrogated with anti-prion antibody PRC5 via western blot. PK indicates usage (+) of proteinase K to ablate PrP^C signal and allow detection of PrP^{Sc}, lack of PK (-) indicates total PrP^C and PrP^{Sc} fraction.

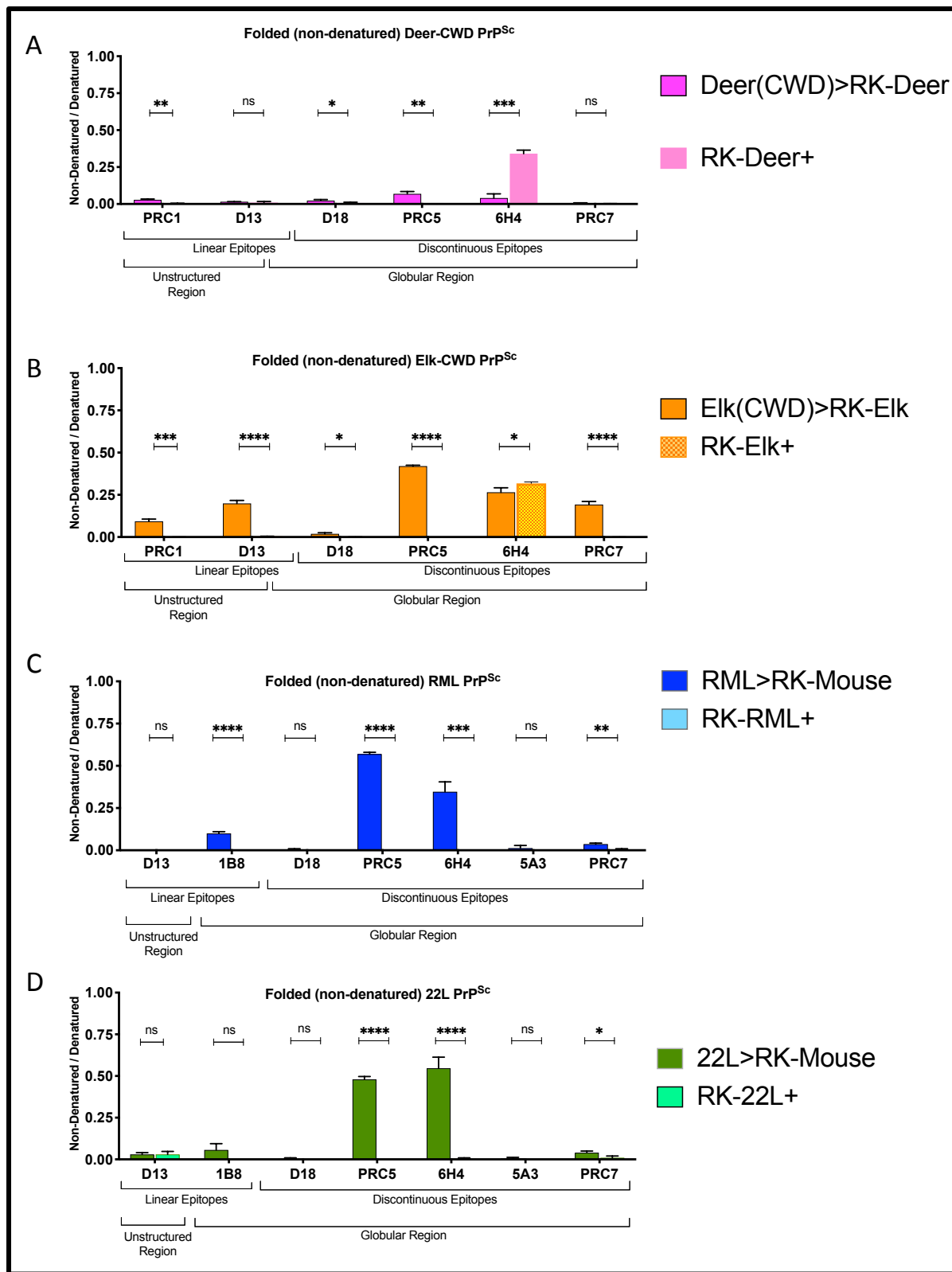


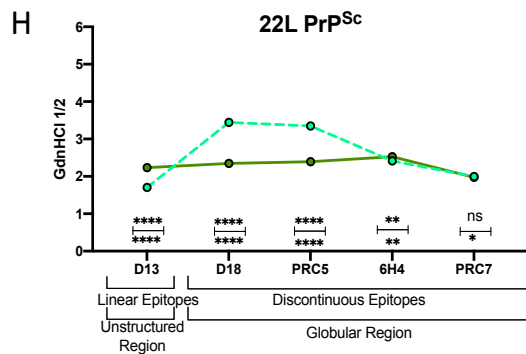
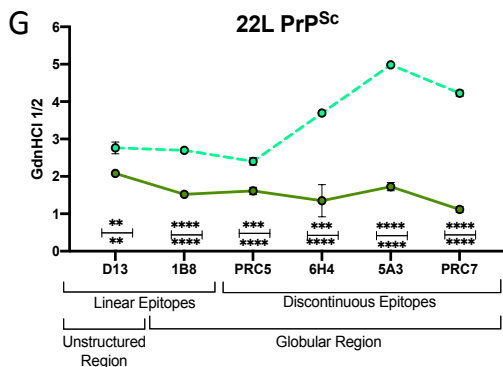
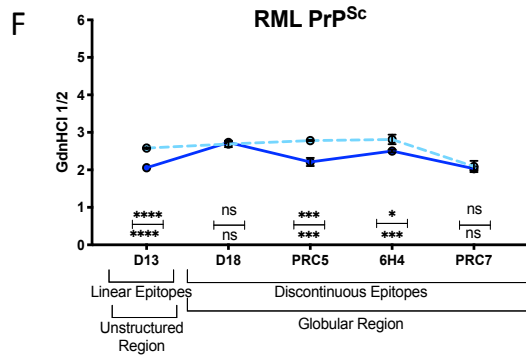
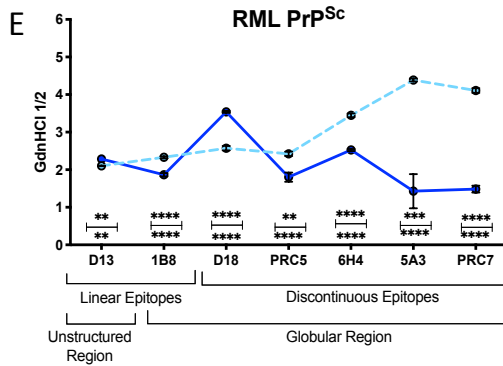
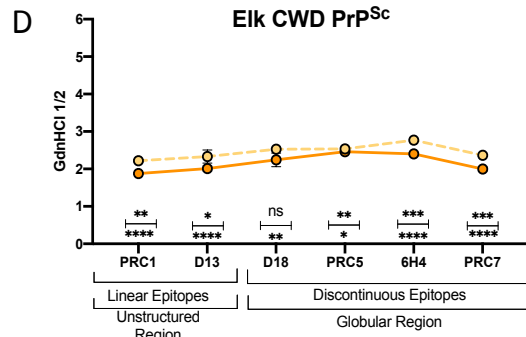
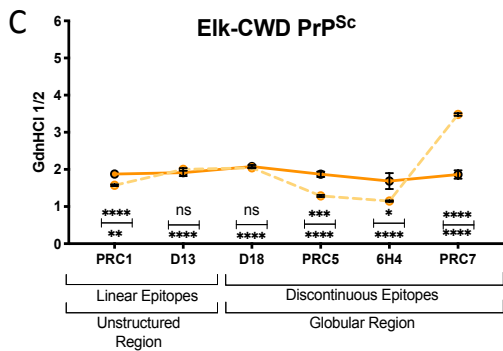
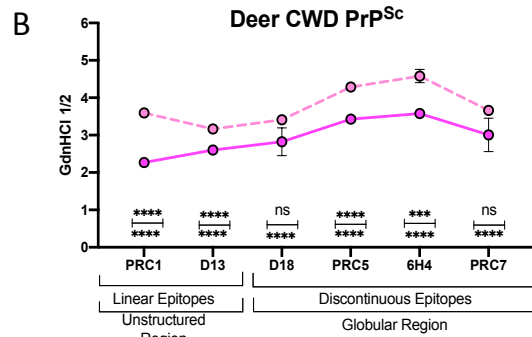
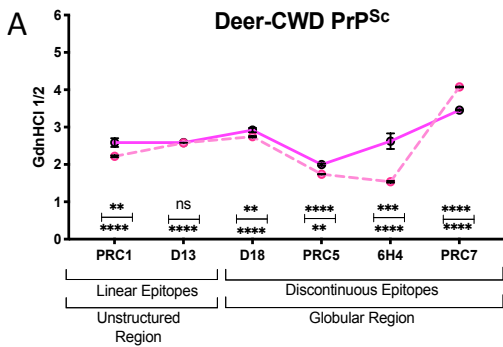
FIGURE 4.5: Chronic prion infection alters PK-treated, non-denatured PrP^{Sc} epitopes accessibility. All prions were examined with an array of epitope-mapped antibodies

(Figure 3.1B) via the ESA (Figure 3.2); however, antibody 5A3 is murine-specific and not used to detect cervid prion strains, and PRC1 is cervid-specific and not used to detect murine-adapted prion strains. **(A)** The chronically infected (RK-Deer+) cell line originated from RK-Deer cells infected with brain homogenate from terminally ill Tg(DeerPrP)1536^{+/-} mice infected with elk CWD isolate 012-9442, then passaged a minimum of 15 times, and then single cell cloned³³. The freshly infected cell line, Deer-CWD>RK-Deer, was derived from: brains (n=3) from terminally ill Tg(DeerPrP)1536^{+/-} mice infected with elk CWD isolate Bala05 were used to infect RK-Deer cell line. **(B)** The chronically infected (RK-Elk+) cell line originated from RK-Elk cells infected with brain homogenate from terminally ill Tg(ElkPrP)5037^{+/-} mice infected with elk CWD isolate 012-9442, then passaged a minimum of 15 times, and then single cell cloned³³. The freshly infected cell line, Elk-CWD>RK-Elk, was derived from: brains (n=3) from terminally ill Tg(ElkPrP)5037^{+/-} mice infected with elk CWD isolate Bala05 were used to infect RK-Elk cell line. **(C)** The freshly infected cell line, RML>RK-Mouse, was derived from: brains (n=3) from terminally ill C57BL/6 mice infected with murine-adapted scrapie strain, RML, was used to infect murine- PrP^C expressing RK13 (RK-Mouse) cells. The chronically infected (RK-RML+) cell line were derived from the freshly infected cell population. After collection for the fresh segment of analysis, the remaining cells were combine into one pool, then passaged a minimum of 15 times. **(D)** The freshly infected cell line, 22L>RK-Mouse, was derived from: brains (n=3) from terminally ill C57BL/6 mice infected with murine-adapted scrapie strain, 22L, was used to infect murine- PrP^C expressing RK13 (RK-Mouse) cells. The chronically infected (RK-22L+) cell line were derived from the freshly infected cell population. After collection for the fresh segment of analysis, the remaining cells were combine into one pool, then passaged a minimum of 15 times.

Y-axis: Ratio of non-denatured (GdnHCl 0M) signal by fully denatured (GdnHCl 5.5M) signal. X-axis: anti-prion antibodies used. Error bars SD n=3 animals, or n=3 cells per group. Statistical differences were calculated by t-test (means) of the ratio of non-denatured (GdnHCl 0M) signal by fully denatured (GdnHCl 5.5M) signal.

ESA

C-CSA



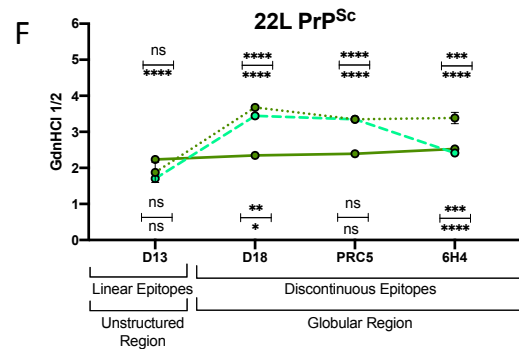
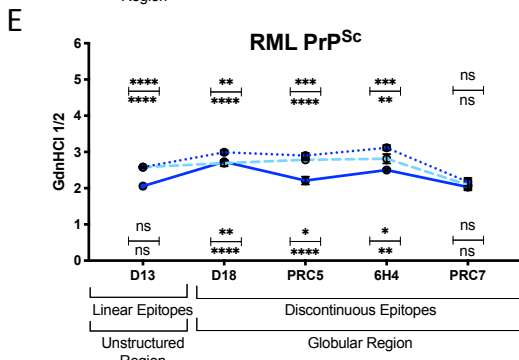
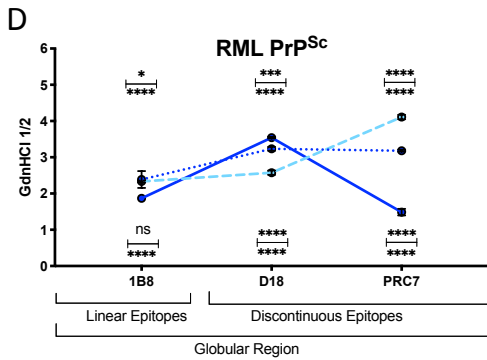
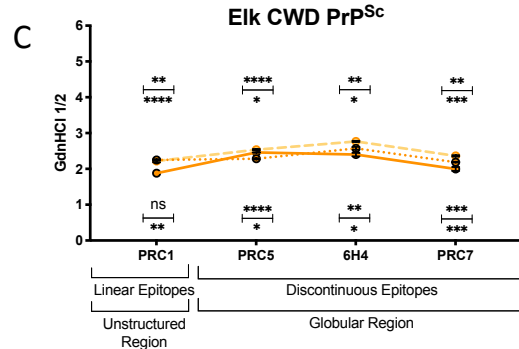
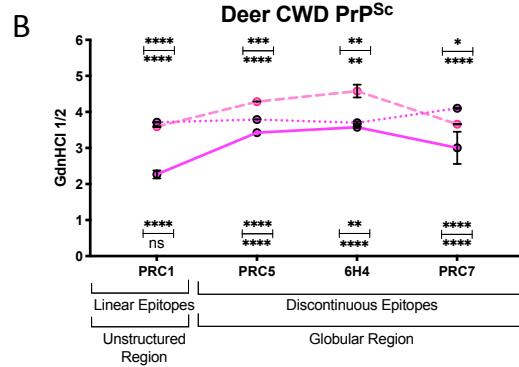
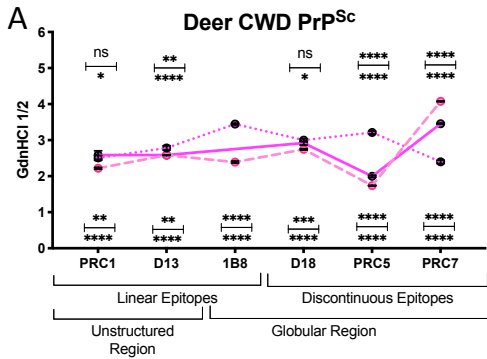
— Freshly Infected - - - Chronically Infected

FIGURE 4.6: Chronically infected cell lines do not have the same PrP^{Sc} structure as Freshly infected cells. Cell line comparisons (Figure 4.5) were compared for GdnHCl_{1/2} values and curve fit across multiple antibodies (Figure 3.1B) with the ESA method (Figure 3.2) and the C-CSA method (Figure 2.2). The GdnHCl_{1/2} value and curve fit comparisons further supports that PrP^{Sc} structure in chronically infected lines is not identical to freshly infected lines. Comparison between chronically infected RK-Deer+ PrP^{Sc} and freshly infected Deer(CWD)>RK-Deer PrP^{Sc} via the **(A)** ESA method and **(B)** C-CSA method. Comparison between chronically infected RK-Elk+ PrP^{Sc} and freshly infected Elk(CWD)>RK-Elk PrP^{Sc} via the **(C)** ESA method and **(D)** C-CSA method. Comparison between chronically infected RK-RML+ PrP^{Sc} and freshly infected RML>RK-Mouse PrP^{Sc} via the **(E)** ESA method and **(F)** C-CSA method. Comparison between chronically infected RK-22L+ PrP^{Sc} and freshly infected 22L>RK-Mouse PrP^{Sc} via the **(G)** ESA method and **(H)** C-CSA method.

The sigmoidal dose-response curve was plotted using a four parameter algorithm and nonlinear least-squares fit; with best fit curve comparison. Error bars, SD from n=3 animals or cells per group. Statistical significance: ns p > 0.05; * p ≤ 0.05, ** p ≤ 0.01; *** p ≤ 0.001; **** p ≤ 0.0001. Statistical differences from the GdnHCl_{1/2} values between matched, curves were calculated by curve fit parameters and via t-test (means)

ESA

C-CSA



— Freshly Infected
 - - Chronically Infected
 . . . Chronic Lysate Infected
 means
 ——— curve fit

Top (Freshly Infected: Chronic Lysate)
 Bottom (Chronically Infected: Chronic Lysate)

FIGURE 4.7: PrP^{Sc} structure from chronically infected cell lysate does not recapitulate the brain source material or the cells they were derived from in chronically infected; the PrP^{Sc} structure in chronically infected cells is not stable, and undergoes changes when it is passaged Cell lysate from chronically prion infected cell lines was used to infect naïve RK-PrP cells and the resultant prions were compared for GdnHCl_{1/2} values and curve fit across multiple antibodies (Figure 3.1B) with the ESA method (Figure 3.2) and the C-CSA method (Figure 2.2). The new cell lysate infection was compared to fresh infection with brain homogenate and the chronically infected cells used for the lysate infection. The GdnHCl_{1/2} value and curve fit comparisons further supports that PrP^{Sc} structure in chronically infected lines is not stable when passaged into naïve RK-PrP cells. Comparison between RK-Deer+ cell lysate (RK-Deer+>RK-Deer, dotted line), chronically CWD infected RK-Deer+ (dashed line), and freshly infected Deer-CWD>RK-Deer (solid line) were compared via the **(A)** ESA method and **(B)** C-CSA method. Comparison between RK-Elk+ cell lysate (RK-Elk+>RK-Elk, dotted line), chronically CWD infected RK-Elk+ (dashed line) and freshly infected Elk(CWD)>RK-Elk (solid line) via the **(C)** C-CSA method. Comparison between RK-RML+ cell lysate (RK-RML+>RK-Mouse, dotted line), chronically infected RK-RML+ (dashed line) and freshly infected RML>RK-Mouse (solid line) via the **(D)** ESA method and **(E)** C-CSA method. Comparison between RK-22L+ cell lysate (RK-22L+>RK-Mouse, dotted line), chronically infected RK-22L+ (dashed line) and freshly infected 22L>RK-Mouse (solid line) via the **(F)** C-CSA method.

The sigmoidal dose-response curve was plotted using a four parameter algorithm and nonlinear least-squares fit; with best fit curve comparison. Error bars, SD from n=3 animals or cells per group. Statistical significance: ns p > 0.05; * p ≤ 0.05, ** p ≤ 0.01; *** p ≤ 0.001; **** p ≤ 0.0001. Statistical differences from the GdnHCl_{1/2} values between matched, curves were calculated by curve fit parameters and via t-test (means). Top statistics indicated are comparing (Freshly Infected : Chronic Cell Lysate Infected); and the bottom statistics indicated are comparing (Chronically Infected : Chronic Cell Lysate Infected). Both statistical comparisons allow the PrP^{Sc} from chronic cell lysate infected to be compared to the brain homogenate PrP^{Sc}, and chronically prion infected cell PrP^{Sc}.

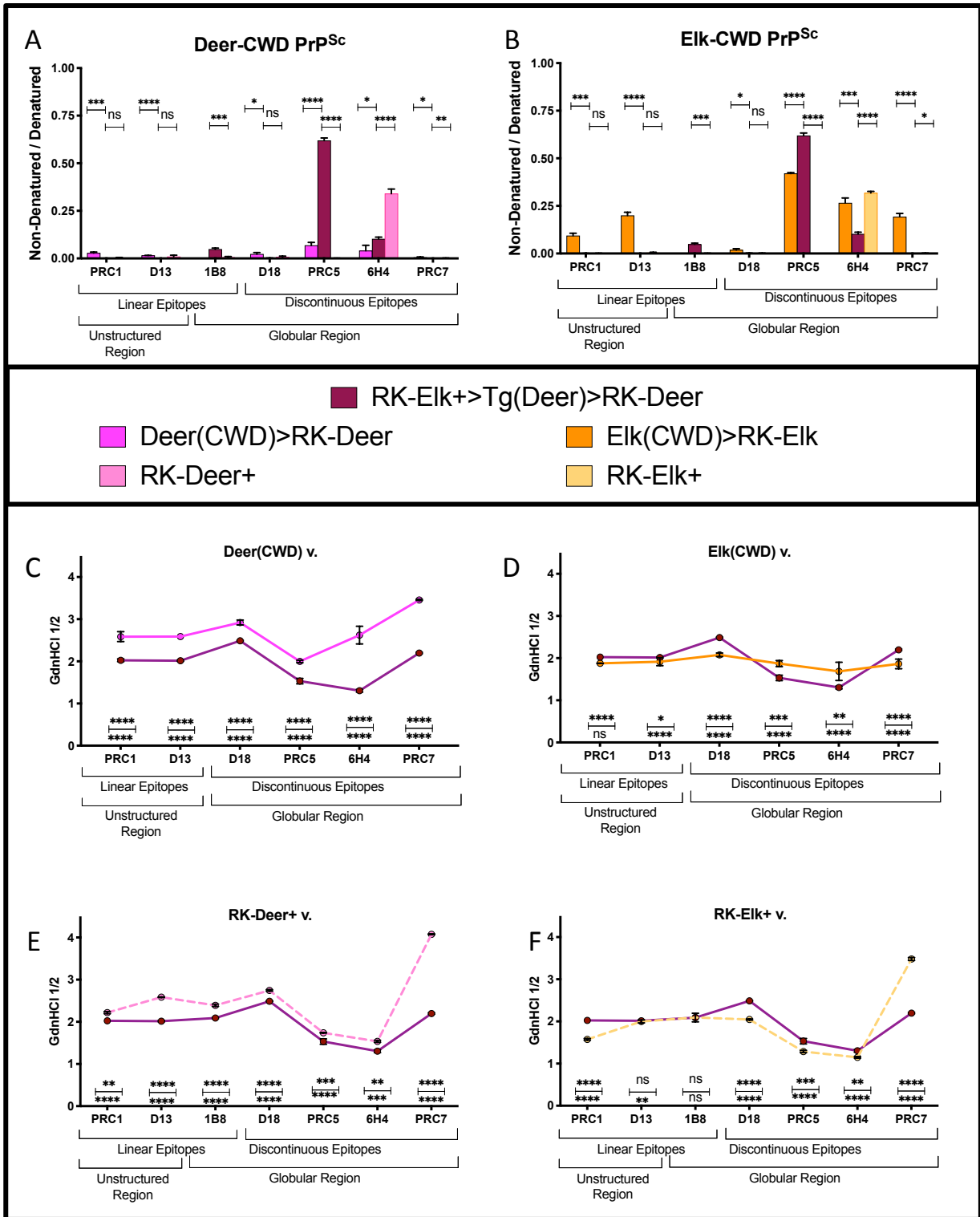


FIGURE 4.8: Passing chronically infected cell material through Tg(Deer) mice alters PK-treated, non-denatured PrP^{Sc} epitopes accessibility. Additionally, PrP^{Sc} structure from chronically infected cell material passaged through Tg(Deer) mice does not recapitulate the brain source material or the chronically infected cells they

were derived from; the PrP^{Sc} structure in chronically infected cells is not stable, and undergoes changes when it is passaged. Brains (n=3) from terminally ill Tg(DeerPrP)1536^{+/-} mice infected with cell lysate from chronically prion infected RK-Elk+ cells were used to infect RK-Deer cells; noted as RK-Elk+>Tg(Deer)>RK-Deer. This bioassay material was compared to fresh infections: brains (n=3) from terminally ill Tg(ElkPrP)5037^{+/-} and Tg(DeerPrP)1536^{+/-} mice infected with elk CWD isolate Bala05 were used to infect RK-Elk and RK-Deer, respectively; noted as Elk-CWD>RK-Elk and Deer-CWD>RK-Deer. This bioassay material was additionally compared to chronically infected cell lines that perpetually propagate CWD prion infection; noted as RK-Deer+, RK-Elk+. All prions were examined with an array of epitope-mapped antibodies (Figure 3.1B) via the ESA (Figure 3.2). **(A)** Comparisons between non-denatured (folded) RK-Elk+>Tg(Deer)>RK-Deer, Deer-CWD>RK-Deer, and RK-Deer+ **(B)** Comparisons between non-denatured (folded) RK-Elk+>Tg(Deer)>RK-Deer, Elk-CWD>RK-Elk, and RK-Elk+. Comparisons between GdnHCl ½ value and curve fit of RK-Elk+>Tg(Deer)>RK-Deer and **(C)** Deer(CWD)>RK-Deer. **(D)** Elk(CWD)>RK-Elk. **(E)** RK-Deer+. **(F)** RK-Elk+.

A - F:

Error bars SD RK-Elk+>Tg(Deer)>RK-Deer was n=3 and experimental replicated (n=6), fresh infections (Deer-CWD>RK-Deer, and Elk-CWD>RK-Elk) n=3 animals, and n=3 chronically infected (RK-Elk+, and RK-Deer+) cells per group. Statistical significance: ns p > 0.05; * p ≤ 0.05, ** p ≤ 0.01; *** p ≤ 0.001; **** p ≤ 0.0001.

A & B:

Y-axis: Ratio of non-denatured (GdnHCl 0M) signal by fully denatured (GdnHCl 5.5M) signal. X-axis: anti-prion antibodies used. Statistical differences were calculated by t-test (means) of the ratio of non-denatured (GdnHCl 0M) signal by fully denatured (GdnHCl 5.5M) signal.

C - F:

Y-axis: GdnHCl Moles X-axis: anti-prion antibodies used. The sigmoidal dose-response curve was plotted using a four parameter algorithm and nonlinear least-squares fit; with best fit curve comparison. Statistical differences from the GdnHCl_{1/2} values between matched, curves were calculated by curve fit parameters and via t-test (means).

D. DISCUSSION

We tracked prion evolution daily as it occurred, re-evaluating selection pressures on the faithful propagation of a specific misfolded prion form in a cell culture model. The results can be summarized into two components based on the forms of evolution evaluated: (1) drug-induced evolution, and (2) strain evolution in cell culture.

Drug-induced strain evolution

Understanding of prion evolution due to drug influence is important in understanding prion biology and is a necessary step along the path to find viable drug treatment options. A prominent limitation was that this was done in a single cell line: RK-Elk+. This limitation can be removed by performing the quinacrine experiment on RK-Deer+ cell line. Unexpectedly, the quinacrine-induced prion evolution in RK-Elk+ cell culture was subtle but detectable within 24 hours of treatment (Figure 4.2 and 4.3). The following days of treatment further significantly alter PrP^{Sc} structure; with drug-induced structural changes to PrP^{Sc} occur in the unstructured (PRC1) and globular regions (PRC5, 1B8, and 6H4), at linear (PRC1 and 1B8) and discontinuous (PRC5 and 6H4) epitopes. Furthermore, the structural changes are not stable, but in daily flux. This implies that prion structural evolution is a moving target that is not as stable as once thought. Additionally, this variation could be happening within animal models. This phenomenon needs to be kept in mind as a cautionary tail as the field moves forward locating a drug treatment for prion diseases.

The GdnHCl $\frac{1}{2}$ values were closer together at 6H4, a discontinuous epitope that spans the prion protein from before α helix-1 into α helix-3. 6H4 is a widely,

traditionally, used anti-prion antibody. Although subtle differences were seen with 6H4, massive discrete changes are occurring at other epitopes throughout the prion protein due to quinacrine. Overall, quinacrine has a greater impact on epitope accessibility at the linear epitope in the unstructured region (PRC1), discontinuous epitope straddles α helix-1 (PRC5), and linear epitope embedded in α helix-1 (1B8). Reliance on a single epitope will not reveal how changes can occur in micro-domains, and further reinforces the need to use multiple epitopes when exploring the complexities of prion structure. A limitation was that the study was limited to 5 days and taken in 24-hour periods. It would be advantageous to track the quinacrine-induced changes over more days to assess if the epitope accessibility changes stabilize. Additionally, the 24-hour periods are only giving snapshots of the changes occurring. Since the exact action of quinacrine on the prion protein is unknown, the time needed for quinacrine to perturb the prion protein is, also, unknown.

One future direction for this project could be to tracking daily changes of quinacrine treatment past the 5 days, to see if the structure stabilizes. Another future direction could be tracking drug-induced changes from other potential anti-prion therapies. Further, the stability of $GdnHCl$ $\frac{1}{2}$ and curve fit in RK-Elk+ treated with vehicle across five days further supports that the ESA method [Chapter 3] is reliable. However, when comparing PBS-treated RK-Elk+ treated with PBS to the evolution in cell culture RK-Elk+ data set, the $GdnHCl$ $\frac{1}{2}$ values are not identical. This could imply that the passage number of the RK-Elk+ cell line has some bearing on the structure of PrP^{Sc}. This could

be further explored by examining chronically infected lines at various passage numbers to see if PrP^{Sc} stays stable within chronic cell culture models.

Strain evolution in cell culture

Humans do not easily change fundamental ideas; we inherently resist ideas that challenge the status quo. However, to ensure scientific facts are accurate and for science to move forward, we must continually challenge our assumptions. A fundamental prion biology assumption that is challenged: chronically prion infected cell models will recapitulate molecular characteristics of a biological prion infection. This fundamental assumption rests on the faithfulness of prion strains to maintain strain properties through bioassay. It was a reasonable hypothesis that the strain specific PrP^{Sc} structure is stable in cell culture. Overall, chronically prion infected cell lines do not recapitulate fresh biological prion infection; this is seen when examining folded / non-denatured PrP^{Sc} (Figure 4.5), GdnHCl $\frac{1}{2}$ values and curve fits (Figure 4.6). Furthermore, the PrP^{Sc} in chronically prion infected cell lines is not stable upon passage into naïve cells (Figure 4.7) or into transgenic mice (Figure 4.8). It implies that new strains are being created through serial passage or that there is a selection for a specific conformation from the original quasi-species potluck. A future direction for the project would be tracking daily changes of from fresh infection into chronic infection status, or tracking chronic infection at various passages.

Serial passaging prions reduces epitope accessibility at folded / non-denatured PrP^{Sc} (Figure 4.5) for Deer-CWD, Elk-CWD, RML, and 22L. The exception is at epitope 6H4 for CWD prions, where there was clearly detectable signal without denaturation.

This could mean that serial passaging a prion selects for a more stable, inaccessible form without denaturation. The overall expectation that the GdnHCl $\frac{1}{2}$ values would be equal to fresh infection did not hold true for most epitopes examined (Figure 4.6) with the ESA [Chapter 3] or C-CSA [Chapter 2]. In general, serial passaging made prions more resistant to protease degradation after denaturation in three different species (deer PrP^C, elk PrP^C, and mouse PrP^C) with three different prions CWD, RML, and 22L. This is further evidence that supports this as a repeatable phenomenon. The overall epitope accessibility is less unified than resistant to protease degradation after denaturation. The single consistent change in epitope accessibility is at the glycosylation specific epitope, PRC7; in all three different species (deer PrP^C, elk PrP^C, and mouse PrP^C) with three different prions CWD, RML, and 22L the epitope is less accessible. This could imply that the glycosylation phenotype becomes unified with chronic passaging. In CWD, the epitope accessibility mirrors or varies from fresh infection dependent on the epitope examined. Again, this further shows the importance of using multiple epitopes in determining similarity or difference between prions. It, also, reinforces the importance of looking at the denaturation curve and GdnHCl $\frac{1}{2}$ values.

Once it was shown that chronically prion infected cell lines do not recapitulate fresh biological prion infection, we examined if the chronically prion infected cell lines maintained their PrP^{Sc} structure upon passage into naïve RK-PrP cells (Figure 4.7). Unlike the faithful recapitulation of a prion strain in bioassay, infection with chronic cell lysate did not maintain the PrP^{Sc} structure of chronic cells. The PrP^{Sc} structure of chronic cell lysate did not recapitulate chronic cell PrP^{Sc} structure or the PrP^{Sc} structure

of fresh infection. The differences were subtle and pronounced, depending on the epitope. Interestingly enough, chronic cell lysate PrP^{Sc} is similar to fresh brain infection PrP^{Sc} nearly as often as it is similar to chronic cell PrP^{Sc}. This implies that PrP^{Sc} is in a state of flux and not stable.

This instability is recapitulated when chronic prion cell lysate (RK-Elk+) is used to infect naïve transgenic Deer-PrP mice then used to infect RK-Deer cells (Figure 4.8). Although the paradigm is complex, it reinforces that that CWD PrP^{Sc} is in a state of flux and is not stable. The folded / non-denatured PrP^{Sc} of RK-Elk+>Tg(Deer)>RK-Deer is unlike CWD (in deer or elk) or chronically CWD infected cell lines (RK-Deer+ or RK-Elk+). Of all folded / non-denatured CWD PrP^{Sc} forms, RK-Elk+>Tg(Deer)>RK-Deer is the most exposed at PRC5. This is interesting because the other epitopes in the α helix-1 (1B8 and D18) are barely accessible. Even though the PRC5 epitope is more accessible without denaturation, RK-Elk+ is more has a more accessible GdnHCl ½ at PRC5. Although the final PrP^{Sc} of RK-Elk+>Tg(Deer)>RK-Deer is Deer-PrP, the GdnHCl ½ and curve fit do not match Deer-CWD>RK-Deer or RK-Deer+ at any epitope examined. It shares more similarities with Elk-CWD>RK-Elk and RK-Elk+. This means that although RK-Elk+ was passaged through mouse Deer-PrP^C and RK-Deer-PrP^C it retained more similarity with Elk-PrP^{Sc} structure. This could have bearing on how CWD structure acts transmitting in wild populations of Deer-PrP^C and Elk-PrP^C. This has special bearing on the transmission of CWD in Europe.

Ultimately, reliance of chronically infected cells as a basis for anti-prion therapeutic testing is not advisable as chronically infected lines do not resemble freshly infected

lines PrP^{Sc} structure. However, they still serve as a model system for understanding prion structure.

BIBLIOGRAPHY

-
- ¹ Prusiner SB (1982) Novel proteinaceous infectious particles cause scrapie. *Science* 216: 136-144
 - ² Oesch, B., Teplow, D. B., Stahl, N., Serban, D., Hood, L. E., & Prusiner, S. B. (1990). Identification of cellular proteins binding to the scrapie prion protein. *Biochemistry*, 29(24), 5848-5855.
 - ³ Basler, K., Oesch, B., Scott, M., Westaway, D., Wälchli, M., Groth, D. F., & Weissmann, C. (1986). Scrapie and cellular PrP isoforms are encoded by the same chromosomal gene. *Cell*, 46(3), 417-428.
 - ⁴ Bett C, Joshi-Barr S, Lucero M, Trejo M, Liberski P, et al. (2012) Biochemical Properties of Highly Neuroinvasive Prion Strains. *PLoS Pathog* 8(2)
 - ⁵ Belt, P. B., Muileman, I. H., Schreuder, B. E., Bos-de Ruijter, J., Gielkens, A. L., & Smits, M. A. (1995). Identification of five allelic variants of the sheep PrP gene and their association with natural scrapie. *Journal of General Virology*, 76(3), 509-517.
 - ⁶ Angers, R. C., H. E. Kang, D. Napier, S. Browning, T. Seward, C. Mathiason, A. Balachandran, D. McKenzie, J. Castilla, C. Soto, J. Jewell, C. Graham, E. A. Hoover, and G. C. Telling. 2010. Prion strain mutation determined by prion protein conformational compatibility and primary structure. *Science* 328:1154-1158.
 - ⁷ Goldfarb, L. G., Petersen, R. B., Tabaton, M., Brown, P., LeBlanc, A. C., Montagna, P., & Haltia, M. (1992). Fatal familial insomnia and familial Creutzfeldt-Jakob disease: disease phenotype determined by a DNA polymorphism. *SCIENCE-NEW YORK THEN WASHINGTON-*, 806-806.
 - ⁸ Colby, D. W., Giles, K., Legname, G., Wille, H., Baskakov, I. V., DeArmond, S. J., & Prusiner, S. B. (2009). Design and construction of diverse mammalian prion strains. *Proceedings of the National Academy of Sciences*, 106(48), 20417-20422.
 - ⁹ Peretz, D., Scott, M. R., Groth, D., Williamson, R. A., Burton, D. R., Cohen, F. E., & Prusiner, S. B. (2001). Strain-specified relative conformational stability of the scrapie prion protein. *Protein Science*, 10(4), 854-863.
 - ¹⁰ Collinge, J., Sidle, K. C., Meads, J., Ironside, J., & Hill, A. F. (1996). Molecular analysis of prion strain variation and the aetiology of 'new variant' CJD. *Nature*, 383(6602), 685.
 - ¹¹ Cobb, N. J., Apostol, M. I., Chen, S., Smirnovas, V., & Surewicz, W. K. (2014). Conformational stability of mammalian prion protein amyloid fibrils is dictated by a packing polymorphism within the core region. *Journal of Biological Chemistry*, 289(5), 2643-2650.
 - ¹² Telling, G. C., Scott, M., Hsiao, K. K., Foster, D., Yang, S. L., Torchia, M., & Prusiner, S. B. (1994). Transmission of creutzfeldt-jakob disease from humans to transgenic mice expressing chimeric human- mouse prion protein. *Proceedings of the National Academy of Sciences*, 91(21), 9936-9940.

-
- ¹³ Telling, G. C., M. Scott, J. Mastrianni, R. Gabizon, M. Torchia, F. E. Cohen, S. J. DeArmond, and S. B. Prusiner. 1995. Prion propagation in mice expressing human and chimeric PrP transgenes implicates the interaction of cellular PrP with another protein. *Cell* 83:79–90.
- ¹⁴ Torres, J. M., Espinosa, J. C., Aguilar-Calvo, P., Herva, M. E., Relañó-Ginés, A., Villadiaz, A., & Castilla, J. (2014). Elements modulating the prion species barrier and its passage consequences. *PloS one*, 9(3), e89722.
- ¹⁵ Collinge, J. (2012). The risk of prion zoonoses. *Science*, 335(6067), 411-413.
- ¹⁶ Bruce, M. E., Will, R. G., Ironside, J. W., McConnell, I., Drummond, D., Suttie, A., & Cousens, S. (1997). Transmissions to mice indicate that ‘new variant’ CJD is caused by the BSE agent. *Nature*, 389(6650), 498-501.
- ¹⁷ Collinge, J., & Clarke, A. R. (2007). A general model of prion strains and their pathogenicity. *Science*, 318(5852), 930-936.
- ¹⁸ Tixador, P., Herzog, L., Reine, F., Jaumain, E., Chapuis, J., Le Dur, A., & Beringue, V. (2010). The physical relationship between infectivity and prion protein aggregates is strain-dependent. *PLoS Pathog*, 6(4), e1000859.
- ¹⁹ Klohn, P. C., L. Stoltze, E. Flechsig, M. Enari, and C. Weissmann. 2003. A quantitative, highly sensitive cell-based infectivity assay for mouse scrapie prions. *Proc Natl Acad Sci U S A* 100:11666-71.
- ²⁰ van Der Merwe, J., Aiken, J., Westaway, D., & McKenzie, D. (2015). The standard scrapie cell assay: development, utility and prospects. *Viruses*, 7(1), 180-198.
- ²¹ Bosque, P. J., and S. B. Prusiner. 2000. Cultured cell sublines highly susceptible to prion infection. *J. Virol.* 74:4377–4386.
- ²² Mahal, S. P., C. A. Demczyk, E. W. Smith, Jr., P. C. Klohn, and C. Weissmann. 2008. Assaying prions in cell culture: the standard scrapie cell assay (SSCA) and the scrapie cell assay in end point format (SCEPA). *Methods Mol. Biol.* 459:49–68.
- ²³ Christofinis, G. J., & Beale, A. J. (1968). Some biological characters of cell lines derived from normal rabbit kidney. *The Journal of Pathology*, 95(2), 377-381.
- ²⁴ Lawson, V. A., L. J. Vella, J. D. Stewart, R. A. Sharples, H. Klemm, D. M. Machalek, C. L. Masters, R. Cappai, S. J. Collins, and A. F. Hill. 2008. Mouse-adapted sporadic human Creutzfeldt-Jakob disease prions propagate in cell culture. *Int. J. Biochem. Cell Biol.* 40:2793–2801.
- ²⁵ Courageot, M. P., N. Daude, R. Nonno, S. Paquet, M. A. Di Bari, A. Le Dur, J. Chapuis, A. F. Hill, U. Agrimi, H. Laude, and D. Vilette. 2008. A cell line infectible by prion strains from different species. *J. Gen. Virol.* 89:341–347.
- ²⁶ Vilette, D., O. Andreoletti, F. Archer, M. F. Madelaine, J. L. Vilotte, S. Lehmann, and H. Laude. 2001. Ex vivo propagation of infectious sheep scrapie agent in heterologous epithelial cells expressing ovine prion protein. *Proc. Natl. Acad. Sci. U. S. A.* 98:4055–4059
- ²⁷ Vilette, D., O. Andreoletti, F. Archer, M. F. Madelaine, J. L. Vilotte, S. Lehmann, and H. Laude. 2001. Ex vivo propagation of infectious sheep scrapie agent in heterologous epithelial cells expressing ovine prion protein. *Proc. Natl. Acad. Sci. U. S. A.* 98:4055–4059

-
- ²⁸ Moore, R. A., Vorberg, I., & Priola, S. A. (2005). Species barriers in prion diseases – brief review. In *Infectious Diseases from Nature: Mechanisms of Viral Emergence and Persistence* (pp. 187-202). Springer Vienna.
- ²⁹ Sweeting B., Brown, E., Chakrabartty, A., & Pai, E. F. (2009). The structure of rabbit PrPC: clues into species barrier and prion disease susceptibility. *Canadian Light Source*, 28.
- ³⁰ Sweeting, B, Brown E, Khan MQ, Chakrabartty A, Pai EF (2013) N-Terminal Helix-Cap in a-Helix 2 Modulates b-State Misfolding in Rabbit and Hamster Prion Proteins. *PLoS ONE* 8(5)
- ³¹ Chianini, F., Fernández-Borges, N., Vidal, E., Gibbard, L., Pintado, B., de Castro, J., & Pang, Y. (2012). Rabbits are not resistant to prion infection. *Proceedings of the National Academy of Sciences*, 109(13), 5080-5085.
- ³² Bian, J., Napier, D., Khaychuck, V., Angers, R., Graham, C., & Telling, G. (2010). Cell-based quantification of chronic wasting disease prions. *Journal of virology*, 84(16), 8322-8326.
- ³³ Khaychuk, V. (2012). Prion Characterization Using Cell Based Approaches. Doctoral Dissertation, University of Kentucky
- ³⁴ Arellano-Anaya, Z. E., Savistchenko, J., Mathey, J., Huor, A., Lacroux, C., Andréoletti, O., & Vilette, D. (2011). A simple, versatile and sensitive cell-based assay for prions from various species. *PLoS One*, 6(5), e20563.
- ³⁵ Leblanc, P., S. Alais, I. Porto-Carreiro, S. Lehmann, J. Grassi, G. Raposo, and J. L. Darlix. 2006. Retrovirus infection strongly enhances scrapie infectivity release in cell culture. *EMBO J.* 25:2674–2685.
- ³⁶ Kocisko, D. A., & Caughey, B. (2006). Searching for Anti-Prion Compounds: Cell-Based High-Throughput In Vitro Assays and Animal Testing Strategies. *Methods in enzymology*, 412, 223-234.
- ³⁷ Korth, C., May, B. C., Cohen, F. E., & Prusiner, S. B. (2001). Acridine and phenothiazine derivatives as pharmacotherapeutics for prion disease. *Proceedings of the National Academy of Sciences*, 98(17), 9836-9841.
- ³⁸ Oelschlegel, A. M., Fallahi, M., Ortiz-Umpierre, S., & Weissmann, C. (2012). The Extended Cell Panel Assay (ECPA) characterizes the relationship of RML, 79A and 139A prion strains and reveals conversion of 139A to 79A-like prions in cell culture. *Journal of virology*, JVI-00181.
- ³⁹ Saborio, G. P., Permanne, B., & Soto, C. (2001). Sensitive detection of pathological prion protein by cyclic amplification of protein misfolding. *Nature*, 411(6839), 810-813.
- ⁴⁰ Soto, C., Saborio, G. P., & Anderes, L. (2002). Cyclic amplification of protein misfolding: application to prion-related disorders and beyond. *Trends in neurosciences*, 25(8), 390-394
- ⁴¹ Atarashi, R., Wilham, J. M., Christensen, L., Hughson, A. G., Moore, R. A., Johnson, L. M., & Caughey, B. (2008). Simplified ultrasensitive prion detection by recombinant PrP conversion with shaking. *Nature Methods*, 5(3), 211-212.

-
- ⁴² Oelschlegel, A. M., Fallahi, M., Ortiz-Umpierre, S., & Weissmann, C. (2012). The Extended Cell Panel Assay (ECPA) characterizes the relationship of RML, 79A and 139A prion strains and reveals conversion of 139A to 79A-like prions in cell culture. *Journal of virology*, JVI-00181.
- ⁴³ Molloy, B., & McMahon, H. E. (2014). A cell-biased effect of estrogen in prion infection. *Journal of virology*, 88(2), 1342-1353.
- ⁴⁴ Pulford, B., Reim, N., Bell, A., Veatch, J., Forster, G., Bender, H., & Wyckoff, A. C. (2010). Liposome-siRNA-peptide complexes cross the blood-brain barrier and significantly decrease PrP C on neuronal cells and PrP RES in infected cell cultures. *PloS one*, 5(6), e11085.
- ⁴⁵ Nishizawa, K., Oguma, A., Kawata, M., Sakasegawa, Y., Teruya, K., & Doh-ura, K. (2014). Efficacy and mechanism of a glycoside compound inhibiting abnormal prion protein formation in prion-infected cells: implications of interferon and phosphodiesterase 4D-interacting protein. *Journal of virology*, 88(8), 4083-4099.
- ⁴⁶ Bosque, P. J., & Prusiner, S. B. (2000). Cultured cell sublines highly susceptible to prion infection. *Journal of virology*, 74(9), 4377-4386.
- ⁴⁷ Marbiah, M. M., Harvey, A., West, B. T., Louzolo, A., Banerjee, P., Alden, J., & Bloom, G. S. (2014). Identification of a gene regulatory network associated with prion replication. *The EMBO journal*, e201387150.
- ⁴⁸ Bian, J., Kang, H. E., & Telling, G. C. (2014). Quinacrine promotes replication and conformational mutation of chronic wasting disease prions. *Proceedings of the National Academy of Sciences*, 111(16), 6028-6033.
- ⁴⁹ Lu D, et al. (2013) Biaryl amides and hydrazones as therapeutics for prion disease in transgenic mice. *J Pharmacol Exp Ther* 347(2):325-338.
- ⁵⁰ Li Z, et al. (2013) Discovery and preliminary SAR of arylpiperazines as novel, brain-penetrant antiprion compounds. *ACS Med Chem Letters* 4(4):397-401.
- ⁵¹ Kimata A, et al. (2007) New series of antiprion compounds: Pyrazolone derivatives have the potent activity of inhibiting protease-resistant prion protein accumulation. *J Med Chem* 50(21):5053-5056.
- ⁵² Geissen M, et al. (2011) From high-throughput cell culture screening to mouse model: Identification of new inhibitor classes against prion disease. *ChemMedChem* 6(10): 1928-1937.
- ⁵³ Ghaemmaghami S, May BC, Renslo AR, Prusiner SB (2010) Discovery of 2-aminothiazoles as potent antiprion compounds. *J Virol* 84(7):3408-3412.
- ⁵⁴ Bate, C., Salmona, M., Diomedea, L., & Williams, A. (2004). Squalostatins cure prion-infected neurons and protect against prion neurotoxicity. *Journal of Biological Chemistry*, 279(15), 14983-14990.
- ⁵⁵ Kocisko, D. A., & Caughey, B. (2006). Searching for Anti-Prion Compounds: Cell-Based High-Throughput In Vitro Assays and Animal Testing Strategies. *Methods in enzymology*, 412, 223-234.
- ⁵⁶ Li, J., Browning, S., Mahal, S. P., Oelschlegel, A. M., & Weissmann, C. (2010). Darwinian evolution of prions in cell culture. *Science*, 327(5967), 869-872.

-
- ⁵⁷ Doh-ura, K., Tamura, K., Karube, Y., Naito, M., Tsuruo, T., & Kataoka, Y. (2007). Chelating compound, chrysoidine, is more effective in both antiprion activity and brain endothelial permeability than quinacrine. *Cellular and molecular neurobiology*, 27(3), 303-316.
- ⁵⁸ Berry, D. B., Lu, D., Geva, M., Watts, J. C., Bhardwaj, S., Oehler, A., ... & Giles, K. (2013). Drug resistance confounding prion therapeutics. *Proceedings of the National Academy of Sciences*, 110(44), E4160-E4169.
- ⁵⁹ Murakami-Kubo, I., Doh-Ura, K., Ishikawa, K., Kawatake, S., Sasaki, K., Kira, J. I., ... & Iwaki, T. (2004). Quinoline derivatives are therapeutic candidates for transmissible spongiform encephalopathies. *Journal of virology*, 78(3), 1281-1288.
- ⁶⁰ Thi, H. T. N., Lee, C. Y., Teruya, K., Ong, W. Y., Doh-ura, K., & Go, M. L. (2008). Antiprion activity of functionalized 9-aminoacridines related to quinacrine. *Bioorganic & medicinal chemistry*, 16(14), 6737-6746.
- ⁶¹ Nguyen, T., Sakasegawa, Y., Doh-ura, K., & Go, M. L. (2011). Anti-prion activities and drug-like potential of functionalized quinacrine analogs with basic phenyl residues at the 9-amino position. *European journal of medicinal chemistry*, 46(7), 2917-2929.
- ⁶² Nishizawa, K., Oguma, A., Kawata, M., Sakasegawa, Y., Teruya, K., & Doh-ura, K. (2014). Efficacy and mechanism of a glycoside compound inhibiting abnormal prion protein formation in prion-infected cells: implications of interferon and phosphodiesterase 4D-interacting protein. *Journal of virology*, 88(8), 4083-4099.
- ⁶³ Hamanaka, T., Nishizawa, K., Sakasegawa, Y., Oguma, A., Teruya, K., Kurahashi, H., ... & Doh-ura, K. (2017). Melanin or a melanin-like substance interacts with the N-terminal portion of prion protein and inhibits abnormal prion protein formation in prion-infected cells. *Journal of virology*, 91(6), e01862-16.
- ⁶⁴ Hamanaka, T., Nishizawa, K., Sakasegawa, Y., Teruya, K., & Doh-ura, K. (2015). Structure-activity analysis and antiprion mechanism of isoprenoid compounds. *Virology*, 486, 63-70.
- ⁶⁵ Doh-Ura, K., Iwaki, T., & Caughey, B. (2000). Lysosomotropic agents and cysteine protease inhibitors inhibit scrapie-associated prion protein accumulation. *Journal of virology*, 74(10), 4894-4897.
- ⁶⁶ Mead S, et al. (2011) PRION-1 scales analysis supports use of functional outcome measures in prion disease. *Neurology* 77(18):1674-1683.
- ⁶⁷ Collinge J, et al. (2009) Safety and efficacy of quinacrine in human prion disease (PRION-1 study): A patient-preference trial. *Lancet Neurol* 8(4):334-344.
- ⁶⁸ Benito-León J (2004) Combined quinacrine and chlorpromazine therapy in fatal familial insomnia. *Clin Neuropharmacol* 27(4):201-203.
- ⁶⁹ Nakajima M, et al. (2004) Results of quinacrine administration to patients with Creutzfeldt-Jakob disease. *Dement Geriatr Cogn Disord* 17(3):158-163.
- ⁷⁰ Kobayashi Y, Hirata K, Tanaka H, Yamada T (2003) [Quinacrine administration to a patient with Creutzfeldt-Jakob disease who received a cadaveric dura mater graft: An EEG evaluation]. *Rinsho Shinkeigaku* 43(7):403-408.

-
- ⁷¹ Geschwind MD, et al. (2013) Quinacrine treatment trial for sporadic Creutzfeldt-Jakob disease. *Neurology* 81(23):2015–2023.
- ⁷² Doolan, K. M., & Colby, D. W. (2015). Conformation-dependent epitopes recognized by prion protein antibodies probed using mutational scanning and deep sequencing. *Journal of molecular biology*, 427(2), 328-340.
- ⁷³ Kang, H. E., Weng, C. C., Saijo, E., Saylor, V., Bian, J., Kim, S., Ramos, L., Angers, R., Langenfeld, K., Khaychuk, V., & Calvi, C. (2012). Characterization of conformation-dependent prion protein epitopes. *Journal of Biological Chemistry*, jbc-M112.

CHAPTER 5 - DISCUSSION

A. OVERALL SUMMARY

Understanding prion disease transmission, the species barrier, and finding treatment options depends on resolving the structure of PrP^{Sc}; yet, this very basic need is still unfulfilled. It remains a driving question that the research presented in this dissertation aims to shed light on. The overarching goal of this dissertation was to *understand structural differences within and between strains of prions* (infectious proteinaceous agents) by examining prion structure after exposure to denaturing chaotropic agents. **My overall hypothesis** was that detailed structural information about the prion protein can be garnered through new and innovative techniques we developed; specifically, chaotropic agents used to probe epitope-mapped regions of the prion protein will allow us to create a map of specific regional differences between strains.

The Cell-Based Conformational Stability Assay (C-CSA, Figure 2.2) uses a cell model expressing PrP^C gene of choice in rabbit kidney epithelial (RK13) cells as a tool to assess how strains differ (Figure 2.2). This technique was specifically developed as a quantitative measure of prions. RK13 cells expressing either elk (RK-Elk) or deer (RK-Deer) PrP^C perpetually propagate CWD prion infection, i.e. chronically infected cell lines. To this end, I first validated the significant ($p < 0.001$) difference (Figure 2.3A) due to the different amino acid at position 226 [deer (Q), elk (E)] has on the stability of chronic wasting disease (CWD) in chronically infected cell lines. Then, I examined the

possibility of analyzing freshly infected, as opposed to chronically infected, cell lines (Figure 2.3B). The prion stability difference seen between CWD chronically infected RK-Deer and RK-Elk ($p < 0.001$) was recapitulated in freshly infected cells ($p < 0.001$) (Figure 2.3).

I, then, expanded the range of antibodies used within the C-CSA to examine multiple epitope-mapped regions of the prion molecule (Figure 2.5, 2.6). The resultant data yielded some unexpected results. First, the response to denaturation is not equivalent across the CWD prion molecule (Figure 2.5A, B, C). The epitopes within a single strain produced a variety of conformational stabilities. Moreover, the Q/E difference between Deer-CWD and Elk-CWD showed pronounced differences at all epitopes examined (Figure 2.6). The range of responses (Figure 2.5D) and individual epitope responses (Figure 2.6) were significantly different when comparing Deer-CWD and Elk-CWD. This means that fundamentally, even when a single original infectious source is used, Deer-CWD and Elk-CWD present with differences at linear and discontinuous epitopes located in the unstructured and globular regions of the prion protein.

To ensure the expanded C-CSA technique was not limited to cervids and CWD, I then examined classically defined murine-adapted scrapie strains (Figure 2.4) and newly murine-adapted CWD (Figure 2.7, 2.8). Unlike Elk-CWD and Deer-CWD, the three murine adapted prion strains all contain the same amino acid sequence. Given that, any variations uncovered with the expanded C-CSA could be the foundation of how these prions conformationally propagate their strain properties. There were less

pronounced differences between these strains, but significant differences did occur. Like CWD, within each murine-adapted strain there were various individual responses to the various epitopes (Figure 2.7). Unlike CWD, the slope of the denaturation curve varied between the murine-adapted strains (Figure 2.7G) while the summed Guanidine Hydrochloride $\frac{1}{2}$ values did not differ (Figure 2.7F). When murine-adapted strains were compared to each other at multiple epitopes, there were subtle but significant differences at most comparisons.

These technological improvements to quantitatively examine prion strains led to the desire to be innovative and create novel techniques. We previously developed epitope-mapped anti-prion antibodies (Figure 3.1B) that were applied in a 7-5 sandwich ELISA format: PRC7 anti-prion antibody is the capture antibody, and PRC5 anti-prion antibody is the detecting antibody. PRC7 is glycosylation specific and only binds to unglycosylated, and monoglycosylated (residue 196) species of the prion protein. Whereas, PRC5 is not glycosylation specific, it binds to residues (132 and 158) on either side of α helix-1. The 7-5 ELISA requires denaturation (Figure 3.3A-B), does not require PK (Figure 3.3C-D) and, above all, is infection specific (Figure 3.3). Moreover, like the C-CSA, the 7-5 ELISA can be used as a 'CSA' to differentiate between different prion strains (Figure 3.3E-F).

I sought to conceptually merge the C-CSA and 7-5 ELISA-CSA to create a new assay that would examine epitope accessibility/stability in a cell-based format. From this endeavor the ESA (Figure 3.2) was created. Like the C-CSA, the ESA is able to differentiate between different prions Elk-CWD and Deer-CWD (Figure 3.5), and within

a single prion (Figure 3.7). The unforeseen data generated by this technique was derived from the PK-treated, non-denatured fraction of PrP^{Sc} (Figure 3.7). The ESA allows, essentially 'native PrP^{Sc}' to be quantitatively detectable. Overall Deer-PrP^{Sc}, regardless of the infectious origin, is not accessible without denaturation; whereas, Elk-PrP^{Sc}, dependent on the infectious origin, is accessible without denaturation (Figure 3.7). Additionally, murine-adapted prion strains are highly accessible at some epitopes, e.g. PRC5 and 6H4, while being completely inaccessible at other epitopes, e.g. D18 and 5A3. This implies that the curve of the prion amyloid, or the individual misfolded prion proteins available have regions that are available and inaccessible dependent on prion strain, and epitope examined. This further emphasizes the unique conformational variation between and within prion strains.

The ESA was then used to examine cross-matched infectious routes (Figure 3.8) where Deer-CWD was used to infect both RK-Deer and RK-Elk cell lines, and Elk-CWD was used to infect both RK-Deer and RK-Elk cell lines. This was done to further show the conformational changes that occur when adaption occurs. The single amino acid difference between Deer-PrP^C and Elk-PrP^C causes massive changes to the structure of PrP^{Sc} at multiple epitopes across the molecule (Figure 3.8). Overall, CWD prions lose accessibility when there is a mismatch between PrP^C and PrP^{Sc}. Additionally, mismatching causes similar CWD prion structures to emerge (Figure 3.8C).

Furthermore, the ESA was tasked to examine larger adaption events (Figure 3.9). Scrapie that was murine-adapted, RML, was then adapted into PrP^C-cervidized mice, Tg(Deer) or Tg(Elk) mice, creating Deer-RML and Elk-RML. These newly adapted,

prions that had been through three species (sheep > mouse > cervid) were then used to infect RK-Deer and RK-Elk cell lines. Unfortunately, the Deer-RML did not efficiently infect the RK-Elk cell line. However, Deer-RML infected RK-Deer, Elk-RML infected RK-Deer, and Elk-RML infected RK-Elk provided data about how adaptation puts pressure on the conformational variation of prions. This is especially evident when comparing cervidized-RML to CWD (Figure 3.10). Likewise, the ESA shows variation amongst murine-adapted prion strains (Figure 3.11).

Moreover, the C-CSA and ESA are different techniques (Figure 3.12) because the prion resistance to protease degradation after partial denaturation (C-CSA) is not equivalent to the epitope accessibility (ESA). The ESA allows for the creation of prion strain-specific 'fingerprints' or 'patterns', which may be useful to future examination of prion strain classification.

Finally, I turned these novel techniques to assess prion evolution [Chapter 4]. I did this in two ways: (1) Drug-induced prion evolution, and (2) prion evolution in cell culture. Prion evolution due to quinacrine-drug related selection pressures caused rapid emergence of conformational perturbation of the prion protein, measurable within 24 hours of drug application (Figure 4.3, 4.4). Importantly, the control-PBS treated samples maintained a steady signal throughout the multi-day treatment schedule. Quinacrine had an impact on epitope accessibility at the linear epitope in the unstructured region (PRC1), discontinuous epitope straddles α helix-1 (PRC5), and linear epitope embedded in α helix-1 (1B8). Overall, quinacrine-induced evolution yields a more epitope-inaccessible protein. Moreover, as the treatment progressed, further significant

alterations to PrP^{Sc} structure occurred. This indicates that the drug-induced structural changes to PrP^{Sc} are not stable, but in flux. This should be taken as a cautionary tale for those seeking to cure prions with a drug treatment, because the drug treatment may cause unknown alterations to the conformation of PrP^{Sc}.

The final evolution assessed, was in cell culture. The C-CSA and ESA were effective tools to show the evolution that occurs with serial passaging within cell culture (Figure 4.5, 4.6). The changes to prion conformation and epitope accessibility reach further, unlike previously established norms in the prion field, serially cell-passaged prions, when used as the infectious source, do not faithfully recapitulate either their original material or the serially passaged material (Figure 4.7). Taken a step further, serially cell-passaged prions when bioassayed and used as the infectious source, do not faithfully recapitulate either their original material or the serially passaged material (Figure 4.8). This is instructive; one of the defining features of prion strains is the faithful propagation of specific strain properties, within the same host. If prion conformations are continually changing in response to environmental pressures, then the prions occurring in the real world may not recapitulate those used in laboratories.

B. AIMS WITH CONJOINING CONCLUSIONS

The aims of this dissertation focused on two questions:

QUESTION 1: What are the subtle structural ways that infectious proteins encrypt strain information?

Aims:

1: Expand the prion Cell-Based Conformational Stability Assay to better understand prion strain structural characteristics.

2: Create a new prion Epitope Stability Assay (ESA) to more directly examine epitope accessibility differences in prion strain structural characteristics and provide previously inaccessible structural information about the prion protein.

Conclusions [Chapter 2 & 3]:

The hypothesis for question one was supported; structural characteristics of the prion protein can be elucidated through new assays via examination of stability and epitope availability within the infectious prion protein. Research becomes stymied by current technological tools and the confounding complexity found in natural systems; the answer is to find novel, innovative techniques that can expand our ability to ask important questions. Consequently, the C-CSA (Figure 2.2), ESA (Figure 3.2), and 7-5 ELISA-CSA represent new tools to reveal more details about prion strain structure in a facile and expedient process. The C-CSA and ESA methodologies reveal different aspects of PrP^{Sc} structure (Figure 3.12). These new methodologies allow data to be gathered across multiple species, with multiple infectious prions, in both chronically infected and freshly infected paradigms. Surprisingly, the optimization rounds of the ESA methodology revealed a capacity to evaluate the folded (non-denatured) fraction of PrP^{Sc}.

We addressed the molecular basis for prion strains seen in murine-adapted prions. The basis for murine prion strains can be uncovered with detailed structural characteristics via examination of prion stability. Specifically, we infected the RK-Mouse

cell line with brain homogenate from terminally ill C57Bl/6 mice infected with classically defined mouse-adapted scrapie (RML, 22L, and 139A) and newly mouse-adapted chronic wasting disease (mD10). Mouse prion strains (RML, 22L, 139A, and mD10) all share the same amino acid sequence; yet, each ultimately produce different diseases. Tertiary structural differences between each infectious particle must be the culprit since they share the same amino acid sequence. Using the experimental methodology we developed, we compared differences in prion structure between these strains with the C-CSA [Aim 1, Chapter 2], ESA [Aim 2, Chapter 3], and 7-5 ELISA-CSA [Chapter 3].

New molecular differences between murine prion strains were uncovered; specifically, a map of specific regional differences between strains. The ESA allows the folded (non-denatured) fraction of PrP^{Sc} to be examined (Figure 3.7 C); moreover, the region around the α helix-1 of the folded (non-denatured) fraction of mouse-adapted PrP^{Sc} is highly accessible. Conformational stability structural differences between mouse-adapted prion strains further delineate classically defined and newly adapted prions (Figure 2.5A-F). Conformational stability structural differences between classically defined mouse-adapted scrapie strains (22L and RML) range between the N-terminal unstructured region and α helix-1 region; whereas, the glycosylation specific epitope (aglycosylated, and monoglycosylated at residue 196), and α helix-3 are similar (Figure 2.5A-F). The epitope accessibility differences between RML and 22L occur at all epitopes except the area straddling the α helix-1 region (Figure 3.11B). Overall, newly murine-adapted CWD contains a unique structure distinct to 22L, RML, and 139A;

conformational stability structural differences between mD10:22L and mD10:RML range through the entire molecule with an exception on the region straddling α helix-1. The epitope accessibility differences between mD10:22L and mD10:RML range at all epitopes (Figure 3.11 D, E); interestingly, mD10:139A have more similar epitope accessibility (Figure 3.11G) than other comparisons. The differences between RML, 22L and mD10 are recapitulated with the 7-5 ELISA-CSA (Figure 3.3F). Overall, each mouse-adapted prion strain has an independent structure with every assay examined.

We addressed the molecular basis for prion strains, prion strain adaption and species barriers seen in cervids. Single amino acid changes to the prion protein can have intense impact on transmission and susceptibility¹; e.g. the difference amino acid at position 226 [deer (Q), elk (E)] has profound effects on the presentation of Chronic Wasting Disease². Specifically, we infected RK-Deer and RK-Elk cell lines with brain homogenate from Tg(DeerPrP)¹⁵³⁶^{+/-} and Tg(ElkPrP)⁵⁰³⁷^{+/-} mice terminally ill with CWD, or newly adapted cervidized-RML. Using the experimental methodology we developed, we compared differences in prion structure between these strains with the C-CSA [Aim 1, Chapter 2], ESA [Aim 2, Chapter 3], and 7-5 ELISA-CSA [Chapter 3].

Molecular differences between cervid prion strains were uncovered; specifically, a map of specific regional differences between strains. Deer-CWD is more resistant than Elk-CWD to degradation by proteinase K after denaturation with a chaotropic agent (Figure 2.3); Deer-CWD, also, has more inaccessible epitopes than Elk-CWD (Figure 3.5). The differences between Deer-CWD and Elk-CWD are recapitulated with the 7-5 ELISA-CSA (Figure 3.3E). The differences seen with CWD caused deer and elk (Q/E

226) residue difference is recapitulated when examining cervid-adapted RML (Figure 3.9). Furthermore, when the PrP^{Sc} and host-PrP^C are not matched, further differences emerge (Figure 3.8, 3.9). Although both Elk and Deer passaged CWD prion share the same initial inoculum (Bala05), each ultimately produces a different disease phenotype dependent on the host PrP^C primary structure. The matching or mismatching PrP^{Sc} - PrP^C combination can spawn new PrP^{Sc} structures. Overall comparisons between elk and deer CWD further supported previous work that the single amino acid difference between elk and deer PrP^C plays an important role in prion structure. This difference is even more crucial now that CWD is in Europe and Camelid prions have been discovered. The differences and similarities that occur between cervid-adapted RML and CWD [Chapter 3] add to the concern that when adaptation occurs, new prions emerge. Perhaps European CWD or the new camelid prions will make the zoonotic leap into humans and create an entirely new prion.

Overall (Figure 3.12), Elk-CWD presented more similar C-CSA and ESA GdnHCl $\frac{1}{2}$ values than other compared prions and mouse-adapted CWD (mD10) had the least similarities between C-CSA and ESA GdnHCl $\frac{1}{2}$ values. This could indicate that adaptation drastically alters the original structure of the prion. GdnHCl $\frac{1}{2}$ values derived from PrP^{Sc} conformational stability and epitope accessibility along with PrP^{Sc} epitope folded (non-denatured) values create strain and host-PrP^C specific patterns, essentially creating an individual strain fingerprint. This pattern can be altered by adaptation into new species, i.e. RML (Figure 3.13A) into cervids (Figure 3.13E, F, I). It can also be altered by the amino acid composition of the host PrP^C substrate or the amino acid

composition infectious PrP^{Sc}. The GdnHCl 1/2 values derived from PrP^{Sc} conformational stability and PrP^{Sc} epitope accessibility were not identical within each strain implying that the prions have molecular micro-regions with discreet denaturation responses. Additionally, PrP^{Sc} epitope folded (non-denatured) values were not identical within each strain implying that the epitopes are not evenly available along a folded (non-denatured) prion. These techniques provide a high-throughput method to examine the prion protein at multiple epitopes, giving a more complete view of PrP^{Sc} structure.

QUESTION 2: What are the subtle structural ways that prion structure evolves?

Aim 3: Compare emerging and evolving strains to better understand the basis of strain/species adaption and ultimately the species barrier.

Conclusions [Chapter 4]:

The hypothesis for question two was supported; subtle tertiary structural changes occurring as prions emerge/evolve can be tracked via chaotropic agents and epitope-mapped antibodies. We examined two forms of prion evolution with the C-CSA (Figure 2.2) and ESA (Figure 3.2) methodology: (1) drug-induced evolution, and (2) strain evolution in cell culture. Understanding of prion evolution due to drug influence is important in understanding prion biology and is a necessary step along the path to find viable drug treatment options.

Conclusions [Chapter 4], Quinacrine-Induced Prion Evolution:

We tracked daily drug-induced effects change in epitope-localized prion structure. Specifically, the RK-Elk+ cell line was grown to near confluence, split into a treatment group (quinacrine) and control group (vehicle-PBS). The PrP^{Sc} structure was

monitored daily for five days during treatment. Quinacrine-induced evolution of chronic wasting disease causes unexpected rapid emergence of conformational perturbation of the prion protein, measurable within 24 hours of drug application (Figure 4.3, 4.4). The following days of treatment further significantly alter PrP^{Sc} structure; the drug-induced structural changes to PrP^{Sc} are not stable, but in daily flux.

Overall, quinacrine has a greater impact on epitope accessibility at the linear epitope in the unstructured region (PRC1), discontinuous epitope straddles α helix-1 (PRC5), and linear epitope embedded in α helix-1 (1B8). The drug-induced evolution yields a more epitope-inaccessible protein.

Conclusions [Chapter 4], Prion Evolution in Cell Culture:

A fundamental prion biology assumption that is being challenged: chronically prion infected cell models will recapitulate molecular characteristics of a biological prion infection. To test the validity that prion strains are truly stable within cell culture, chaotropic agents and epitope-mapped antibodies (Aim1, Aim 2) were used to compare fresh prion infection to chronic (long-term) prion infection in cell culture. Specifically, RK-PrP cell lines that were chronically infected with Deer-CWD, Elk-CWD, RML, and 22L were compared to freshly infected cells. Overall, chronically prion infected cell lines do not recapitulate fresh biological prion infection; this is seen when examining folded / non-denatured PrP^{Sc} (Figure 4.6), GdnHCl $\frac{1}{2}$ values and curve fits (Figure 4.7).

Chronic cell line establishment makes folded (non-denatured) PrP^{Sc} epitopes for Deer-CWD, Elk-CWD, RML, and 22L more inaccessible without denaturation (Figure 4.6), essentially PrP^{Sc} structural epitopes evolve in the cell culture systems. The overall

expectation that the GdnHCl $\frac{1}{2}$ values would be equal to fresh infection did not hold true for most epitopes examined (Figure 4.7) with the ESA (Figure 3.2) or C-CSA (Figure 2.2). In general, serial passaging made prions more resistant to protease degradation after denaturation in three different species (deer PrP^C, elk PrP^C, and mouse PrP^C) with three different prions CWD, RML, and 22L. This is further evidence that supports this as a repeatable phenomenon. The overall epitope accessibility is less unified than resistant to protease degradation after denaturation. The single consistent change in epitope accessibility is at the glycosylation specific epitope, PRC7; in all three different species (deer PrP^C, elk PrP^C, and mouse PrP^C) with three different prions CWD, RML, and 22L the epitope is less accessible. This could imply that the glycosylation phenotype becomes unified with chronic passaging. In CWD, the epitope accessibility mirrors or varies from fresh infection dependent on the epitope examined. Again, this further shows the importance of using multiple epitopes in determining similarity or difference between prions. It, also, reinforces the importance of looking at the denaturation curve and GdnHCl $\frac{1}{2}$ values.

Furthermore, the PrP^{Sc} in chronically prion infected cell lines is not stable upon passage into naïve cells (Figure 4.8) or into transgenic mice (Figure 4.9). Specifically, lysate from RK-PrP cell lines that were chronically infected with Deer-CWD, Elk-CWD, RML, and 22L were used to freshly infected naïve RK-PrP cell lines (Figure 4.8); lysate from the RK-Elk+ cell line that were chronically infected CWD was used to infect Tg(DeerPrP)1536^{+/-} and then brain homogenate from terminally ill mice was used to infect naïve RK-Deer cells (Figure 4.9). Analyses were then done with the ESA (Figure

3.2) or C-CSA (Figure 2.2). Unlike the faithful recapitulation of a prion strain in bioassay, infection with chronic cell lysate did not maintain the PrP^{Sc} structure of chronic cells. The PrP^{Sc} structure of chronic cell lysate did not recapitulate chronic cell PrP^{Sc} structure or the PrP^{Sc} structure of fresh infection. The differences were subtle and pronounced, depending on the epitope. Interestingly enough, chronic cell lysate PrP^{Sc} is similar to fresh brain infection PrP^{Sc} nearly as often as it is similar to chronic cell PrP^{Sc}. This implies that PrP^{Sc} is in a state of flux and not stably propagating. This instability is recapitulated when chronic prion cell lysate (RK-Elk+) is used to infect naïve transgenic Deer-PrP mice then used to infect RK-Deer cells (Figure 4.9). Although RK-Elk+ was passaged through mouse Deer-PrP^C and RK-Deer-PrP^C it retained more similarity with Elk-PrP^{Sc} structure but still had a unique structure. This could have bearing on how CWD structure acts transmitting in wild populations of Deer-PrP^C and Elk-PrP^C. This has special bearing on the transmission of CWD in Europe. Overall, implies that new prion strain structures are being created through serial passage or that there is a selection for a new specific conformation from the original quasi-species potluck.

C. FUTURE DIRECTIONS

This dissertation reinforces that reliance on a single epitope is not advisable to reveal how changes can occur in micro-domains; multiple epitopes are needed when exploring the complexities of prion structure. Future research needs to expand how it evaluates prion strains and prion evolution.

Ultimately, reliance of chronically infected cells as a basis for anti-prion therapeutic testing is not advisable as chronically infected lines do not resemble freshly infected lines PrP^{Sc} structure. However, they still serve as a model system for understanding prion structure. Additionally, the stability of GdnHCl $\frac{1}{2}$ and curve fit in RK-Elk+ treated with vehicle across five days (Figure 4.3, 4.4) further supports that the ESA method (Figure 3.2) is reliable. However, when comparing PBS-treated RK-Elk+ treated with PBS to the evolution in cell culture RK-Elk+ (Figure 4.7), the GdnHCl $\frac{1}{2}$ values are not identical. This could imply that the passage number of the RK-Elk+ cell line has some bearing on the structure of PrP^{Sc}. This could be further explored by examining chronically infected lines at various passage numbers to see if PrP^{Sc} stays stable within chronic cell culture models. Further analysis could be done to track prion evolution in cell culture from fresh infection into the chronically infected state. Daily, or weekly monitoring would provide the field with an opportunity to better understand the structural evolution that can occur to the tertiary structure of an infectious protein. Perhaps prion structural evolution is a moving target that is not as stable as once thought; this variation could be happening within animal models. This phenomenon needs to be kept in mind as the field moves forward locating a drug treatment for prion diseases.

It is crucial for the overall survival of cervids and protection of humans that we understand CWD and the structure of the cervid prion protein better. Human risk due to exposure to animal prion diseased tissues is a prevailing concern. The CWD prion has a resoundingly different structure and resistance to denaturation due to the single

amino acid difference in the substrate (PrP^C) of infected species, i.e. Deer-Q226/Elk-E226. Moreover, these new assays could potentially reveal subtle variations between North American and European CWD.

The drug-induced prion structural changes could be tracked daily past the 5 days indicated (Figure 4.3, 4.4), to see if the drug-induced structural changes eventually stabilize. Another future direction could be tracking drug-induced changes from other potential anti-prion therapies.

To ensure scientific facts are accurate and for science to move forward, we must continually challenge our assumptions and expand our understanding of natural phenomenon. By using multiple techniques we further characterized the unique structure of prion strains. The GdnHCl_{1/2} values for C-CSA, 7-5 ELISA-CSA, and ESA were not identical across the same epitopes examined, indicating that each methodology is interrogating PrP^{Sc} differently. These techniques could be expanded in the future for use with other prions; i.e. scrapie (sheep/goats), CJD (humans), TME (mink), etc. Ideally, future prion researchers will use this data, generated by these three methodologies, to create more accurate molecular models of prion structure and better understand the subtle variation between prion strains.

Moreover, the data contained in this dissertation expands our understanding of the structure of infectious prions, prion strains, prion adaption, and prion cell culture models. Ultimately, better understanding prion structure is vital to more than the prototypical transmissible spongiform encephalopathies (TSE's)³, other neurodegenerative disorders (Alzheimer's, Parkinson's, and Huntington's) are now

being recognized as prion disorders^{4, 5}. Until recently, the concept of a protein folding into a pathological conformation and propagating the misfolded form to cause disease was limited to prion diseases; however, other devastating neurodegenerative diseases (e.g. Alzheimer's⁶, Parkinson's⁷, etc.) share similar etiology⁸. The reliance on the primary structure to dictate seeding potential is shared with other amyloidogenic proteins⁹; there is a link between amyloid structure and disease seen in prions, Hyp-FN protein¹⁰, α -synuclein¹¹, Alzheimer's¹², and other amyloidogenic diseases. Understanding prion diseases may further our ability to understand other neurodegenerative diseases¹³. This allows the prion protein to serve as a model for these human diseases and increases the need for stringent well-designed prion protein experiments. As such, new techniques that capitalize on nuances of antibody epitope binding can further illuminate the complexities of PrP^{Sc} structure. If the techniques generated in this dissertation can be adapted to other amyloidogenic proteins, the possibilities to better understand a grander biological phenomenon would emerge.

BIBLIOGRAPHY

- ¹ Belt, P. B., Muileman, I. H., Schreuder, B. E., Bos-de Ruijter, J., Gielkens, A. L., & Smits, M. A. (1995). Identification of five allelic variants of the sheep PrP gene and their association with natural scrapie. *Journal of General Virology*, 76(3), 509-517.
- ² Angers, R. C., H. E. Kang, D. Napier, S. Browning, T. Seward, C. Mathiason, A. Balachandran, D. McKenzie, J. Castilla, C. Soto, J. Jewell, C. Graham, E. A. Hoover, and G. C. Telling. 2010. Prion strain mutation determined by prion protein conformational compatibility and primary structure. *Science* 328:1154-1158.
- ³ Gajdusek, D. C. (1972). Spongiform virus encephalopathies. *Journal of Clinical Pathology. Supplement (Royal College of Pathologists)*, 6, 78.
- ⁴ Soto, C., Estrada, L., & Castilla, J. (2006). Amyloids, prions and the inherent infectious nature of misfolded protein aggregates. *Trends in Biochemical Sciences*, 31(3), 150-155.
- ⁵ Soto, C. (2012). Transmissible proteins: Expanding the prion heresy. *Cell*, 149(5), 968-977.
- ⁶ Bernstein, S. L., Dupuis, N. F., Lazo, N. D., Wytttenbach, T., Condrón, M. M., Bitan, G., & Bowers, M. T. (2009). Amyloid- β protein oligomerization and the importance of tetramers and dodecamers in the aetiology of Alzheimer's disease. *Nature chemistry*, 1(4), 326-331.
- ⁷ Cremades, N., Cohen, S. I., Deas, E., Abramov, A. Y., Chen, A. Y., Orte, A., & Bertocchini, C. W. (2012). Direct observation of the interconversion of normal and toxic forms of α -synuclein. *Cell*, 149(5), 1048-1059.
- ⁸ Soto, C. (2012). Transmissible proteins: Expanding the prion heresy. *Cell*, 149(5), 968-977.
- ⁹ Krebs, M. R., Morozova-Roche, L. A., Daniel, K., Robinson, C. V., & Dobson, C. M. (2004). Observation of sequence specificity in the seeding of protein amyloid fibrils. *Protein Science*, 13(7), 1933-1938.
- ¹⁰ Campioni, S., Mannini, B., Zampagni, M., Pensalfini, A., Parrini, C., Evangelisti, E., & Chiti, F. (2010). A causative link between the structure of aberrant protein oligomers and their toxicity. *Nature chemical biology*, 6(2), 140.
- ¹¹ Cremades, N., Cohen, S. I., Deas, E., Abramov, A. Y., Chen, A. Y., Orte, A., & Bertocchini, C. W. (2012). Direct observation of the interconversion of normal and toxic forms of α -synuclein. *Cell*, 149(5), 1048-1059.
- ¹² Bernstein, S. L., Dupuis, N. F., Lazo, N. D., Wytttenbach, T., Condrón, M. M., Bitan, G., & Bowers, M. T. (2009). Amyloid- β protein oligomerization and the importance of tetramers and dodecamers in the aetiology of Alzheimer's disease. *Nature chemistry*, 1(4), 326-331.
- ¹³ Aguzzi, A., & O'Connor, T. (2010). Protein aggregation diseases: Pathogenicity and therapeutic perspectives. *Nature Reviews Drug Discovery*, 9(3), 237-248.

LIST OF ABBREVIATIONS

22L	Murine-Adapted Sheep Scrapie, Strain (22L)
139A	Murine-Adapted, Hamster-Adapted Sheep Scrapie
BSE	Bovine Spongiform Encephalopathy
7-5 ELISA	PRC7-PRC5 sandwich Enzyme-Linked Immunosorbent Assay
BCA	Bicinchonic Acid Assay
BSA	Bovine Serum Albumin
C57Bl/6	Wild-Type (Inbred) mouse strain
C-CSA	Cell-Based Conformational Stability Assay
cerRML	Cervid-Adapted Murine-Adapted Scrapie (Rocky Mountain Labs)
CJD	Creutzfeldt-Jacob Disease
vCJD	Variant Creutzfeldt-Jacob Disease
fCJD	Familial Creutzfeldt-Jacob Disease
iCJD	Iatrogenic Creutzfeldt-Jacob Disease
CSA	Conformational Stability Assay
CWD	Chronic Wasting Disease
ELISA	Enzyme-Linked Immunosorbent Assay
ESA	Epitope Stability Assay
FFI	Fatal Familial Insomnia
FSI	Fatal Sporadic Insomnia
FVB	Wild-Type (Inbred) mouse strain
GdnHCl	Guanidine Hydrochloride
GSS	Gerstmann-Straussler-Scheinker
Gt	Gene-targeted mouse model
GTC	Guanidinium thiocyanate
Gt(Deer)	Gene-targeted mouse model expressing Deer PrP ^C
Gt(Elk)	Gene-targeted mouse model expressing Elk PrP ^C
mD10	Murine-Adapted chronic wasting disease, Strain (D10)
N2a	Neuro-2a murine cell line model
NMR	Nuclear Magnetic Resonance
PBS	Phosphate-buffered Saline
PBS-T	Phosphate-buffered Saline with 10% w/ v Tween-20
PK	Proteinase K
PMSF	Phenylmethylsulfonyl fluoride
PrP	Prion Protein
PrP ^C	Prion Protein (cellular)
PrP-KO	PrP ^C knockout (lacks PrP ^C expression)
PrP ^{Sc}	Prion Protein (infectious)
RK13	Rabbit Kidney Epithelial Cell Model
RK-22L+	Established line of RKM7 cells chronically infected with Murine-Adapted Scrapie, Strain 22L

RK-Deer	RK13 cell line with heterologous expression of Puromycin-PrP ^C Vector, Deer PrP ^C
RK-Deer+	Established line of RK-Deer cells chronically infected with CWD
RK-Elk	RK13 cell line with heterologous expression of Puromycin-PrP ^C Vector, Elk PrP ^C
RK-Elk+	Established line of RK-Elk cells chronically infected with CWD
RK-Mouse	RK13 cell line with heterologous expression of Puromycin-PrP ^C Vector, Mouse PrP ^C
RML	Murine-Adapted Sheep Scrapie, Strain (Rocky Mountain Labs)
RK-RML+	Established line of RK-Mouse cells chronically infected with Murine-Adapted Scrapie, Strain RML
RKV	RK13 cell line with heterologous expression of Puromycin Vector (but no PrP ^C expression)
TBS	Tris-buffered Saline
TBS-T	Tris-buffered Saline with 10% w/ v Tween-20
Tg	Transgenic mouse model
Tg(Deer)	Transgenic mouse model expressing Deer PrP ^C
Tg(Elk)	Transgenic mouse model expressing Elk PrP ^C
TME	Transmissible Mink Encephalopathy
TSE	Transmissible Spongiform Encephalopathy
w/v	Weight / Volume

Vanessa Villegas Selwyn

Phone: (575) 650-2357

Email: VSelwyn@rams.colostate.edu

Education:

- Ph.D. (2019): Colorado State University
 - Ph.D. in Cell and Molecular Biology with an emphasis in Molecular, Cellular and Integrative Neuroscience
 - *Novel in vitro approaches to delineate prion strain conformational variation*
 - Advisor: Dr. Glenn Telling
 - Department/Program:
 - Cell and Molecular Biology Program
 - Microbiology, Immunology, and Pathology Department
 - Molecular, Cellular, and Integrative Neurosciences Program
- Masters (2011): New Mexico State University
 - Master of Arts in Curriculum and Instruction
 - Emphasis: Secondary (7th – 12th grade) Science Education
 - Minors: Molecular Biology and Psychology
- Undergraduate (2008): New Mexico State University
 - Bachelor of Science in Biology (minor: Biochemistry, Molecular Biology)
 - Bachelor of Arts in Psychology (minor: Human Biology)
 - Undergraduate Honors Thesis: Understanding Recent Divergence: A study of Round-headed katydids. (genus *Amblycorypha*).

Publications and Presentations:

Publications

- Ross, C.L., Benedix J.H., Garcia, C., Lambeth, K., Perry, R., **Selwyn V.**, & Howard D.J. Scale-independent criteria and scale-dependent agents determining the structure of a ground cricket mosaic hybrid zone (*Allonemobius socius* – *A. fasciatus*). *Biological Journal of the Linnean Society*. 2008.
- **Selwyn, V.** (2008) Understanding Recent Divergence: A study of Round-headed katydids. (genus *Amblycorypha*). Undergraduate Honors Thesis, New Mexico State University, Las Cruces, New Mexico, USA

Presentations

- MCIN/CMB/MIP/BMB Spring Poster Symposium 2019 Poster:
 - *Interrogating Prion Strain differences Using a Newly Expanded Conformational Assay*
- *El Centro Awards Ceremony* 2018 Invited Speaker:
 - *The Latinx graduate student perspective: United we stand*
- MCIN/CMB/MIP/BMB Spring Poster Symposium 2018 Poster:
 - *Understanding Prion Strain Structural Variability*
- PRION international conference 2017 Poster:

- *Deciphering how infectious proteins encrypt strain information*
- *El Centro Awards Ceremony 2017 Invited Speaker:*
 - *The Latinx graduate student perspective: Mentorship and the path to success*
- *Center of Environmental Medicine Symposium 2017 Poster:*
 - *The core of the prion hypothesis: Deciphering how infectious proteins encrypt strain information*
- *MCIN/CMB/MIP/BMB Spring Poster Symposium 2017 Poster:*
 - *Understanding Prion Strain Structural Variability*
- *Cell and Molecular Biology Recruitment at Northern New Mexico College 2017 Seminar:*
 - *Graduate Opportunities at Colorado State University*
 - *Deciphering how infectious proteins encrypt strain information*
- *Colorado State University Cell and Molecular Biology Graduate Seminar 2016:*
 - *The core of the prion hypothesis: Deciphering how infectious proteins encrypt strain information*
- *Prion Research Center Works in Progress Seminar 2016:*
 - *The core of the prion hypothesis: Deciphering how infectious proteins encrypt strain information*
- *Rocky Mountain Virology Conference 2016 Poster:*
 - *Revealing Prion Strain Fingerprints*
- *Hispanic/Black Cultural Center 40th Anniversary, Colorado State University 2016:*
 - *The true meaning of “El Centro”: the Latinx graduate student perspective*
- *TRIO Graduate School Visitation Day 2016 Presentation:*
 - *Overview of Graduate Programs at Colorado State University*
- *Cell and Molecular Biology Retreat 2016 Poster:*
 - *Understanding Prion Strain Structural Variability*
- *Prion Research Center Works in Progress Seminar 2016:*
 - *Understanding Prion Strain Structural Variability*
- *MCIN/CMB/MIP/BMB Spring Poster Symposium 2016 Poster:*
 - *Understanding Prion Strain Structural Variability*
- *2016 CVMBS Research Day Presentation:*
 - *Uncovering prion strain structural differences via examination with epitope-mapped antibodies and chaotropic agents*
- *2015 Annual Biomedical Research Conference for Minority Students (ABRCMS) Poster:*
 - *Examining Prion Isoform Conformational Stability Associated with Strain Properties*
 - Presented by REU 2015 mentee: Adrian Garcia
- *Colorado State University Cell and Molecular Biology Seminar 2015:*
 - *Examining Prion Strain differences*
- *Center of Environmental Medicine Symposium 2015 Poster:*
 - *Addressing the Molecular Basis of Prion Strains*
- *MCIN/CMB/MIP/BMB Spring Poster Symposium 2015 Poster:*
 - *Addressing the Molecular Basis of Prion Strains*
- *Colorado State University Cell and Molecular Biology Seminar 2014:*
 - *Understanding Prion Strains*
- *Colorado State University Cell and Molecular Biology Seminar 2013:*
 - *Can prion infection be found in lymphoid tissues of CWD inoculated humanized mice?*
- *Colorado State University Prion Research Center 2013 Expanding Prion Horizons Conference Presentation:*

- *Can prion infection be found in lymphoid tissues of CWD inoculated humanized mice?*
- MCIN/CMB/MIP/BMB Spring Poster Symposium 2013 Poster:
 - *Can prion infection be found in lymphoid tissues of CWD inoculated humanized mice?*
- American Chemical Society 241st ACS National Meeting 2010 Presentation:
 - *Getting the foot in the door: Recruitment tool for Chemistry, Biomedicine and STEM through the Medicinal Plants of the Southwest*
- Leadership Alliance 2007 Presentation:
 - *Running Away from Alcohol Use; Why it just might work!*
- Undergraduate Research and Creative Arts Symposium 2007 Poster:
 - *Understanding Recent Divergence: A study of Katydid*
- American Physiological Society, Intersociety Meeting: Comparative Physiology National Conference 2006 Poster:
 - *Metabolic Fuel Utilization in Hibernators*
- Research Experience for Undergraduates 2006 Presentation:
 - *To eat or not to eat, that is the question; the role of ACC/pACC in feeding cycle of golden mantle ground squirrels.*
- ISV Conference at Toronto 2006 Poster:
 - *Eavesdropping and the Evolution of Signal Complexity in Amblycorypha*
- Undergraduate Research and Creative Arts Symposium 2006 Presentation:
 - *Understanding Recent Divergence: A study of Katydid*
- Undergraduate Research and Creative Arts Symposium 2005 Poster:
 - *Understanding Recent Divergence: A study of Katydid*

Honors and Awards:

- Scientific Conference:
 - Cell and Molecular Biology Registration Award for CSU Data Integrity Conference and/or Data Carpentry Workshop. (Spring 2015)
 - Cell and Molecular Biology Travel Grant for PRION 2013 (Summer 2013)
 - NSF - Alliances for Graduate Education and the Professoriate Travel Grant for PRION 2013 (Summer 2013)
- Scholastic:
 - Graduate Assistance in Areas of National Need (GAANN) Fellow (Summer 2015 – Spring 2019)
 - Program in Research & Scholarly Excellence (PRSE) Scholar (Fall 2011 – Spring 2014)
 - NSF - Alliances for Graduate Education and the Professoriate (AGEP) Fellowship (Fall 2011 – Spring 2012)
 - Amy Lyster Montgomery Memorial Endowment (Spring 2009)
 - Crimson Scholar (Spring 2004 - Spring 2008)
 - Regents Scholarship (Fall 2003)
- Research / Training Awards
 - Undergraduate Honors Thesis (2008)
 - Summer Multicultural Access to Research Training (Summer 2007)
 - MBRS-RISE: Research Initiative for Scientific Enhancement Scholar (Fall 2007 - Spring 2008)
 - Research Experience for Undergraduates (Summer 2006)
 - Minority Access to Research Careers Fellowship (Summer 2005 - Spring 2007)

- Other:
 - El Centro Outstanding Graduate Student Award (2012, 2013, 2015)
 - MBRS-RISE Outstanding Graduate Summer Coordinator (2010, 2011)

Research Experience:

Ph.D. Colorado State University Cell and Molecular Biology Program

- 2012- current Advisor: Dr. Glenn Telling
 - Ph.D. in Cell and Molecular Biology with an emphasis in Molecular, Cellular and Integrative Neuroscience
 - *Novel in vitro approaches delineate prion strain conformational variation*
- Ph.D. Rotation Projects (Molecular, Cellular, and Integrative Neuroscience Program)
 - (2011) Advisor: Dr. Kathy Partin: *Structural characteristics of GluR2-AMPA receptors*
 - (2011) Advisor: Dr. Kim Hoke: *Behavioral analysis of shoaling behaviors in guppies*
 - (2012) Advisor: Dr. James Bamburg: *Examining actin rods in hippocampal neurons*
 - (2012) Advisor: Dr. Richard Bessen: *Neurophysiological effects of prion infection in hamsters*

Undergraduate New Mexico State University Biology Department

- 2004-2008 Advisor: Dr. Daniel Howard Lab of Ecological and Evolutionary Genetics
 - Undergraduate Honors Thesis: Understanding Recent Divergence: A study of Round-headed katydids. (genus *Amblycorypha*).
- 2007-2008 Advisor: Dr. James Kroger Mind and Brain Laboratory
 - *Memory: Comparing Episodic and Semantic encoding*

Undergraduate Summer Research Programs

- Summer 2007: Advisor: Dr. Marissa Ehringer Genetics of Substance Abuse Laboratory
 - University of Colorado, Boulder
 - Summer Multicultural Access to Research Training (SMART) program
 - *Running Away from Alcohol Use; Why it just might work!*
- Summer 2006: Advisor: Dr. Gregory Florant Physiology Lab
 - Colorado State University
 - Research Experience for Undergraduates (REU) program
 - *Metabolic Fuel Utilization in Hibernators*

Research Techniques:

- Care and preparation of Human Subjects

- E-Prime programming and execution, Data statistical analyses
- Electric Encephalography: Preparation, Data monitoring and coalition
- fMRI: Data monitoring and coalition
- Use of Animal models
 - Animal care – Genetically Modified Mice
 - Creation of new transgenic mouse models
 - Bioassay and diagnosing clinical signs (prions)
 - Behavioral studies (alcohol/running behavior)
 - Using tissues to examine prion diseases
 - Animal care – Guppies
 - Shoaling behavioral studies
 - *in situ* hybridization studies
 - Trapping animal subjects in nature (Golden Mantle Ground Squirrels and Marmots)
 - Behavioral studies
 - Hibernation studies
 - Cryostat slicing of tissues
- Cell culture
 - Primary (neuronal): Actin Rod studies for Alzheimer’s research
 - RK13 Cells: Transformation, maintenance of mutants, prion studies
 - Cell-based Conformational Stability Assay
 - Cell-based Epitope Stability Assay
 - 10X Gold Cells: Transformation and maintenance of mutants, genetic studies
 - HEK 293 Cells: Transformation and maintenance of mutants, GluR2-AMPA studies
 - Dictyostelium discoideum
- DNA techniques
 - Creating/Ordering Primers
 - Extraction
 - PCR
 - Sequencing
 - Data statistical analyses & Phylogenetic Software
 - SNP’s analyses
 - Creating GluR2-AMPA receptor mutants (QuickChange Mutagenesis)
- Protein Analyses
 - Allozyme starch gels
 - Western Blot
- Bioinformatics
 - PyMol and ImageJ computer programs
- Biochemical analyses
 - Extractions (HPLC & ACE) and analyses (GCMS) for anti-cancer compounds
 - IR, GCMS, Melting Point, and TLC for anti-cancer compounds
- Imagery

- Basic Microscopy
- Confocal imagery

Teaching/Mentoring Experience and Training:

Teaching / Mentoring

- Colorado State University Diversity Coordinator (Fall 2016 – Spring 2017)
 - Graduate Preparatory Academy Instructor (Fall 2016 – Spring 2017)
 - TRIO Graduate School Visitation Day (Fall 2016)
 - Veterans Symposium - Graduate Involvement (Fall 2016)
- Colorado State University Graduate Teaching Assistant
 - LIFE 102: Attributes of Living systems
 - Laboratory Instructor (Fall 2015)
 - BZ 310: Cell Biology
 - Lecture Instructor (Spring 2016)
 - Microbiology Prep Room
 - Preparing supplies for all microbiology, and biology undergraduate classes (Spring 2019)
- Science Teacher
 - Gadsden Independent School District, Chaparral High School (2008-2010)
 - Classes Taught:
 - Integrated Science 3 – Chemistry and Honors Chemistry
 - *Note: I was the only Chemistry teacher in the High School*
 - Integrated Science 3 – Biology
 - Integrated Science 2 – Sophomore Science (Physical Science)
 - MESA (Math Engineering Science Advancement) Coordinator:
 - Innoventure Competition: 1st Place overall state winner (2009)
- Medicinal Plants of the Southwest Summer Research Program facilitator
 - MBRS-RISE (Research Initiative for Scientific Enhancement) Program, New Mexico State University, P.I. Dr. Antonio Lara (Summer 2010)
 - Responsible for:
 - Training underprivileged minority undergraduates in biochemistry and scientific method
 - Curriculum and Instructional planning
 - Attendance and timesheets
 - Creating a presentation for the American Chemistry Society National Meeting
- RISE Graduate Facilitator
 - MBRS-RISE (Research Initiative for Scientific Enhancement) Program, New Mexico State University, Director Dr. Elba Serrano (2010-2011)
 - Responsible for:
 - Instruction and support for underprivileged minority students to complete Summer Research and Graduate School Applications
 - Recruited Undergraduates and Graduates (ABRCMS 2010)
 - Serve as resource for underprivileged minority students
 - Create cohesive curriculum for future Summer Research Programs
- Summer Research Facilitator

- MBRS-RISE (Research Initiative for Scientific Enhancement) Program (New Mexico State University, Director Dr. Elba Serrano (Summer 2011))
- Medicinal Plants of the Southwest facilitator (P.I. Dr. Laura Rodriguez)
- Cell Discovery Workshop facilitator (P.I. Dr. Kevin Houston)
- Genomes Discovery Workshop facilitator (P.I. Dr. Brook Milligan)
- Responsible for (all 3 programs):
 - Purchasing
 - Curriculum and activity binder
 - Guest lecturer
- Research Experience for Undergraduates Mentor
 - Research Experience for Undergraduates in Molecular Biosciences, Colorado State University, P.I. Dr. Paul Laybourn (Summer 2015)
 - Responsible for:
 - Training underprivileged minority undergraduate in molecular bioscience and scientific method

Training / Certification

- Masters of Arts, Curriculum and Instruction (Graduation Year: 2011)
 - Specialized in Secondary (7th – 12th grade) Science Education
 - Minors in Molecular Biology and Psychology
 - Training in:
 - Curriculum
 - Instruction
 - Science Education
 - Educational Research
 - Multicultural Education / Teaching for Diversity
- New Mexico Level 1 (7-12) Secondary Teaching License (Certification Year: 2010)
 - Science Endorsement
 - Psychology Endorsement

Outreach and Memberships:

Outreach and Leadership Activities:

- Committee member: Creutzfeldt-Jakob Disease Foundation: Strides for CJD event (2015-2017)
- Founding member: Graduate Students of Color Advisory Council Founding Member (Colorado State University Graduate Minority Association) (2011-2018)
- President:
 - *Todos Juntos* President (Colorado State University Hispanic Graduate Association) (2011-2017)
 - CSU RAMbler Toastmasters Organization (2014-2016)
- Recruitment Facilitator:
 - PhD recruitment weekend, Cell and Molecular Biology Program (2013-2019)
 - PhD recruitment weekend, Microbiology, Immunology, and Pathology Department (2013-2018)

- PhD recruitment weekend, Molecular, Cellular, and Integrative Neuroscience Program (2012-2014)
- Judge:
 - Celebrate Undergraduate Research and Creativity (2015 – 2019)
 - Colorado Science and Engineering Fair (2012 – 2019)
 - MURALS (Multicultural Undergraduate Research Art and Leadership Symposium) (2015 – 2019)
 - El Centro Awards Ceremony (2014-2019)
 - Odyssey of the Mind Tournament (2013-2017)
 - Judge 5th Grade Science Fair (2012-2018)
 - Radiation Biology Class (ERHS300) Poster Final (2014)
- Instructor:
 - Brain Awareness Week (2012 – 2018)
- Newsletter Editor
 - Cell and Molecular Biology Newsletter (Spring 2015)
 - El Centro Focus (Colorado State University Hispanic Cultural Center Newsletter) (2011-2014)
 - Desert SunRISE (New Mexico State University MBRS-RISE Newsletter) (2010-2011)
- Advisor
 - QWEEN (Queer Women Engaging in an Encouraging Nexus) (2015 – 2019)
- Panelist
 - TRIO undergraduate to graduate seminar (2012-2018)
 - TRIO Collegiate mentorship seminar (2012-2014)
 - Research Experience for Undergraduates (REU): The path to Graduate School (2012-2018)

Memberships:

- CSU RAMblers Toastmasters Organization
- Microbiology, Immunology, and Pathology – Graduate Student Organization
- Graduate Student Council – Representative for Cell and Molecular Biology program and Microbiology, Immunology, and Pathology department (2015-2016)
- QWEEN (Queer Women Engaging in an Encouraging Nexus)
- Cell and Molecular Biology Newsletter
- *Todos Juntos* (Colorado State University Hispanic Graduate Association)
- Graduate Student of Color Advisory Council (Colorado State University Graduate Minority Association)
- National Society of Collegiate Scholars
- Phi Eta Sigma (Honors Society)
- American Physiological Society
- National Science Teachers Association
- American Chemical Society

Please feel free to contact me <vselwyn@rams.colostate.edu> if you would like a comprehensive list of coursework and/or additional information.